

Improved techniques to estimate mean sea level, velocity and acceleration from long ocean water level time series to augment sea level (and climate change) research

Author:

Watson, Phillip

Publication Date:

2018

DOI:

<https://doi.org/10.26190/5d47b04de6df4>

License:

<https://creativecommons.org/licenses/by-nc-nd/3.0/au/>

Link to license to see what you are allowed to do with this resource.

Downloaded from <http://hdl.handle.net/1959.4/59571> in <https://unsworks.unsw.edu.au> on 2024-05-02

Improved techniques to estimate mean sea level, velocity and acceleration from long ocean water level time series to augment sea level (and climate change) research

Phil J. Watson

A thesis in fulfilment of the requirements for the degree of

Doctor of Philosophy



UNSW
AUSTRALIA

School of Civil and Environmental Engineering

Faculty of Engineering

January 2018

<http://doi.org/10.26190/5d47b04de6df4>

THE UNIVERSITY OF NEW SOUTH WALES
Thesis/Dissertation Sheet

Surname or Family name: Watson
First name: Phillip Other Names: John
Abbreviation for degree as given in the University calendar: PhD
School: Civil & Environmental Engineering Faculty: Engineering
Title: Improved techniques to estimate mean sea level, velocity and acceleration from long ocean water level time series to augment sea level (and climate change) research.

Abstract 350 words maximum: (PLEASE TYPE)

The prominence of the climate change issue has placed more emphasis on examination of the extensive global repository of mean sea level records, which along with temperature and carbon dioxide, remain the key proxy data sets used to monitor and quantify changes in the global climate system. Over the past decade, the scientific literature is replete with conflicting conclusions regarding the detection (or otherwise) of a measurable acceleration in mean sea level attributable to climate change. The key aim of the research program is to develop improved techniques (and associated tools) for estimating mean sea level and associated velocity and acceleration from long individual ocean water level time series to augment climate change research. This task involved extensive time series analysis which identified Singular Spectrum Analysis (SSA) as an optimal analytic for resolving estimates of mean sea level from long tide gauge records with improved accuracy and temporal resolution. SSA was further tested and optimised, then integrated into an open source analytical software package (“msltrend”), specifically customised for sea level research, providing enhanced estimates of mean sea level and associated velocity and acceleration on a year to year basis. The application of this package to the data rich margins of USA and Europe have provided more insight into the temporal and regional characteristics of mean sea level than previously available. In general, key findings across both margins suggest that not only are more recent accelerations no different to other periods elsewhere in the historical records, but, they are neither sufficiently strong nor sustained enough (yet) to accord with those associated with climate change projection models. Further, until such time as the velocities and accelerations are sufficiently large not to be obscured by complex influences inducing decadal to multi-decadal variability and other background noise, the search for accelerations in ocean water level records require more intuitive, diagnostic considerations which are explored in the research. The techniques espoused in this research form an integral part of the evolutionary process by which to measure kinematic properties of mean sea level with improving robustness and consistency.

Declaration relating to disposition of project thesis/dissertation

I hereby grant to the University of New South Wales or its agents the right to archive and to make available my thesis or dissertation in whole or in part in the University libraries in all forms of media, now or here after known, subject to the provisions of the Copyright Act 1968. I retain all property rights, such as patent rights. I also retain the right to use in future works (such as articles or books) all or part of this thesis or dissertation.

I also authorise University Microfilms to use the 350 word abstract of my thesis in Dissertation Abstracts International (this is applicable to doctoral theses only).

.....
Signature Witness Date

The University recognises that there may be exceptional circumstances requiring restrictions on copying or conditions on use. Requests for restriction for a period of up to 2 years must be made in writing. Requests for a longer period of restriction may be considered in exceptional circumstances and require the approval of the Dean of Graduate Research.

FOR OFFICE USE ONLY Date of completion of requirements for Award: 30 January 2018

ORIGINALITY STATEMENT

'I hereby declare that this submission is my own work and to the best of my knowledge it contains no materials previously published or written by another person, or substantial proportions of material which have been accepted for the award of any other degree or diploma at UNSW or any other educational institution, except where due acknowledgement is made in the thesis. Any contribution made to the research by others, with whom I have worked at UNSW or elsewhere, is explicitly acknowledged in the thesis. I also declare that the intellectual content of this thesis is the product of my own work, except to the extent that assistance from others in the project's design and conception or in style, presentation and linguistic expression is acknowledged.'

Signed

Date

COPYRIGHT STATEMENT

'I hereby grant the University of New South Wales or its agents the right to archive and to make available my thesis or dissertation in whole or part in the University libraries in all forms of media, now or here after known, subject to the provisions of the Copyright Act 1968. I retain all proprietary rights, such as patent rights. I also retain the right to use in future works (such as articles or books) all or part of this thesis or dissertation.

I also authorise University Microfilms to use the 350 word abstract of my thesis in Dissertation Abstract International (this is applicable to doctoral theses only).

I have either used no substantial portions of copyright material in my thesis or I have obtained permission to use copyright material; where permission has not been granted I have applied/will apply for a partial restriction of the digital copy of my thesis or dissertation.'

Signed

Date

AUTHENTICITY STATEMENT

'I certify that the Library deposit digital copy is a direct equivalent of the final officially approved version of my thesis. No emendation of content has occurred and if there are any minor variations in formatting, they are the result of the conversion to digital format.'

Signed

Date

ACKNOWLEDGEMENTS

Numerous individuals have been acknowledged in each of the respective published works forming this PhD research program.

Notwithstanding, the author would like to expressly acknowledge the following individuals whose various contributions have in one form or another, proved pivotal to success of the overall research program (in alphabetical order):

Associate Professor Ron Cox, UNSW (Co-Supervisor). Provided a professional and supportive framework within which to conduct the research program.

Emeritus Professor Robert Dean (late), University of Florida. A constant source of inspiration and encouragement from the development of the project throughout until his passing in 2015.

Associate Professor Nina Golyandina, Department of Mathematics, St. Petersburg University, Russia. Provided extensive and timely advice on Singular Spectrum Analysis and the application of the Rssa package in R, both of which were pivotal to development of the msltrend package.

Dr James Houston, retired former Director, Engineer Research and Development Center (ERDC), US Army Corps of Engineers. A constant source of inspiration and encouragement and always happy to review and critique draft manuscripts.

Professor Rob Hyndman, Department of Econometrics and Business Statistics, Monash University, Australia. Provided extensive and timely advice on time series analysis, R programming and statistical analysis techniques, all of which were pivotal to development of the msltrend package.

Associate Professor Bill Pierson, UNSW (Co-Supervisor). Provided a professional and supportive framework within which to conduct the research program.

Associate Professor Andrew Robinson, School of Mathematics and Statistics, University of Melbourne, Australia. Provided extensive advice and resources to learn the R programming language.

Linda Watson. Devoted wife who provided unlimited support throughout to enable the research program to be undertaken whilst juggling full time careers and raising our family.

Table of Contents

Chapter 1.....	1
Introduction	1
Chapter 2.....	8
Development of Synthetic Ocean Water Level Data Set	8
2.1 Background	9
2.2 Key philosophies underpinning the design approach.....	9
2.3 Mean Sea Level	11
2.4 Cyclical Dynamic Influences	12
2.4.1 Seasonal Influences.....	12
2.4.2 Long Period Tidal Harmonic Influence	14
2.4.3 Pole Tide Influence.....	17
2.4.4 Climate Mode Influences	20
2.4.4.1 El Niño-Southern Oscillation	22
2.4.4.2 Pacific Decadal Oscillation (PDO).....	24
2.4.4.3 Northern Annular Mode (NAM) and North Atlantic Oscillation (NAO)	26
2.4.4.4 Southern Annular Mode (SAM) and Antarctic Oscillation (AAO)	28
2.4.5 Noise	29
2.5 Other Considerations	31
2.6 Summary	33
2.7 Acknowledgements.....	34
Chapter 3.....	36
Testing to identify the optimum performing analytic for isolating mean sea level with improved temporal accuracy	36
3.1 Background	37
3.2 Testing Methodology	39
3.2.1 Application of analysis methods to extract trend from synthetic data sets.....	41
3.2.2. Multi-criteria assessment of analytical methods for isolating mean sea level.....	43
3.3 Results.....	45
3.4 Discussion and limitation of analysis and testing framework.....	50
3.5 Conclusion.....	54
3.6 Acknowledgements.....	55
Chapter 4.....	57
Methodology to Improve Estimates of Velocity and Acceleration in the Mean Sea Level Signal.....	57
4.1 Introduction	58

4.2 What is SSA and how does it work?	58
4.3 Optimising SSA for mean sea level analysis	59
4.3.1 Minimum length annual average time series	60
4.3.2 Embedding Dimension	60
4.3.3 Automatic identification of “trend-like” components	61
4.3.4 Gap filling of time series	67
4.4 Additional considerations to enhance velocity and acceleration estimates	68
4.5 Summary of key findings	69
4.6 Development of analytical software package	70
4.6.1 Input Data	72
4.6.2 Estimation of Errors	72
4.6.3. Key Functions	73
4.7 Acknowledgements	74
Chapter 5	75
Application of “msltrend” Analytical Software Package to the Data Rich Margins of the USA	75
5.1 Introduction	76
5.2 Data	77
5.3 Methodology	79
5.4 Results	81
5.5 Discussion	87
5.5.1 Accounting for vertical land motions at tide gauge sites	88
5.5.2 Accounting for dynamic influences contained within tide gauge time series	89
5.5.3 Measuring mean sea level acceleration	90
5.5.4 Recent literature concerning MSL acceleration around the USA	91
5.5.5 Reconciling historical and future projected MSL accelerations	94
5.6 Conclusions	96
5.7 Acknowledgements	99
Chapter 6	100
Application of “msltrend” Analytical Software Package to the Data Rich Margins of Europe	100
6.1 Introduction	101
6.2 Physical Setting	102
6.3 Methodology	107
6.4 Data	107
6.5 Results	110
6.6 Discussion	116

6.6.1. Reconciling historical and future projected MSL accelerations.....	117
6.6.2. Selected Literature concerning MSL acceleration around Europe	120
6.7 Conclusion.....	123
6.8 Acknowledgements.....	125
Chapter 7.....	126
Conclusions and Recommendations	126
7.1 Key Learnings and Insights from Research	129
7.2 Future Research	132
Chapter 8.....	134
Bibliography	134
Appendix A.....	160
PSMSL Stations Used to Develop Core Synthetic Data Set.....	160
Appendix B	162
Extraction of Noise Component from PSMSL Stations Used to Develop Synthetic Data Set	162
Appendix C	166
Comparison of Real and Synthetic Data Set Mean Sea Level Time Series.....	166
Appendix D.....	169
Comparison of Components 1 and 2 to optimise and automate SSA decomposition	169
Appendix E	176
“Msltrend” User Manual.....	176

Figures

Figure 1.1: Projections from process-based models of (a) global mean sea level (GMSL) rise relative to 1986–2005 and (b) the rate of GMSL rise and its contributions as a function of time for the four RCP scenarios and scenario SRES A1B.....	4
Figure 1.2: Rate of GMSL rise from AR5 RCP central projections.	5
Figure 2.1: Schematic representation of components of the core synthetic data set.	10
Figure 2.2: Generated Monthly Time Series Signal of Mean Sea Level (MSL).	11
Figure 2.3: Schematic Representation of Seasonal Component.	13
Figure 2.4: Schematic Representation of Nodal Tide Component.	16
Figure 2.5: Temporal Variability of Polar Tide Influence at Chandler Period.	19
Figure 2.6: Schematic Representation of Pole Tide Component.	20
Figure 2.7: Schematic Representation of Climate Mode Component.	22
Figure 2.8: Comparison of SOI and ICI.	23
Figure 2.9: Maximum Monthly Sea-Surface Anomaly Attributable to ENSO.	24
Figure 2.10: Comparison of PDO and DCI.	25

Figure 2.11: Maximum Monthly Sea-Surface Anomaly Attributable to PDO. 25

Figure 2.12: Maximum Monthly Sea-Surface Anomaly Attributable to NAO..... 27

Figure 2.13: Maximum Monthly Sea-Surface Anomaly Attributable to SAM..... 29

Figure 2.14: Datum Shift in Tide Gauge Record at Hanasaki, Japan. 32

Figure 3.1: Indicative monthly average ocean water level time series from synthetic data set. 40

Figure 3.2: Analysis overview based on Criteria A_1 47

Figure 4.1: Spectral characteristics of leading SSA components from long PSMSL records..... 65

Figure 4.2: Differencing vs smoothing spline for kinematic properties of Cuxhaven trend..... 70

Figure 5.1: Location of tide gauge records analysed. 79

Figure 5.2: Temporal characteristics of mean sea level at selected sites (Seattle, San Francisco, New York, and Key West)..... 82

Figure 5.3: Peak estimates of velocity and acceleration for all stations..... 83

Figure 5.4: Periods of positive acceleration (95% CI). 85

Figure 5.5: Estimates of Geocentric Rate of Sea-Level Rise (95% CI). 86

Figure 5.6: Relative velocity time series for Central Pacific and west coast U.S. station records. 92

Figure 5.7: Indicative implications of projected sea-level rise of 800 mm at San Francisco and New York from end of 2014 to 2100. 95

Figure 6.1: Location of tide gauge records analysed. 104

Figure 6.2: North Sea tide gauge records analysed. 105

Figure 6.3: Baltic Sea tide gauge records analysed..... 106

Figure 6.4: Temporal characteristics of mean sea level for the longest records within the study area (Amsterdam, Stockholm, Brest and Swinoujscie). 111

Figure 6.5: Peak estimates of velocity and acceleration for all stations..... 112

Figure 6.6: Periods of positive acceleration (95% CI). 114

Figure 6.7: Estimates of Current Geocentric Rate of Sea-Level Rise (95% CI). 115

Figure 6.8. Indicative implications of projected sea-level rise of 800 mm at Cuxhaven, Germany, and Kronstadt, Russian Federation, from 2015 to 2100..... 119

Figure A1: Location of PSMSL stations used to derive seasonal components..... 161

Figure B1: Noise component of PSMSL station records used for synthetic data set..... 163

Figure C1: Selected monthly average ocean water level data sets from PSMSL..... 167

Figure C2: Selected monthly average ocean water level time series from synthetic data set. 168

Figure D1: Leading 2 components of SSA decomposition for Brest and San Francisco mean sea level records..... 170

Figure D2: Leading 2 components of SSA decomposition for Helsinki and Nedre Sodertalje mean sea level records. 171

Figure D3: Leading 2 components of SSA decomposition for Batumi and Bergen mean sea level records. 172

Figure D4: Leading 2 components of SSA decomposition for Sydney and Hanko mean sea level records. 173

Figure D5: Leading 2 components of SSA decomposition for Kobenhavn and Klaipeda mean sea level records..... 174

Figure D6: Leading 2 components of SSA decomposition for Hornbaek and Portland mean sea level records..... 175

Tables

Table 2.1: Summary of Core Synthetic Data Set. 33

Table 2.2: Generated Monthly and Annual Average Data Sets for Analysis..... 34

Table 3.1: Summary of Analysis Techniques Applied to Synthetic Data Set..... 42

Table 3.2: Summary of Number of Analyses Applied to Each Data Set..... 43

Table 3.3: Multi-Criteria Assessment by Method Across Annual Synthetic Data Sets. 49

Table 4.1: PSMSL Records tested to optimise performance of Singular Spectrum Analysis. 63

Table 4.2: Station records with significant component 2 contribution in the low frequency band [0 – 0.01]. 66

Table 4.3: Key features necessary to optimise the temporal resolution of mean sea level and associated kinematic properties. 71

Table 5.1: Summary of data used in USA analysis. 78

Table 6.1: Summary of data used in European analysis. 108

Table 7.1: Snapshot of Key Findings and Learnings. 131

Table 7.2: Priority Research Projects. 133

Table A1: Summary of PSMSL stations used to derive seasonal components. 161

Chapter 1

Introduction

Climate change is predicted to have far reaching physical, social, environmental and economic impacts (e.g., Houser *et al.*, 2015; IPCC, 2014; Melillo *et al.*, 2014; Neumann *et al.*, 2015; Watkiss, 2011). The capacity for mankind to adapt will (in part) be governed by the pace at which impacts will manifest and the success of global adaptation endeavours which might offset (or delay) the inevitability of impacts from longer term climate change commitments associated with radiative forcings, such as sea level rise.

Sea level rise is one of the more insidious (or irreversible) of the postulated climate change impacts. This is due to the fact that thermal expansion and ice sheet response (as key elements of the sea level rise budget) will continue for centuries after stabilization of radiative forcing owing to the thermal inertia and long response time scale of the deep ocean (Zickfeld *et al.*, 2013) and ice sheets (Levermann *et al.*, 2013). For example, Gillett *et al.* (2011) demonstrated in zero-emission commitment simulations with complex Earth System Models, that thermo-steric sea level rise continued for some 900 years after the cessation of emissions.

The continued trend for coastal global population migration (Neumann *et al.*, 2015) fuels the increasing projected risks associated with sea level rise. In July 2015, the world's population reached 7.3 billion. The world has added one billion people since 2003 and two billion since 1990 with the global population projected to increase somewhere between 9.5 and 13.3 billion by 2100 at the 95% confidence level (United Nations, 2015). In 2000, the global coastal population residing within the low elevation coastal zone (commonly defined as the contiguous and hydrologically connected zone of land along the coast and below 10 m of elevation (Lichter *et al.*, 2011; McGranahan *et al.*, 2007)) was estimated at around 625 million (Neumann *et al.*, 2015).

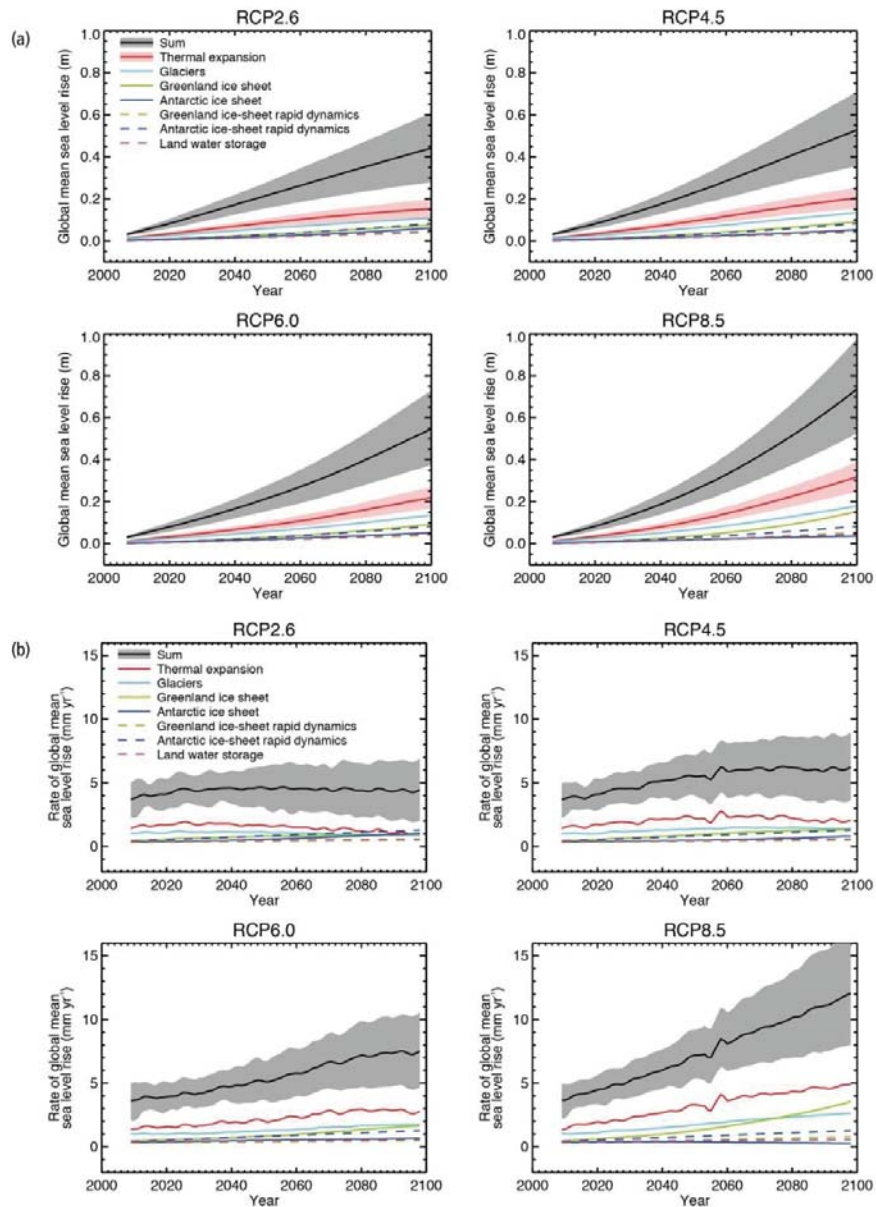
Flood exposure is increasing in coastal cities owing to growing populations and assets, the changing climate, and land subsidence (Hallegatte *et al.*, 2013). Similarly environmentally sensitive delta regions, which are extremely vulnerable to storm surges and sea level rise account for only 1% of the global land area, but, accommodate approximately 7% of the global population (Ericson *et al.*, 2006). The threat of sea level rise in these margins is exacerbated by the propensity of the founding fluvial sediments to readily compact, leading to enhanced land subsidence (Szabo *et al.*, 2016).

The prominence of the climate change issue has placed more emphasis on examination of the extensive global repository of relative mean sea level records (Holgate *et al.*, 2012), which along with temperature and carbon dioxide, remain the key proxy data sets used to monitor and quantify changes in the global climate system (Watson, 2016e). In particular, considerable research effort has been invested over the past decade in detecting evidence of a measurable acceleration in mean sea level commensurate with forecast projections associated with climate change. However, these research endeavours fit within a broader, integrated framework of sea level science designed to understand sea level change and its implications both present and future (e.g. Intergovernmental Panel on Climate Change; World Climate Research Programme, etc).

Climate models are key tools in assisting to understand and plan for the predicted impacts of a changing climate system, forming central elements of the Assessment Reports of the Intergovernmental Panel on Climate Change (IPCC, 2007, 2013a) with great reliance placed on projection outputs to facilitate appropriate policy, adaptation and mitigation responses. By coordinating the design and distribution of global climate model simulations of the past, present, and future climate, the Coupled Model Intercomparison Project (CMIP) has become one of the foundation elements of climate science (Eyring *et al.*, 2016), providing an ensemble of climate models to support the IPCC's Fifth Assessment Report (AR5) (Church *et al.*, 2013a).

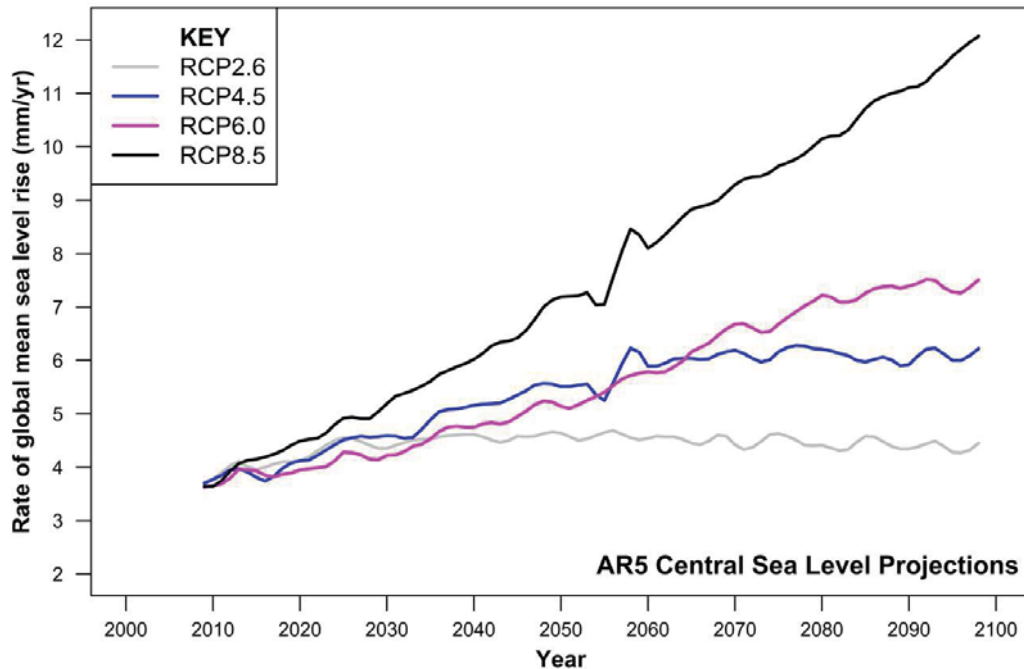
Various Representative Concentration Pathway (or RCP) experiments were modelled in AR5 providing future projections of sea level based on changes to radiative (or external) forcing (Moss *et al.*, 2010). Global mean sea level projection model outputs from AR5 for each of the RCP experiments are provided in Figure 1.1 (Figure 13.11, Church *et al.*, 2013a). Church *et al.* (2013a) observes that in all the projections, the rate of rise initially increases. More specifically, in RCP2.6 it becomes roughly constant (central projection 4.5 mm/yr) before the middle of the century, and subsequently declines slightly. The rate of rise becomes roughly constant in RCP4.5 and RCP6.0 by the end of the century, whereas acceleration continues throughout the century in RCP8.5, reaching 11 [8 to 16] mm/yr by 2100. Figure 1.2 directly compares the global rate of rise in the central projection for each RCP experiment, highlighting key differences between the respective simulated model projections over time.

Figure 1.1: Projections from process-based models of (a) global mean sea level (GMSL) rise relative to 1986–2005 and (b) the rate of GMSL rise and its contributions as a function of time for the four RCP scenarios and scenario SRES A1B.



Notes:

The lines show the median projections for GMSL rise and the thermal expansion contribution, the likely range is shown as a shaded band. The contributions from ice sheets include the contributions from ice-sheet rapid dynamical change, which are also shown separately. The rates in (b) are calculated as linear trends in overlapping 5-year periods. Only the collapse of the marine-based sectors of the Antarctic ice sheet, if initiated, could cause GMSL to rise substantially above the likely range during the 21st century. This potential additional contribution cannot be precisely quantified but there is medium confidence that it would not exceed several tenths of a metre of sea level rise. Source: Figure 13.11 (Church *et al.*, 2013a).

Figure 1.2: Rate of GMSL rise from AR5 RCP central projections.**Notes:**

The rate of global mean sea level rise from each of the RCP central projections depicted above are derived directly from panel (b) of Figure 1.1 using data made available by the IPCC (Church *et al.*, 2013b).

From the start of the projection models (2007) to around the mid-2030s, the rate of rise in the central estimate for each of the RCP experiments (with the exception of RCP8.5) is relatively consistent from 3.7 mm/yr to \approx 4.5 mm/yr (refer panel (b) of Figure 1.1 and Figure 1.2), commensurate with a sustained, though relatively low rate of acceleration. By comparison, at this time the rate of rise in the central sea level projection for the RCP8.5 experiment is almost 1 mm/yr higher than for the other RCP experiments (at \approx 5.5 mm/yr) and continuing to diverge further over the remainder of the century. The influence of the radiative forcing built into each RCP experiment only really starts to diverge significantly over the latter half of the 21st century. The aforementioned temporal characteristics of the projected rate of global rise in the central projections, provide a coarse reference frame against which long tide gauge and other records (such as satellite altimetry) can be compared to augment scientific understanding and adaptive planning endeavours.

Fasullo *et al.* (2016) note that among the major unanswered questions associated with climate change is why Global Mean Sea Level (GMSL) acceleration has not yet been detected in the

altimeter record, given the increasing rates at which glacial and ice sheet melt are estimated to have occurred (Hanna *et al.*, 2013; Shepherd *et al.*, 2012) and as greenhouse gas concentrations have risen (Haigh *et al.*, 2014). Various theories have been proposed to account for the lack of acceleration in GMSL over the altimetry period (post 1992) including the masking influence associated with the Mt Pinatubo volcanic eruption in 1991 (Fasullo *et al.*, 2016) and the identification of a significant non-zero systematic drift (satellite-specific), most notably affecting the first 6 years of the GMSL record (Watson *et al.*, 2015).

Numerous studies and their conclusions regarding the prospect of whether there is a measurable acceleration in ocean water level records have spawned energetic scientific debate in the recent literature (e.g., Baart *et al.*, 2012a; Donoghue and Parkinson, 2011; Houston and Dean, 2011a, 2011b; Rahmstorf and Vermeer, 2011; Visser *et al.*, 2015; Watson, 2011). In particular, the published works of Watson (2011) and Houston and Dean (2011a) generated extensive political, social, and media debate around the issue (e.g., ABC-TV, 2011; Australia, 2011; Rintoul, 2011; Tamino, 2011).

In addition to discussion on physical process drivers (such as Fasullo *et al.*, 2016), much of the professional debate has centred on the manner in which acceleration is estimated. Almost exclusively, estimates of acceleration in global or basin scale mean sea level studies have been derived from the fitting of comparatively simple second order polynomial (or quadratic function of the form $Ax^2 + Bx + C$). With these simple functions, the acceleration can be conveniently and directly calculated by doubling the quadratic coefficient (i.e., $2A$). These approaches are extremely limited because they inherently assume a constant rate of acceleration applying over the course of the record (Watson, 2016c,e), which is not the case in reality with sea level records (refer Watson, 2016e,f; Woodworth *et al.*, 2009).

As a result, trends determined via simple linear regression and acceleration determined through simple quadratic fits are likely to be unduly influenced by the particular time slice chosen (Rahmstorf and Vermeer, 2011). These comparatively simple approaches work well at a coarse scale where real-time changes in the kinematic properties of the mean sea level signal are unimportant. Given the prominence of mean sea level acceleration and its intrinsic linkages to climate change science, the key aim of the research program is to develop improved techniques (and associated tools) for estimating mean sea level and associated real-

time velocity and acceleration from long individual ocean water level time series to augment climate change research. Thesis chapters have been designed as essentially standalone bodies of work that sequentially build on the findings of each other in order to achieve the objective of the research program as summarised briefly below. Specific literature reviews are included within each chapter:

Chapter 2: Development of a detailed synthetic ocean water level data set to test time series analysis techniques for their utility in isolating mean sea level with improved temporal accuracy;

Chapter 3: Detailed testing of time series analysis techniques for their utility in isolating mean sea level with improved temporal accuracy;

Chapter 4: Development of a methodology to improve estimates of velocity and acceleration in the mean sea level signal incorporated into the build of an analytical software package;

Chapter 5: Apply the analytical software package developed on the data rich margins of continental USA to improve knowledge of real-time acceleration for regional sea level and climate change research;

Chapter 6: Apply the analytical software package developed on the data rich margins of Europe to improve knowledge of real-time acceleration for regional sea level and climate change research; and

Chapter 7: Conclusions.

Chapter 2

Development of Synthetic Ocean Water Level Data Set

Synopsis: An authoritative, effective and transparent process by which to identify the most accurate analytical technique for isolating the mean sea level signal is to test such approaches against “synthetic” (or custom built) data sets with a known mean sea level signal. In order to be effective, the synthetic data set developed for this research has been specifically designed to mimic key physical characteristics of real-world data, comprising a range of known components added to a nonlinear, non-stationary time series of mean sea level. The key components embedded within conventional ocean water level data sets have been established from the extensive literature available and via direct consultation with some of the world’s leading oceanographers, sea level researchers and subject matter experts relevant to various components of the proposed synthetic data set.

Publication I

Watson, P.J., 2015. Development of a unique synthetic data set to improve sea-level research and understanding. *Journal of Coastal Research*, 31(3), 758–770. Coconut Creek (Florida), ISSN 0749-0208.

Declaration

I certify that this publication was a direct result of my research towards this PhD, and that reproduction in this thesis does not breach copyright regulations.

Phil J. Watson [Candidate]

2.1 Background

The complexity of the influences embedded within conventional monthly and annual average ocean water level data sets has led sea level research toward successively more sophisticated time series analytical techniques. The key prerogative for sea level researchers remains isolating the comparatively small, non-stationary, non-linear mean sea level signal from the significant and substantial dynamic inter-decadal (and other) influences and noise.

Without an absolute knowledge of the mean sea level signal, the extracted signal (or trend) will only ever be an estimate of the true signal. The veracity of the extracted mean sea level signal has universally been inferred from the assumed sophistication of the underpinning analytical approach applied to ocean water level data sets. In effect, comparison from one estimate of mean sea level to another, in part, has become an indirect qualitative view of the merit of the analytical approach applied.

An authoritative, effective and transparent process by which to identify the most appropriate analytical technique for isolating the mean sea level signal is to test such approaches against “synthetic” (or custom built) data sets with a known mean sea level signal.

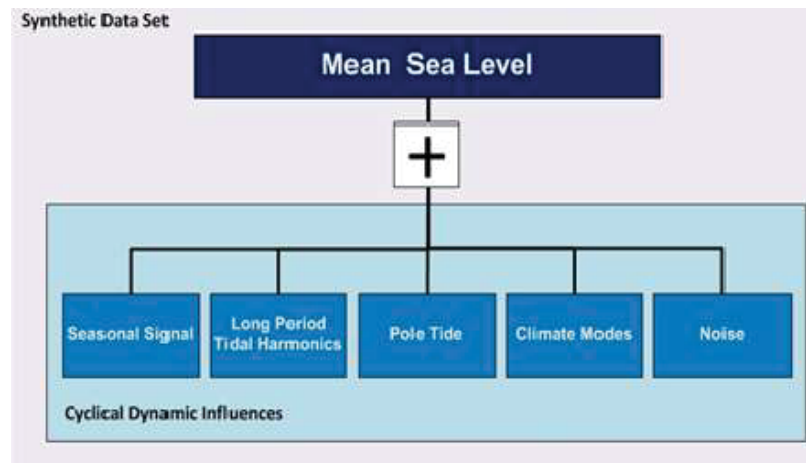
2.2 Key philosophies underpinning the design approach

In order to be effective, the synthetic data set developed for this research has been designed to be as generically applicable as possible (i.e. reflective of the environmental attributes and signals captured by a tide gauge located anywhere worldwide) and thus mimic the key physical characteristics embedded within real-world ocean water-level data. The key components of the synthetic data set have been established from the extensive literature available and via direct consultation with some of the world’s leading oceanographers, sea level researchers and subject matter experts (refer Section 2.7). A schematic representation of the elements comprising the core synthetic data set is depicted at Figure 2.1.

This data set has been designed as a monthly average time series spanning a 160-year period from 1850–2010. This time period has been selected to reflect the predominant date range for the longer Permanent Service for Mean Sea Level (PSMSL) data holdings. The core data set can then be aggregated to annual data and separately divided into 2 X 80 year and 4 X 40 year subsets to further examine not only the capacity of the respective analytical methods to

extract the embedded mean sea level signal, but, also any issues associated with record length, end effects as well as monthly versus annual data.

Figure 2.1: Schematic representation of components of the core synthetic data set.



Details concerning the construction of the fixed mean sea level signal are detailed in Section 2.3. Details concerning the cyclical dynamic components and how they have been used to construct the data set are detailed in Section 2.4.

In order for the core synthetic data set to be as globally representative as possible, each of the key dynamic influences are represented by a bin of monthly time series spanning the full 160-year period, reflecting the range of real-world measured influences for each particular component. The synthetic data set contains 20,000 separate time series, with each time series generated by successively adding a randomly sampled signal from within each of the dynamic components to the fixed mean sea-level signal.

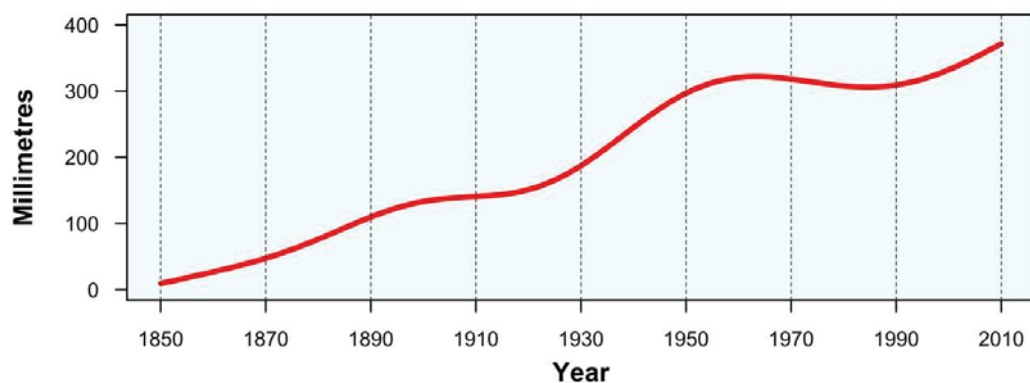
The selection of 20,000 randomly generated time series represents a reasonable balance between optimising the widest possible set of complex combinations of real-world signals and the extensive computing time required to analyse the synthetic data set. Further, the 20,000 generated trend outputs from each analysis applied to the data set provides a robust means of statistically identifying the better performing techniques for extracting the trend (Chapter 3).

In addition to the published literature, the data from 43 selected PSMSL sites have been analysed and decomposed to estimate genuine seasonal signals and noise components using the respective methods detailed in the following sections pertaining to these components. The selected sites (refer Appendix A) were based on maximising a range of factors including global spatial coverage, length and quality of records, and range of environmental influencing factors. The other dynamic components and the fixed mean sea-level signal have been specifically based on the scientific literature, and the methods used to generate the bins of real-world signals are detailed in the following sections dedicated to each component.

2.3 Mean Sea Level

Mean sea level has been created as a smoothed, non-linear time series signal reflective of the global trend of mean sea level (Bindoff *et al.*, 2007) and key “inflexion” points evident in the majority of long ocean water level data sets (Woodworth *et al.*, 2009). This monthly time series signal (refer Figure 2.2) is the key fixed signal embedded within each time series of the core synthetic data set.

Figure 2.2: Generated Monthly Time Series Signal of Mean Sea Level (MSL).



It is important to note that the intention here is not to seek to have the “perfect” representation of mean sea level over the period in question as there are numerous and differing representations of assumed global mean sea level (e.g., Church and White, 2011; Hamlington *et al.*, 2011; Hay *et al.*, 2015; Jevrejeva *et al.*, 2006; Jevrejeva *et al.*, 2014; Meyssignac *et al.*, 2012a; Ray and Douglas, 2011; Wenzel and Schröter, 2014). Rather, this embedded feature is designed to represent the type of signatures and characteristics anticipated of this feature against which one can critically test (Chapter 3).

2.4 Cyclical Dynamic Influences

The key cyclical dynamic influences embedded within ocean water level data sets can be generally classified within one of five key areas which include seasonal signals, long-period tidal harmonic responses, pole tides, climate modes (global and regional) and noise (as indicated in Figure 2.1).

In addition to the published literature and consultation with key international oceanographers and sea level researchers, the data from 43 selected PSMSL sites have been analysed and decomposed to estimate the seasonal influence and noise components. The selected sites (refer Appendix A for details) were based on maximising a range of factors including global spatial coverage, length and quality of records and range of environmental influencing factors.

2.4.1 Seasonal Influences

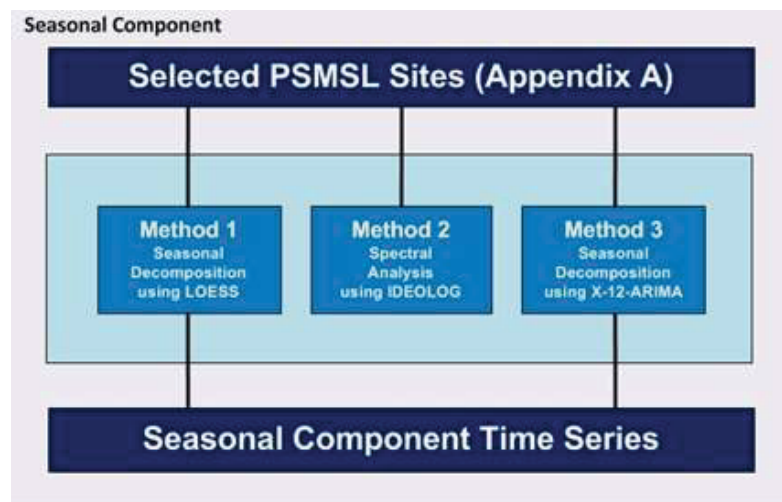
The seasonal signal is highly variable in nature and one of the larger components of sea level time series. Gauge records located near river mouths in glaciological or monsoonal regions will also be embedded with seasonal influences attributed to large river outflows at certain times of the year. The 43 PSMSL gauge sites used for seasonal decomposition (refer Appendix A) provide a broad mix of locations which encompass significant monsoonal and glaciological cycles as well. The seasonal signal has been extracted from each of the gauge records using three (3) separate established methodologies (refer Figure 2.3), including:

- ❑ **Method 1:** locally weighted polynomial regression smoothing (or “loess”) of the seasonal sub-series (ie. the series of all January, February, March values, etc). This approach has been undertaken using the “stl decomposition” function in the R analytical software package (Cleveland *et al.*, 1990; R Core Team, 2013). This methodology produces a repetitive seasonal cycle throughout the data record;
- ❑ **Method 2:** spectral analysis using a de-seasonalising band stop filter available in the IDEOLOG software package (Pollock, 2008). Similar to the loess smoothing approach, the frequency domain filtering approach produces a repetitive seasonal cycle throughout the data record; and
- ❑ **Method 3:** fitting an autoregressive integrated moving average (or ARIMA) model to the data. This approach has been undertaken using the X-12-ARIMA seasonal adjustment software package developed by the US Census Bureau (US Census Bureau, 2009) run within the GRETl analytical software package (GRETl, 2013). X-12-ARIMA automatically

selects the optimum “additive” or “multiplicative” seasonal model based on the parameters of the data set. Unlike the afore-mentioned techniques, the X-12-ARIMA model outputs produce a time varying seasonal signal. The software limits the input data to 70 years. Where the available tide gauge data record exceeded this limit, only the latter 70 years of the record were used to extract the seasonal signal. Outputted seasonal signals were then looped ‘top to tail’ backwards over time to estimate the seasonal signal corresponding to the complete time period (1850 to 2010).

The seasonal signals extracted via Methods 1 and 2 produced remarkably similar results for the respective monthly amplitude at each station. To avoid unnecessary duplication of results, only the Method 1 and Method 3 outputs from the analysis of the 43 PSMSL stations have been used to compose the seasonal time series components in the synthetic data set.

Figure 2.3: Schematic Representation of Seasonal Component.



From the analysis, the phase and amplitude of the seasonal signals varied significantly ranging from the smallest amplitude signal (-24 to +3 mm) recorded at the Argentine Islands gauge (Antarctica) to the largest amplitude signal (-630 to +1220 mm) recorded at the Trois-Rivières gauge (Quebec, Canada) situated at the confluence of the Saint-Maurice and Saint Lawrence Rivers and significantly affected by snow accumulation and melting cycles.

Based upon the above-mentioned analysis, a total of 82 time series have been generated to represent the range of seasonal influences expected within ocean water level data sets.

2.4.2 Long Period Tidal Harmonic Influence

Cherniawsky *et al.* (2009) advises that modern harmonic analysis of tidal heights (Foreman, 1977; Godin, 1972) can be expressed broadly as a linear superposition of six astronomical forcing harmonics, including:

- mean rates of change of lunar time (with a mean period of 24.84 hours);
- longitudes of the moon (27.3 days);
- sun (365.24 days);
- lunar perigee (8.85 years);
- moon's ascending node (18.61 years); and
- solar perigee (20392 years).

Other than the nodal tide (governed by the moon's ascending node), all other above-mentioned forcings have little direct relevance as separate components for inclusion within the synthetic data set. The high frequency daily harmonic signals are largely removed through monthly averaging and therefore not relevant. The monthly and annual harmonic signals are relatively small compared to the seasonal signal operating in the same frequency band and thus can be similarly ignored. The lunar perigee with an 8.85 year harmonic cycle has relevancy for consideration of extremes, but, is a relatively small signal that cancels out in the consideration of mean sea levels and has also not been considered further (Haigh ID 2013, pers. comm., 22 October; Woodworth PL 2013, pers. comm., 8 October). Similarly, the influence of the long period solar perigee over such a comparatively short period of the harmonic cycle (160 years of 20392 year period or 0.8% of cycle) deems that the influence of this signal is insignificant and can be ignored in this context.

However, the 18.61 year nodal harmonic cycle has relevancy for the construction of the core synthetic data set. The nodal influence at a particular location, in accordance with equilibrium theory, is based on latitude and angle relative to the moon's position (Pugh, 1987) with the theoretical signal amplitude ranging from zero at latitudes of around 35.3°N and S to a maximum of approximately 12 mm at the poles (Woodworth, 2012). The phase angle of the nodal signal varies over the 18.6 year cycle in accordance with equilibrium theory but is

considered to be latitude dependent (Pugh, 1987). The phase of the cycle at higher latitudes is anti-phased to those at the tropics (Woodworth PL 2013, pers. comm., 22 October).

Woodworth (2012) notes however, that loading and self-attraction and mass conservation processes modify the simple spatial dependence of any long-period tide that would otherwise “follow the equilibrium law”. Woodworth (2012) further advises that these processes are likely to enhance the nodal amplitude at higher latitudes by as much as 25% above that proposed by equilibrium theory. However, within tropical areas, the nodal signal is within 5-10% of the classical theory.

Discussion around the amplitude of the nodal tide has taken on particular prominence in recent years as researchers attempt to improve sea level trend and acceleration estimates by accounting for this longer period phenomenon (Baart *et al.*, 2012b; Cherniawsky *et al.*, 2009; Houston and Dean, 2011c; Iz, 2006; Woodworth, 2012).

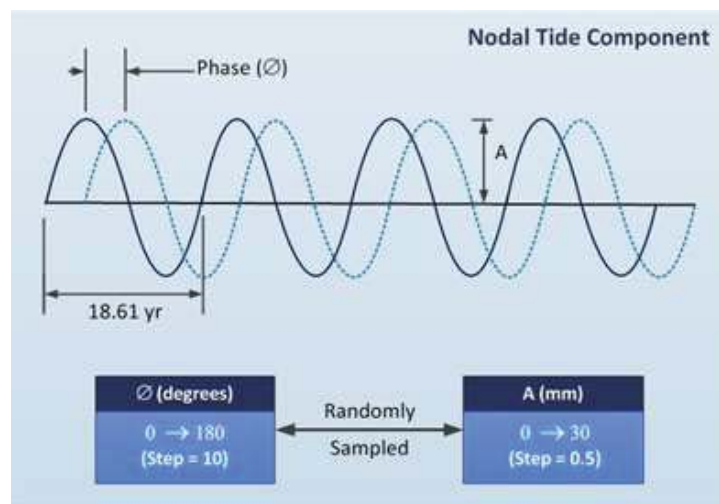
An extensive study by Trupin and Wahr (1990) concluded the aggregate nodal signal to be consistent with equilibrium theory. Woodworth (2012) advises that further unpublished work conducted by the Permanent Service for Mean Sea Level (PSMSL) using a data set twice as large as that analysed by Trupin and Wahr (1990) obtained similar findings. Woodworth (2012) notes that some situations can be envisaged in which significant non-equilibrium nodal signals might occur in sea level records, in particular, shelf areas where shallow water dynamics somehow generate nodal aliases (Loder and Garrett, 1978). Similarly, Cherniawsky *et al.* (2009) notes local effects, such as friction in shallow water, or tidal resonance, also affect the observed nodal ratios, thus making them different from their astronomical values.

Iz (2006) reported on the unpublished findings of analysis of the complete PSMSL data set indicating nodal amplitudes substantially exceeding that described by equilibrium theory (Pugh 1987). From consideration of Figure 5 in Iz (2006), approximately 170 station records have estimated nodal amplitudes exceeding 25 mm with some 80 records exceeding 40 mm. Recent unpublished further research concerning 27 long globally distributed station records indicated an average nodal amplitude of 9.1 ± 0.3 mm with a maximum of 20 ± 4.2 mm (HB Iz 2013, pers. comm., 8 October).

Cherniawsky *et al.* (2009) harmonically analysed 16 years of satellite altimetry data which indicated measured amplitudes at nodal frequencies in the range of 15 – 35 mm, substantially larger than suggested by equilibrium theory. Cherniawsky *et al.* (2009) concluded that the discrepancy with theoretical amplitudes was likely of non-tidal origin, due to broad-band ocean variability with non-stationary phases at nodal frequencies. Baart *et al.* (2012b) analysed all records in the PSMSL exceeding 57 years (or 3 nodal cycles) concluding that measured amplitudes of signals at the nodal frequency exceeded those based purely on equilibrium theory (such as described in Pugh (1987, 1996)). Baart *et al.* (2012b) also observed clear differences between the phase determined from the analyses and equilibrium theory consistent with findings in Cherniawsky *et al.* (2009).

In consideration of the above-mentioned literature, the component of the synthetic data set representative of the lunar nodal tide signal will be randomly sampled from a bin of sinusoidal curves with an 18.61 year period, amplitudes ranging from zero to 30 mm (in 0.5 mm increments) and phase angles ranging from zero to 180° (in 10° increments) as described in Figure 2.4. Based upon this analysis, a total of 1141 time series (including a zero time series) have been generated to represent the range of nodal tide influences expected with ocean water level data sets.

Figure 2.4: Schematic Representation of Nodal Tide Component.



2.4.3 Pole Tide Influence

The pole tide is an interesting phenomena which results from variations in the axis of the Earth's rotation rather than tidal forcing (Woodworth, 2012). In order to conserve angular momentum, a freely rotating body will wobble about its spin axis when the mass distribution deviates from spherical symmetry (Miller, 1973). Although polar motions are driven by a range of processes described in Gross (2000), Desai (2002) observes that the polar motion of the earth is almost predominantly described by two key harmonic variations, namely an elliptical motion at an annual (365 day) period and an almost circular motion at a period of 14 months (433 days), otherwise known as the "Chandler wobble".

The annual elliptical polar motion has near constant amplitude of about 100 milliarcseconds (Gross, 2000) and is forced by the seasonal displacement of air and water masses, beating with each other to give a characteristic pulsating shape to the motion (IERS, 2013). Unlike the annual motion, the circular polar motion at the Chandler period (433 days) is a free oscillation having variable amplitude ranging between about 100 to 200 milliarcseconds (Gross, 2000). Gross (2000) demonstrated that the Chandler wobble was excited by a combination of atmospheric and oceanic processes, with the dominant excitation mechanism being ocean-bottom pressure fluctuations.

Desai (2002) observes that the incremental centrifugal potential associated with these polar motions are referred to as the pole tide potential, with the resulting deformations referred to as the pole tide (Munk and Macdonald, 1960). The displacement of the oceans caused by the pole tide potential is dependent on the inherent dynamics of the oceans (Desai, 2002).

Numerous studies searching for the pole tide in long sea surface records have generally proven inconclusive owing to the relatively small amplitude of the tide (typically 10 mm, Carton and Wahr, 1986) and problems associated with high background noise levels of comparative scale (Xie and Dickman, 1996). Pugh (1987) notes that even with careful analysis the theoretical maximum amplitude of the pole tide, is so small that very broad confidence limits are inevitable. The latitudinal dependence of the pole tide differs from that of the nodal tide, instead maintaining the same dependence as the equilibrium diurnal tides. Spatially, diurnal tides exhibit maximum amplitudes at latitudes of 45°N and S with zero amplitude at the

equator and the poles with variations north and south of the equator in opposite phase (Pugh, 1987).

Desai (2002) analysed almost nine years of data from the TOPEX/Poseidon satellite altimetry mission to observe the geocentric pole tide deformations of the sea surface. The analysis indicated the maximum amplitude of the pole tide at the Chandler period exhibited time varying characteristics ranging from 8 – 18 mm (corresponding to polar motions ranging from 120 – 260 milliarcseconds) over the period from 1993 to 2001. Over the longer term, Malkin and Miller (2010) have estimated the amplitude of polar motion around the Chandler period varied between about 20 and 280 milliarcseconds over the period from 1846 to 2009. Although Desai (2002) notes the altimetric record used only spanned some eight cycles of the Chandler wobble and that results might be contaminated with oceanographic noise, the work demonstrated the pole tide could be reasonably modelled from knowledge of polar motion using an equilibrium assumption for the ocean response.

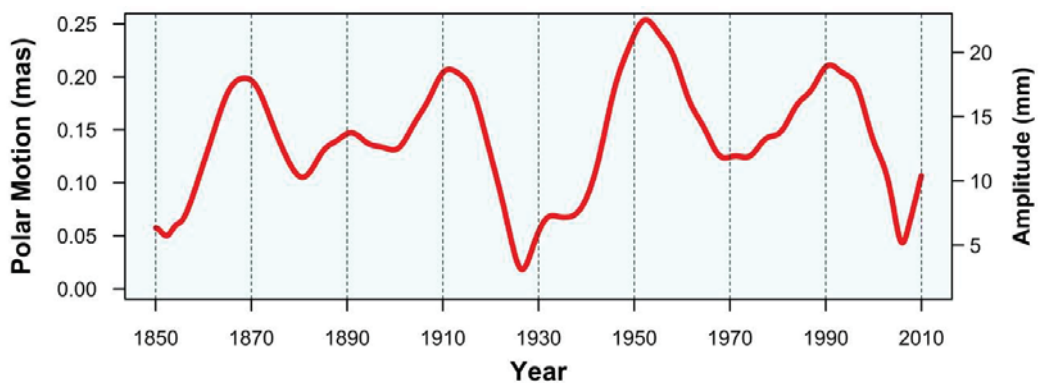
The literature contains considerable discussion on both the existence and rationale for the anomalously high pole tide amplitudes observed in the North and Baltic Seas which are several times larger than the equilibrium pole tide (e.g., Chao *et al.*, 2001; Currie, 1975; Ekman and Stigebrandt, 1990; Haubrich and Munk, 1959; Jessen, 1964; Maksimov and Karklin, 1965; Medvedev *et al.*, 2017; Miller and Wunsch, 1973; O'Connor, 1986; O'Connor *et al.*, 2000; Plag, 1988; Tsimplis *et al.*, 1994; Wunsch, 1974, 1986, 2001; Xie and Dickman, 1995, 1996). Analysing records from Northern Europe spanning the period from 1900 to 1964, Miller and Wunsch (1973) confirmed amplitudes of the pole tide at the Chandler period rose markedly as one progressed from the North Sea into the Baltic and the Gulf of Bothnia, with the exception of the values in the constricted waters of the Kattegat. In this region, pole tide amplitudes of up to 37 mm were evident. Unfortunately, due to the shortness of the record and the level of background noise, the altimetric records analysed by Desai (2002) were not able to observe short-wavelength departures from equilibrium in the North Sea area that might provide some temporal context to previously measured values in this region.

In consideration of the above-mentioned literature, the amplitude of the annual pole tide harmonic (less than ≈ 5 mm) is relatively small compared to that of the seasonal signal (refer Section 2.4.1) at the same frequency, and thus has not been considered further for addition to

the synthetic data set. However, in order to represent the component of the pole tide at the Chandler frequency, sinusoidal curves with a period of 433 days have been developed with time varying amplitudes. The maximum amplitude of 18 mm in early 1993 determined by Desai (2002) from satellite altimetry data, has been fitted to the time varying time series of polar motions determined by Malkin and Miller (2010) spanning the period from 1850 to 2010. To accommodate the range of amplitudes of this signal that can vary from zero to the peak, the maximum time varying time series has been factored from zero to unity in 50 equal increments. These sinusoids have been determined both for phase angles of zero and 180° to represent the diurnal characteristics of the signal.

Using a factor of unity, the maximum amplitude of the time varying signal (refer Figure 2.5) is approximately 22 mm in 1952. Therefore in order to represent the larger amplitude signals experienced in the North Sea region, 5 additional time series have been generated with factors [1.08, 1.26, 1.44, 1.62 and 1.8] corresponding to maximum time varying amplitudes of 24, 28, 32, 36 and 40 mm with zero phase. Figure 2.6 provides a pictorial representation of the pole tide component derived for the synthetic data set. Based upon this analysis, a total of 106 time series (including a zero time series) have been generated to represent the range of pole tide influences expected with ocean water level data sets.

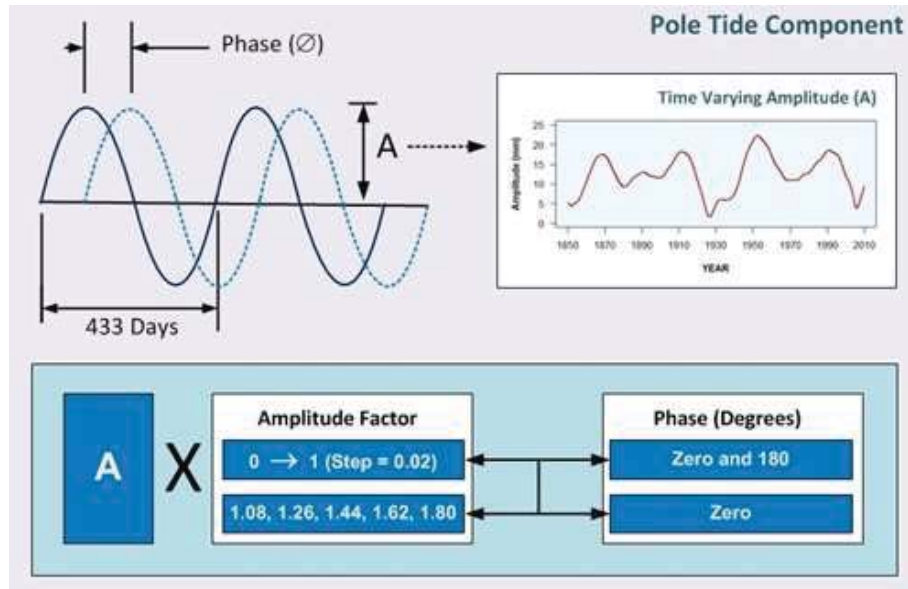
Figure 2.5: Temporal Variability of Polar Tide Influence at Chandler Period.



Notes:

1. Polar motion described relates to the portion corresponding to the Chandler period (433 days). The left-hand axis corresponds to the polar motion described by the SSA analysis in Malkin and Miller (2010). Data kindly supplied by Dr Zinovy Malkin; and
2. The right hand axis is an approximation for the associated maximum amplitude of the pole tide based on the work of Desai (2002) fitted to the time-series of Malkin and Miller (2010).

Figure 2.6: Schematic Representation of Pole Tide Component.



2.4.4 Climate Mode Influences

The global atmospheric circulation has a number of preferred patterns of variability, all of which have expressions in surface climate. Many teleconnections have been identified, but combinations of only a small number of patterns can account for much of the inter-annual variability in the circulation and surface climate (Trenberth *et al.*, 2007). Trenberth *et al.* (2005) analysed global atmospheric mass and found four key rotated Empirical Orthogonal Function (EOF) patterns: the two annular modes (Southern Annular Mode (SAM) and Northern Annular Mode (NAM)), a global El Niño-Southern Oscillation (ENSO) related pattern and a fourth closely related to the North Pacific Index and the Pacific Decadal Oscillation (PDO), which in turn is closely related to ENSO and the Pacific-North American (PNA) pattern (Trenberth *et al.*, 2007).

Numerous studies have identified significant relationships between the various climate mode indices and mean sea level at both a regional and global scale. Although the PDO has been identified as a strong signal with multi-decadal cycles predominantly influencing the North Pacific, considerable debate exists concerning whether this mode can be confidently treated as independent to ENSO (Deser *et al.*, 2010; Schneider and Cornuelle, 2005; Trenberth *et al.*, 2007).

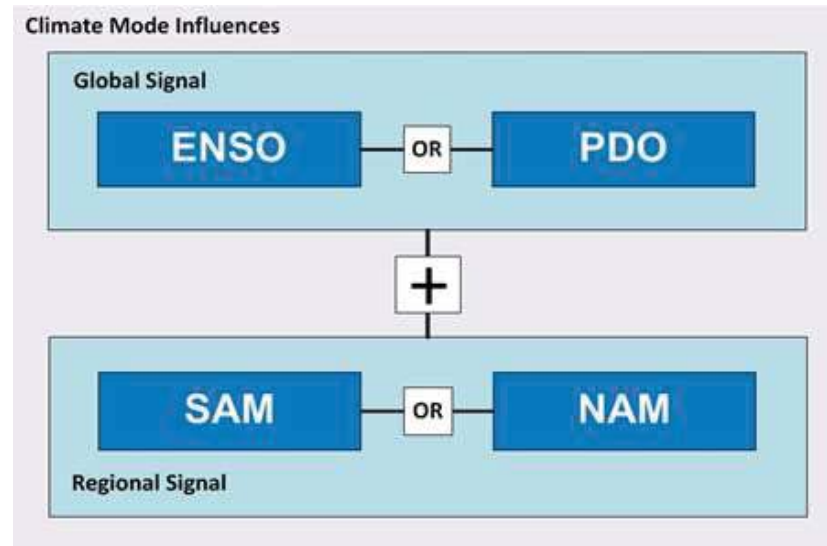
ENSO events are known to occur on cycles generally ranging from 3-7 years (Trenberth *et al.*, 2007) whereas the PDO exhibits key cycles that play an important role in the climate phenomenon over the North Pacific on bidecadal and pentadecadal scales (Minobe, 1999). Whilst numerous regional studies have demonstrated clear correlations to sea level anomalies and the PDO (Merrifield *et al.*, 2012; Meyssignac *et al.*, 2012b; Senjyu, 2006; Zhang and Church, 2012), Hamlington *et al.*, (2013) provide evidence of the relationship between PDO and global averaged mean sea level.

Zhang and Church (2012) note the PDO and ENSO are highly correlated in the low (decadal) frequency band (Newman *et al.*, 2003; Power and Coleman, 2006). Through detailed wavelet analysis, Newman *et al.* (2003) determined the PDO to be dependent upon ENSO on all timescales with the PDO (at least to first order) considered the “reddened” response to both atmospheric noise and ENSO, resulting in more decadal variability than either. Merrifield *et al.* (2012) undertook detailed regression analysis of regional sea levels across the western pacific in which substitution of either the PDO or Southern Oscillation Index (SOI) produced very similar results, providing credence to interpretations of Newman *et al.* (2003).

For the purposes of constructing a synthetic data set to mimic “real-world” climate mode influences, it is proposed to construct each time series by separately sampling a contribution from both a “global” and “regional” signature climate mode influence. ENSO is the dominant, global signal with power in the inter-annual to decadal frequency band, with varying localised influence. Although closely correlated to ENSO with key influence in the north and western pacific region, the PDO has also been shown to have a global influence on mean sea level at bi-decadal and longer frequencies.

In order to encompass the widest possible range of climate mode influences likely to be embedded within ocean water level data sets, the “global” climate mode influence will be a composite of signals reflective of both ENSO and PDO influences. In addition to the “global” signal, there commonly exist climate mode signals with a strong “regional” influence such as SAM, NAM, which are also well described in the literature. A schematic representation of the construction of the climate mode influence within the synthetic data set is described in Figure 2.7.

Figure 2.7: Schematic Representation of Climate Mode Component.



2.4.4.1 El Niño-Southern Oscillation

Analysis of satellite altimetry data spanning the period post 1993 provide clear evidence that ENSO events are the most statistically significant source of inter-annual variations in global mean sea level (Nerem *et al.*, 2010). Nerem *et al.* (1999) observed a direct correlation between the 20 mm rise and fall in the time series of global averaged mean sea level and the significant ENSO event in 1997-1998. Similarly, a drop in global mean sea level of about 7 mm has been attributed to the exceptionally strong La Niña event in 2011 (Fasullo *et al.*, 2013).

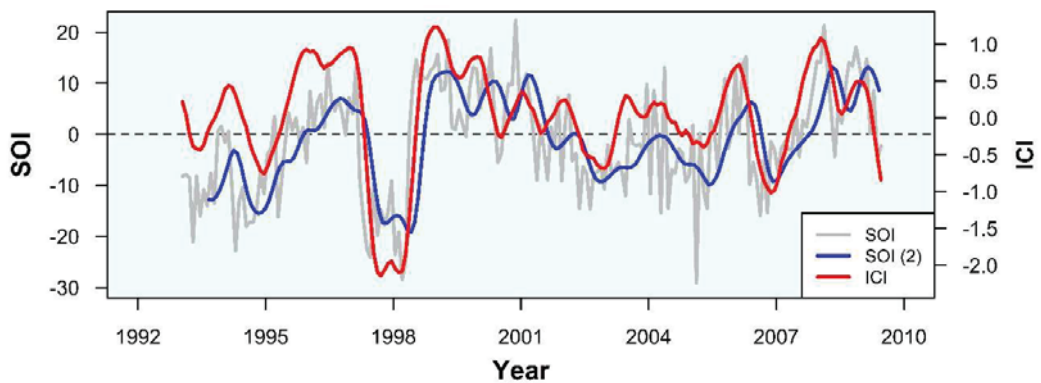
Zhang and Church (2012) analysed satellite altimeter data spanning the period from 1993 to 2009 in order to isolate inter-annual and decadal climate variability associated with ENSO. This analysis found that only 20% of the observed variance was described by simple single variable linear regression analysis. However, multiple variable linear regression including filtered indices of the El Niño-Southern Oscillation and the Pacific Decadal Oscillation accounted for almost 60% of the observed variance. Zhang and Church (2012) determined an Inter-annual Climate Index (ICI) and Decadal Climate Index (DCI) based on high-pass filtering of the Multivariate ENSO Index (MEI) and low-pass filtering of the Pacific Decadal Oscillation (PDO), respectively.

Zhang and Church (2012) identified the inter-annual sea level fingerprint to have a higher signal in the eastern and western extremities of the tropical Pacific, with maximum amplitudes of +70 mm per unit Inter-annual Climate Index (ICI) change in the east and -70 mm in the west. The peak ICI determined during the analysis period was 2.14 (associated with the 1997/98 El Niño event) equating to an amplitude of approximately ± 150 mm.

The ICI (Zhang and Church, 2012) and a smoothed monthly SOI (BoM, 2013) provide a strong temporal correlation (refer Figure 2.8). Fitting the maximum amplitude (150mm) to the peak of the smoothed SOI during the 1997/98 El Niño enables a time series of peak amplitude representative of the ENSO signal to be extended back to 1876 (refer Figure 2.9). A portion of this smoothed time series has been recycled to extend an “ENSO-like” signal over the full width of the synthetic data set (1850-2010).

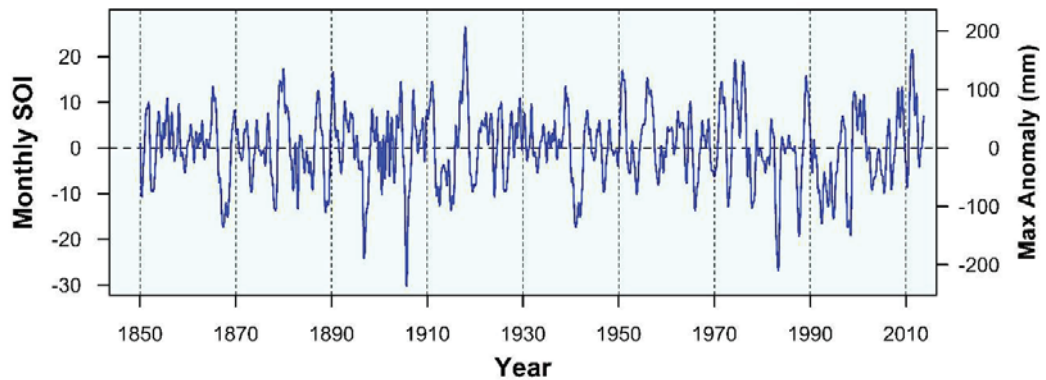
To construct the ENSO induced signal in the synthetic data set, the maximum amplitude time series signal (refer Figure 2.9) has been factored between ± 1 at 0.02 increments, creating 101 time series data sets (including a zero time series).

Figure 2.8: Comparison of SOI and ICI.



Notes:

1. Monthly SOI values from BoM (2013). SOI(2) has been smoothed using a modified Daniell kernel with variable weighting 4 months either side; and
2. Inter-annual Climate Index (ICI) based on Zhang and Church (2012).

Figure 2.9: Maximum Monthly Sea-Surface Anomaly Attributable to ENSO.**Notes:**

1. Monthly SOI (1876-2013) from BoM (2013) smoothed using a convoluted modified Daniell kernel with variable weighting 4 months either side;
2. Smoothed SOI extended back to 1850 by replicating a section of the record (1923-1950) to match the 1876 start point; and
3. Maximum anomaly equates to the maximum inter-annual water surface influence of ENSO based on Zhang and Church (2012).

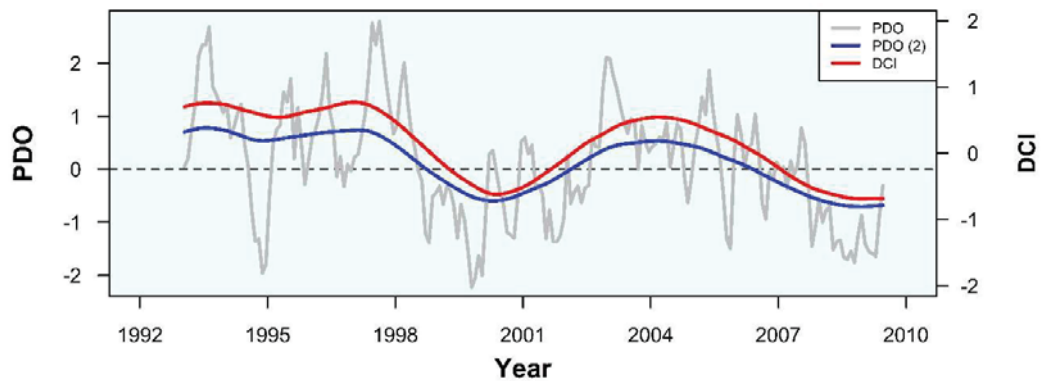
2.4.4.2 Pacific Decadal Oscillation (PDO)

By integrating satellite altimetry (post 1993) with long record length tide gauge records, Hamlington *et al.* (2013) examined long (decadal and longer) time scale climate signals to quantify their contribution to sea level trends at a regional and global scale. This study quantified the significance of the PDO on decadal sea level trends at both the regional and global scale, in particular defining the extent to which the PDO has induced acceleration and deceleration in global averaged mean sea level over the period from 1950-2010.

The Decadal Climate Index (DCI) determined by Zhang and Church (2012) low-pass filtering of the Pacific Decadal Oscillation (PDO), determined a maximum positive sea level variation in the central and eastern tropical pacific of 80 mm per unit DCI analysing global satellite altimetry data spanning the period 1993-2009. Similarly, this analysis determined maximum negative sea level responses in a narrow western tropical region of the order of -150 mm per unit DCI.

The peak positive DCI determined during the analysis period (February 1997) of 0.77 equates to a maximum amplitude of approximately +62 mm. The DCI (Zhang and Church, 2012) and a smoothed monthly PDO (JISAO, 2014) provide a strong temporal correlation (refer Figure 2.10). By fitting the maximum amplitude (62mm) to the corresponding peak of the smoothed

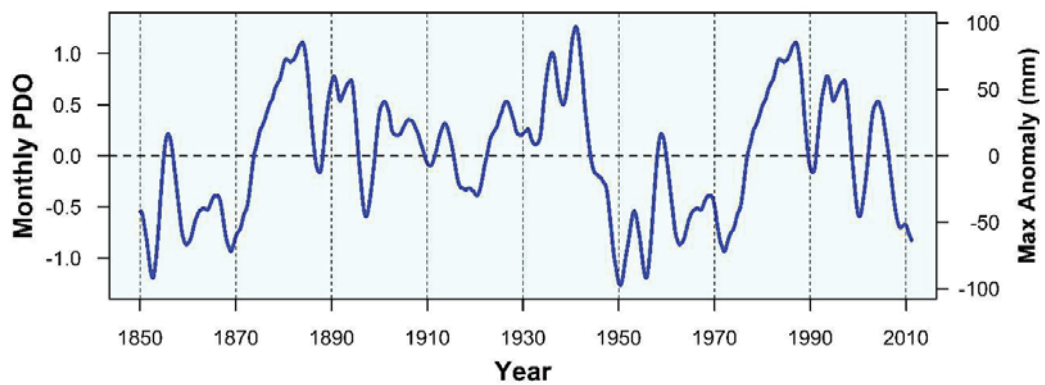
Figure 2.10: Comparison of PDO and DCI.



Notes:

1. Monthly PDO values from JISAO (2014). PDO(2) has been smoothed using a modified Daniell kernel with variable weighting 16 months either side; and
2. Decadal Climate Index (DCI) based on Zhang and Church (2012).

Figure 2.11: Maximum Monthly Sea-Surface Anomaly Attributable to PDO.



Notes:

1. Monthly PDO (1900-2013) from JISAO (2014) smoothed using a convoluted modified Daniell kernel with variable weighting 16 months either side;
2. Smoothed PDO extended back to 1850 by replicating the latter section of the record to match the 1900 start point; and
3. Maximum anomaly equates to the maximum positive water surface influence of PDO based on Zhang and Church (2012).

PDO enables a time series of peak positive sea surface anomaly representative of the PDO signal to be extended back to 1900 (refer Figure 2.11). A portion of this smoothed time series has been recycled to extend a “PDO-like” signal over the full width of the synthetic data set (1850-2010). To construct the PDO induced signal in the synthetic data set reflective of the range between peak positive and negative sea surface anomalies determined by Zhang and Church (2012), the maximum positive amplitude time series signal (refer Figure 2.11) has been factored between + 1 and – 1.9 at 0.05 increments, creating 59 time series data sets (including a zero time series).

2.4.4.3 Northern Annular Mode (NAM) and North Atlantic Oscillation (NAO)

Woolf *et al.* (2003) notes the atmosphere in the northern-hemisphere winter features five large-scale perturbations in lower-level pressure fields or “Centers of Action” (Rossby, 1939). The Icelandic Low and the Azores High are the most significant Centres for the Atlantic/Europe region. These features dictate the mean zonal flow in the region and strongly affect surface fluxes. Whilst not fixed in intensity or position, these features exhibit significant inter-annual and inter-decadal variability. One important feature is a significant tendency of pressure in the Icelandic Low and Azores High to vary in anti-phase, a see-saw known as the North Atlantic Oscillation (NAO). The NAO is closely related to the NAM, which has similar structure over the Atlantic but is more zonally symmetric (Trenberth *et al.*, 2007).

The NAO is considered to be a singular major atmospheric, basin scale pattern, which affects sea-level around Europe and further afield (Tsimplis and Josey, 2001; Tsimplis *et al.*, 2006; Wakelin *et al.*, 2003; Woolf *et al.*, 2003; Yan *et al.*, 2004). The NAO index, defined as the difference of normalised mean sea level pressure anomalies between Lisbon, Portugal and Stykkisholmur, Iceland has become the most widely used NAO index and extends back in time to 1864 (Hurrell, 1995), and further back in time to 1821 if Reykjavik is used instead of Stykkisholmur and Gibraltar instead of Lisbon (Jones *et al.*, 1997).

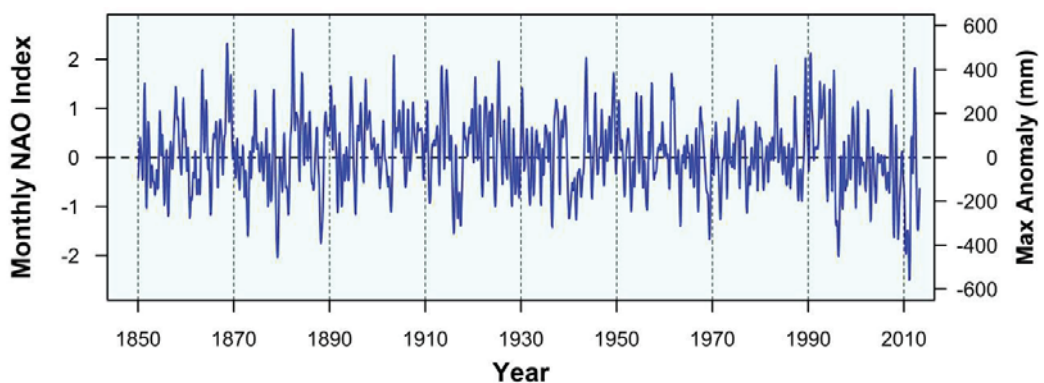
Woolf *et al.* (2003) analysed Topex/Poseidon (T/P) satellite data for the period 1993–2001, determining that a linear relationship between the winter sea-level anomalies and the NAO Index (December – March) can be used to explain the majority of the variability in the North Sea, the Mediterranean and the eastern parts of the North Atlantic (Tsimplis *et al.*, 2006). Woolf *et al.* (2003) confirmed that the correlation between the NAO and sea level is not

uniform but positive only for the northern part of Europe and negative for the south. The zone with negative correlation extended from the subtropics up to southwest England.

Yan *et al.* (2004) notes that the linear relationship between sea-level anomalies and the winter averaged NAO index in northwest Europe ranged from about -100 to $+200$ mm per NAO unit (Wakelin *et al.*, 2003; Woolf *et al.*, 2003). The peak winter (December – March) averaged NAO index (2.44) during the period of analysis of Woolf *et al.* (2003) equates to a maximum sea-level anomaly attributable to the NAO of approximately $+450$ mm. By fitting the maximum anomaly (450 mm) to the peak of the smoothed NAO index (CRU, 2013; Jones *et al.*, 1997) between 1993 and 2001 enables a time series of peak sea surface anomaly attributable to the NAO signal to be estimated from 1850 to present (refer Figure 2.12).

Woolf *et al.* (2003) also noted the significant negative correlation to the NAO index around areas of the North Atlantic (subtropics to southwest England) producing a maximum sea surface anomaly half that of the positively correlated maximum influence. Therefore, in order to construct a component that mimics the NAO induced signal in the synthetic data set, the maximum amplitude time series signal (refer Figure 2.12) has been factored between -0.5 and $+1$ at 0.02 increments, creating 76 time series data sets (including a zero time series).

Figure 2.12: Maximum Monthly Sea-Surface Anomaly Attributable to NAO.



Notes:

1. Monthly NAO index (CRU, 2013; Jones *et al.*, 1997) smoothed using a convoluted modified Daniell kernel with variable weighting 4 months either side;
2. Maximum anomaly equates to the maximum average winter water surface influence of NAO between September 1992 and August 2001 (Woolf *et al.*, 2003) fitted to the smoothed monthly NAO index time series.

2.4.4.4 Southern Annular Mode (SAM) and Antarctic Oscillation (AAO)

The principal mode of variability of the atmospheric circulation in the southern-hemisphere extra-tropics is now known as the Southern Annular Mode (Trenberth *et al.*, 2007). Various known as the Antarctic Oscillation (AAO) or the Southern Annular Mode (SAM) (Thompson and Wallace, 2000), this climate mode consists of an oscillation of sea level atmospheric pressure between polar and subtropical latitudes, associated with oscillations in circumpolar winds in the troposphere and stratosphere, including at the sea surface (Hughes *et al.*, 2003).

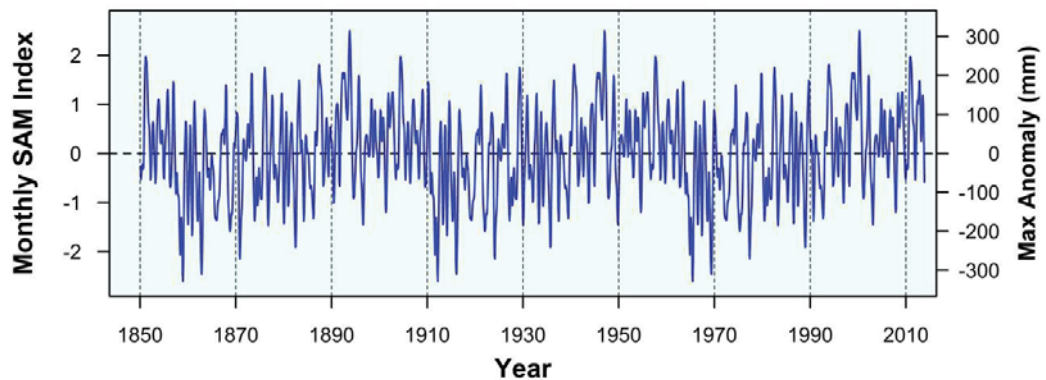
Trenberth *et al.* (2007) noted the imprint of SAM variability on the Southern Ocean system is observed as a coherent sea level response around Antarctica (Aoki, 2002; Hughes *et al.*, 2003) and by its regulation of Antarctic Circumpolar Current flow through the Drake Passage (Meredith *et al.*, 2004). Trenberth *et al.* (2007) describe the SAM Index as a measure of either the difference in average MSLP between southern-hemisphere middle and high latitudes (usually 45°S and 65°S), from gridded or station data (Gong and Wang, 1999; Marshall, 2003), or the amplitude of the leading empirical orthogonal function of monthly mean southern-hemisphere 850 hPa height poleward of 20°S (Thompson and Wallace, 2000). This index was formerly known as the Antarctic Oscillation (AAO) Index or High Latitude Mode (HLM) Index.

Aoki (2002) analysed available hourly tide gauge data from five stations around Antarctica (Vernadsky, Syowa, Mawson, Davis and Casey) for the period January 1993 to December 1999, determining a high negative correlation in the linear relationship between the sea level variations and the daily AAO Index. Linear regressions of the high-passed AAO signal explained 17–25% of the sea level variance with variations of approximately -25 mm corresponding to each unit of AAO Index (Aoki, 2002). Analysis of the Vernadsky (Faraday) record indicates a regression coefficient of -9.2 mm per unit of AAO Index (up to 4 years) but, with considerable frequency dependence in the relationship (Hughes CW 2013, pers. comm., 19 December).

For the period of analysis of Aoki (2002), the daily AAO Index (NWS, 2013) ranged from +4.009 to -4.855 equating to a maximum sea level anomaly attributable to the AAO of approximately -101 mm to +122 mm. By fitting these maximum amplitudes to the respective positive and negative peaks of the smoothed monthly SAM Index (BAS, 2013) over the corresponding timeframe, enables a time series of peak amplitude representative of the SAM signal to be extended back to 1957 (refer Figure 2.13). The major portion of this smoothed time series has

been recycled to pad the record over the full width of the synthetic data set (1850-2010). To construct the SAM induced signal in the synthetic data set, the maximum amplitude time series signal (refer Figure 2.13) has been factored from zero to 1 at 0.02 increments, creating 51 time series data sets (including a zero time series).

Figure 2.13: Maximum Monthly Sea-Surface Anomaly Attributable to SAM.



Notes:

1. Monthly SAM Index (1957-2013) from NWS (2013) smoothed using a convoluted modified Daniell kernel with variable weighting 4 months either side;
2. Smoothed SAM Index extended back to 1850 by replicating the actual record (1957-2013); and
3. Maximum anomaly attributable to SAM based on fitting the results of Aoki (2002) to monthly SAM Index (NWS, 2013).

2.4.5 Noise

Ocean water levels measured at tide gauges are a composite of numerous complex oceanographic and meteorological phenomena with global, ocean basin and local scale process origins.

Environmental time series data records are inherently embedded with considerable noise. This is particularly the case with monthly ocean water level records. Following the removal of the underlying trend, dominant cyclical dynamic influences (refer Sections 2.4.1 to 2.4.4) and serial correlation between successive measurements, the residual is characterised generally as stationary, normally distributed, random white noise (Grieser *et al.*, 2002).

The 43 PSMSL gauge sites selected for this analysis (refer Appendix A) provide good global coverage with considerable local variability from which to extract estimates of the likely range of noise attributes within conventional monthly averaged ocean water level data sets. The following process has been applied to each of these monthly average water level time series to estimate the white noise component embedded within the records:

- ❑ isolate and remove seasonal influences from monthly average water level data sets using “stl decomposition” function in the R analytical software package (Cleveland *et al.*, 1990; R Core Team, 2013)(refer Method 1, Section 2.4.1);
- ❑ fit generalised least squares (GLS) linear regression model to “de-seasonalised” monthly time series data to extract residuals using “nlme” package in R (Pinheiro *et al.*, 2013); and
- ❑ fit an autoregressive (AR) model to the residuals from the fitted GLS regression model to remove the serial correlation using R (R Core Team, 2013). Analysis of the correlogram of the Partial Autocorrelation Function (PACF) has then been used to determine the optimum lagged AR model to remove serial correlation from the residuals (to represent white noise).

Only 5 sites (Arrecife, Canary Islands; Churchill, Canada; Jolo, Philippines; Mossel Bay, South Africa; Visakhapatnam, India) proved unsuitable for extraction of noise via the process adopted, largely due to either significance of gaps in the available data record or significance of the deviation from linear of the assumed underlying trend.

Visual inspection of the histogram of uncorrelated residuals from each station record (refer Appendix B) indicates close resemblance to optimum Gaussian normal distribution, in turn exhibiting properties of white noise. From the above-mentioned analysis, the standard deviation of the residuals ranged from a low of 23 mm (Magueyes Island, Puerto Rico) to a high of 290 mm (Trois-Rivieres, Canada), the latter affected by significant variations in glaciological discharges. The next highest standard deviations recorded were 144 mm (Helsinki, Finland) and 143 mm (Cuxhaven, Germany).

In order to generate a white noise component reflective of real-world attributes, a Gaussian (normal) distributed set of residuals of length 1920 months will be randomly sampled for each

time series in the synthetic data set. The scale of each set of normally distributed white noise residuals will be determined by randomly sampling from a bin of standard deviations ranging from 20 to 300 mm (between 20 and 150 in single increments plus 200, 250 and 300; 134 standard deviations in total) to reflect the results from analysis of the gauge records sampled.

2.5 Other Considerations

In addition to the range of cyclical influences, noise and mean sea level components mentioned in this chapter, ocean water level data sets measured at land based tide gauges are also comprised of datum shifts and other vertical land motion processes. In particular, small (< 10 mm) vertical step jumps (positive and negative) are likely in lengthy tide gauge records due to absolute levelling errors at specific junctures in the record associated with the installation of improved measuring technologies and/or relocation of the recording instrument.

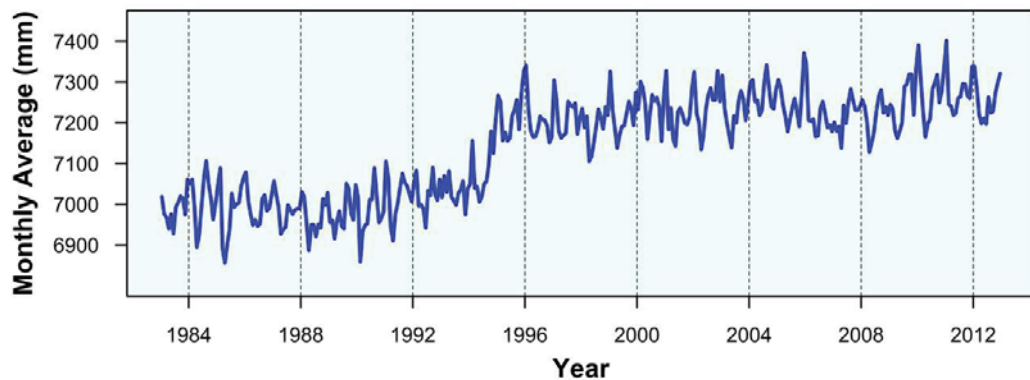
Hannah and Bell (2012) note a 20 mm datum shift in the long Wellington, New Zealand record, associated with the installation of a new tide gauge facility in 1944. Similarly, Breaker and Ruzmaikin (2013) identified an increase in the average mean sea level record at San Francisco between 1877 and 1897, which in part was attributable to moving the tide gauge from Fort Point to Sausalito in San Francisco Bay. Examination of tidal records within San Francisco Bay indicate a positive gradient in the mean tidal elevation between these two locations resulting from complex geographic and bathymetric influences (Conomos, 1979) estimated at approximately 20 mm (Breaker and Ruzmaikin, 2013).

Douglas (2008) noted the possibility of a previously unrecognised vertical offset between the long Brest (France) and Newlyn (UK) gauge records of approximately 23 mm for the common period between records prior to 1945. Wöppelmann *et al.* (2006) notes the Brest tide gauge was destroyed during bombing at the end of World War II and though the gauge recording facility was reconstructed during the 1950s, the quality of the observations deteriorated.

The above-mentioned examples are postulated to be relatively commonplace artefacts within lengthy time series tide gauge records. Similarly, vertical datum shifts are routine for tide gauge records in regions experiencing tectonic or geological instability. Such datum shifts can be quite significant as evidenced in the tide gauge record at Hanasaki on the north shore of Hokkaido Island, Japan. This gauge was the closest Japanese station to the great Kurile Islands

earthquake on 4 October 1994 (Katsumata *et al.*, 1995). Inspection of the monthly average ocean water level records at the Hanasaki II gauge (PSMSL, 2014) indicate a distinct vertical offset of approximately 200 mm in the record either side of the earthquake event indicative of significant subsidence of the land mass in the vicinity of the tide gauge (refer Figure 2.14).

Figure 2.14: Datum Shift in Tide Gauge Record at Hanasaki, Japan.



Notes:

1. Monthly average ocean water level for Hanasaki II station, Hokkaido Island, Japan obtained from PSMSL (2014); and
2. Sharp discontinuity in record of the order of 200 mm evident around the timing of the earthquake and associated tsunami which occurred in the Kuril Islands on 4 October 1994.

The above-mentioned circumstances give rise to positive and negative vertical offsets (or step functions) in tide gauge records of varying magnitude. Although recognised, it is not proposed to include a separate component within the synthetic data set to accommodate such influences. Unlike the other components comprising the synthetic data set, there is very little published information within the scientific literature sufficient to rigorously estimate the scale, timing and global scope of such datum shift influences.

The data repositories of the PSMSL are quality controlled and where possible, reduced to a common datum, known as the Revised Local Reference (RLR) ensuring they are suitable for use in research quality time series analysis. Metadata for each station provides information on **known** datum shifts with associated quality assurance warning flags.

2.6 Summary

The core synthetic data set comprises 20,000 generated monthly average water level time series spanning the period from January 1850 to December 2009 (160 years). Each time series comprises separately randomly sampled components of seasonal influence, nodal tide, pole tide, global and regional climate mode influences and white noise added to a fixed mean sea level as summarised in Table 2.1.

In addition to examining the utility of various analytical methodologies to isolate the mean sea level signal, the core data set will also be used to investigate any issues associated with record length and end effects as well as monthly versus annual data. Core synthetic monthly and annual average water level data sets for analysis are summarised in Table 2.2.

Appendix C provides a visual comparison of selected long monthly average ocean water level data sets with randomly generated time series from the synthetic data set.

Table 2.1: Summary of Core Synthetic Data Set.

Component	Sampling		Details
	Type	Sampling Bins	
Mean Sea Level	Fixed	1	Section 2.3
Seasonal Influence	Random	82	Section 2.4.1
Nodal Tide	Random	1141	Section 2.4.2
Pole Tide	Random	106	Section 2.4.3
Global Climate Mode:			
ENSO	Random ^(Note 1)	101	Section 2.4.4.1
PDO	Random ^(Note 1)	59	Section 2.4.4.2
Regional Climate Modes:			
NAM/NAO	Random ^(Note 2)	76	Section 2.4.4.3
SAM/AAO	Random ^(Note 2)	51	Section 2.4.4.4
White Noise	Random	^(Note 3)	Section 2.4.5

Notes:

1. Only one global climate mode component will be randomly sampled per time series;
2. Only one regional climate mode component will be randomly sampled per time series; and
3. White noise residuals are generated by randomly sampling within the defined standard deviation range to create a normal distribution (refer Section 2.4.5). The generated normal distribution is then randomly sampled to derive the white noise component for each respective time series.

Table 2.2: Generated Monthly and Annual Average Data Sets for Analysis.

Ref No. (M=Monthly, A=Annual)	Time Span	
	Months	Years
M1, A1	Jan 1850 - Dec 2009	160
M2A, A2A	Jan 1850 - Dec 1929	80
M2B, A2B	Jan 1930 - Dec 2009	80
M3A, A3A	Jan 1850 - Dec 1889	40
M3B, A3B	Jan 1890 - Dec 1929	40
M3C, A3C	Jan 1930 - Dec 1969	40
M3D, A3D	Jan 1970 - Dec 2009	40

Notes:

1. All time-series have been generated from the core monthly synthetic data set (M1). M2* and M3* datasets have been subsetted from data set M1 using R (R Core Team, 2013); and
2. A* datasets generated through aggregating associated M* dataset using R (R Core Team, 2013).

2.7 Acknowledgements

The development of the core synthetic data set is one of the key underpinning elements of this PhD research program. This research has benefitted significantly from direct consultations with some of the world’s leading oceanographers, sea level researchers and subject matter experts relevant to various components of the proposed synthetic data set. By consequence, I am indebted to the following individuals whose contributions have helped considerably to shape the final product and have ranged from providing specific and general expert advice, guidance and review, through to provision of original research data outputs for use:

- ❑ Dr Shailen Desai, California Institute of Technology, Jet Propulsion Laboratory, NASA, Pasadena, USA;
- ❑ Dr Bruce Douglas (retired), Department of Geography, University of Maryland, College Park and Laboratory for Coastal Research, Florida International University, Miami, USA;
- ❑ Dr Ivan Haigh, National Oceanography Centre, University of Southampton, UK;
- ❑ Dr Angela Hibbert, National Oceanography Centre, Natural Environment Research Council, UK;
- ❑ Professor Chris Hughes, National Oceanography Centre, Natural Environment Research Council, UK;

- ❑ Professor Rob Hyndman, Department of Econometrics and Business Statistics, Monash University, Australia. Editor-in-Chief, *International Journal of Forecasting*. Editor, *Journal of Statistical Software*;
- ❑ Professor Huseyin Baki Iz, Department of Land Surveying and Geo-Informatics, Hong Kong Polytechnic University, Kowloon, Hong Kong;
- ❑ Dr Zinovy Malkin, Laboratory of Radioastrometry and Geodynamics, Pulkovo Observatory, St Petersburg, Russia;
- ❑ Professor Philip Woodworth, National Oceanography Centre, Natural Environment Research Council, UK. Former Director of the Permanent Service for Mean Sea Level (PSMSL) and Chairman of the Global Sea Level Observing System (GLOSS) of the Intergovernmental Oceanographic Commission; and
- ❑ Dr Xuebin Zhang, Centre for Marine and Atmospheric Research, CSIRO, Hobart, Australia.

Chapter 3

Testing to identify the optimum performing analytic for isolating mean sea level with improved temporal accuracy

Synopsis: A broad range of analytical techniques were tested against the synthetic data set (Chapter 2) for their utility to isolate the trend with improved temporal accuracy from conventional, long, individual ocean water level data sets. Time series techniques considered included linear and polynomial regression, LOESS smoothing, smoothing splines, moving averages, structural models, digital filters, singular spectrum analysis (SSA), empirical mode decomposition, wavelets and the respective derivatives of these techniques. Sensitivity testing around key parametrization was undertaken to optimize performance of each of the analytics specifically for application with conventional ocean water level data. In total, some 1462 separate analyses were applied to the synthetic data set, resulting in over 29 million individual time series analyses. This work is likely the largest undertaking of its type for time series analysis. Key findings were that enhanced accuracy in resolving the temporal resolution of the trend were achieved through the use of longer, annual average data, coupled with the use of so called “data adaptive” analytics, in particular, SSA and multi-resolution wavelet decomposition. SSA is more instructive and convenient for the process at hand given the technique’s enhanced capability to separate key harmonic components of the time series.

Publication II

Watson, P.J., 2016a. Identifying the best performing time series analytics for sea-level research. In: Rojas, I., and Pomares, H. (eds.), *Time Series Analysis and Forecasting: Contributions to Statistics*. Springer International Publishing, 261-278, doi: 10.1007/978-3-319-28725-6.

Declaration

I certify that this publication was a direct result of my research towards this PhD, and that reproduction in this thesis does not breach copyright regulations.

Phil J. Watson [Candidate]

3.1 Background

Monthly and annual average ocean water level records used by sea level researchers are a complex composite of numerous dynamic influences of largely oceanographic, atmospheric or gravitational origins operating on differing temporal and spatial scales, superimposed on a comparatively low amplitude signal of sea level rise driven by climate change influences (see Chapter 2 for more detail).

The mean sea level (or trend) signal results directly from a change in volume of the ocean attributable principally to melting of snow and ice reserves bounded above sea level (directly adding water), and thermal expansion of the ocean water mass. This low amplitude, non-linear, non-stationary signal is quite distinct from all other known dynamic processes that influence the ocean water surface which are considered to be stationary; that is, they cause the water surface to respond on differing scales and frequencies, but do not change the volume of the water mass.

In reality, improved real-time knowledge of velocity and acceleration rests entirely with improving the temporal resolution of the mean sea level signal by isolating and removing the “contaminating” dynamic signals from the time series record. In theory, this sounds straightforward, but the tools available to undertake such a task, in part rely on our ability to accurately understand and quantify the relative contributions of all influences embedded within ocean water level data. Much of the contemporary science around elements of the sea level “equation” continues to evolve at global and ocean basin scales and remains highly contested in the literature. Some key recent examples include:

- ❑ influence of and potential slowing of the Atlantic Meridional Overturning Circulation (Buckley and Marshall, 2016);
- ❑ contribution of the 1991 Mt Pinatubo volcanic eruption to masking GMSL acceleration (Fasullo *et al.*, 2016);
- ❑ possible reversal in the long held theory pertaining to the surface mass balance of the Antarctica ice sheet (Zwally *et al.*, 2015);
- ❑ potential bias in the drift of the first 6 years of satellite altimetry missions (Watson *et al.*, 2015); and

- temporal characteristics of longer scale oceanographic and meteorological artefacts that might have cycles exceeding many decades to a century (Chambers *et al.*, 2012; Minobe, 1999)

The simple examples listed above serve merely to highlight the complex nature of sea level rise and the many processes which can affect the water level recorded at a particular place and point in time and the evolving nature of the science pertaining to same. With so much critical reliance on accurate estimates of these physical parameters to understand climate change and improve future projections, there is a heightened urgency in identifying the better performing analytics for defining the temporal characteristics of mean sea level (including associated velocity and acceleration) from available long monthly and annual average water level data sets.

To date, the wide range of techniques employed to detect mean sea level (and associated velocities and accelerations) have proven difficult to compare directly, particularly when some of the more widely used techniques (such as linear and quadratic approaches) provide erroneous or misleading estimates due to the insensitivity of the technique or inherent method bias or “trends” increasingly corrupted by inter-decadal influences (in particular) as the time base of the available data record shortens. As a result, the key debate around detecting critical changes in the long-term rate of sea level rise has been unwittingly side-tracked by the application of inadequate analytical techniques and debate over the limitations and intuitive application of more sophisticated spectral analytics applied to ocean water level records.

Over recent decades, the emergence and rapid improvement of data adaptive approaches to isolate trends from nonlinear, non-stationary and comparatively noisy environmental data sets such as Empirical Mode Decomposition (EMD) (Huang *et al.*, 1998, Wu and Huang, 2009), Singular Spectrum Analysis (SSA) (Broomhead and King, 1986; Golyandina *et al.*, 2001; Vautard and Ghil, 1989) and Wavelet analysis (Daubechies, 1992; Grossmann and Morlet, 1984; Grossmann *et al.*, 1989) are theoretically encouraging for the task at hand. The continued development of data adaptive and other spectral techniques (Tary *et al.*, 2014) have given rise to recent variants such as Complete Ensemble EMD (Han and van der Baan, 2013; Torres *et al.*,

2011) and Synchrosqueezed Wavelet Transform (SWT) (Daubechies *et al.*, 2011; Thakur *et al.*, 2013).

The utility of the application of various techniques to isolate the mean sea level signal from conventional long, ocean water level time series has largely been left to the assumed sophistication of the analytic, based on the attendant literature. This chapter provides a summary of the detailed time series analysis testing regime employed to identify the most efficient method(s) for estimating/isolating the mean sea level (trend) from conventional monthly and annual average time series data used extensively in sea level research (such as the global data repositories of the PSMSL).

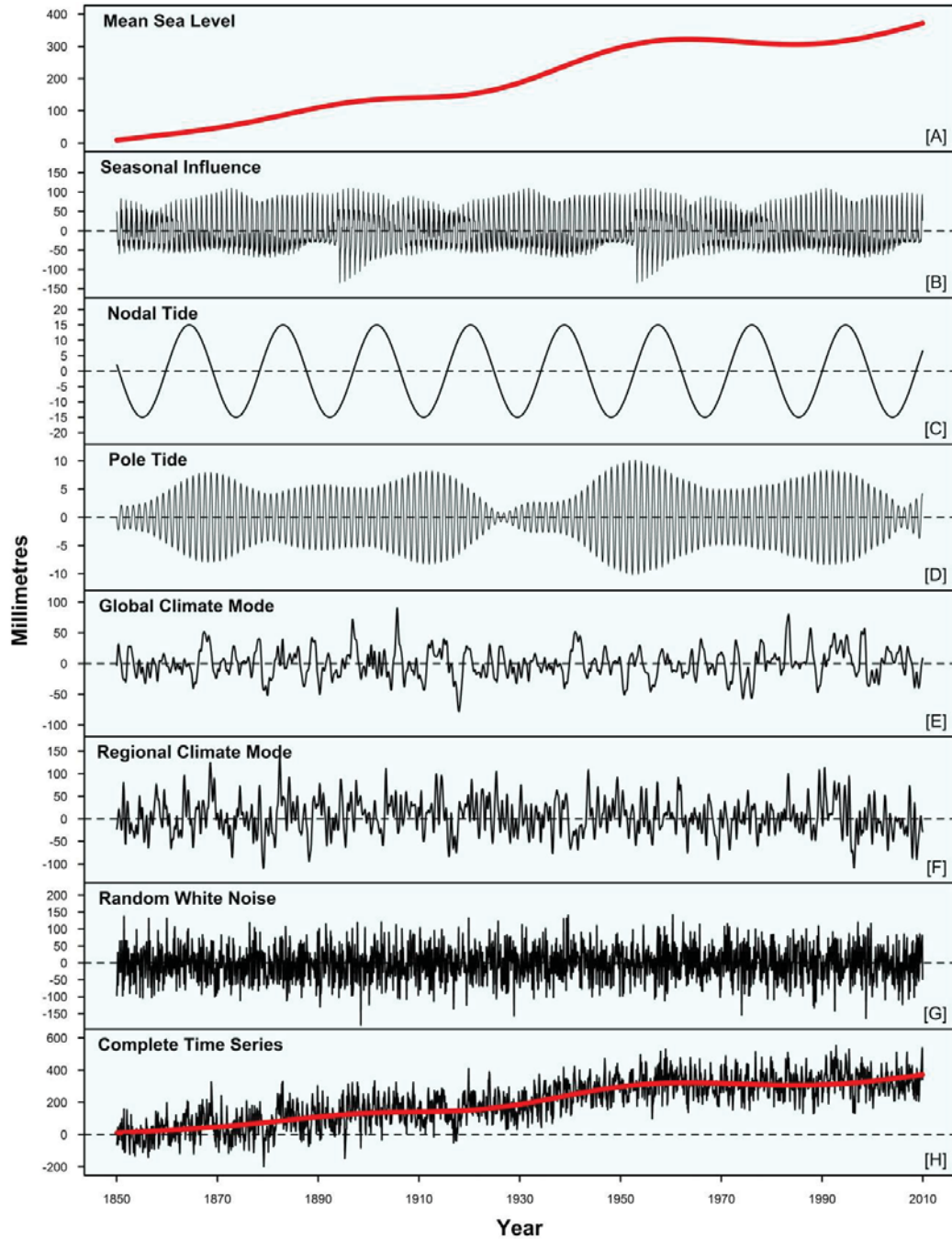
The synthetic data set developed as part of this research program (Chapter 2) provides the ideal platform against which to test a wide range of analytical approaches for their utility to isolate the fixed mean sea level signal embedded within each of the 20,000 time series of the data set. Refer Figure 3.1 for example synthetic time series.

3.2 Testing Methodology

The method to determine the most robust time series method for isolating mean sea level with improved temporal accuracy is relatively straightforward and has been based on 3 key steps, namely:

- Step 1:** development of synthetic data sets to test (refer Chapter 2);
- Step 2:** application of a broad range of analytical methods to isolate the mean sea level trend from the synthetic data set; and
- Step 3:** comparative assessment of the performance of each analytical method using a multi-criteria analysis (MCA) based on some key metrics and a range of additional qualitative criteria relevant to its applicability for broad, general use on conventional ocean water level data worldwide.

Figure 3.1: Indicative monthly average ocean water level time series from synthetic data set.



Notes:

The scale of signals highlighted in Panels [B] to [G] are indicative only and vary in amplitude based on global position and local influencing factors. Panel [H] is the composite time series of all contributory signals denoted with the mean sea level signal highlighted in red. For specific detail on the nature of signals embedded within the synthetic ocean water level data set, refer Chapter 2.

3.2.1 Application of analysis methods to extract trend from synthetic data sets

The time series analysis methods that have been applied to the synthetic data set to estimate the trend are summarised in Table 3.1. This research has not been designed to consider every time series analysis tool available. Rather, the testing regime is aimed at appraising the wide range of tools currently used for mean sea level trend detection of individual records, with a view to improving generalised tools that can be customized (or optimized) for sea level researchers.

Some additional, more recently developed data adaptive methods such as CEEMD (Torres *et al.*, 2011) and SWT (Daubechies *et al.*, 2011; Thakur *et al.*, 2013) have also been included in the analysis to consider their utility for sea level research. It is acknowledged that various methods permit a wide range of parameterisation that can critically affect trend estimation. In these circumstances, broad sensitivity testing has been undertaken to identify the better performing combination and range of parameters for a particular method when applied specifically to ocean water level records (as represented by the synthetic data sets).

In some cases the sensitivity testing of a particular method might involve several sub-methods in combination with a range of additional conditions, which are also detailed in Table 3.1. Every combination of sub-method and additional condition has been tested on the complete synthetic data set (refer Chapter 2, Table 2.2).

With methods such as SSA and SWT, it has been necessary to develop auto detection routines to isolate specific elements of decomposed time series with characteristics that resemble low frequency trends. Direct consultation with leading time series analysts and developers of method specific analysis tools has assisted to optimise sensitivity testing (refer Section 3.6).

The R open source language for statistical computing and graphics (R Core Team, 2014) has been used as the framework for undertaking the extensive computing tasks required to undertake the time series analysis. Where possible, relevant extension packages in R have been used to facilitate method specific analysis as indicated in Table 3.1. Owing to the size of the core synthetic data set (20,000 time series) and the sheer computational expense of some of the algorithms tested (e.g., EEMD and CEEMD) it has been necessary to undertake large portions of the analysis in combination with cluster computing systems made available by

Table 3.1: Summary of Analysis Techniques Applied to Synthetic Data Set.

METHOD	SUB-METHOD	ADDITIONAL CONDITION	SOFTWARE PACKAGE/ ADDITIONAL COMMENT
Linear Regression	n/a	n/a	n/a
Polynomial Regression	Second order	n/a	n/a
LOESS Smoothing	n/a	n/a	$\alpha = 0.75$, order = 2, weighted least squares
Smoothing Splines	Cubic smoothing; Thin plate PRS; and B-Spline	λ based on both GCV and REML	"mgcv" package in R (Eilers and Marx, 1996; O'Sullivan, 1986, 1988; Wood, 2006).
Moving average ⁽¹⁾	10-40 year smooth (10 yr increment)	Single, triple and quad averaging.	"zoo" package in R (Zeileis and Grothendieck, 2005).
Structural models ⁽²⁾	Seasonal decomposition & basic structural model	Based on LOESS and ARIMA	Stl decomposition in R (Cleveland <i>et al.</i> , 1990). StructTS in R (Durbin and Koopman, 2012).
Butterworth filter ⁽³⁾	10-80 yr cycles removed (10 yr increment)	n/a	GRETL (2013)
SSA ^(4,6)	1d and Toeplitz variants	Win: 10-80 yr (10 yr increment)	"Rssa" package in R (Golyandina and Korobeynikov, 2014).
EMD	<u>Envelope:</u> Interpolation; Spline smoothing; Locfit smoothing; Sifting by interpolation and spline smoothing.	<u>Boundary condition:</u> None; Symmetric; Wave; Periodic.	"EMD" package in R (Huang <i>et al.</i> , 1998; Kim and Oh, 2009; Kim <i>et al.</i> , 2012).
EEMD ⁽⁵⁾	<u>Noise amplitude:</u> 20, 50, 100, 200 mm	<u>Trials:</u> 20, 100, 200	"hht" package in R (Wu and Huang, 2009; Bowman and Lees, 2013).
CEEMD ⁽⁵⁾	<u>Noise amplitude:</u> 20, 50, 100, 200 mm	<u>Trials:</u> 20, 100, 200	"hht" package in R (Torres <i>et al.</i> , 2011; Bowman and Lees, 2013).
Wavelet Analysis	Multi-resolution decomposition using MODWT.	Daubechies filters: Symmlet (S2, S4, S6, S8, S10)	"wmtsa" package in R (Daubechies, 1988, 1992; Percival and Walden, 2006).
Synchrosqueezed Wavelet Transform (SWT) ⁽⁶⁾	<u>Wavelet filters:</u> "Bump" (mu=1, s=0.2); "CMHat" (mu=1, s=5); "Morlet" (mu=0.05PI); "Gauss" (mu=2, s=.083.)	<u>Gen parameter:</u> 100 1000 10,000 100,000	"SynchWave" package in R (Daubechies <i>et al.</i> , 2011; Thakur, 2013).

Notes:

The above-mentioned table provides a general summary of the analytical techniques applied to the 14 synthetic data sets (refer Table 2.2 and Table 3.2) in order to test the utility of extracting the embedded mean sea level (trend) component. The "Sub-Method" and "Additional Condition" provide details on the sensitivity analysis pertaining to the respective methodologies. Where possible, relevant analytical software from the R open source suite of packages have been used (R Core Team, 2014).

- (1) Moving (or rolling) averages are centred on the data point in question and therefore the determined trend is restricted to half the averaging window inside both ends of the data set;
- (2) Structural models are only relevant for monthly average data sets;
- (3) For the respective 40 year monthly and annual synthetic data sets, only cycles up to and including 40 years have been removed by the digital filter;
- (4) For the respective 40 year data sets, only window lengths from 10 - 30 years have been considered. Similarly, for the respective 80 year data sets, only window lengths from 10 - 70 years have been considered;
- (5) The noise amplitude for the annual data sets includes the full range, but, for the monthly data sets only ranges from 50 - 200 mm; and
- (6) Auto-detection routines have been specifically written to isolate decomposed elements of the time series with low frequency trend characteristics.

Table 3.2: Summary of Number of Analyses Applied to Each Data Set.

METHOD	SYNTHETIC DATASETS														SUM
	M1	M2	M3	M4	M5	M6	M7	A1	A2	A3	A4	A5	A6	A7	
Linear Regression	1	1	1	1	1	1	1	1	1	1	1	1	1	1	14
Polynomial Regression	1	1	1	1	1	1	1	1	1	1	1	1	1	1	14
LOESS Smoothing	1	1	1	1	1	1	1	1	1	1	1	1	1	1	14
Smoothing Splines	6	6	6	6	6	6	6	6	6	6	6	6	6	6	84
Moving average	12	11	11	6	6	6	6	12	11	11	6	6	6	6	116
Structural models	2	2	2	2	2	2	2	-	-	-	-	-	-	-	14
Butterworth filter	8	8	8	4	4	4	4	8	8	8	4	4	4	4	80
SSA	32	28	28	12	12	12	12	32	28	28	12	12	12	12	272
EMD	16	16	16	16	16	16	16	16	16	16	16	16	16	16	224
EEMD	12	12	12	12	12	12	12	12	12	12	12	12	12	12	168
CEEMD	12	12	12	12	12	12	12	12	12	12	12	12	12	12	168
Wavelet Analysis	5	5	5	5	5	5	5	5	5	5	5	5	5	5	70
Synchrosqueezed Wavelet Transform (SWT)	16	16	16	16	16	16	16	16	16	16	16	16	16	16	224
SUM	124	119	119	94	94	94	94	122	117	117	92	92	92	92	1462

Notes:

The above-mentioned table provides a general summary of the number of analyses applied to each of the 14 synthetic data sets (refer Table 2.2). Refer Table 3.1 for details of the parametrisation relevant to each method. Each dataset contains 20,000 individual time series.

University of New South Wales Faculty of Engineering (*Leonardi System*) and Water Research Laboratory (*Manning System*). All scripting code to facilitate data preparation, analysis, remote UNIX batching and post analysis statistical processing have all been developed by the candidate as part of the research program.

3.2.2. Multi-criteria assessment of analytical methods for isolating mean sea level

In addition to identifying the analytic that provides the greatest temporal precision in resolving the trend, the intention is to further optimize this analytic (where possible) to underpin the development of tools for wide applicability by sea level researchers. Comparison of techniques identified in Table 3.1, have been assessed across a relevant range of quantitative and qualitative criteria, including:

- ❑ **Measured accuracy (Criteria A₁).** This criteria is based upon the cumulative sum of the squared differences between the fixed mean sea level signal and the trend derived from a particular analytic for each time series in the synthetic data set. This metric has then been normalised per data point for direct comparison between the different length synthetic data sets (40, 80 and 160 year of the 14 identified in Table 2.2) as follows:

$$A_1 = \frac{1}{n} \sum_{i=1}^{20,000} (x_i - X)^2 \quad (1)$$

Where:

- X represents the fixed mean sea level signal embedded within each time series;
- x_i represents the trend derived from the analysis of the synthetic data set using a particular analytical approach; and
- n represents the number of data points within each of the respective synthetic data sets (or lesser outputs in the case of moving averages).

It is imperative to note that particular combinations of key parameters used as part of the sensitivity testing regime for particular methods (refer Table 3.1), resulted in no (or limited) outputs for various time series analysed. This occurred either due to the analytic not resolving a signal within the limitations established for a trend (particularly for auto detection routines necessary for SSA and SWT) or where internal thresholds and/or convergence protocols were not met for a particular algorithm and the analysis terminated. Where such circumstances occurred, the determined A_1 metric was prorated to equate to 20,000 time series for direct comparison across methods. Where the outputs of an analysis resolved a trend signal in less than 75% (or 15,000 time series) of a particular synthetic data set, the result was not included in the comparative analysis.

- ❑ **Maximum standard deviation (Criteria A_2).** This straightforward statistical measure is based on the outputted trends from the application of a particular analytical method to the synthetic data sets, providing a measure of the scale of the spread of outputted trend estimates. Intuitively, the better performing analytic will minimise both criterions A_1 and A_2 .

- ❑ **Computational expense (Criteria A_3).** This criterion provides a comparative assessment of the average processing time to isolate the trend from the longest synthetic data set (160 year, datasets A1 and M1). This metric provides an intuitive appraisal of the value of some of the more computationally demanding analytical approaches when weighed against, in particular, the measured accuracy (criteria A_1).

- ❑ **Consistency across differing length datasets (Criteria A₄).** This criteria is based on a qualitative assessment of the consistency in the performance of the respective method across the 3 key length data sets (40, 80 and 160 years) which cover the contemporary length of global data used by sea level researchers. It is important to gain an understanding of how the relative accuracy changes in the extraction of the trend (if at all) from shorter to longer length data sets. A simple tick indicates a general consistency in the level of accuracy across all datasets. A cross indicates that the analytic may not have been able to consistently isolate a signal with “trend-like” characteristics across all length datasets within the limits established through the sensitivity testing regime.

- ❑ **Capacity to improve temporal resolution of trend characteristics (Criteria A₅).** This criteria is similarly based on a qualitative assessment of the capacity for the isolated trend to inform changes to associated real-time velocity and accelerations, which are of great contemporary importance to sea level and climate change researchers.

- ❑ **Resolution of trend over full data record (Criteria A₆).** This criteria relates to the ability of a particular analytic to resolve the trend over the full length of the data record. It has become increasingly important for sea level researchers to gain a real-time understanding of any temporal changes in the characteristics of the mean sea level (or trend) signal in the latter portion of the record.

- ❑ **Ease of application by non-expert practitioners (Criteria A₇).** Several analytical approaches considered require extensive expert judgement to optimise performance. Despite the sensitivity analyses undertaken to broadly identify the optimal settings of a specific analytic in relation to the signals within the synthetic data sets, the sensitivity of key parameters can be quite high. Where limited (or no) specific knowledge of the analytic is required to optimise its performance, the analytic has been denoted with a tick.

3.3 Results

In total, 1462 separate analyses have been undertaken as part of the testing regime, translating to precisely 29.24 million individual time series analyses. Figure 3.2 provides a pictorial summary of the complete analysis of all monthly and annual data sets (40, 80 and 160

year synthetic data sets) plotted against the key metric, criteria A_1 . Equivalent scales for each panel provide direct visual and quantitative comparison between monthly and annual and differing length data sets. For the sake of completeness, it is worth noting a further 36 monthly analysis results lie beyond the limit of the scale chosen and therefore are not depicted on the chart. Where analysis resolves a trend signal across more than 75% (or 15,000 time series) of a synthetic data set, the output is used for comparative purposes and depicted on Figure 3.2 as “complete”.

From Figure 3.2, it is evident that the cumulative errors of the estimated trend (criteria A_1) are appreciably lower for the annual datasets when considered across the totality of the analysis undertaken. For example, of the 579 “complete” monthly outputs, 408 (or 71%) fall below an A_1 level of $30 \times 10^6 \text{ mm}^2$ (where notionally the optimum methods reside). By comparison, of the 632 “complete” annual outputs, 566 (or 90%) are below this A_1 level.

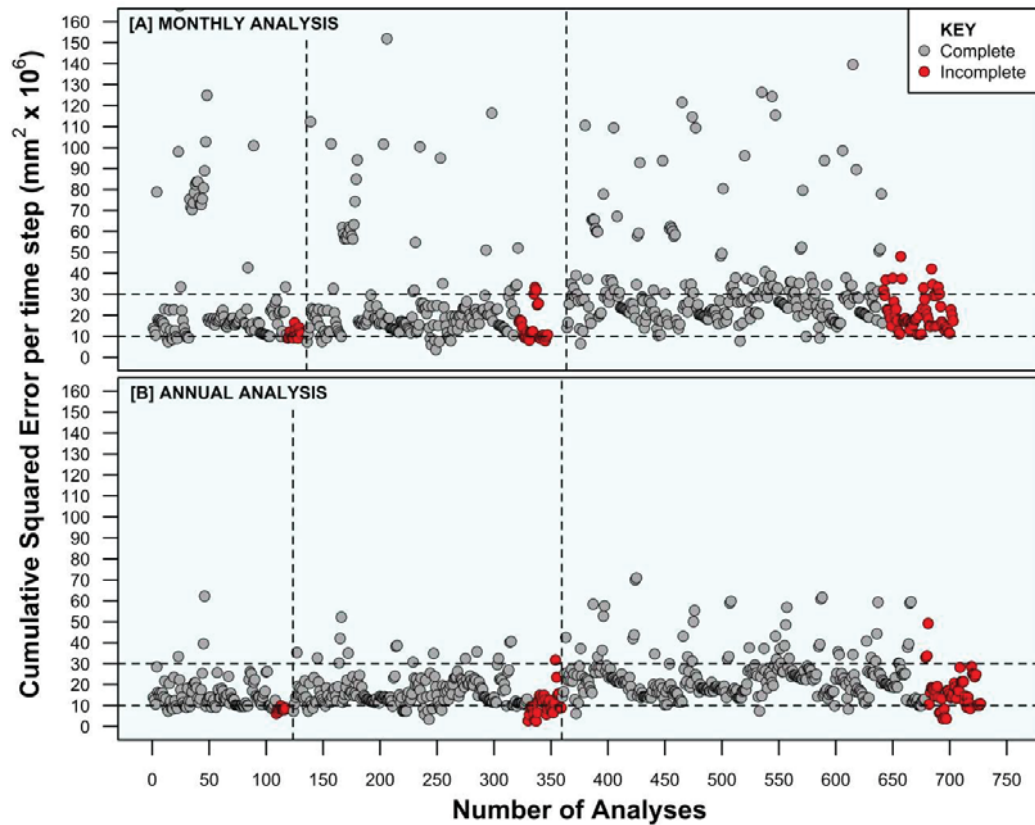
The key reason for this is that the annualised data sets not only provide a natural low frequency smooth (through averaging calendar year monthlies), but, the seasonal influence (at monthly frequency) is largely removed, noting the bin of seasonal signals sampled to create the synthetic data set also contains numerous time varying seasonal signals derived using ARIMA.

Based on visual inspection of Figure 3.2 alone, it is difficult to distinguish the influence of record length on capacity to isolate the trend component. However, detailed examination of the “complete” monthly outputs indicates that 77% of the 160 year dataset are contained below the A_1 threshold level of $30 \times 10^6 \text{ mm}^2$, falling to 62% for the 40 year datasets. Similarly for the “complete” annual outputs, 98% of the 160 year dataset are contained below this threshold, falling to 85% for the 40 year datasets. The above-mentioned results provide strong evidence that estimates of mean sea level are enhanced generally through the use of longer, annual average ocean water level data.

Based upon the appreciably reduced error in the estimate of the trend by using annual over monthly average ocean water level data, the multi-criteria assessment of the various methodologies advised in Table 3.1, have been limited to analysis outputs based solely on the annual synthetic data sets. Table 3.3 provides a summary of the multi-criteria assessment of

the better performing methods, based on optimisation of relevant parameters for each specific analytic. From this assessment, and within the limits of the analysis framework, multi-resolution decomposition using short maximal overlap discrete wavelet transform (MODWT) and short length wavelets has proven generally to be the optimal analytic over the broad range of criteria outlined in section 3.2.3, whereby limited expert judgment is required to optimise performance.

Figure 3.2: Analysis overview based on Criteria A_1 .



Notes:

This chart provides a summary of all analysis undertaken (refer Table 3.1). Scales for both axes are equivalent for direct comparison between respective analyses conducted on the Monthly (top panel) and Annual (bottom panel) synthetic data sets. The vertical dashed lines demarcate the results of each method on the 160, 80 and 40 year length data sets in moving from left to right across each panel. Where the analysis permitted the resolution of a trend signal across a minimum of 75% (or 15,000 time series) of a synthetic data set, this has been represented as “complete”. Those analyses resolving trends over less than 75% of a synthetic data set are represented as “incomplete”.

In addition to the results discussed above, there are some other interesting observations to be gleaned from the weight of analysis undertaken as part of this work. Of all methods considered in Table 3.1, the comparatively simple structural models applied to the monthly data sets provided the least utility in extracting the mean sea level trend component. This is not unexpected given that the range of complex signals within the synthetic data set are forced to be resolved into trend, seasonal and noise components only by these general models.

Similarly, methods such as EMD with inherent limitations associated with mode mixing and splitting, aliasing, and end effects (Mandic *et al.*, 2013), performed comparatively poorly across the range of synthetic data sets and across the range of parameters varied to optimise performance. The EEMD variant (Wu and Huang, 2009) which effectively combines EMD with noise stabilisation to offset the propensity for mode mixing and aliasing (Tary *et al.*, 2014), exhibited substantially enhanced performance compared to EMD. Across all 14 monthly and annual average synthetic data sets, EEMD exhibited more stable and consistent results across all sensitivity tests with the best performing EEMD on average reducing the squared error by 15% compared to the best performing EMD combination.

A further advancement in the form of CEEMD (Torres *et al.*, 2011) was developed to overcome a nuance of EEMD in which the sum of the intrinsic mode functions determined by the algorithm does not necessarily reconstruct the original signal (Tary *et al.*, 2014). When similarly averaged across all synthetic data sets, the best performing combination of CEEMD parameterisation only reduced the squared error by less than 5% compared to the best performing EMD combination. Further, it should be noted the CEEMD algorithm was not able to resolve a trend for every time series where internal thresholds/convergence protocols were not met.

Based on the testing regime performed on the synthetic data sets, EEMD outperformed CEEMD. Both variants of the ensemble EMD, using the sensitivity analysis advised, proved the most computationally expensive of all the algorithms tested. Both of these EMD variants were substantially outperformed by the MODWT and SSA, but importantly, processing times were of the order of 3000 - 4000 times that of these better performing analytics.

Table 3.3: Multi-Criteria Assessment by Method Across Annual Synthetic Data Sets.

METHOD	CRITERIA						
	A ₁ (mm ² x 10 ⁶) (note 1)	A ₂ (mm) (note 1)	A ₃ (seconds) (note 2)	A ₄	A ₅	A ₆	A ₇
Single MA (30YR)	26.0	81	< 0.01	✓	✓	✗	✓
SWT (Wavelet: CMH, generalization param 10 ⁵)	37.1	89	0.36	✗	✓	✓	✗
Linear Regression	37.2	71	< 0.01	✓	✗	✓	✓
Multi-resolution Wavelet Decomposition (MODWT) (Wavelet: s2)	37.8	65	< 0.01	✓	✓	✓	✓
SSA (1-D Toeplitz, auto select, window = 30YR)	39.3	63	0.01	✓	✓	✓	✗
EEMD (Noise = 100mm, trials = 200)	40.9	94	24.06	✓	✓	✓	✗
2nd Order Polynomial	43.7	102	< 0.01	✓	✗	✓	✓
Butterworth Digital Filter (removal up to 40YR cycles)	45.5	115	< 0.01	✓	✓	✓	✓
CEEMD (Noise = 100mm, trials = 100)	49.3	106	26.80	✗	✓	✓	✗
LOESS Smoothing	49.7	139	< 0.01	✓	✓	✓	✓
B-Spline Smoothing (λ based on REML)	50.8	122	0.01	✓	✓	✓	✓
EMD (Spline smooth sifting, symmetric end, λ based on golden search)	51.0	125	20.57	✓	✓	✓	✗

Notes:

The above-mentioned table provide a summary of the better performing methods based on optimisation of relevant parameters for each specific analytic (refer Table 3.1 for full range of sensitivity analyses). Only methods which resolved a trend component for a minimum of 75% of each of the respective annual datasets (160, 2 x 80 and 4 x 40 year) have been considered. The multi-resolution wavelet decomposition highlighted, demonstrates optimal performance across all criteria considered. Only the top 12 methods are indicated based on criteria A₁ ranking.

- (1) Criteria A₁ and A₂ are based on the sum of the metrics for the 160 year data set added to the respective averages for the 2 x 80 year and 4 x 40 year data sets.
- (2) Criteria A₃ represents the average time in seconds to analyse a single time series from the 160 year annual average synthetic data set.

Clearly for these particularly complex ocean water level time series, the excessive computational expense of these algorithms has not proven beneficial. One of the more inconsistent performers proved to be the SWT. This algorithm proved highly sensitive to the combination of wavelet filter and generalisation parameter. Certain combinations of

parameters provided exceptional performance on individual synthetic datasets but proved less capable of consistently resolving low frequency “trend-like” signals across differing length datasets. Of the analytics tested, this algorithm proved the most complex to optimise in order to isolate and reconstruct trends from the ridge extracted components. Auto detection routines were specifically developed to test and isolate the low frequency components based on first differences. However, a significant portion of the sensitivity analyses for SWT had difficulty isolating the low frequency signals across the majority of the datasets tested.

SSA has also been demonstrated to be a superior analytical tool for trend extraction across the range of synthetic data sets. For example, from Table 3.3, the A_1 parameter is only 4% higher than the MODWT, whilst having the lowest A_2 parameter of all the methods. However, like the SWT, SSA requires an elevated level of expertise to select appropriate parameters and internal methods to optimise performance. Auto detection routines were also developed to isolate the key SSA eigentriple groupings with low frequency “trend-like” characteristics, based on first differences. With this approach, not all time series could be resolved to isolate a trend within the limits established. Auto detection routines based on frequency contribution (Alexandrov and Golyandina, 2005) were also provided by Associate Professor Nina Golyandina (St Petersburg State University, Russia) to test, proving comparable to the first differences technique.

3.4 Discussion and limitation of analysis and testing framework

With so much reliance on improving the temporal resolution of the mean sea level signal due to its association as a key climate change indicator, it is imperative to maximise the information possible from the extensive global data holdings of the PSMSL. Numerous techniques have been applied to these data sets to extract trends and infer accelerations based on local, basin or global scale studies. Ocean water level data sets, like any environmental time series, are complex amalgams of physical processes and influences operating on different spatial scales and frequencies. Further, these data sets will invariably also contain influences and signals that might not yet be well understood (if at all).

With so many competing and sometimes controversial findings in the scientific literature concerning trends and more particularly, accelerations in mean sea level (refer Chapter 1), it is difficult to definitively separate sound conclusions from those that might unwittingly be

influenced by the analytical methodology applied (and to what extent). This research has been specifically designed as a necessary starting point to alleviate some of this uncertainty and improve knowledge of the better performing trend extraction methods for individual long ocean water level data. Identification of the better performing methods enables the temporal resolution of mean sea level to be improved, enhancing the knowledge that can be gleaned from long records which includes associated real time velocities and accelerations. In turn, key physically driven changes can be identified with improved precision and confidence, which is critical not only to sea level research, but climate change more generally at increasingly finer (or localised) scales.

The importance of resolving trends from complex environmental and climatic records has led to the application of increasingly sophisticated, so called “data adaptive” spectral and empirical techniques (Ghil *et al.*, 2002; Moore *et al.*, 2005; Tary *et al.*, 2014; Wu and Huang, 2009) over comparatively recent times. In this regard, it is readily acknowledged that whilst the testing undertaken within this research has indeed been extensive, not every time series method for trend extraction has been examined. The methods tested are principally those applied to individual ocean water level data sets within the literature to estimate the trend of mean sea level.

Therefore spatial trend coherence and multiple time series decomposition techniques such as Principal Component Analysis (PCA)/Empirical Orthogonal Functions (EOF), Singular Value Decomposition (SVD), Monte Carlo SSA (MC-SSA), Multichannel SSA (M-SSA), Cross Wavelet Transform (XWT), some of which are used in various regional and global scale sea level studies (Church *et al.*, 2004; Church and White, 2006, 2011; Domingues *et al.*, 2008; Hendricks *et al.*, 1996; Jevrejeva *et al.*, 2008; Meyssignac *et al.*, 2012a) are beyond the scope of this work and have not been considered. In any case, the synthetic data sets developed for this work have not been configured with spatially dependent patterns to facilitate rigorous testing of these methods. In developing the synthetic data sets to test for this research, Watson (2015) noted specifically that a natural extension (or refinement) of the work might be to attempt to fine tune the core synthetic data set to reflect the more regionally specific signatures of combined dynamic components.

Other key factors for consideration include identifying the method(s) that prove robust over the differing length time series available whilst resolving trends efficiently, with little pre-conditioning or site specificity. Whilst recognising that various studies investigating mean sea level trends at long gauge sites have utilised the construction of comparatively detailed site specific general additive models, these models have little direct applicability or transferability to other sites and have not been considered further for this work.

Of the analysis methods considered, the comparatively simple 30 year moving (or rolling) average filter proved the optimal performer against the key A_1 criterion when averaged across all length data sets. Although not isolating and removing high amplitude signals or contaminating noise, the sheer width of the averaging window proves to be very efficient in dampening their influence for ocean water level time series. However, the resulting mean sea level trend finishes 15 years inside either end of each data set, providing no temporal understanding of the signal for the most important part of the record – the recent history, which is keenly desired to better inform the trajectory of the climate related signal. Although well performing on a range of criteria, this facet is a critical shortcoming of this approach. Whilst triple and quadruple moving averages were demonstrated to marginally lower the A_1 criteria, respectively, compared to the equivalent single moving average, the loss of data from the ends of the record was further amplified by these methods.

It is also noted that the simple linear regression analysis also performed exceptionally well against the A_1 criteria when averaged across all data sets. Based on the comparatively limited amplitude and curvature of the mean sea level trend signal embedded within the synthetic data set it is perhaps not surprising that the linear regression performs well. But, like the moving average approach, its simplicity brings with it a profound shortcoming, in that it provides limited temporal instruction on the trend other than its general direction (increasing or decreasing). No information on how (or when) this signal might be accelerating is possible from this technique, which regrettably, is a facet of critical focus for contemporary sea level research. Further, it should also be noted that physics based projection models used by the IPCC (Church *et al.*, 2013a) forecast mean sea level to increase at increasing rate over the 21st century (refer Chapter 1, Figures 1.1 and 1.2). In effect, the linear model will have increasingly less utility under these circumstances in accurately charting the subtleties of time varying velocity given the model assumes zero acceleration at all times.

It has been noted that unfortunately, many studies using wavelet analysis have suffered from an apparent lack of quantitative results. The wavelet transform has been regarded by many as an interesting diversion that produces colourful pictures, yet purely qualitative results (Torrance and Compo, 1998). The initial use of this particular multi-resolution decomposition technique (MODWT) for application to a long ocean water level record can be found in the work of Percival and Mofjeld (1997). From the techniques applied that satisfied all qualitative criteria (A_4 to A_7 , refer Table 3.3), MODWT produced the best measurable qualitative performance overall (criteria A_1 to A_3 , refer Table 3.3), providing evidence of its strong utility for isolating mean sea level from long individual records.

Importantly, it is worth noting that the sensitivity testing and MCA used to differentiate the utility of the various methods, unduly disadvantages the SSA method. In reality the SSA method performs optimally with a window length varying between $L/4$ and $L/2$ (where L is the length of the time series). Varying the window length permits necessary optimisation of the separability between the trend, oscillatory and noise components (Hassani *et al.*, 2011). However, for the sensitivity analysis around SSA, only fixed window lengths were compared across all data sets. Although SSA (with a fixed 30 year window) performed comparably for the key A_1 criteria with MODWT (refer Table 3.3), a method that optimizes the window length parameter would, in all likelihood have further improved this result.

Only a modest improvement of less than 4% would be required to put SSA on parity with the accuracy of MODWT. In addition, auto-detection routines designed to select “trend-like” SSA components are unlikely to perform as well as the interactive visual inspection techniques commonly employed by experienced practitioners decomposing individual time series (Ghil *et al.*, 2002). Clearly visual inspection techniques were not an option for the testing regime described herein, which involved processing 14 separate data sets (Table 2.2) each containing 20,000 time series.

It is important that both the intent and the limitations of the research work presented here are clearly understood. The process of creating a detailed synthetic ocean water level data set, embedded with a fixed non-linear, non-stationary mean sea level signal to test the utility of trend extraction methods is unique for sea level research. Despite broad sensitivity testing designed herein, this work should be viewed as a starting point rather than a *fait accompli* in

providing a transparent appraisal of the utility of currently used techniques for isolating the mean sea level trend from individual ocean water level time series.

3.5 Conclusion

The monthly and annual average ocean water level data sets used to estimate mean sea level are like any environmental or climatic time series data, ubiquitously “contaminated” by numerous complex dynamic processes operating across differing spatial and frequency scales, often with very high noise to signal ratio. Whilst the primary physical processes and their scale of influence are known generally (Watson, 2015), not all processes in nature are fully understood and the quantitative attribution of these associated influences will always have a degree of imprecision, despite improvements in the sophistication of time series analyses methods (Moore *et al.*, 2005). In an ideal world with all contributory factors implicitly known and accommodated, the extraction of a trend signal would be straightforward.

In recent years, the controversy surrounding the conclusions of various published works, particularly concerning measured accelerations from long, individual ocean water level records necessitate a more transparent, qualitative discussion around the utility of various analytical methods to isolate the mean sea level signal with improved accuracy. The synthetic data set developed in Chapter 2 was specifically designed for long individual records, providing a robust and unique framework within which to test a range of time series methods to augment sea level research (Watson, 2015).

The testing and analysis framework summarised in this research is extensive, involving 1462 separate analyses across monthly and annual data sets of length 40, 80 and 160 years. In total, over 29 million individual time series were analysed, which represents the largest body of time series analysis testing undertaken to date for mean sea level research. From this work, there are some broad general conclusions to be drawn concerning the extraction of the mean sea level signal from individual ocean water level records with improved temporal accuracy:

- ❑ Precision is enhanced by the use of the longer, annual average data sets;
- ❑ The technique resulting in the best measured accuracy (Criteria A_1) across all length annual data sets was the simple 30 year moving average filter. However, the outputted trend finishes half the width of the averaging filter inside either end of the data record,

providing no temporal understanding of the trend signal for the most important part of the record – the recent history;

- ❑ The technique requiring minimum expert judgment and parameterisation to optimise performance was multi-resolution decomposition using maximal overlap discrete wavelet transform (MODWT); and
- ❑ The optimum performing technique is most likely to be Singular Spectrum Analysis (SSA) whereby interactive visual inspection techniques are used by experienced practitioners to optimise window length and component separability.

The testing and analysis framework for this work provides a very strong argument for the utility of Singular Spectrum Analysis (SSA) and multi-resolution decomposition using maximal overlap discrete wavelet transform (MODWT) techniques to isolate mean sea level with improved temporal resolution from long individual ocean water level data using a unique, robust, measurable approach. Notwithstanding, there remains scope to improve the utility of several of the data adaptive approaches using more extensive tuning of alternative parameters to optimise their performance to enhance mean sea level research. Of the two approaches, it is considered that SSA provides a superior capability to separate the key harmonic components of the time series and a wider scope to further optimize key internal parameters through testing by decomposing a wide range of long records in the Permanent Service for Mean Sea Level (Chapter 4).

3.6 Acknowledgements

The computing resources required to facilitate this research have been considerable. It would not have been possible to undertake the testing program without the benefit of access to high performance cluster computing systems. In this regard, I am indebted to John Zaitseff and Dr Xavier Barthelemy for facilitating access to the “Leonardi” and “Manning” systems at the Faculty of Engineering, University of NSW and Water Research Laboratory, respectively.

Further, this component of the research has benefitted significantly from direct consultations with some of the world’s leading time series experts and developers of method specific analysis tools. Similarly, I would like to thank the following individuals whose contributions have helped considerably to shape the final product and have ranged from providing specific and general expert advice, to guidance and review (in alphabetical order):

- ❑ Daniel Bowman (Department of Geological Sciences, University of North Carolina at Chapel Hill);
- ❑ Dr Eugene Brevdo (Research Department, Google Inc, USA);
- ❑ Emeritus Professor Dudley Chelton (College of Earth, Ocean and Atmospheric Sciences, Oregon State University, USA);
- ❑ Associate Professor Nina Golyandina (Department of Statistical Modelling, Saint Petersburg State University, Russia);
- ❑ Professor Rob Hyndman (Department of Econometrics and Business Statistics, Monash University, Australia);
- ❑ Professor Donghoh Kim (Department of Applied Statistics, Sejong University, South Korea);
- ❑ Alexander Shlemov (Department of Statistical Modelling, Saint Petersburg State University, Russia);
- ❑ Associate Professor Anton Korobeynikov (Department of Statistical Modelling, Saint Petersburg State University, Russia);
- ❑ Emeritus Professor Stephen Pollock (Department of Economics, University of Leicester, UK);
- ❑ Dr Natalya Pya (Department of Mathematical Sciences, University of Bath, UK);
- ❑ Dr Andrew Robinson (Department of Mathematics and Statistics, University of Melbourne, Australia); and
- ❑ Professor Ashish Sharma (School of Civil and Environmental Engineering, University of New South Wales, Australia).

Chapter 4

Methodology to Improve Estimates of Velocity and Acceleration in the Mean Sea Level Signal

Synopsis: The extensive testing of time series analytics (Chapter 3) identified Singular Spectrum Analysis (SSA) as an optimal tool to improve the isolation of mean sea level with improved temporal resolution from long, individual ocean water level data sets. This chapter details further testing and optimisation of SSA to enhance isolation of the mean sea level signal along with methods to improve estimates of the associated real-time velocity and acceleration over the length of the time series. This chapter also details the consolidation and integration of these facets into an open source analytical software package titled “msltrend” within the R Project for Statistical Computing (R Core Team, 2016).

Publications III and IV

Watson, P.J., 2016c. How to improve estimates of real-time acceleration in the mean sea level signal. In: Vila- Concejo, A.; Bruce, E.; Kennedy, D.M., and McCarroll, R.J. (eds.), Proceedings of the 14th International Coastal Symposium (Sydney, Australia). *Journal of Coastal Research*, Special Issue, No. 75, pp. 780-784. Coconut Creek (Florida), ISSN 0749-0208.

Watson, P.J., 2016b. msltrend: Improved Techniques to Estimate Trend, Velocity and Acceleration from Sea Level Records. *R Project for Statistical Computing*, published 12 January. URL: <http://cran.ms.unimelb.edu.au/web/packages/msltrend/index.html>

Declaration

I certify that these publications are a direct result of my research towards this PhD, and that reproduction in this thesis does not breach copyright regulations.

Phil J. Watson [Candidate]

4.1 Introduction

The time series analysis testing regime summarized in Chapter 3, highlighted the utility and efficiency of Singular Spectrum Analysis (SSA) and multi-resolution decomposition using maximal overlap discrete wavelet transform (MODWT) for isolating the trend component from the contaminating dynamic influences and noise embedded within long ocean water level data sets. Isolating the trend with improved temporal resolution is the key to refining the associated kinematic properties of mean sea level, in particular velocity and acceleration.

From the conclusions of Chapter 3, SSA has been selected as the data adaptive tool of choice for furthering this research program in developing a customized analytical software package (“msltrend”) to augment sea level (and climate change) research. This chapter summarises the process by which SSA has been specifically optimized to enhance resolution of the mean sea level trend from long ocean water level time series and the development of “msltrend”.

4.2 What is SSA and how does it work?

SSA is a powerful data adaptive technique capable of decomposing the observed time series into the sum of interpretable components with no *a priori* information about the time series structure (Alexandrov *et al.*, 2012; Ghil *et al.*, 2002; Golyandina and Zhigljavsky, 2013; Unal and Ghil, 1995; Vautard and Ghil, 1989).

SSA amplifies signal-to-noise ratio by separating the original time series into low-frequency trends and narrow-band quasi-periodic signals, with the rest (assumed to be noise) distributed among the filters (Moore *et al.*, 2005). Golyandina and Shlemov (2014) note the separability of respective components is closely related to the properties of the singular value decomposition (SVD), which is the essential part of many statistical and signal processing methods: principal component analysis (Jolliffe, 2002), low-rank approximations (Markovsky, 2012), several subspace-based methods (Van Der Veen *et al.*, 1993) including singular spectrum analysis among many others.

Through use of an embedding dimension, the original time series is projected via a series of lagged copies of the original time series into the form of what is referred to as a trajectory matrix (Golyandina *et al.*, 2001). SVD functions can then be performed on the matrix to resolve

individual components in order of rank of contribution to the time series from trend and oscillatory signals all the way down to dimensionless noise.

Since SSA uses data-adaptive basis functions, rather than the predetermined sines and cosines of classical spectral analysis, it can detect weak, non-harmonic oscillations in short, noisy time series (Unal and Ghil, 1995). A significant advantage of SSA is that it can detect a nonlinear, anharmonic oscillation by only two empirical orthogonal functions (EOFs), while in applying conventional Fourier analysis, one would require a large number of sine and cosine pairs to represent the same oscillation (Unal and Ghil, 1995). The method has significant advantages over, e.g., low-pass filtering or fitting by polynomial functions in that as the fit is data adaptive, no preconceived functions are forced on the data; the errors associated with the trend are then usually much smaller than individual measurement errors (Moore *et al.*, 2005).

Despite the improved capacity of these functions, a crucial problem remains selection of an appropriate embedding dimension (Unal and Ghil, 1995) which in effect is a quasi-smoothing parameter defining the number of lagged copies of the time series to be considered. Maximum recommended embedding dimensions range from one-quarter to one-half of the length of the data record (Moore *et al.*, 2005; Unal and Ghil, 1995), reflecting a trade-off between spectral resolution and optimal noise reduction. Moore *et al.* (2005) notes the smaller the embedding dimension, the shorter the length of the window over which the resolved components are calculated, and the less resolved is each component. On the other hand it is noted that the longer the window, the greater the frequency resolution of each component, but the greater the chance that noise is mistaken for signal and that a greater proportion of the time series is affected by the data boundaries. The trend is considered to be the collection of reconstructed components that have a periodicity longer than about twice the length of the embedding dimension (Moore *et al.*, 2005).

4.3 Optimising SSA for mean sea level analysis

A combination of lessons learned from the time series testing (Chapter 3) and parameter optimisation targeted specifically at mean sea level data has greatly enhanced the capacity of SSA for the task at hand in the following key areas:

- minimum length annual average time series;

- ❑ embedding dimension;
- ❑ automatic identification of “trend-like” components; and
- ❑ gap-filling routines.

4.3.1 Minimum length annual average time series

This is a critical consideration to improving the robustness of trend, velocity and acceleration estimates derived from long, individual ocean water level records. For example, Douglas (2001) advised minimum length data sets of 50-60 years to measure acceleration in order to lower the likelihood of key contamination from the influences of decadal to multi-decadal variability which ostensibly result from winds driven by climate modes (refer Qiu and Chen, 2012; Sturges and Douglas, 2011). Through further detailed analysis, Houston and Dean (2013) advised that, because of decadal variations, record lengths of at least 75 years should be used to determine acceleration, and even longer records should be used to determine trend differences.

Importantly, Chambers *et al.*, 2012 identified the existence of a significant oscillation with a period around 60 years in the majority of the tide gauges examined during the 20th Century, and that it appears in every ocean basin, with amplitudes exceeding 20 mm in several long records. Chambers *et al.* (2012) and Calafat and Chambers (2013) advise that estimates of global and regional acceleration must account for these multi-decadal fluctuations.

The times series analysis testing (Chapter 3) highlighted generally that precision in resolving the trend is enhanced by the use of the longer, annual average data sets. By recommending the use of annual time series of minimum length 80 years, ensures the trend signal (or in this case mean sea level) is optimally separable from the contaminating dynamic cyclical signals (including the quasi 60-year ocean oscillation proposed by Chambers *et al.* (2012)) and noise.

4.3.2 Embedding Dimension

The embedding dimension (or “window” as it is also commonly referred to) is a critical SSA parameter which establishes the number of lagged copies of the time series in the form of what is known as a trajectory matrix (Golyandina *et al.*, 2001). Ghil *et al.* (2002) describes this as equivalent to representing the behaviour of the system by a succession of overlapping

“views” of the series through a sliding M -point window, where “ M ” is known as the embedding dimension.

The embedding dimension is recommended in the range of one-quarter to one-half the length of the time series with one-half the maximum possible (Moore *et al.*, 2005; Unal and Ghil, 1995). Selecting the maximum range ensures optimal possible separability between the resolved components of the time series. In effect, small (or shorter) embedding dimensions act like smoothing linear filters of width $2M - 1$ (Moore *et al.*, 2005), risking suboptimal separability and potential mixing of signals across components, where the singular values of the decomposition are close. Alternatively, by using a small embedding dimensions, risks retaining contaminating power bands (albeit smoothed), spread across a smaller number of components, distinct from their isolation and removal.

As the exercise at hand is to isolate the trend with improved temporal resolution, it is strongly recommended to use the maximum embedding dimension (half the time series length) afforded by the data record so as to optimise the separability of resolved components and minimise mixing across signals. Although SSA performed extremely well in the time series testing (Chapter 3), each SSA test was based on a fixed embedding dimension (e.g., 10, 20, 30, 40 years) compared across all 14 data sets (Table 2.2). Had the testing protocols automatically set the embedding dimension to half the time series length (by default), separability between key components (and trend extraction) would have been improved.

4.3.3 Automatic identification of “trend-like” components

One of the strengths of SSA is the efficient decomposition of the original time series into individual components that can be visually examined and diagnostically tested using extension packages like *Rssa* (Golyandina and Korobeynikov, 2014). The visual diagnostic element enables trained analysts to readily confirm separability and components of specific interest. However, the extent of expert knowledge required to optimise SSA’s performance was identified as an impediment for using the technique to underpin the building of an analytical software tool for broad general use by sea level (and climate change) practitioners (see Table 3.3, Criteria A₇).

Automatic identification of specific types of components from an SSA decomposition has been an active area of scientific interest. Of primary consideration in setting an automatic identification threshold, is that one needs to be able to process every time series from a prescribed class with appropriate quality and consistent outcomes (Alexandrov and Golyandina, 2005).

The sheer scale of the time series testing regime undertaken in Chapter 3 negated use of visual inspection techniques but, necessitated the instigation of comparatively crude techniques to automatically detect “trend-like” components based on presupposing the maximum limit of first differences. At a coarse level this worked reasonably within the tolerance of the testing regime. However, such applications would not be sufficiently robust to underpin the development of a general purpose software tool for broad scale use by non (time series analysis) experts to produce reliable, consistent, high quality results.

In order to robustly establish an automatic identification regime for the isolation of components with intrinsically “trend-like” characteristics, it has been necessary to consult with SSA experts (refer Section 4.7) and undertake further testing using the data repositories of the PSMSL to establish what the key “characteristics” of “trend-like” components actually are. In particular, frequency thresholding based on Alexandrov and Golyandina (2005) has been trialled via application to the longest records in the PSMSL to isolate and diagnostically examine the characteristics of trend components from the SSA decomposition. Only annual average records in the PSMSL which meet the following notional criteria have been tested:

- minimum of 100 years in length; and
- maximum limit of 15% missing data from the complete time series.

Some 63 records which met the abovementioned criteria (refer Table 4.1 for summary details) have been tested. In order to decompose records using SSA the time series must be complete so the initial step involves filling gaps using simple linear interpolation. With gaps filled, univariate time series have been decomposed using 1 dimensional SSA via the Rssa extension package (Golyandina and Korobeynikov, 2014) in R (R Core Team, 2015).

Table 4.1: PSMSL Records tested to optimise performance of Singular Spectrum Analysis.

Station Name/Location	Reference Station ID	PSMSL (ID)	Length (Years)	Gaps (Years)
Brest, France	1	1	209	23
Swinoujscie, Poland	2	2	189	8
Cuxhaven, Germany	3	7	168	0
Wismar, Germany	4	8	167	1
Maassluis, Netherlands	5	9	168	0
San Francisco, USA	6	10	162	1
Warnemunde, Germany	7	11	160	1
New York, USA	8	12	161	18
Travemunde, Germany	9	13	160	8
Helsinki, Finland	10	14	137	0
Vlissingen, Netherlands	11	20	154	0
Aberdeen, UK	12	21	104	1
Hoek van Holland, Netherlands	13	22	152	0
Den Helder, Netherlands	14	23	151	0
Delfzijl, Netherlands	15	24	151	0
Harlingen, Netherlands	16	25	151	0
Nedre Sodertalje, Sweden	17	31	102	0
Ijmuiden, Netherlands	18	32	144	0
Poti, Georgia	19	41	142	9
Mumbai, India	20	43	133	15
Batumi, Georgia	21	51	134	18
Cascais, Portugal	22	52	112	11
Vaasa, Finland	23	57	132	11
Bergen, Norway	24	58	100	8
Marseille, France	25	61	131	7
Fort Denison, Australia	26	65	108	0
Landsort, Sweden	27	68	119	0
Olands Norra Udde, Sweden	28	69	129	0
Kungsholmsfort, Sweden	29	70	129	0
Hanko, Finland	30	71	127	24
Aarhus, Denmark	31	76	124	8
Stockholm, Sweden	32	78	127	0
Oulu, Finland	33	79	127	18
Esbjerg, Denmark	34	80	124	3
Fredericia, Denmark	35	81	123	3
Kobenhavn, Denmark	36	82	124	4
Ratan, Sweden	37	88	124	1
Hirtshalls, Denmark	38	89	121	10
Frederikshavn, Denmark	39	91	119	8
North Shields, UK	40	95	120	12
Slipshavn, Denmark	41	98	117	10
Fremantle, Australia	42	111	119	13
Fernandina Beach, USA	43	112	119	21
Korsor, Denmark	44	113	116	6
Klaipeda, Lithuania	45	118	114	11
Hornbaek, Denmark	46	119	122	4

Table continued over page.

Table 4.1 (continued).

Station Name/Location	Reference Station ID	PSMSL (ID)	Length (Years)	Gaps (Years)
Gedser, Denmark	47	120	121	2
Seattle, USA	48	127	118	0
Philadelphia, USA	49	135	116	5
Baltimore, USA	50	148	114	1
Trieste, Italy	51	154	141	22
Honolulu, USA	52	155	112	0
San Diego, USA	53	158	111	3
Galveston, USA	54	161	108	1
Balboa, Panama	55	163	108	1
Victoria, Canada	56	166	106	2
Mantyluoto, Finland	57	172	105	4
Smogen, Sweden	58	179	105	0
Atlantic City, USA	59	180	105	13
Portland, USA	60	183	105	1
Key West, USA	61	188	104	1
Pietarsaari, Finland	62	194	101	5
Fort Denison(II), Australia	63	196	101	3

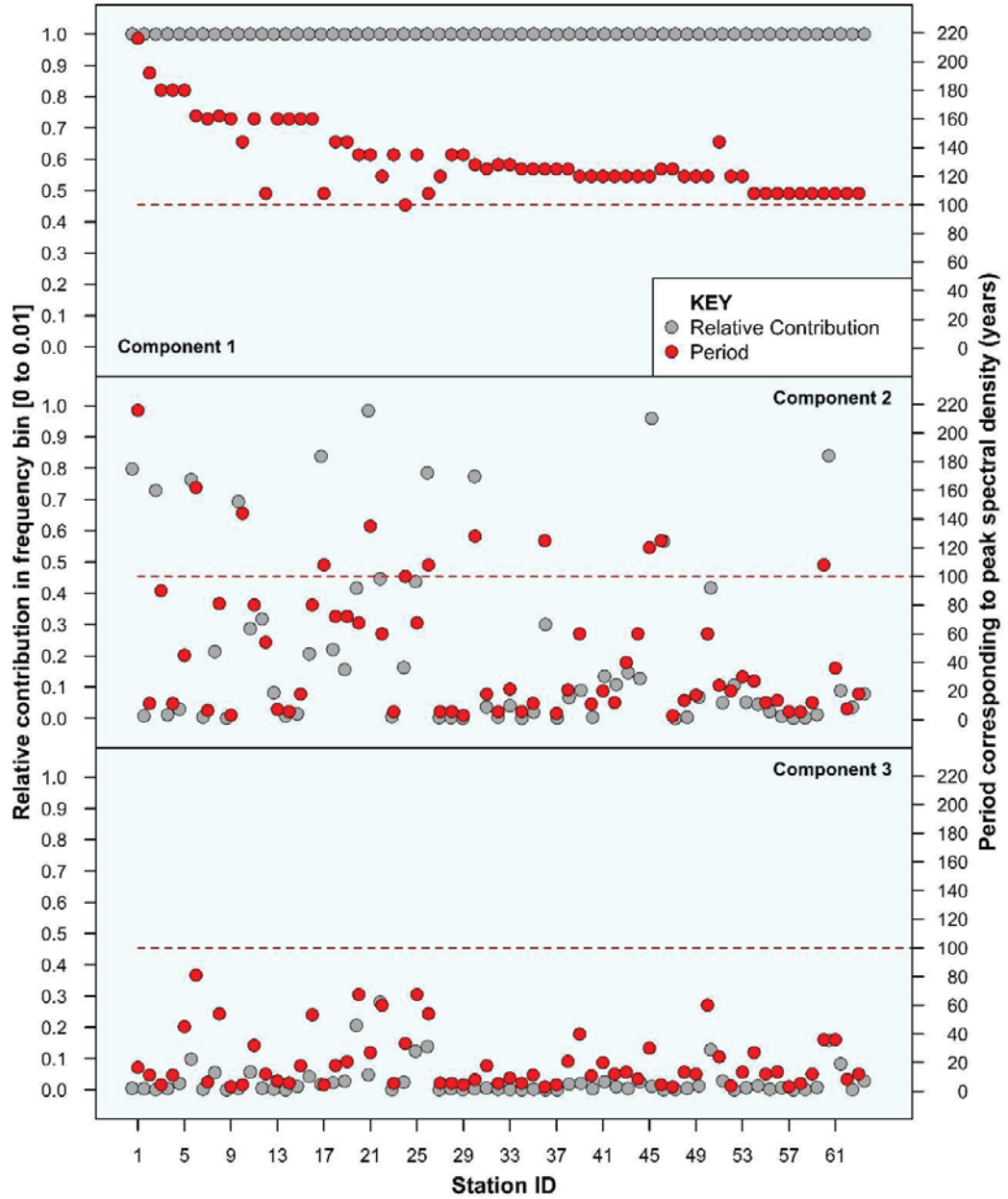
Notes:

These are the longest annual average time series records in the PSMSL exceeding 100 years with a maximum amount of missing data limited to 15% of the time series. The “Station ID” has been notionally assigned for presentation of graphical outputs.

Moore *et al.*, (2005) advises that the trend is considered to be the collection of reconstructed components that have a periodicity longer than about twice the length of the embedding dimension. Based on the records tested this means that the trend components have a minimum periodicity of at least 100 years. Alternatively, for annual time series, the trend components will be quarantined within the lowest frequency band [0 to 0.01] using a spectrogram analysis.

Each of the records summarised in Table 4.1 have been decomposed with the 10 leading components visually inspected and diagnostically analysed using a spectrogram to understand the spectral characteristics of the trend components. The spectrogram analysis has been undertaken by setting frequency bins at 0.01 and considering the contribution of each component that is contained within the lowest frequency bin [0 to 0.01]. The results for the 3 leading components are summarised in Figure 4.1.

Figure 4.1: Spectral characteristics of leading SSA components from long PSMSL records.



Notes:

This chart summarises the spectral analysis of the 3 leading components of the SSA decomposition of each record in Table 4.1 (refer to Station ID for details of specific records). The relative contribution (left hand axis) indicates the proportion of the component contained within the lowest frequency band [0 to 0.01] from the spectrogram analysis and is denoted on the chart by a grey dot. The periodicity corresponding to the peak spectral energy in each of the respective components (right hand axis) is denoted on the chart by a red dot. The red horizontal line highlights the 100 year periodicity which provides a clear visual point of demarcating trend-like components.

Table 4.2: Station records with significant component 2 contribution in the low frequency band [0 – 0.01].

Station ID	Station Location	Component 2 Contribution
1	Brest, France	0.80
6	San Francisco, USA	0.76
10	Helsinki, Finland	0.69
17	Nedre Sodertalje, Sweden	0.84
21	Batumi, Georgia	0.98
24	Bergen, Norway	0.16
26	Sydney, Australia	0.79
30	Hanko, Finland	0.77
36	Kobenhavn, Denmark	0.30
45	Klaipeda, Lithuania	0.96
46	Hornbaek, Denmark	0.57
60	Portland, USA	0.84

Notes:

The table summarises the records for which the component 2 has a peak spectral period matching component 1 (refer middle panel Figure 4.1). The leading 2 components of these records are visually depicted in Appendix D.

The results of the visual and spectral analysis of the leading 10 components of the SSA decomposition of all records in table 4.1 can be summarised in the following:

- ❑ Component 1 is a pure trend for all records analysed, with the relative contribution contained within the lowest frequency bin [0 to 0.01] exceeding 0.999;
- ❑ Components 3 and below contain no signals that could be considered as characteristic of a trend;
- ❑ 12 station records exhibit a component 2 which has a peak spectral period matching that of its associated component 1, meaning that it exhibits similar trend-like characteristics but the contribution in the lowest frequency bin [0 to 0.01] is diminished. This infers other (minor) frequency bands (and or noise) are also partially embedded within this component; and
- ❑ Visual examination of these 12 stations records (refer appendix D) highlights that genuine trend characteristics are retained by component 2 when the relative contribution in the lowest frequency bin [0 to 0.01] is set above a threshold of ≈ 0.75 (refer Table 4.2). The addition of these component 2 contributions matches known inflexions that have been keenly observed in long mean sea level records by others (e.g., Woodworth *et al.*, 2009). Relative contributions below this notional threshold appear to

be increasingly contaminated by other oscillatory signals and possibly noise and depart from the shape of mean sea level curves over the relevant period as understood from the body of the literature available (e.g., Church and White, 2011; Jevrejeva *et al.*, 2014).

4.3.4 Gap filling of time series

Mean sea level time series, like numerous geophysical and climate related data, are synonymous with missing data (Kondrashov and Ghil, 2006) owing to a wide variety of causes. For example, of the longest time series tested in the PSMSL in section 4.3.3 (Table 4.1), only 18 of the 63 time series were complete.

Given SSA can only be performed on complete time series, it is necessary to look at the potential optimisation of gap filling routines to improve the retention of key geophysical signals in the record (where possible). Douglas (1992) noted the importance of gaps in mean sea level records due to the presence of low-frequency sea-level variations. There are of course numerous, quite sophisticated gap filling techniques available reliant in part, on spatio-temporal covariance (e.g., Beckers and Rixon, 2003; Johns *et al.*, 2003; Kaplan *et al.*, 1997; Reynolds and Smith, 1994; Sherwood, 2001; Schneider, 2001; Smith *et al.*, 1996).

However, these techniques utilize spatial correlations only (Kondrashov and Ghil, 2006) deeming they are reliant on near neighbour correlations and sufficient spatial data density over both the gap and regional area of interest. In addition to the data requirements not being available, it also might not be practical to go to this level of endeavour to fill relatively small gaps in individual time series analysis. In many circumstances where small gaps are required to be filled in annual average time series, it might be entirely appropriate to fill the gaps using comparatively unsophisticated techniques that might include for example, linear interpolation, spline interpolation, Stineman's interpolation (Stineman, 1980) and weighted moving average, amongst numerous others. Within the SSA literature, a variety of gap filling options have been developed including:

- ❑ iterative approach proposed by Kondrashov and Ghil (2006);
- ❑ sequential method of forecasting complete portions of the time series onto incomplete sections (Golyandina and Osipov, 2007); and

- simultaneous method involving projections of the time series onto the signal subspace (Golyandina and Osipov, 2007).

Perceived advantages of using the available SSA gap filling routines are that one has the theoretical ability to preserve the principal spectral structures of the complete portions of the original data set in filling the gaps. Intuitively this would be an advantage. Irrespective, it should always be remembered that gap-filling is a synthetic process and where required, it is strongly recommended to sensitivity test using the different filling options available and most importantly, visually inspect the filled time series to provide a necessary sanity check on the synthetic data sections generated.

The less reliance one has on synthetically filling data gaps, the lower the likelihood that the gap-filling procedures will affect the underlying integrity of records and by consequence affect trend determination. One way of limiting such a circumstance is to restrict the scale of missing data permissible prior to trend analysis. From manual inspection of the PSMSL records considered in Table 4.1 and sensitivity testing the error of different gap filling procedures, it is recommended to limit maximum total and continuous gaps to 15% and 5% respectively, of the length of the record.

4.4 Additional considerations to enhance velocity and acceleration estimates

Mean sea level trends determined from an SSA decomposition are not governed by *a priori* parametric form or model constraints. As such the trend components are comparatively free form elements. By convention, associated velocity and accelerations are readily determined from the first and second differences of the mean sea level time series. Although this works well with smooth and naturally curvilinear trends, the isolated trend components from the SSA decomposition are portions of linearly additive components that reconstruct the original time series and thus are not precisely smooth or curvilinear at point to point scale.

Therefore in estimating comparatively low time varying velocity and accelerations, the first and second differences from the SSA derived trend components can induce unwanted and misleading kinematic properties owing to the “sawtooth” characteristic associated with point to point discontinuities. This is particularly evident in the second differences when the actual

time varying accelerations are generally low and principally confined in the range of ± 0.04 mm/yr² (Watson 2016e, 2017).

An alternative approach to estimating the time varying velocity and acceleration is to determine the first and second derivatives, respectively, of a fitted cubic smoothing spline. This approach provides a more realistic representation of a smoothly varying trend so long as the cubic smoothing spline model fit can accurately describe the reconstructed trend-like components of the SSA decomposition.

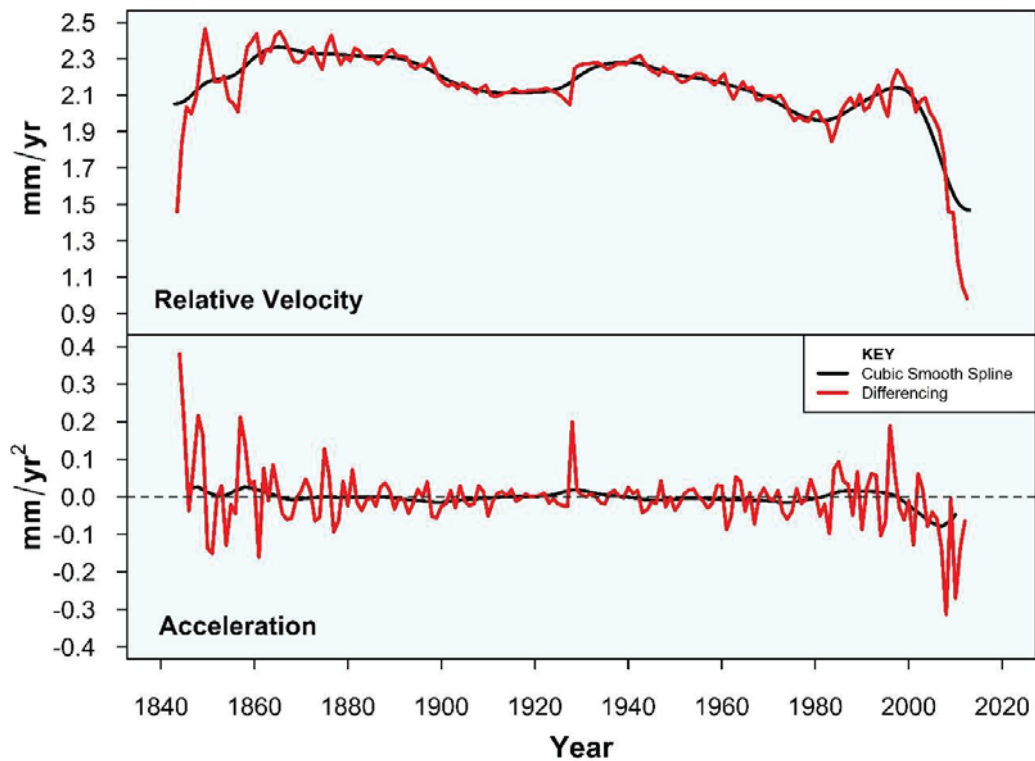
Sensitivity testing on a wide variety of long records in Table 4.1 indicates that by fitting a cubic smoothing spline with approximately 1 degree of freedom per every 8 years of record length, the fit is optimised whilst removing the extraneous effects of the sawtoothing. Figure 4.2 highlights the relevant differences discussed above using the long Cuxhaven (Germany) record. For the numerous records tested, the coefficient of determination (R^2) of the fitted spline to the sea level trend exceeds 0.99 in all cases, providing a high degree of confidence in this form of model to estimate the associated time varying velocities and accelerations.

Notwithstanding, care is required in fitting smoothing splines and deriving second derivatives near the end of the time series. The reason for caution here is that the knots at the end of a fitted cubic smoothing spline are fixed in order to be differentiable, resulting in a second derivative at the ends which must converge to zero, which is purely an *a priori* artefact of the model fit, not the characteristics of the data. For this reason, the first and last 3 derived acceleration points for each time series using a fitted cubic spline will likely have reduced accuracy and should be ignored in any prospective analysis.

4.5 Summary of key findings

Table 4.3 summarises the key learnings from the body of testing and further optimisation of SSA to be incorporated into an analytical software package to enhance mean sea level (and climate change) research.

Figure 4.2: Differencing vs smoothing spline for kinematic properties of Cuxhaven trend.



Notes:

This chart shows the kinematic properties of the mean sea level trend from the Cuxhaven record determined separately from 1st and 2nd differences and also from the 1st and 2nd derivatives of a fitted cubic smoothing spline with 1 degree of freedom per every 8 years of record length. Decomposed mean sea level trend provided by Watson (2017).

4.6 Development of analytical software package

Key research findings (Section 4.5, Table 4.3) have been consolidated into a purpose-built analytical software package titled “msltrend” and published as an extension package within the open source R Project for Statistical Computing (R Core Team, 2016). R is the world’s most popular programming language for statistical computing and predictive analytics; used by more than 2 million people worldwide (Sirosh, 2015). A key feature of R is the capacity for the user to custom build innovative diagnostic tools to augment research and analysis problems through access to an extensive range of contributed objects, functions and customised packages already available.

Table 4.3: Key features necessary to optimise the temporal resolution of mean sea level and associated kinematic properties.

Feature	Recommended Optimisation
Type of time series	Annual average
Length of time series	Minimum length 80 years
Analytic to isolate mean sea level	1 dimensional Singular Spectrum Analysis (SSA) thereafter fitted with a cubic smoothing spline using 1 degree of freedom per 8 years of record length
Embedding dimension (SSA)	Maximum width (half length of time series)
Selection of trend components	Isolated automatically by aggregating components in which the relative contribution of the lowest frequency bin [0-0.01] exceeds 75%
Total missing data	15 % of record length
Maximum continuous data gap	5% of record length
Gap filling	Irrespective of what method is used, visual inspection of filled time series is recommended as a first order sanity check
Gap filling method	SSA techniques which use the broad spectral characteristics of the time series to fill the data gaps (Golyandina and Osipov, 2007; Kondrashov and Ghil, 2006)
Velocity	1 st derivative of a cubic smoothing spline fitted to the SSA derived trend using 1 degree of freedom per 8 years of record length
Acceleration	2 nd derivative of a cubic smoothing spline fitted to the SSA derived trend using 1 degree of freedom per 8 years of record length. Remove 1 st and last 3 acceleration estimates due to reduced accuracy at end of time series

The “msltrend” package has been built to provide improved trend estimates based on Singular Spectrum Analysis methods. Various gap-filling options are included to accommodate incomplete time series records. Another central feature of the package is the inclusion of a forecasting module to consider the implication of user defined quantum of sea level rise between the end of the available historical record and the year 2100. A wide range of screen and pdf plotting options are included in the package along with a detailed User Manual to guide the analyst in the application of the software (refer Appendix E).

Published packages such as “msltrend” are required to satisfy extensive third party testing protocols on multiple operating system platforms before being accepted within the Comprehensive R Archive Network (CRAN) and available for download worldwide, including all the original code (Watson, 2016b). The following sections provide an insight into some of the basic elements that underpin the package, along with a discussion on some of the key functions and outputted products.

4.6.1 Input Data

Input data files must be annual average time series data (in *.csv format), which are publicly accessible from the global data repository of the Permanent Service for Mean Sea Level (PSMSL, 2016). Critical additional conditions have been imposed on the input time series regarding length of record and extent of data gaps (where relevant) to ensure the robustness and integrity of the estimated trends derived (refer Table 4.3). Where the specified conditions are not met, the function terminates with appropriate warnings to instruct the analyst about the cause of the problem.

4.6.2 Estimation of Errors

The estimation of errors in the trend and associated instantaneous velocity and accelerations is one of the more significant features of the package and is based on bootstrapping techniques. This process initially involves fitting an autoregressive time series model to remove the serial correlation in the residuals between the SSA derived trend and the original (or gap-filled) time series input data (refer Foster and Brown, 2015). This process is undertaken by importing the *auto.arima* function from the “forecast” package (Hyndman and Khandakar, 2008). The uncorrelated residuals are then tested to identify change points in the statistical variance along the time series by importing the *cpt.var* function in the “change point” package (Killick and Eckley, 2014), using a minimum segment length of 15 years.

Where a change point is detected in the variance, bootstrapping processes to randomly sample uncorrelated residuals are quarantined between identified variance change points (otherwise known as “block” bootstrapping). The randomly sampled uncorrelated residuals are then added to the SSA derived trend and the process repeated 10,000 times (default). From the extensive pool of outputted trends, associated velocities and accelerations, standard deviations are readily calculated to derive robust confidence intervals. The analyst is given the option of selecting the number of iterations for bootstrapping between 500 and 10,000. It is strongly recommended to use the lower bound figure for preliminary analysis, trialling different gap-filling methods, etc, in order to limit processing time associated with bootstrapping procedures. However, the default value (10,000) is recommended for final analysis. 95% confidence intervals are generated as defaults throughout, though other confidence intervals can be selected by the analyst.

4.6.3. Key Functions

The *msl.trend* function is the key entry point within the package. This function deconstructs annual average time series data into a trend and associated real-time velocities and accelerations, whilst filling necessary internal structures to facilitate all other functions in the package.

The outputted *msl.trend* object contains summary information in the form of a data frame incorporating the original data, gap-filled time series (where necessary), trend, velocity, acceleration, associated standard deviations and uncorrelated residuals. The outputted object also retains various meta-data including relevant details about the input arguments, input data set, peak velocities and accelerations and the time at which they occur. A full description of the *msl.trend* object and relevant examples are also provided in the “msltrend” User Manual (see Appendix E).

The package is underpinned by the most extensive testing (Chapter 3) and optimisation regime (Sections 4.1 - 4.5) undertaken for long individual ocean water level records. Thus, key functions and settings have been specifically optimised and “hard-wired” into the scripting code to ensure unsuspecting, inexperienced or untrained analysts using ocean water level data, would not inadvertently produce misleading results by tampering with internal settings.

The *msl.forecast* function is the other key element of the package, directly integrating the historical record with a user defined quantum of sea level rise to the year 2100, providing an invaluable tool to augment coastal adaptation planning endeavours. All internal parameters captured in the *msl.trend* function are parsed directly to *msl.forecast* with outputted velocities, accelerations and associated error margins extended to 2100.

The permissible user defined quantum of sea level rise ranges from 200 to 1500 mm with 800 mm set as the default. Simple equations of motion are used, based on constant acceleration, to project the defined quantum of sea level rise from the end of the historical trend to the year 2100. The instantaneous velocity at the end of the historical record is parsed directly from the *msl.trend* object and used as the initial velocity in the motion equations. This technique accords with contemporary methods of projecting sea level rise forward into the future.

Instantaneous velocities and accelerations are determined in the same manner detailed for the historical record, but with one small difference. The projection curve naturally permits extending the trend beyond 2100. In doing so, real estimates of acceleration are able to be determined at 2100 as they are not encumbered by the issue of a fixed knot at the end of the smoothing spline which affects the decomposition of the historical record (refer Section 4.4).

The estimation of errors in the trend and associated instantaneous velocity and accelerations is undertaken in a similar, though not identical manner, to that advised for the historical record. Despite any apparent change points in the variance of the random residuals in the historical portion of the record, bootstrapping procedures randomly resample (with replacement) from the whole pool of uncorrelated residuals to accommodate the projected portion of the time series out to 2100. The number of iterations used in the bootstrapping process to generate confidence intervals is automatically parsed forward from the *mstrend* object to maintain consistency.

The outputted *mstforecast* object is near identical in format to the *mstrend* object, with the exception that associated summary and meta-data information extend up to 2100, incorporating the defined sea level rise. A full description of the *mstforecast* object and relevant examples are provided in the “mstrend” User Manual (see Appendix E).

4.7 Acknowledgements

In order to assist with the optimization of SSA and subsequent development of the “mstrend” analytical software package, I am indebted to the expert advice provided by the following individuals (in alphabetical order):

- Professor Karl Broman (Department of Biostatistics and Medical Informatics, University of Wisconsin-Madison, USA);
- Associate Professor Nina Golyandina (Department of Statistical Modelling, Saint Petersburg State University, Russia); and
- Professor Rob Hyndman (Department of Econometrics and Business Statistics, Monash University, Australia).

Chapter 5

Application of “msltrend” Analytical Software Package to the Data Rich Margins of the USA

Synopsis: The analytical software package “msltrend” (Section 4.6) has been applied to the data rich margins of continental USA to enhance estimates of trend, real-time velocity and acceleration in the relative mean sea level signal. This research presents a fresh approach in the literature to considering acceleration that overcomes the limitations of other applied methodologies (refer Section 5.5) that have largely proven inadequate in charting the subtle temporal changes in the characteristics of mean sea level. The techniques employed within form an integral part of the evolutionary process by which to measure accelerations in mean sea level with improving robustness and consistency. Key findings are that at the 95% confidence level, there is no consistent or substantial evidence (yet) that recent rates of rise are higher or abnormal in the context of the historical records available for the USA, nor is there any evidence that geocentric rates of rise are above the global average. It is likely a further 20 years of data will identify whether recent increases east of Galveston and along the east coast are evidence of the onset of climate change induced acceleration.

Publication V

Watson, P.J., 2016e. Acceleration in US Mean Sea Level? A New Insight using Improved Tools. *Journal of Coastal Research*, 32(6), pp.1247-1261.

Declaration

I certify that this publication was a direct result of my research towards this PhD, and that reproduction in this thesis does not breach copyright regulations.

Phil J. Watson [Candidate]

5.1 Introduction

Neumann *et al.* (2011) estimated the global population living within areas deemed at threat from a 1-in-100 year storm surge event, coupled with 210 mm of projected sea level rise, to be of the order of 315 to 410 million people. Within this estimate, some 6.5 to 8 million people are located within the Northern American region.

Whilst the scale of these projected statistics are indeed confronting from an overall global adaptation perspective, the domestic economic threat posed by sea level rise is also daunting. The Third National Climate Assessment report provides a detailed examination of the range of climate impacts affecting the USA (Melillo *et al.*, 2014). This assessment advised that in 2010, economic activity in shoreline counties around the USA accounted for approximately 66 million jobs and USD 3.4 trillion in wages (NOAA, 2012) through diverse industries and commerce. In many instances, economic activity is fundamentally dependent on the physical and ecological characteristics of the coast.

Moser *et al.* (2014) estimated more than 15,000 km² and more than USD 1 trillion of property and structures are at risk of inundation from sea level rise of approximately 600 mm (or two feet) above current sea level around coastal USA. In addition, coastal recreation and tourism comprises the largest and fastest-growing sector of the U.S. service industry, accounting for 85% of the USD 700 billion annual tourism-related revenues, making this sector especially vulnerable to increased impacts from climate change (Moser *et al.*, 2014).

Whilst the afore-mentioned assessments predominantly deal with projections and estimates, it is worth noting that 2015 experienced the highest number of global natural catastrophes (198), the highest ever recorded in one year (Swiss Re, 2016) on a steadily upward trending trajectory. Of the total economic losses caused by disasters in 2015 (USD 92 billion), some 75% were due to natural catastrophes, of which storms and floods comprised around 90%. Further, of the 40 most costly global disasters since 1970, nearly 50% are directly or partially related to floods (Swiss Re, 2016). Flooding more generally will of course be substantially exacerbated by forecast sea level rise into the future, foreboding an increasingly ominous threat from natural disasters.

Improved understanding of how and when climate change impacts will occur and evolve over time will be critical to developing robust strategies to adapt and minimise risks (Watson, 2016c).

This chapter provides an updated appraisal of acceleration in mean sea level records around continental USA through use of ‘msltrend’ (Watson, 2016b) within the R Project for Statistical Computing (R Core Team, 2016). The ‘msltrend’ package has been specifically designed to substantially enhance estimates of trend, real-time velocity and acceleration in relative mean sea level derived from contemporary ocean water level data sets, based on unprecedented time series research, development, testing and analysis (refer Chapters 3 and 4).

The outputs of this research tool provide a more consistent, transparent appraisal of acceleration in mean sea level records around continental USA; overcoming many of the evident shortcomings from the wide body of scientific literature on this topic (refer Section 5.5).

5.2 Data

The ‘msltrend’ package was specifically developed for application to annual average time series data available from the PSMSL, with a minimum record length of 80 years (refer Section 4.3.1). In addition, the time series data must also conform to protocols concerning missing data, including maximum missing data and maximum continuous gaps limited to 15% and 5%, respectively, of the length of the time series (refer Section 4.3.4). Only Revised Local Reference (RLR) datasets from the PSMSL have been used as they are commensurate with quality control procedures and complete tide gauge datum histories provided by the supplying national authority (PSMSL, 2016).

In addition, Hogarth (2014) explores the potential for extending tide gauge time series from the PSMSL using historical documents, PSMSL ancillary data, and by developing additional composite time series using near neighbour tide gauges. Several long US records have been further extended by Hogarth (2014), including Honolulu, Ketchikan, San Francisco, New York and Boston. The complete portions of these extended time series have been used in this study. Annual average time series were available from the PSMSL for the study area up to and including 2014.

All data records used in this study have notionally been assigned a ‘Station ID’ (refer Table 5.1) commencing with Honolulu (1) in the Central Pacific, progressing north to south along the west coast (2-12), west to east along the Gulf coast (13, 14) and south to north up the east coast (15-29). By graphically representing characteristics associated with records based on the Station ID, spatially dominant patterns are more readily apparent. A total of 29 annual average time series records from the PSMSL fit the above-mentioned criteria and have been analysed within this study (refer Figure 5.1, Table 5.1).

Table 5.1: Summary of data used in USA analysis.

Tide Gauge Data							GNSS (GPS) Data ⁽³⁾			
Station ID ⁽¹⁾	Location	PSMSL ID	Start (yr)	End (yr)	Length (yrs)	Gaps (yrs)	SONEL Station	Length (yrs)	Distance to tide gauge (m)	VLM (mm/yr)
1	Honolulu ⁽²⁾	155	1891	2014	124	-	HNLC	16.04	1	-0.22 ± 0.18
2	Ketchikan	225	1919	2014	96	2	-	-	-	-
3	Friday Harbour	384	1934	2014	81	3	SC02	12.13	359	0.26 ± 0.24
4	Victoria	166	1910	2014	105	2	ALBH	18.99	12,000	0.72 ± 0.14
5	Neah Bay	385	1935	2014	80	4	NEAH	17.56	7,776	3.28 ± 0.28
6	Seattle	127	1899	2014	116	-	SEAT	16.69	5,900	-0.97 ± 0.22
7	Astoria	265	1925	2014	90	2	TPW2	13.74	2	0.38 ± 0.15
8	Crescent City	378	1933	2014	82	4	PTSG	11.48	7,195	3.23 ± 0.17
9	San Francisco ⁽²⁾	10	1855	2014	160	-	TIBB	18.99	9,551	0.08 ± 0.14
10	Los Angeles	245	1924	2014	91	2	VTIS	15.05	2,168	-0.03 ± 0.15
11	La Jolla	256	1925	2014	90	8	SIO3	17.18	671	0.77 ± 0.38
12	San Diego	158	1906	2014	109	3	PLO5	7.56	8,400	-2.60 ± 0.20
13	Galveston ⁽⁴⁾	161	1909	2014	106	1	TXGA	8.81	2,856	-3.42 ± 0.79
14	Pensacola	246	1924	2014	91	4	PCLA	9.71	7,500	-0.43 ± 0.36
15	Key West	188	1913	2014	102	1	KYW5	6.21	15,946	-1.78 ± 0.42
16	Charleston	234	1922	2014	93	-	SCHA	4.97	200	-1.84 ± 0.64
17	Sewells Point	299	1928	2014	87	-	-	-	-	-
18	Washington	360	1931	2014	84	2	USNO	16.53	6,380	-0.12 ± 0.20
19	Annapolis	311	1929	2014	86	5	ANP5	6.24	11,577	-2.48 ± 0.37
20	Baltimore	148	1903	2014	112	1	SA15	9.19	11,287	-1.22 ± 0.26
21	Atlantic City	180	1912	2014	103	13	NJGT	4.85	16,342	-1.62 ± 0.67
22	Philadelphia	135	1901	2014	114	5	PAPH	6.17	9,390	-0.55 ± 0.38
23	Sandy Hook	366	1933	2014	82	4	SHK5	7.66	553	-2.68 ± 0.27
24	New York ⁽²⁾	12	1853	2014	162	-	NYBP	4.68	49	-2.09 ± 0.62
25	Newport	351	1931	2014	84	2	NPRI	8.14	500	0.17 ± 0.23
26	Woods Hole	367	1933	2014	82	8	-	-	-	-
27	Boston ⁽²⁾	235	1902	2014	113	10	-	-	-	-
28	Portland	183	1912	2014	103	1	-	-	-	-
29	Eastport	332	1930	2014	85	11	EPRT	13.26	853	0.24 ± 0.25

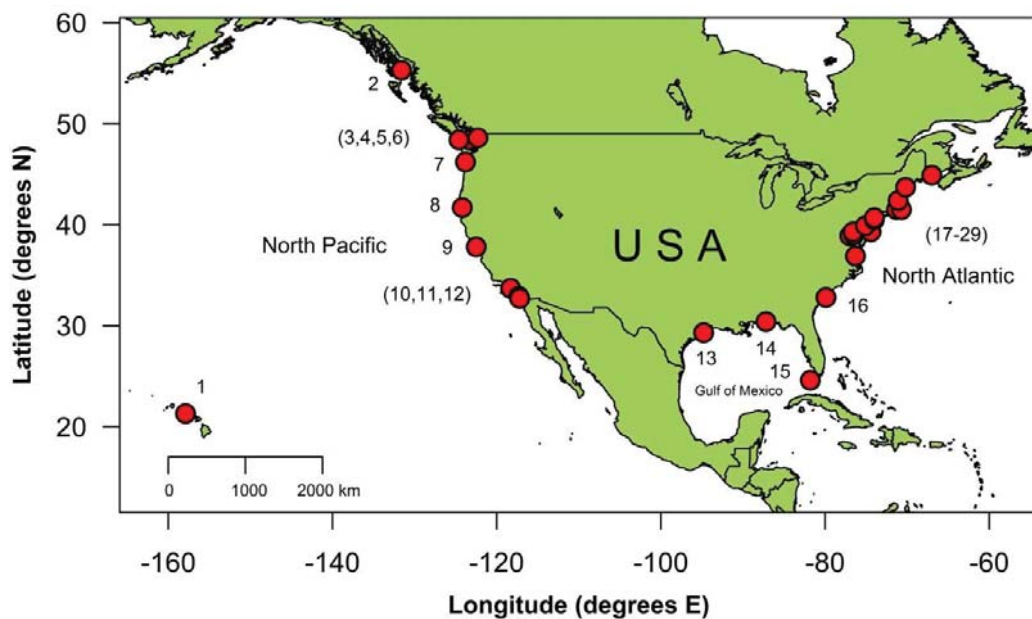
Notes:

- ⁽¹⁾ The ‘Station ID’ is a local referencing protocol used throughout this study, particularly the graphical outputs;
- ⁽²⁾ Extended data sets advised in Hogarth (2014) have been used for this study; and
- ⁽³⁾ All GPS data kindly provided by SONEL using updated ULR6a solutions (Santamaría-Gómez *et al.*, 2012) with 1 sigma error estimates advised.
- ⁽⁴⁾ The Galveston site is known to be affected by accelerated relative subsidence resulting from the removal of groundwater and hydrocarbons (Emery and Aubrey, 1991).

Systeme d’Observation Du Niveau Des Eaux Littorales (SONEL, 2016) vertical land movement data have been used to correct relative rates of sea level rise at each site to estimate geocentric rates. SONEL serves as the Global Navigation Satellite System (GNSS) data assembly

centre for the Global Sea Level Observing System (GLOSS). SONEL recently updated vertical land velocities for GNSS sites within approximately 15 km of long tide gauge records used in this study. In situations where several alternative SONEL stations were available to choose from, selection was based upon the Global Positioning System (GPS) site located closest to the tide gauge, where the GPS antennae is still active (refer Table 5.1).

Figure 5.1: Location of tide gauge records analysed.



Notes:

Each record is denoted by a Station ID with further details provided in Table 5.1.

5.3 Methodology

The methodology applied to the records in Table 5.1 to extract mean sea level and estimate associated velocities and accelerations are built into the ‘msltrend’ package (refer Section 4.6), but, can be broadly summarised in the following 4 key steps:

- ❑ **Step 1 - Gap Filling.** Msltrend is underpinned by SSA and thus times series must be complete in order to be decomposed. The iterative gap filling using SSA (Konrashov and Ghil, 2006) option has been preferred given the gap is reconstructed from SSA components in which the peak spectral frequency is ≤ 0.2 (alternatively, corresponding

to peak periods ≥ 5 years), thus utilising the principal spectral structures evident in the complete parts of the record. Each gap filling procedure has been visually inspected as a sanity check and where filling via SSA proves sub-optimal, alternative options of linear and spline interpolation, respectively have been employed.

- ❑ **Step 2 - Isolating Trend Using SSA.** Once gap filling has been completed, 'msltrend' decomposes the time series using 1D-SSA whereby the trend can be isolated by reconstructing only the components that possess distinctly "trend-like" characteristics. Trend components are automatically detected and reconstructed within 'msltrend' based on having a contribution threshold $\geq 75\%$ contained within frequency bins ≤ 0.01 (refer Section 4.3.3).
- ❑ **Step 3 - Estimating Velocity and Acceleration.** Readily estimated from the first and second derivatives, respectively of a cubic smoothing spline fitted to the trend determined via the SSA decomposition in Step 2 (refer Section 4.4).
- ❑ **Step 4 - Estimation of Errors.** Block bootstrapping techniques are used to randomly sample uncorrelated residuals which are added to the SSA derived trend and steps 2 and 3 repeated 10,000 times. Standard deviations are readily calculated from the extensive pool of outputted trends, velocities and accelerations (refer Section 4.6.2). All error margins in the analysis herein are estimated at the 95% confidence level (unless specified otherwise).

In addition to the above-mentioned, SONEL vertical land movement data (refer Table 5.1) have been applied to the time series of relative rates of sea-level rise in order to estimate geocentric rates.

An important aspect of the analysis is to determine whether more recent peak velocities and accelerations associated with mean sea level are statistically different (higher) than rates measured elsewhere over the course of the historical record. To do this, the statistical significance tests advised by Wolfe and Hanley (2002) have been applied at the 95% confidence level.

5.4 Results

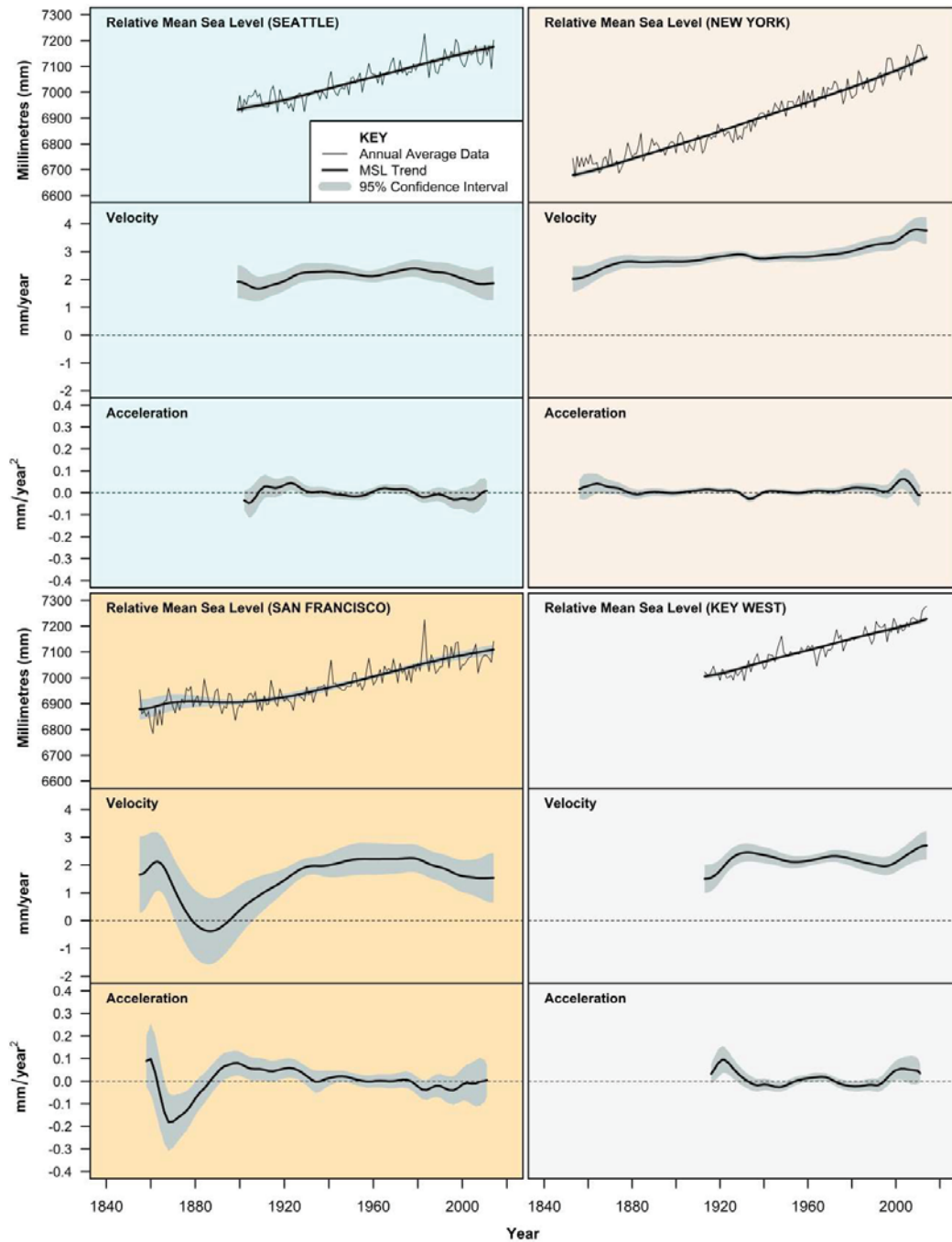
The analysis and outputs provide the means to examine real-time (or instantaneous) velocities and accelerations in greater detail than has been possible to date for the many long US tide gauge records. Figure 5.2 provides an example output from the analysis of four separate station records located around the margins of continental USA that are largely reflective of the regional temporal signatures of velocity and accelerations in relative mean sea level. It is clear that these velocities and accelerations are varying continuously over time.

In particular, the west coast records (Seattle and San Francisco) show evidence of the velocity peaking around 1980, then moderating gradually to present (2014). These distinctive features are consistent with the 1976 - 77 regime (or climate) shift over the Pacific Ocean (Miller *et al.*, 1994). Both records show similar temporal characteristics in the associated accelerations over the common period with no evidence of mean sea level acceleration. Another prominent feature evident in the very long San Francisco record is the levelling off (and slight fall) in mean sea level between 1878 and 1906. However, some caution is recommended in explicitly interpreting such temporal signatures owing to the location of this feature within the very early and somewhat problematic portion of the historical record (Breaker and Ruzmaikin, 2011; Hogarth, 2014), coupled with the fact there are no other Pacific Ocean 'buddy' stations to compare such signatures during this time horizon.

On the east coast, the relative signatures are starkly contrasting, with velocities continuing to rise over the course of the historical record to present, providing some evidence of an accelerating trend. The complete analysis of all the records in this manner provides the means to inspect spatial temporal patterns in greater detail than previously available.

Figure 5.3 provides a breakdown of the peak velocities and accelerations for each record and the time at which they occur. It is relevant to consider these charts simultaneously as velocity and acceleration are intrinsically linked as kinematic properties. For example, acceleration is required to increase velocity and conversely negative acceleration (or deceleration) is required to reduce velocity.

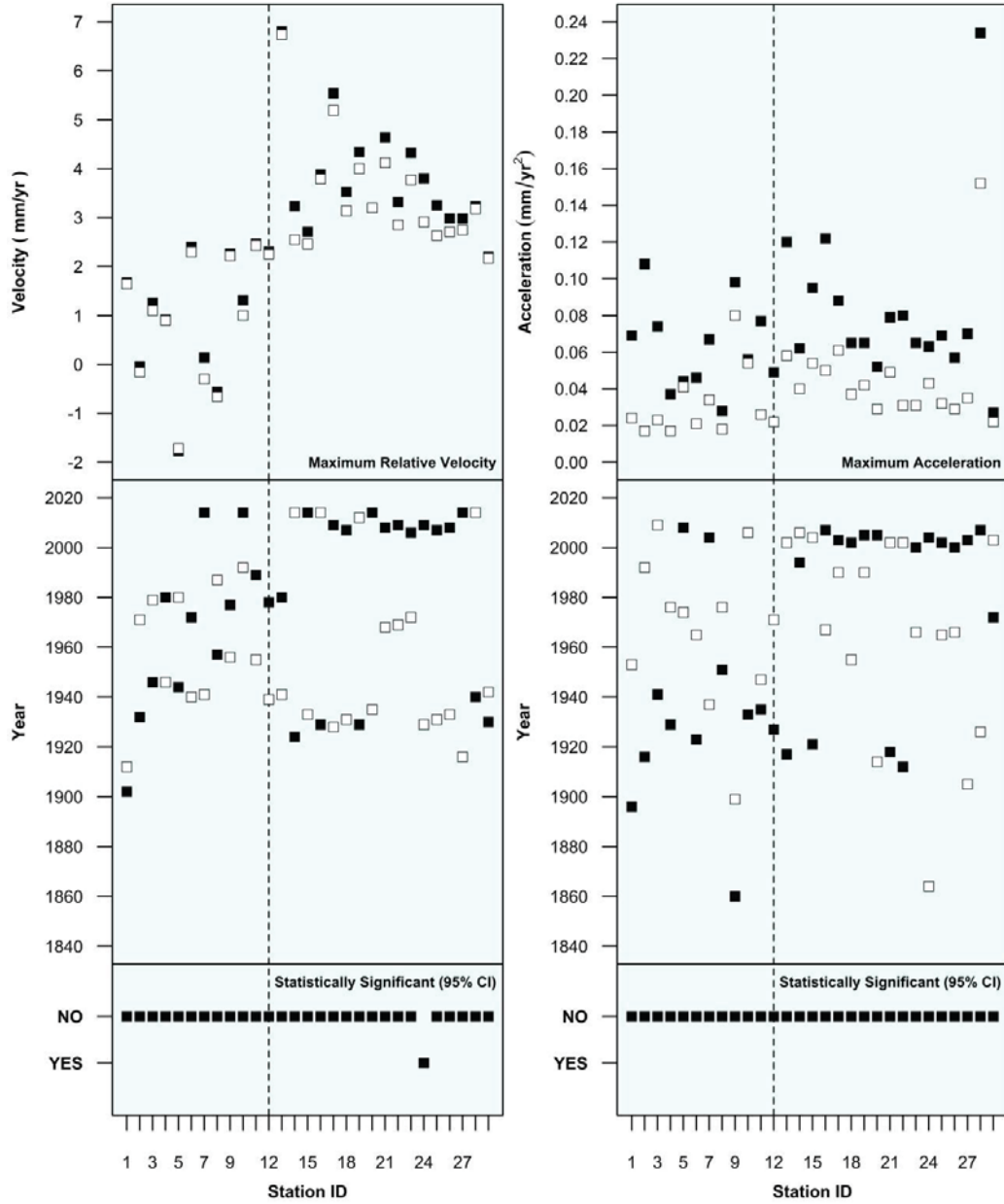
Figure 5.2: Temporal characteristics of mean sea level at selected sites (Seattle, San Francisco, New York, and Key West).



Notes:

Each site is depicted by a three-panel plot of mean sea level, velocity, and acceleration. The respective scales are identical for all stations for direct comparative purposes.

Figure 5.3: Peak estimates of velocity and acceleration for all stations.



Notes:

Peak metrics are denoted as filled boxes, while secondary peaks are denoted by clear boxes. The centre panels indicate the year in which the respective peaks occurred. A vertical dashed line corresponding to Station 12 (San Diego) denotes the spatial limit of the Central Pacific and west coast records. The bottom panel provides an indication as to whether or not the peak metric is statistically different (in this case higher) than all others in the context of the historical record at the 95% confidence level. Station ID references are summarised in Table 5.1.

From inspection of Figure 5.3, the following observations are apparent, including:

- ❑ lowest peak relative rates of velocity are distinctly confined to the Central Pacific and west coast margins;
- ❑ primary and secondary velocity peaks within the Central Pacific and west coast region are not dissimilar, with no clear temporal pattern to their timing (refer middle left panel);
- ❑ from Pensacola (ID=13) to Boston (ID=27), the primary peak in velocity is on average 13% higher than the secondary peaks observed. Further, moving east from Pensacola, there are clear temporal patterns to the timing of the peaks with the peak velocities occurring predominantly post 2006 and secondary peaks clustered in a band centred around 1930. Significant upward inflexions in sea level records are noted in Woodworth *et al.* (2009) coinciding with the period from 1920–1930 which was one of the main periods of sustained rise in global air and sea surface temperatures in the 20th century (Jones *et al.*, 2001);
- ❑ four station records have the maximum relative velocity occurring in 2014, at the end of the data record (Astoria, Los Angeles, Key West and Boston);
- ❑ mean maximum acceleration measured across all records is approximately 0.075 ± 0.041 mm/yr² (1σ) with no particular spatial patterns evident;
- ❑ timing of the respective primary and secondary acceleration peaks follow similar temporal signatures to the associated velocities (as expected). Peak accelerations in the Central Pacific and west coast margins predominantly occur between about 1920 and 1940, but along the east coast these peaks are generally confined to the period post 2000; and
- ❑ significantly, from an analysis of the peak velocities and accelerations for all records considered in this study, only the peak velocity observed at New York (which occurs near the end of the record) is statistically different (or higher) than peaks observed over the historical record (95% confidence level).

Another option for investigating subtleties of acceleration when the metrics are comparatively low is to consider the extent and temporal distribution of positive acceleration statistically different to zero (Figure 5.4). This analysis highlights the absence of acceleration along the west coast and the reasonably limited extent of sustained acceleration evident along the east

coast. Interestingly, for the stations analysed within the so-called ‘hotspot of acceleration’ north of Cape Hatteras (Sallenger Jr *et al.*, 2012), less than 21% of the data years from 1990 exhibit any positive acceleration that is statistically different to zero at the 95% confidence level.

Figure 5.4: Periods of positive acceleration (95% CI).

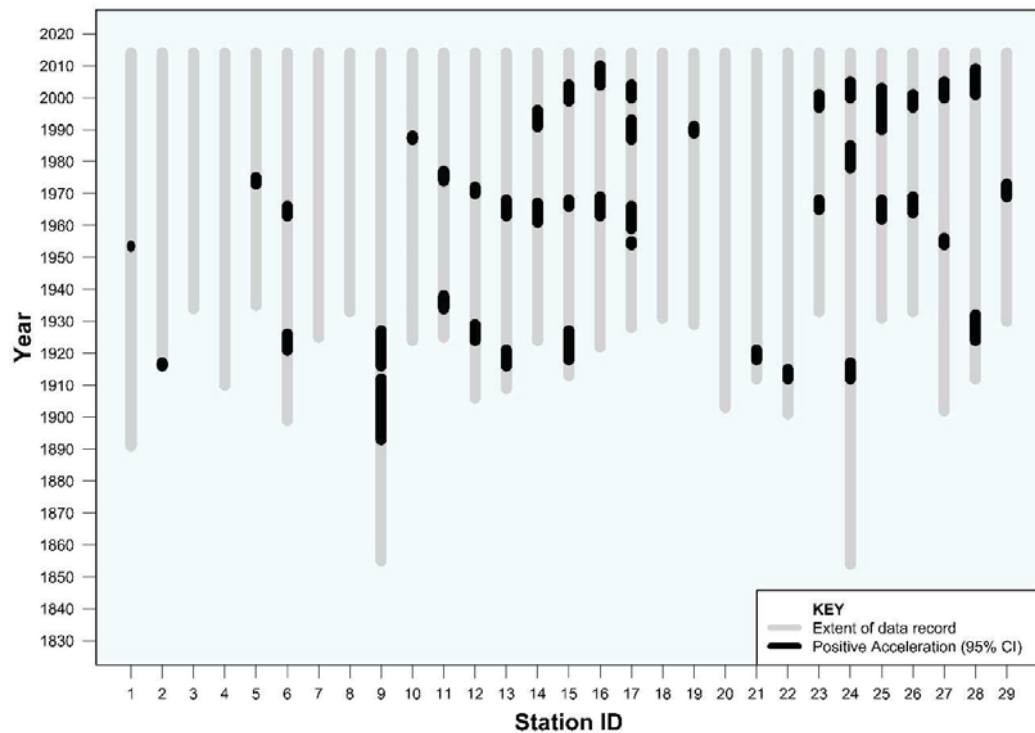
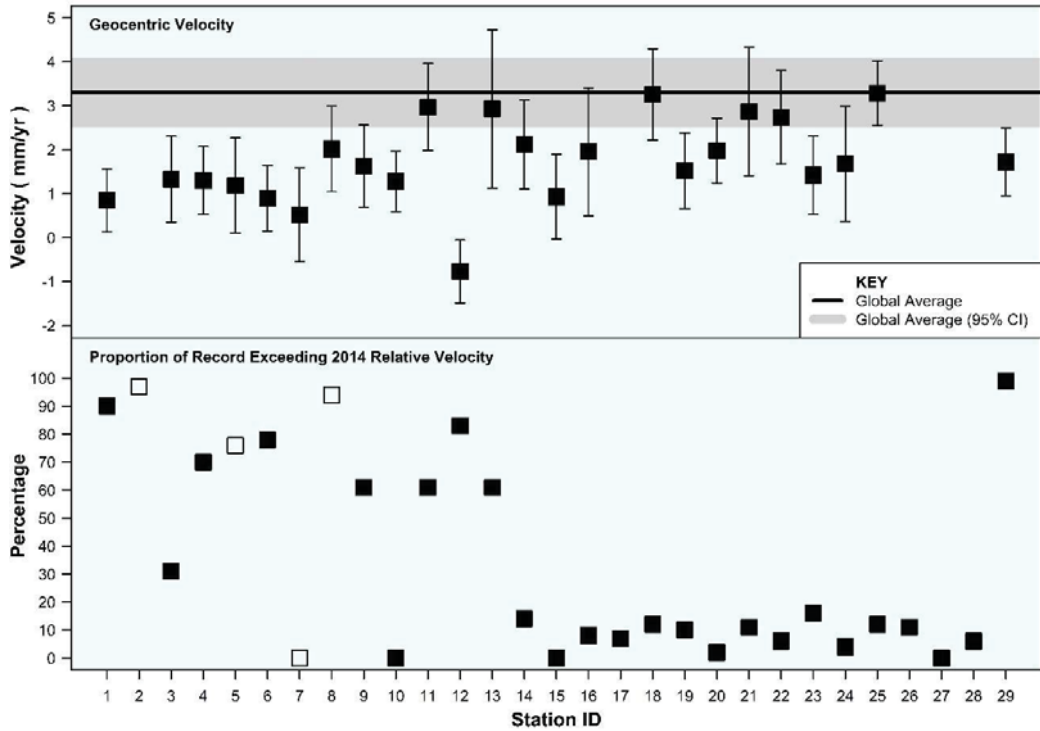


Figure 5.5 provides an appraisal of the current (2014) rate of geocentric sea level rise across the tide gauge network by correcting the relative velocity with GPS derived vertical land movement rates from SONEL (refer Table 5.1), noting that five records do not have an associated SONEL station. There are a number of key spatial features evident from this graphical analysis, including that the mean of the current (2014) geocentric velocity falls into three general bandings around the USA:

- 2.7 to 3.3 mm/yr (predominantly north-east);
- 1.5 to 2.2 mm/yr (predominantly east coast); and
- Less than 1.5 mm/yr (predominantly confined to the Central Pacific and north-west).

The spatial signature of current geocentric sea level rise around the USA is also clearly highlighted by the fact the average rate for the Central Pacific and west coast stations is 1.20 ± 0.45 mm/yr compared to the Gulf of Mexico and along the east coast where the average rate is some 80% higher at 2.19 ± 0.58 mm/yr (95% CI).

Figure 5.5: Estimates of Geocentric Rate of Sea-Level Rise (95% CI).



Notes:

Estimates based on real-time relative velocity derived from msltrend decomposition at the end of 2014 corrected by vertical land movement velocities provided by SONEL. Clear boxes in the bottom panel represent stations in which there is evident relative sea-level fall over the course of the record. Data sources and station ID references are summarised in Table 5.1.

Of particular interest, none of the geocentric velocities determined at the end of 2014 exceed the global average of 3.3 ± 0.4 mm/yr (Nerem *et al.*, 2010; University of Colorado, 2016) at the 95% confidence level. Further, some 8 of the 12 stations in the Central Pacific and west coast region and a further 4 stations along the east coast (Key West, Annapolis, Sandy Hook and Eastport) are lower than the global average (95% CI).

The bottom panel of Figure 5.5 is similarly quite instructive, highlighting that for the majority of records west of Galveston (ID=13), the current instantaneous velocity has been exceeded by 60% or more of the historical record, providing no genuine evidence of acceleration in mean sea level at these stations. However, from Pensacola (ID=14) heading east, near all records exhibit a current velocity exceeded by less than 16% of the historical record. This indicates the latter portions of these records are within the upper bracket of velocities recorded over the historical record, providing tangible evidence of recent acceleration in mean sea level in this region.

5.5 Discussion

Although extensive research has been undertaken into sea level rise, there remains considerable conjecture and scientific debate about the temporal changes in mean sea level and the climatic and associated physical forcings responsible for them (Watson, 2016c). One of the reasons for this is that ocean water level time series data from tide gauge stations are a complex amalgam of key physical contributors which include:

- ❑ **Factor 1:** land movement at the tide gauge site;
- ❑ **Factor 2:** dynamic influences of largely oceanographic, atmospheric or gravitational origins operating on differing temporal and spatial scales; and
- ❑ **Factor 3:** low amplitude signal of mean sea level rise driven by climate change influences (principally melting of snow and ice reserves bounded above sea level (directly adding water), and thermal expansion of the ocean water mass).

For completeness, it is worth noting that long relative sea level records from tide gauges might also contain inevitable datum shifts that have resulted from poor quality control or inadequate datum transfer in updating or relocating instrumentation. Whilst these issues can be very difficult to isolate, data archaeology, careful checking and reconstruction of long and suspect portions of records, are critical facets for improving mean sea level time series (e.g., Breaker and Ruzmaikin, 2011; Hogarth, 2014; Talke and Jay, 2013). The use of 'RLR' datasets from the PSMSL are custom designed for time series analysis purposes and provide the best insurance against these inadvertent complications.

5.5.1 Accounting for vertical land motions at tide gauge sites

Land motions embedded within tide gauge records are difficult contributions to resolve and isolate, in part because the general scale of vertical land motions (see Oostanciaux *et al.*, 2012) and sea level rise trends due to climate change influences (factor 3 above) observed over the 20th and early 21st Centuries, are often of similar scale (although the sign may differ). In attempting to convert ‘relative’ to ‘eustatic’ estimates of sea level rise, the majority of contemporary studies make some allowance for land movements via the application of site specific estimates of long timescale Glacial Isostatic Adjustment (GIA) from the various models available (e.g., Lambeck *et al.*, 1998; Peltier, 2004; Tushingham and Peltier, 1991).

However, GIA models provide only the broadest scale resolution of vertical land motions (VLM) at local scales. Local processes associated with tectonics, volcanism, sediment compaction, and subsurface mineral and water extraction are often of significance and generally not accounted for in the GIA models (Zervas *et al.*, 2013). Tide gauges situated on highly urbanised and densely populated shorelines are becoming increasingly affected by a wide range of anthropogenic processes that predominantly result in localised subsidence (Oostanciaux *et al.*, 2012). The advent of the GNSS has provided the opportunity to continuously measure the total contributions of all land movement processes where GPS recording instruments have been installed enabling estimates of ‘geocentric’ mean sea level (to a fixed reference point). The drawback of the comparatively recent development of these measuring technologies is that maximum record lengths are only around 20 years.

Whilst updated vertical velocities advised by SONEL (ULR6a solutions) are based on a linear regression of the GNSS time series (Santamaría-Gómez *et al.*, 2012), it is evident from inspection that these time series are not necessarily linear. Over time as the length of these valuable records increase, there might be scope to enhance the resolution of the non-linear trend of the GPS derived vertical velocities to improve real-time (say annual resolutions) that will further enhance the accuracy of locally derived corrections for ‘geocentric’ mean sea level.

Another factor highlighted previously by Wöppelmann and Marcos (2012), relates to the common situation where the geodetic connection between the GPS antennae and tide gauge is absent. Under these circumstances it is simply assumed that vertical land movement sensed by the GPS antenna corresponds to the actual land movement affecting the tide gauge record

when the GPS antenna is distant from the tide gauge (e.g., Bevis *et al.*, 2002). This is a ubiquitous problem highlighted in the current study whereby only 4 SONEL GPS records are within 200 m of the tide gauge of interest. A further 16 SONEL GPS records are located in excess of 6 km from the tide gauge, diminishing the inferred representativeness of land motion factors directly at the tide gauge. It is hoped that over time, the long and valuable tide gauge records examined in this study will be better augmented with co-located GPS antennae to more accurately measure localised vertical land motions directly at the tide gauge.

For sea level studies, it is commonly assumed that vertical land motions are generally small and occur in near linear fashion, in which case estimates of acceleration remain unaffected. Whilst geological time scale influences such as GIA will be approximately linear over the timescale of an available tide gauge record, the anthropogenic influences contributing to subsidence in heavily developed coastal margins might not necessarily perpetuate in a linear manner. The latter circumstance, if not properly accounted for, will contaminate real-time estimates of acceleration in the relative mean sea level signal. This facet heightens the necessity of continuing to improve the resolution of GNSS records which are slowly increasing in length to become more useful for time series analysis of mean sea level.

5.5.2 Accounting for dynamic influences contained within tide gauge time series

Assuming that vertical land motions are resolvable and constant, the next step to improving acceleration lies in improving separation of the low amplitude signal of mean sea level rise from the contaminating dynamic influences (factor 2 above) and other residual, unaccounted for artefacts embedded within the time series data (otherwise referred to as noise). It is critical to remove these dynamic influences because these are considered to be ostensibly stationary; that is, they cause the water surface to respond on differing scales and frequencies within generally defined limits, but do not change the volume of the water mass, which is the key signal of interest for mean sea level researchers (Watson 2016a). The resolved signal of mean sea level rising over time is of itself, a complex artefact of the changing physics and mass of the ocean water body.

These contaminating influences which persist on inter-annual to decadal (and longer) timescales ostensibly result from winds driven by climate modes (refer Section 2.4.4) and are often orders of magnitude larger in scale than the low amplitude signal of mean sea level rise,

which is the key artefact of interest. The necessity to remove these influences from the data to enhance acceleration estimates is well noted in the literature (Calafat and Chambers, 2013; Chambers *et al.*, 2012; Douglas, 1992). A key facet of the ‘msltrend’ package used to decompose the records within this study, is the capability of the underpinning singular spectrum analysis algorithm to separate out these complex oscillatory signals with time-varying amplitudes and noise from the low amplitude and low frequency signal of mean sea level rising over time.

5.5.3 Measuring mean sea level acceleration

Since the key published works on mean sea level acceleration in the early 1990’s (Douglas, 1992; Woodworth, 1990), there has been almost universal application of the quadratic model fit to estimate acceleration from individual, regional and global ocean water level records (e.g., Boon, 2012; Boon and Mitchell, 2015; Church and White, 2006, 2011; Douglas, 1997; Haigh *et al.*, 2014; Hannah, 1990, 2004; Hay *et al.*, 2015; Houston and Dean, 2011a, 2013; Jevrejeva *et al.* 2006, 2008, 2014; Maul and Martin, 1993; Spada *et al.*, 2014; Wahl *et al.*, 2013; Watson, 2011; Woodworth *et al.*, 2014; Wöppelmann *et al.*, 2006).

The simple quadratic model is based on a linear term coupled with an acceleration term, in which the acceleration is constant resulting in a linearly increasing rate of rise over time. The simplicity of its application to sea level records, coupled with the direct single measure of acceleration (double the quadratic term) have resulted in its widespread application, despite the evident limitations or suitability of such a model fit to the task at hand.

What is clear from this study is that all real-time velocity time series associated with mean sea level at each site, are distinctly non-linear, in turn reflective of associated acceleration varying over time, directly at odds with the quadratic model assumptions. The same can also be said of the various global mean sea level reconstructions proposed within the literature and commonly used by sea level researchers (e.g., Church and White, 2011; Hamlington *et al.*, 2011; Hay *et al.*, 2015; Jevrejeva *et al.*, 2006, 2014; Meyssignac *et al.*, 2012a; Ray and Douglas, 2011; Wenzel and Schröter, 2014).

Long records and global mean sea level reconstructions contain well recognized signatures of positive and negative ‘inflexions’ (Woodworth *et al.*, 2009) as well as key influences driven

ostensibly by climate modes (Cazenave *et al.*, 2012; Fasullo *et al.*, 2013; Hamlington *et al.*, 2013). As a result, acceleration determined through simple quadratic fits will be unduly influenced by the particular time slice chosen (Rahmstorf and Vermeer, 2011). The considerable vulnerability of the quadratic method to the time period selected is further highlighted in Houston (2016). Much of the considerable scientific debate concerning the existence (or otherwise) of a measurable acceleration in mean sea level records (for details refer Visser *et al.*, 2015; Watson, 2016a) rests almost entirely with the over-use of the unduly simple and ill-suited quadratic model to estimate accelerations in mean sea level records.

Alternative approaches to inferring acceleration such as changes in the average velocity between differing time slices (e.g., Bindoff *et al.*, 2007; Calafat and Chambers, 2013; Hansen *et al.*, 2012; Kemp *et al.*, 2009; Merrifield *et al.*, 2009; Sallenger Jr *et al.*, 2012) are also extremely limited given they are unable to capture the necessary temporal changes evident in the mean sea level velocity and acceleration time series.

The real-time mean sea level velocity and acceleration time series associated with the respective tide gauge records provide a more transparent and robust basis upon which to investigate accelerations.

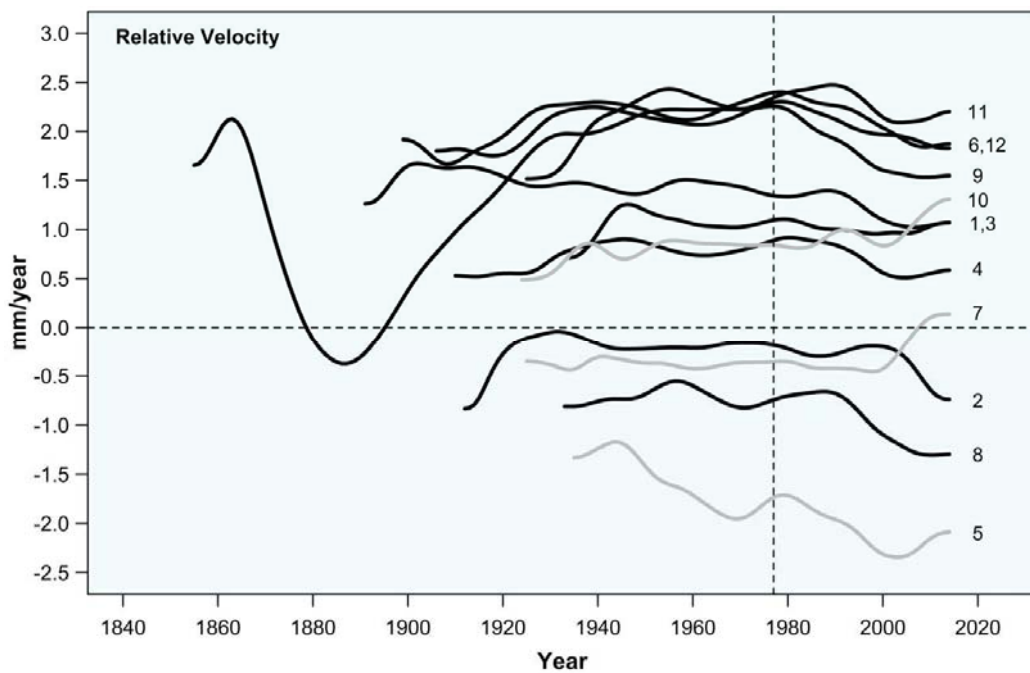
5.5.4 Recent literature concerning MSL acceleration around the USA

Over recent years there have been a range of published papers relating to acceleration determined from tide gauge records around mainland USA, in particular Houston and Dean (2011a), Bromirski *et al.* (2011), Boon (2012); Boon and Mitchell, 2015 and Sallenger Jr *et al.* (2012). Numerous additional papers have been dedicated to the specific role that oceanographic processes and climate mode influences might be playing on measured sea level trends and accelerations (e.g., Bingham and Hughes, 2009; Di Lorenzo *et al.*, 2008; Ezer *et al.*, 2013; Higginson *et al.*, 2015; Kopp, 2013; Park and Sweet, 2015; Piecuch *et al.*, 2016; Qiu, 2002; Sallenger Jr *et al.*, 2012; Woodworth *et al.*, 2014; Yin and Goddard, 2013).

Across the Central Pacific and west coast USA, observations suggest a lower than global average rise in mean sea level post the well documented 1976-77 regime (or climate) shift over the Pacific Ocean (Miller *et al.*, 1994). Bromirski *et al.* (2011) suggests the suppression in mean sea level across this region results from a dynamical steric response of North Pacific

eastern boundary ocean circulation to a dramatic change in wind stress curl evident after the regime shift. Bromirski *et al.* (2011) also suggests that if a recent change in wind stress patterns (evident since 2008) persists, an associated regime shift to the Pacific Decadal Oscillation cold phase may result with a concomitant resumption of relative sea level rise along the west coast approaching or exceeding the global mean sea level rise rate. Figure 5.6 indicates that the majority of station records analysed in the Central Pacific and west coast region show continued lowering of the relative velocity in mean sea level to the end of 2014 post the 1976-77 regime shift. The ‘imminent’ acceleration foreshadowed by Bromirski *et al.* (2011) has not materialised in the records at this point in time. Boon and Mitchell (2015) observe a similar finding.

Figure 5.6: Relative velocity time series for Central Pacific and west coast U.S. station records.



Notes:

A vertical dashed line denotes the commencement of the Pacific regime shift (Miller *et al.*, 1994). Grey time series denote those indicating a noticeable increase in velocity post 2000 (Neah Bay, Washington; Astoria; and Los Angeles). Numbers beside the time series denote the Station “ID” (Refer Table 5.1 for details).

By contrast on the east coast, much gravitas has been given to the so-called ‘hotspot’ of acceleration in the mid-Atlantic region, north of Cape Hatteras. Sallenger Jr *et al.* (2012) suggested evidence of recently accelerated SLR in a unique 1,000-km-long ‘hotspot’ on the

highly populated North American Atlantic coast north of Cape Hatteras and show that it is consistent with a modelled fingerprint of dynamic SLR with rate increases of the order of 3 – 4 times higher than the global average.

Attention has centred on the underpinning oceanographic processes driving this recent pronounced sea level acceleration. The Gulf Stream (GS) system drives the ocean surface circulation on the Western North Atlantic (Higginson *et al.*, 2015), resulting in a distinct ocean surface level ‘tilt’ which persists along the inshore edge of the GS downward from Florida to Cape Hatteras estimated at 2.0 ± 0.4 cm/degree of latitude (Sturges, 1974). It has been generally proposed that a weakening Atlantic Meridional Overturning Circulation (AMOC) driving a slowing in the GS system is producing the accelerated sea level rise north of Cape Hatteras over the past 20 years (Bingham and Hughes, 2009; Ezer *et al.*, 2013; Goddard *et al.*, 2015; Yin and Goddard, 2013).

Higginson *et al.* (2015) note other recent studies (Andres *et al.*, 2013; Rossby *et al.*, 2014) that cast doubt on this theory with in-situ measurements showing no change to the strength of the GS downstream of Cape Hatteras over the noted period of sea level acceleration. Woodworth *et al.* (2014) finds that nearshore wind forcing on the shelf dominate the inter-annual sea level variability along the east coast of the USA, with winds in particular, capable of producing low frequency accelerations in mean sea level comparable to those observed by the tide gauge network. Woodworth *et al.* (2014) question the AMOC fingerprint (Boon, 2012; Sallenger Jr *et al.*, 2012) driving such accelerations, noting that levels have declined again since 2010 at many locations, as can be seen from the latest data on the PSMSL website. Piecuch *et al.* (2016) highlight the limitations and skill levels of various approaches to reconciling the contributory processes associated with recent sea level rises north and south of Cape Hatteras, acknowledging considerable work remains to be done.

Kopp (2013) provides discussion on contributory factors along the mid-Atlantic coast that would result in regional and local sea levels differing from the mean global sea level. This work notes that East of the Fall Line, which passes close to New York City and Washington, bedrock is overlain by the Mesozoic and Cenozoic sediments of the Coastal Plain, which can subside due to natural compaction and therefore experience a faster long-term rate of SLR. From a comparison of sea-level records with climatic and oceanographic indices, Kopp (2013)

concluded that observed changes may at least be partially accounted for by known sources of variability, suggesting that neither the magnitude of the phenomenon, nor its rate of change, nor its acceleration appear to be beyond the bounds of 20th-century variability.

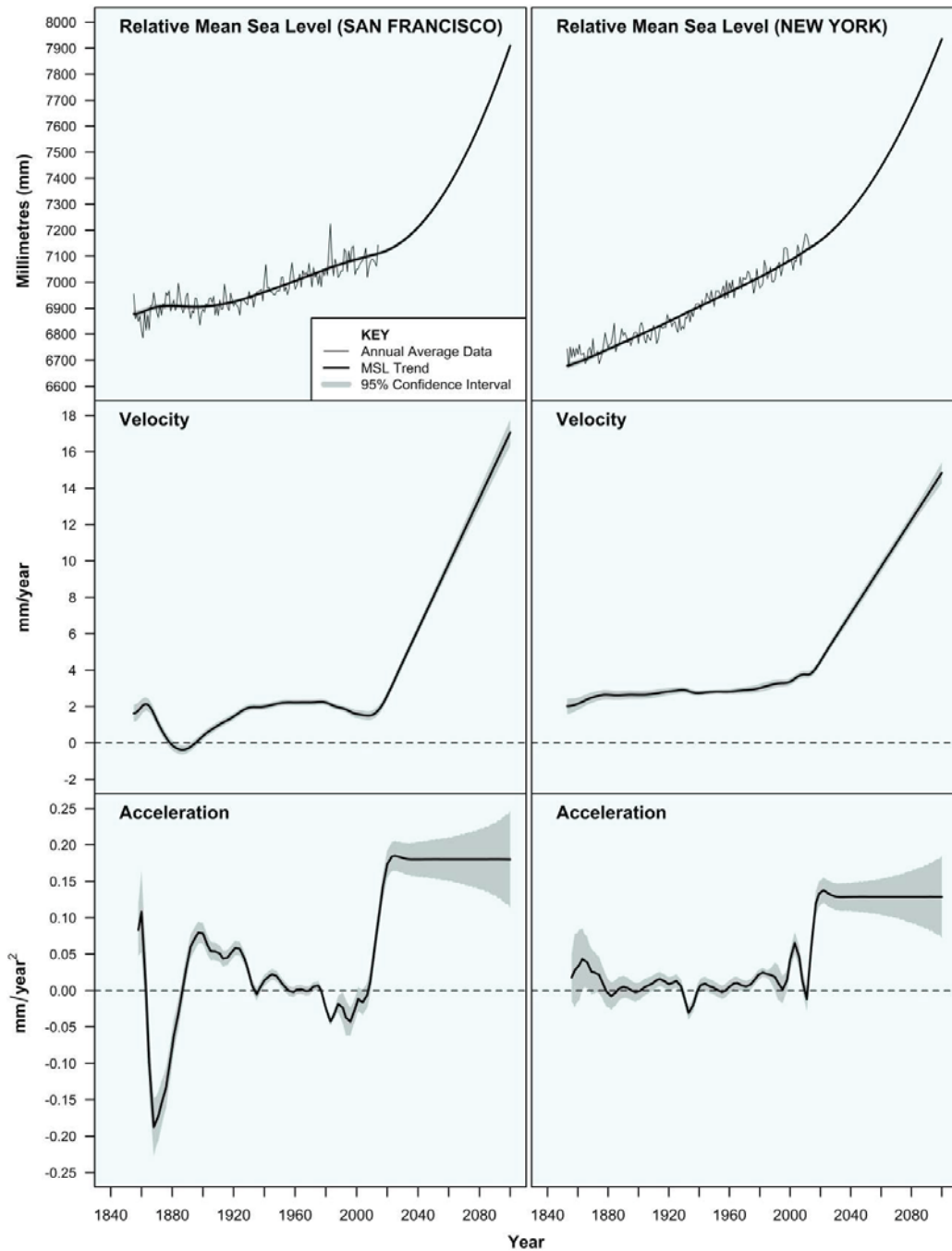
From a longer-term perspective, a range of detailed paleo examinations centred on the US east coast have attempted to reconcile recent rates of relative sea level rise over the instrumental era with rates approximated over the past couple of millennia. Analysis of geological data at Connecticut (Kemp *et al.*, 2015), New Jersey (Kemp *et al.*, 2013), North Carolina (Kemp *et al.*, 2011) and Florida (Kemp *et al.*, 2014), conclude that historic rates of rise commenced around 1850 - 1890 and that it is virtually certain the rate of 20th century relative sea level rise is faster than any of the preceding 20+ centuries. Similar conclusions have recently been observed on a global basis (Kopp *et al.*, 2016).

5.5.5 Reconciling historical and future projected MSL accelerations

Whilst the 20th century rise in relative mean sea level appears unprecedented along the US east coast over the past couple of millennia (Kemp *et al.*, 2015), the scale of velocities and accelerations measured within this analysis (e.g., Figure 5.2) remain lower than those associated with forecasts from physics-based climate models over the course of the 21st century and beyond (Church *et al.*, 2013a; IPCC, 2013b). Under forecasts of high simulated radiative (or external) forcing (RCP8.5 scenario), the current rate of global averaged sea level rise of 3.3 ± 0.4 mm/yr (Nerem *et al.*, 2010; University of Colorado, 2016) is expected to increase to rates of the order of 8 - 16 mm/yr by 2100 (refer Chapter 1, Figures 1.1 and 1.2).

Figure 5.7 provides a visual comparative analysis of how the velocity and acceleration time series might change at San Francisco and New York, based on a mean sea level rise of 800 mm from present (2014) to 2100. Under such a scenario, which assumes simple equations of motion and uniform acceleration, the necessary and significant changes in velocities and accelerations compared to those measured over the historical record, are likely to be readily apparent well within the next 20 years. For example, velocities and accelerations at San Francisco will become statistically different (at the 95% confidence level) from the rest of the historical record at approximately 2021 and 2024, respectively. For the New York record, these timeframes reduce to 2017 and 2019, respectively.

Figure 5.7: Indicative implications of projected sea-level rise of 800 mm at San Francisco and New York from end of 2014 to 2100.



Notes:

Projections based on simple equations of motion with uniform acceleration. Error margins noted are 95% confidence levels.

One should caution these forecasts are highly idealistic and preliminary. However, they do provide a sense of perspective regarding the timing of necessary changes to the kinematic properties of mean sea level at these locations, in order to give effect to such projections.

5.6 Conclusions

The implications of sea level rise, particularly the much larger projected rates of rise under future climate change modelled scenarios (IPCC, 2013b) are profound with far reaching social, economic and environmental implications (amongst others) foreshadowed over the course of the 21st century and beyond. These are well described for the US context in Melillo *et al.* (2014) and Houser *et al.* (2015).

Mean sea level records are pivotal data sources as they provide one of the key proxies by which to measure the impact of a changing climate system. With the very ethos of the climate change science and projection modelling underpinned by accelerations in mean sea level (refer Chapter 1), numerous works in the scientific literature have been dedicated to measuring accelerations that might provide improved instruction on the extent to which external (climate change) forcings are manifesting to assist strategic planning, adaptive responses and policy development in readiness for the challenges ahead.

Douglas (1992) provided the initial attempt at considering whether acceleration in ocean water levels aligned with the primitive sea level forecast models available at the time, concluding *'there is no evidence of an acceleration effect in sea level in the historical record that is in any way comparable to that associated with most global warming predictions for the future.'* The ubiquitously simple quadratic approach to estimate sea level acceleration used in the early studies of Woodworth (1990) and Douglas (1992) has been substantially overused by a following generation of researchers despite the inherent limitations of this simple mathematical model approach. The 'msltrend' package and associated methods applied in this study to enhance estimates of trend, real-time velocity and acceleration in the relative mean sea level signal are long overdue, but welcome advancements for improving sea level research.

This study presents a fresh approach to considering acceleration that overcomes the limitations of other applied methodologies (refer Section 5.5.3) that have largely proven inadequate in charting the subtle temporal changes in the characteristics of mean sea level.

The comparatively low time varying velocities and associated accelerations evident over the period of historical records deem that acceleration is unwisely measured as a simple metric. Until such time as the apparent real-time velocities and accelerations in the MSL signal are sufficiently large not to be obscured by complex influences inducing decadal to multi-decadal variability and other background noise, the search for accelerations in these records require more intuitive, diagnostic considerations.

For example, the search for acceleration is perhaps more practically inferred by considering whether or not peaks in the instantaneous velocity and acceleration time series are increasing, becoming more sustained or statistically abnormal (or different) over time in the context of the historical record (Watson, 2016a). This type of approach will continue to be important until the extent of sea level rise (due to climate change) is sufficient to be statistically differentiated from the remnant historical record with widespread spatial coherence.

From the detailed analysis undertaken herein, there are a number of key findings including:

- ❑ although sea level has risen around continental USA over the period of available tide gauge records (1853 - 2014), clear and differing spatial signatures in sea level rise have emerged between the Central Pacific and west coast compared to those within the Gulf of Mexico and along the east coast;
- ❑ no evidence of acceleration in mean sea level across the Central Pacific and along the west coast of the USA to the end of 2014;
- ❑ subtle evidence of a more recent acceleration in mean sea level within the Gulf of Mexico and along the east coast of the USA which could be inferred from a range of differing diagnostic approaches espoused within this research, including that peak instantaneous velocities within these margins have tended to occur post 2006. However, there is no evidence (at the 95% confidence level) of instantaneous velocity and acceleration peaks post 2000 that are abnormal or higher than secondary peaks occurring elsewhere over the length of the historical records available (with the sole exception of the peak instantaneous velocity at New York near the end of the record);
- ❑ of the 2913 station years of records analysed, less than 9% exhibited a positive acceleration statistically different to zero (95% CI). Of the stations analysed within the

so-called 'hotspot of acceleration' north of Cape Hatteras, less than 21% of the data years from 1990 exhibit a positive acceleration statistically different to zero (95% CI);

- ❑ none of the geocentric velocities determined at the end of 2014 exceed the global average rate of 3.3 ± 0.4 mm/yr (Nerem *et al.*, 2010; University of Colorado, 2016) at the 95% confidence level. Some 8 of the 12 stations in the Central Pacific and west coast region and a further 4 stations along the east coast (Key West, Annapolis, Sandy Hook and Eastport) are lower than the global average (95% CI); and
- ❑ current (2014) geocentric sea level rise around the USA highlights the spatial fingerprint of the sea level rise phenomena. The average rate for the Central Pacific and west coast stations is 1.20 ± 0.45 mm/yr compared to the Gulf of Mexico and along the east coast where the average rate is some 80% higher at 2.19 ± 0.58 mm/yr (95% CI).

These findings are particularly poignant given the various recent published works alluding to a so-called 'hotspot' of accelerated sea level rise, particularly along the east coast margin north of Cape Hatteras. Clearly considerable contentions exist concerning the underpinning mechanics responsible for driving recent increases in the rate of mean sea level that have been measured along this stretch of coastline (e.g., Higginson *et al.*, 2015; Kopp, 2013). It might be probable that the contributory influences have derivations with oceanographic, geological and climate change induced origins. However, nothing in the analysis contained herein hints at recent increases in velocities or accelerations within this region that are outside the natural range of these characteristics measured from the tide gauge time series available (at the 95% confidence level).

It is possible that the recent increase in instantaneous velocities and accelerations within the Gulf of Mexico and along the east coast of the USA might signal the onset of large projected sea level rises due to climate change forecasts over the course of the 21st century (and beyond). For example, 4 of the 29 station records analysed indicate the peak instantaneous relative velocities occurring in 2014, at the end of the available data record (Astoria, Los Angeles, Key West and Boston). However, whilst the accelerated climate change influence is not yet statistically evident in these records, depending on the climate change trajectory, it is highly likely that such changes will take at least 15 - 20 years to manifest in the network of tide gauge records examined within this analysis.

When investigating temporal characteristics of mean sea level it is imperative to make use of the longest, quality controlled records available. This analysis has benefitted from the use of recently extended data sets for the USA (Hogarth, 2014; Talke and Jay, 2013). The techniques employed within this research form an integral part of the evolutionary process by which to measure accelerations in mean sea level with improving robustness and consistency.

5.7 Acknowledgements

I would like to acknowledge the publicly available data archives of the PSMSL and the extended data sets kindly provided by Peter Hogarth that have been used for this study. Similarly, I would like to extend my appreciation to the SONEL data centre for kindly providing the updated ULR6a solutions used to estimate geocentric sea level rise and acknowledge Professor Bob Kopp (Department of earth and Planetary Sciences, Rutgers University, USA) and Dr James Houston (Former Director, Engineer Research and Development Center, USACE) for suggestions that improved this aspect of the study program and associated published paper (Watson, 2016e).

Chapter 6

Application of “msltrend” Analytical Software Package to the Data Rich Margins of Europe

Synopsis: This chapter supplements the detailed analysis of the long USA records (Chapter 5) using the same analytical framework and methodology but, applied to the extensive network of European tide gauge records which encompass a range of complex geophysical and oceanographic settings. This work has significant regional and global implications given that some 28 of the 30 longest records in the Permanent Service for Mean Sea-level (PSMSL) global data holdings are European, extending as far back as 1807 (Brest, France). Key findings are that at the 95% confidence level, there is no consistent or compelling evidence (yet) that recent rates of rise are higher or abnormal in the context of the historical records available across Europe nor is there any evidence that geocentric rates of rise are above the global average. It is likely a further 20 years of data will distinguish whether recent increases are evidence of the onset of climate change induced acceleration.

Publication VI

Watson, P.J., 2017. Acceleration in European Mean Sea Level? A New Insight Using Improved Tools. *Journal of Coastal Research*, 33(1), pp.23-38.

Declaration

I certify that this publication was a direct result of my research towards this PhD, and that reproduction in this thesis does not breach copyright regulations.

Phil J. Watson [Candidate]

6.1 Introduction

Global analysis suggests that coastal population growth and urbanisation rates are outstripping the demographic development of the hinterland, driven by rapid economic growth and coastward migration (McGranahan *et al.*, 2007; Neumann *et al.*, 2015; Smith, 2011). Based on population assessments in 2000, it was estimated that the global population living within the Low Elevation Coastal Zone (LECZ, below 10m above mean sea level) was of the order of 625 million, of which 50 million were estimated to reside in Europe (Neumann *et al.*, 2015).

The *ClimateCost Project* undertaken for the European Union (Watkiss, 2011) provides a sobering economic appraisal of the threat from sea level rise and the costs and benefits of adaptation over the course of the 21st century. For example, assuming no adaptation, it is estimated that under a medium to high greenhouse gas emission scenario (A1B: Meehl *et al.*, 2007) that flooding along with other impacts of sea-level rise (e.g., shoreline recession) will lead to annual damage costs across Europe of up to €11 billion for the 2050s, rising to €25 billion by the 2080s (Brown *et al.*, 2011). Flooding more generally will of course be substantially exacerbated by forecast sea-level rise into the future, foreboding an increasingly ominous threat from natural disasters (Watson, 2016e).

Some 28 of the 30 longest records in the PSMSL global data holdings are European, extending as far back as 1807 (Brest, France). Such records provide the world's best time series data with which to examine how kinematic properties of the trend might be changing over time. This chapter supplements the detailed analysis of the long USA records (Chapter 5) using the same analytical framework and methodology but, applied to the extensive network of European tide gauge records.

This chapter provides an updated appraisal of acceleration in mean sea level records around Europe through use of 'msltrend' (Watson, 2016b, refer Section 4.6) within the R Project for Statistical Computing (R Core Team, 2016). The outputs of this research tool provide a more consistent, transparent appraisal of acceleration in mean sea level records around Europe; overcoming many of the evident shortcomings from the wide body of scientific literature on this topic (refer Section 5.5).

6.2 Physical Setting

Whilst the extensive quantum of quality European relative mean sea-level time series data sets are invaluable for sea-level research, one must also have an understanding of the complex geophysical (and other factors) embedded within the data. The study area (refer Figure 6.1, 6.2 and 6.3) encompasses coastlines on major water bodies including:

- ❑ The **North Atlantic Ocean** between the Strait of Gibraltar, Spain along the open coast to Murmansk Oblast in the Barents Sea. This area includes the adjacent water bodies of the Gulf of Cadiz, Bay of Biscay, English Channel, Celtic Sea, Irish Sea, North Sea, Kattegat and Norwegian Sea;
- ❑ The **Mediterranean Sea** is a semi-enclosed water body of approximately 2.5 million km² connected to the Atlantic Ocean via the Strait of Gibraltar which narrows to a mere 13 km. Owing to this constriction, the tides are low compared to that of the Atlantic (Pugh, 1996). The Mediterranean Sea is divided into two large basins separated by the Sicilian Channel and the Messina Strait, with both basins extending to depths of more than 4 km in places (Arabelos *et al.*, 2011). The Mediterranean is connected to the Black Sea via the Strait of Bosphorus and artificially to the Red Sea via the Suez Canal. Some of Europe's largest rivers drain directly or indirectly into the Mediterranean including the Nile (Egypt), Po (Italy), Ebro (Spain) and Rhône (France);
- ❑ The **Black Sea** is the world's largest inland sea covering an area of 436,000 km² exchanging water with the Mediterranean Sea via the Bosphorus and Dardanelles Straits (Avsar *et al.*, 2016), and the Sea of Azov through the Kerch Strait (Stanev, 2005). At any given time, the level of the Black Sea is principally governed by complex interrelationships between the local water budget (precipitation vs evaporation), eustatic sea-level variations and water exchange through the straits and continental discharges onto the northern coast via the Danube, Dniiper and Don Rivers which drain almost one third of the entire land area of continental Europe (Bakan and Büyükgüngör, 2000). A permanent feature is an upper layer circulation driving the Rim Current, encircling the entire Black Sea and forming a large-scale cyclonic gyre (Korotaev *et al.*, 2003). This circulation induces a rise of sea level toward the coast where velocities increase and conversely sea level decreases in the deeper margins of the Black Sea (Kubryakov and Stanichnyi, 2013). The amplitude of sea level variation in space depends on seasonal influences, ranging from 25 to 40 cm (Korotaev *et al.*, 2003). Volkov and

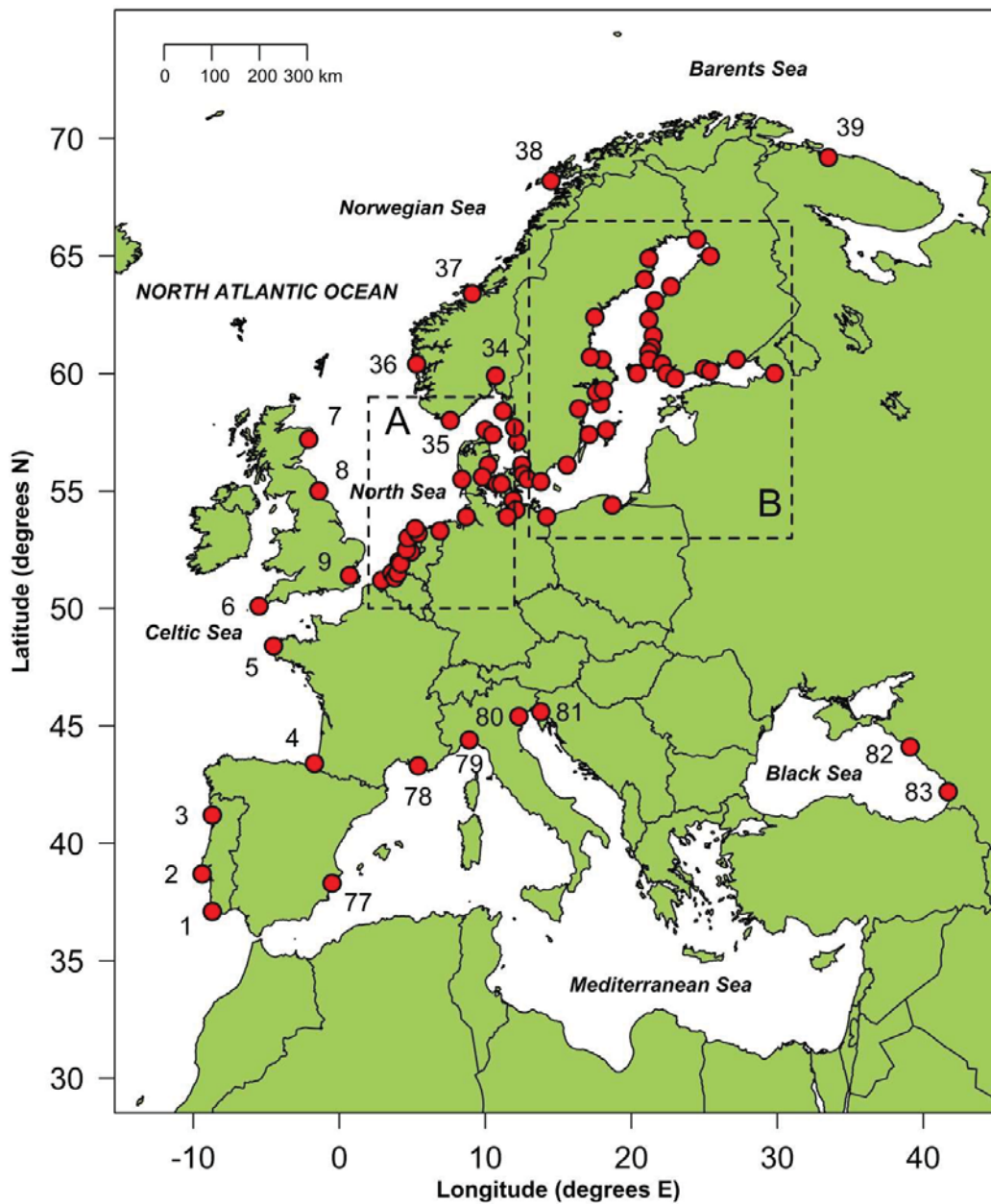
Landerer (2015) note that non-seasonal sea level time series in the Black and Aegean Seas (eastern Mediterranean) are significantly correlated, with the Black Sea lagging by around 1 month; and

- The **Baltic Sea** is another semi-enclosed water body of approximately 350,000 km² connected to the North Sea through the Kattegat and via the three Danish Straits (Øresund, Great Belt and Little Belt) between Sweden and Denmark. The Gulf of Bothnia defines the northernmost extent the Baltic Sea, whilst the Gulf of Finland defines the easternmost extremity, extending all the way to Saint Petersburg, Russia. Based on the limited exchange with the open ocean, the Baltic Sea is virtually tideless but receives considerable freshwater inflows from over 200 river systems (Leithe-Eriksen, 1992). The mean depth of the Baltic is around 50 m, however, the Gulfs of Bothnia and the central Baltic can be up to 500 m deep (Leppäranta and Myrberg, 2009). Ice typically covers the sea in winter months in the Gulfs of Bothnia, Finland and Riga, and in sheltered bays and lagoons (Kullenberg, 1981).

Whilst these water bodies exhibit quite different physical characteristics, the associated land masses around Europe embody distinctive vertical land motions which are embedded within relative sea level records recorded at tide gauges. The most prominent of which are the high rates of post-glacial rebound experienced within the Fennoscandian Region of northern Europe (comprising Sweden, Finland, Norway and parts of Russia) which are amongst the highest rates globally predicted by the ICE-6G(VM5a) model (Argus *et al.*, 2014; Peltier *et al.*, 2015). Land uplift rates around the Baltic Sea margins range from zero in the south to 9 mm/yr in the north (Leppäranta and Myrberg, 2009). Elsewhere across Europe, areas are known to be subsiding such as the eastern margins of the Black Sea and around the southern English, Dutch and German coastlines (Bungenstock and Schäfer, 2009; Minshull *et al.*, 2005, Shennan and Woodworth, 1992; Wahl *et al.*, 2013).

The Mediterranean and Black Sea regions exhibit a complex range of concomitant land movement processes including glacial isostatic adjustment, subsidence due to sediment compaction in key river delta areas such as the Po, Rhône, Ebro and Danube (Ericson *et al.*, 2006; Panin and Jipa, 2002) and tectonic processes whereby collisions between the African, Eurasian and Arabic plates have produced very complex tectonic regimes of microplates that are far from resolved, especially with respect to vertical motions (Garcia *et al.*, 2007).

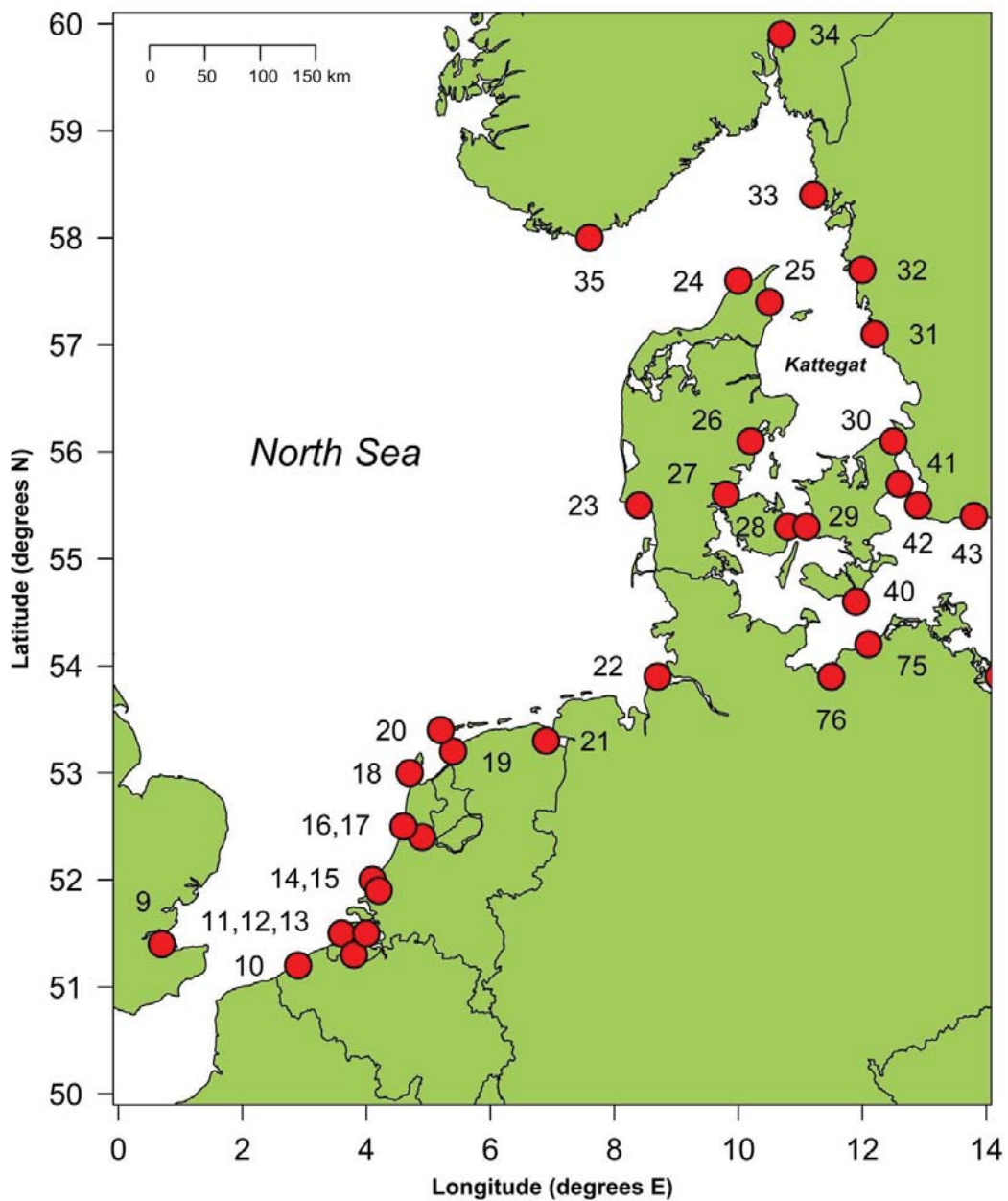
Figure 6.1: Location of tide gauge records analysed.



Notes:

Each record is denoted by a "Station ID" with further details provided in Table 6.1. Refer to Figures 6.2 and 6.3 for insets A and B, respectively.

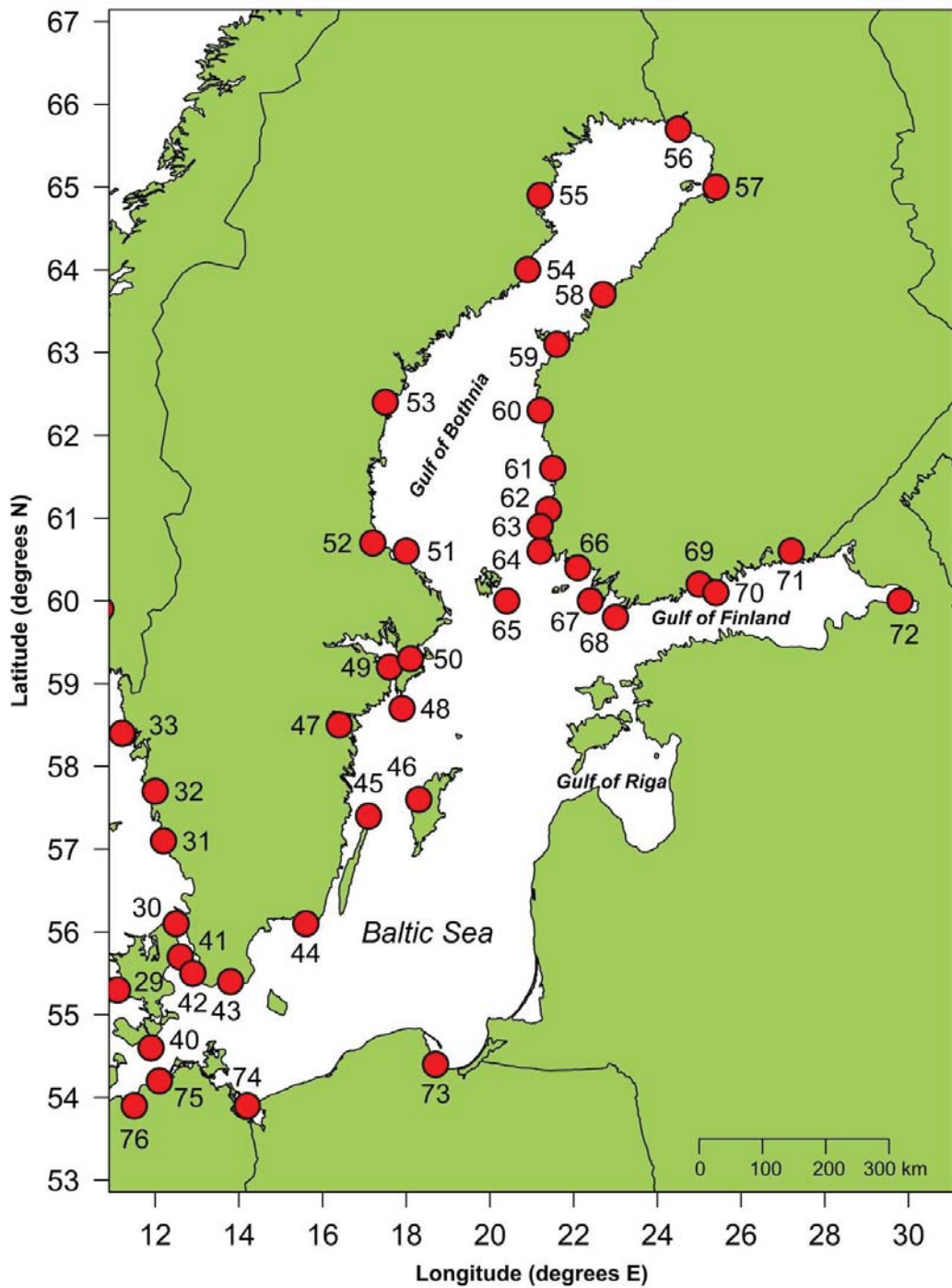
Figure 6.2: North Sea tide gauge records analysed.



Notes:

Refer to Figure 6.1 (inset A) and Table 6.1 for further details.

Figure 6.3: Baltic Sea tide gauge records analysed.



Notes:

Refer to Figure 6.1 (inset B) and Table 6.1 for further details.

6.3 Methodology

The methodology applied to the records in Table 6.1 is identical to that undertaken for the USA records in Chapter 5 (refer Section 5.3).

6.4 Data

Within the study area (refer Figures 6.1, 6.2 and 6.3), some 83 annual average time series records are available for analysis which meet the length and data gap admissibility protocols of the *msltrend* package (advised in Sections 4.3.1, 4.5). Only Revised Local Reference (RLR) datasets from the PSMSL have been used as they are commensurate with quality control procedures and complete tide gauge datum histories provided by the supplying national authority (PSMSL, 2016).

Within these records, the spatial density is highest along the northern and central European mainland bordering the North Sea and for margins around the Baltic Sea, contrasting sharply to the scarcity of comparable records within the Mediterranean and Black Sea. Records used in this study comprise 8,505 station years from the PSMSL plus a further 2,436 station years added through the extensive data archaeology work of Hogarth (2014). The work of Hogarth (2014) extends tide gauge time series from the PSMSL using historical documents, PSMSL ancillary data, and by developing additional composite time series using near neighbour tide gauges (Watson, 2016e). A total of 54 station records used in this study have been extended by Hogarth (2014), with only the complete portions of these extended time series used. Further, only records finishing within the last decade (post 2006) have been considered as the focus of the study is to reconcile recent temporal changes in mean sea level with the historical record available.

All data records used have notionally been assigned a 'Station ID' (refer Table 6.1) based on differentiating key European coastlines including:

- ❑ North Atlantic commencing in the south at Lagos, Portugal (ID=1) heading north around the British Isles, along the North, Norwegian and Barents Seas to Polyarniy, Russian Federation (ID=39)(see Figures 6.1 and 6.2);

- ❑ Baltic Sea beyond the entrance at the Great Belt commencing at Gedser, Denmark (ID=40) moving in a clockwise direction around the Gulf of Bothnia, Gulf of Finland and Gulf of Riga to Wismar, Germany (ID=76) (see Figure 6.3); and
- ❑ Mediterranean and Black Seas beyond the Strait of Gibraltar commencing at Alicante, Spain (ID=77) moving in a clockwise direction around the Balearic, Tyrrhenian, Ionian, Adriatic and Aegean Seas, to Poti, Georgia (ID=83) on the eastern foreshore of the Black Sea (see Figure 6.1).

By graphically representing characteristics associated with records based on the Station ID, spatially dominant patterns are more readily apparent.

Table 6.1: Summary of data used in European analysis.

Tide Gauge Data							GNSS (GPS) Data ⁽³⁾			
Station ID ⁽¹⁾	Location	PSMSL ID	Start (yr)	End (yr)	Length (yrs)	Gaps (yrs)	SONEL Station	Length (yrs)	Distance to tide gauge (m)	VLM (mm/yr)
NORTH ATLANTIC OCEAN (including NORTH SEA, NORWEIGAN SEA and BARENTS SEA)										
1	Lagos ⁽²⁾	162	1909	2012	104	14	LAGO	13.72	134	-0.52 ± 0.15
2	Cascais ⁽²⁾	52	1882	2012	131	14	CASC	15.63	275	-0.08 ± 0.18
3	Leixoes ⁽²⁾	791	1928	2008	81	12	GAIA	NA	12,677	
4	St Jean De Luz ⁽²⁾	469	1889	2013	125	15	SCOA	8.01	2	-2.70 ± 0.28
5	Brest	1	1807	2014	208	23	BRST	15.16	293	-0.02 ± 0.11
6	Newlyn	202	1916	2014	99	2	NEWL	15.24	5	-0.21 ± 0.13
7	Aberdeen ⁽²⁾	21	1862	2014	153	11	ABER	15.28	1	0.90 ± 0.22
8	North Shields ⁽²⁾	95	1895	2014	120	2	NSLG	3.94	495	1.37 ± 0.67
9	Sheerness ⁽²⁾	3	1870	2008	139	1	SHEE	16.57	2	1.09 ± 0.20
10	Oostende ⁽²⁾	413	1927	2012	86	6	OOST	10.65	966	-0.35 ± 0.28
11	Vlissingen	20	1862	2014	153	-	VLIS	7.1	2	0.28 ± 0.51
12	Terneuzen ⁽²⁾	-	1862	2008	147	-	-	-	-	-
13	Hansweert ⁽²⁾	-	1862	2008	147	-	-	-	-	-
14	Hoek Van Holland	22	1864	2014	151	-	-	-	-	-
15	Maassluis	9	1848	2014	167	-	-	-	-	-
16	Amsterdam ⁽²⁾	-	1766	2011	246	-	-	-	-	-
17	Ijmuiden ⁽²⁾	32	1872	2014	143	-	IJMU	9	2	-0.53 ± 0.34
18	Den Helder ⁽²⁾	23	1832	2014	183	-	-	-	-	-
19	Harlingen ⁽²⁾	25	1865	2014	150	-	-	-	-	-
20	West-Terschelling	236	1921	2014	94	-	TERS	17.16	10	-0.20 ± 0.22
21	Delfzijl ⁽²⁾	24	1827	2014	188	1	-	-	-	-
22	Cuxhaven ⁽²⁾	7	1843	2013	171	-	TGCU	5.02	1	0.01 ± 0.86
23	Esbjerg	80	1889	2012	124	3	ESBH	9.13	5	-1.18 ± 0.48
24	Hirtshals	89	1892	2012	121	10	HIRS	9.13	512	2.75 ± 0.45
25	Frederikshavn	91	1894	2012	119	8	-	-	-	-
26	Aarhus	76	1889	2012	124	8	-	-	-	-
27	Frederika	81	1890	2012	123	3	-	-	-	-
28	Slipshavn	98	1896	2012	117	10	-	-	-	-
29	Korsor	113	1897	2012	116	6	-	-	-	-
30	Hornbaek ⁽²⁾	119	1891	2013	123	4	-	-	-	-
31	Varberg ⁽²⁾	73	1887	2012	126	-	-	-	-	-
32	Goteborg-Ringon ⁽²⁾	2133	1887	2012	126	1	-	-	-	-
33	Smogen ⁽²⁾	179	1895	2014	120	-	-	-	-	-
34	Oslo ⁽²⁾	62	1914	2014	101	-	OSLS	13.16	28,041	5.31 ± 1.12
35	Tregde	302	1928	2014	87	5	TGDE	9.78	5	1.64 ± 0.41

Table 6.1 (cont)

Tide Gauge Data							GNSS (GPS) Data ⁽³⁾			
Station ID ⁽¹⁾	Location	PSMSL ID	Start (yr)	End (yr)	Length (yrs)	Gaps (yrs)	SONEL Station	Length (yrs)	Distance to tide gauge (m)	VLM (mm/yr)
36	Bergen ⁽²⁾	58	1915	2014	100	4	-	-	-	-
37	Heimsjo	313	1928	2014	87	11	-	-	-	-
38	Kabelvag ⁽²⁾	45	1928	2014	87	4	-	-	-	-
39	Polyarniy ⁽²⁾	2027	1926	2012	87	6	-	-	-	-
BALTIC SEA REGION										
40	Gedser ⁽²⁾	120	1882	2012	131	2	GESR	9.17	200	0.61 ± 0.66
41	Kobenhavn	82	1889	2012	124	4	BUDP	10.99	8,817	1.99 ± 0.51
42	Klagshamn	330	1930	2014	85	-	-	-	-	-
43	Ystad ⁽²⁾	72	1887	2012	126	-	-	-	-	-
44	Kungsholmsfort	70	1887	2014	128	-	-	-	-	-
45	Olands Norra Udde ⁽²⁾	69	1887	2014	128	-	-	-	-	-
46	Visby	2105	1916	2014	99	1	VISO	14.83	5,195	3.31 ± 0.56
47	Mem ⁽²⁾	75	1864	2013	150	-	-	-	-	-
48	Landsort ⁽²⁾	68	1887	2012	127	-	-	-	-	-
49	Nedre Sodertalje ⁽²⁾	31	1869	2014	146	-	-	-	-	-
50	Stockholm ⁽²⁾	78	1801	2014	214	-	-	-	-	-
51	Bjorn ⁽²⁾	90	1892	2013	122	-	-	-	-	-
52	Nedre Gavle ⁽²⁾	99	1896	2013	118	-	MAR6	14.83	11,000	7.86 ± 0.65
53	Draghallan ⁽²⁾	122	1898	2013	116	1	SUN6	NA	16,017	-
54	Ratan	88	1892	2014	123	1	-	-	-	-
55	Furuogrund ⁽²⁾	203	1892	2014	123	2	SKEO	8.99	9,530	10.43 ± 0.20
56	Kemi	229	1920	2014	95	9	-	-	-	-
57	Oulu	79	1889	2014	126	18	-	-	-	-
58	Pietarsaarj ⁽²⁾	194	1889	2014	126	5	-	-	-	-
59	Vaasa ⁽²⁾	57	1867	2014	148	11	VAAS	14.83	20,000	9.13 ± 0.13
60	Kaskinen	285	1927	2014	88	6	-	-	-	-
61	Mantyluoto ⁽²⁾	172	1889	2014	126	4	-	-	-	-
62	Rauma	376	1933	2014	82	2	-	-	-	-
63	Lyokki ⁽²⁾	16	1858	2013	156	1	-	-	-	-
64	Lypyrnti ⁽²⁾	17	1858	2013	156	1	-	-	-	-
65	Foglo ⁽²⁾	249	1866	2014	149	8	-	-	-	-
66	Turku	239	1922	2014	93	3	-	-	-	-
67	Jungfrusund ⁽²⁾	18	1858	2011	154	17	-	-	-	-
68	Hanko ⁽²⁾	71	1866	2014	149	17	-	-	-	-
69	Helsinki	14	1879	2014	136	-	METS	18.99	31,729	4.48 ± 0.84
70	Soderskar ⁽²⁾	29	1866	2014	149	-	-	-	-	-
71	Hamina ⁽²⁾	315	1889	2014	126	4	-	-	-	-
72	Kronstadt ⁽²⁾	-	1835	2011	177	-	-	-	-	-
73	Gdansk ⁽²⁾	64	1886	2011	126	5	-	-	-	-
74	Swinoujscie ⁽²⁾	2	1811	2012	202	2	-	-	-	-
75	Warnemunde ⁽²⁾	11	1855	2014	160	1	WARN	10.87	126	0.65 ± 0.59
76	Wismar	8	1849	2014	166	1	-	-	-	-
MEDITERRANEAN SEA (including BLACK SEA)										
77	Alicante ⁽²⁾	208	1874	2010	137	11	ALAC	14.4	1	0.33 ± 0.19
78	Marseille ⁽²⁾	61	1885	2014	130	1	MARS	15.45	5	-0.24 ± 0.18
79	Genova ⁽²⁾	59	1884	2013	130	16	GENO	15.43	1,000	-0.22 ± 0.27
80	Venezia ⁽²⁾	168	1872	2012	141	7	VEN1	4.18	5,825	-1.21 ± 0.67
81	Trieste ⁽²⁾	154	1875	2015	141	2	TRIE	10.89	6,707	0.30 ± 0.27
82	Tuapse	215	1917	2014	98	2	TUAP	NA	95	-
83	Poti	41	1874	2013	140	9	-	-	-	-

Abbreviations: VLM = vertical land movements; NA = not available

Notes:

- ⁽¹⁾ The 'Station ID' is a local referencing protocol used throughout this study, particularly the graphical outputs;
- ⁽²⁾ Extended data sets advised in Hogarth (2014) have been used for this study; and
- ⁽³⁾ All GPS data kindly provided by SONEL using updated ULR6a solutions (Santamaría-Gómez *et al.*, 2012) with 1 sigma error estimates advised.

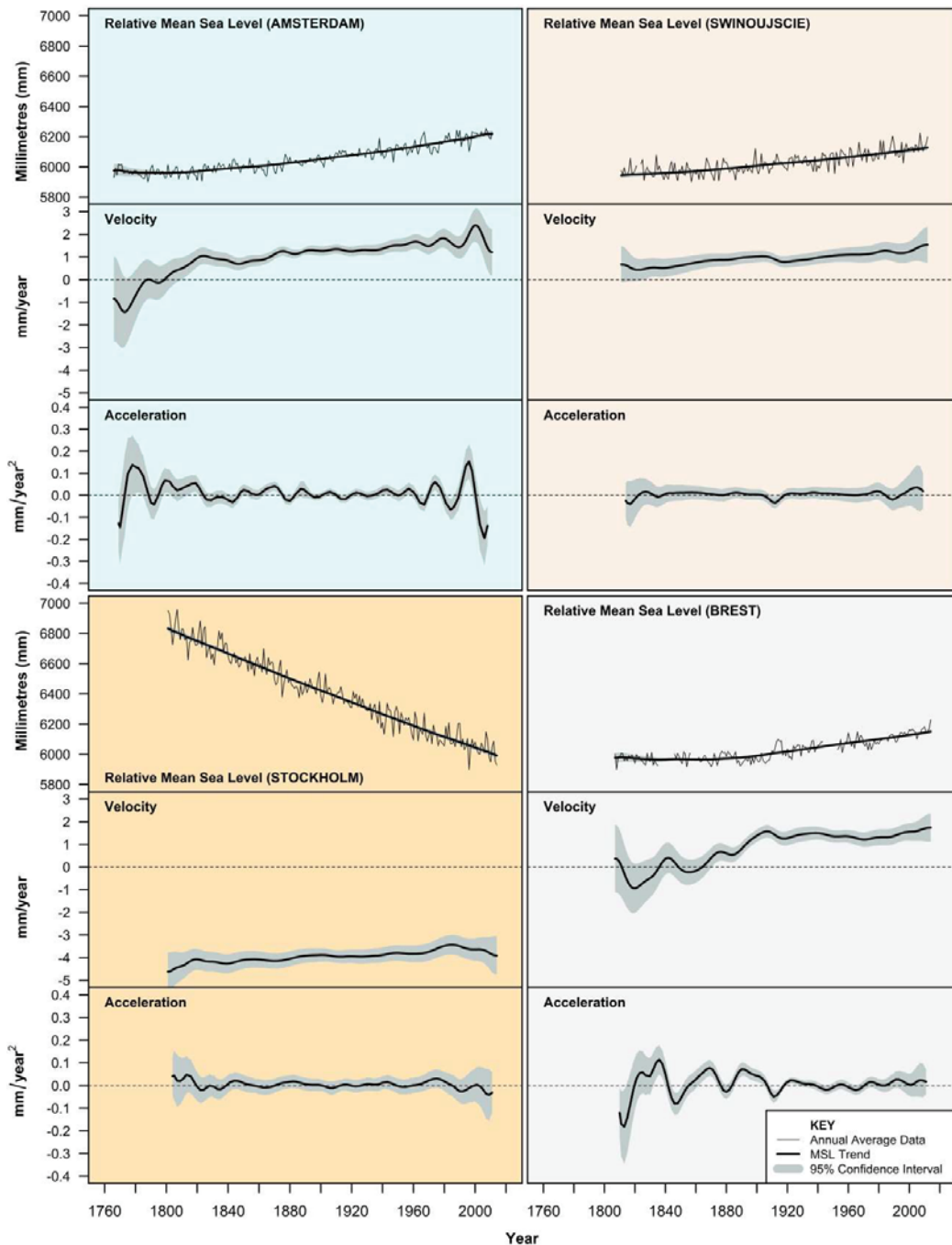
6.5 Results

Figure 6.4 provides an example output from the analysis of the four longest records available within the study area (Amsterdam, Netherlands – 246 years; Stockholm, Sweden – 214 years; Brest, France – 208 years; and Swinoujscie, Poland – 202 years), reflective of the broader regional temporal signatures of velocity and accelerations in relative mean sea-level. It is clear that these velocities and accelerations are varying over time. It is also evident from these long records that relative velocity is steadily increasing over time, peaking at or near the recent end of the time series record, driven by low and continually changing rates of acceleration. For each of the long records depicted in Figure 6.4, the acceleration is predominantly confined to a narrow band within $\pm 0.05 \text{ mm/yr}^2$ and not statistically different to zero at the 95% confidence level for most of the records, despite evidence that relative velocities are continuing to increase. The complete analysis of all the records in this manner provides the means to inspect spatial temporal patterns in greater detail than previously available.

Figure 6.5 provides a breakdown of the peak velocities and accelerations for each record and the time they occur. It is relevant to consider these charts simultaneously as velocity and acceleration are intrinsically linked as kinematic properties. For example, acceleration is required to increase velocity and conversely negative acceleration (or deceleration) is required to reduce velocity. From inspection of Figure 6.5, a range of key observations are apparent, including:

- The spatial signature of peak relative velocity is strongly reflective of the signatures of vertical land movements within the study area. Those areas experiencing high rates of post-glacial rebound are clearly evident moving northward around the Baltic Sea margins with peak relative velocities below -4 mm/yr . Conversely, only 19 stations measure a peak relative velocity throughout the historical record exceeding 2 mm/yr . Principally these high rates correspond with areas that exhibit known subsidence (eastern Black Sea, southern English, Dutch and German coastlines);
- primary and secondary velocity peaks measured across all European records are quite similar in magnitude;

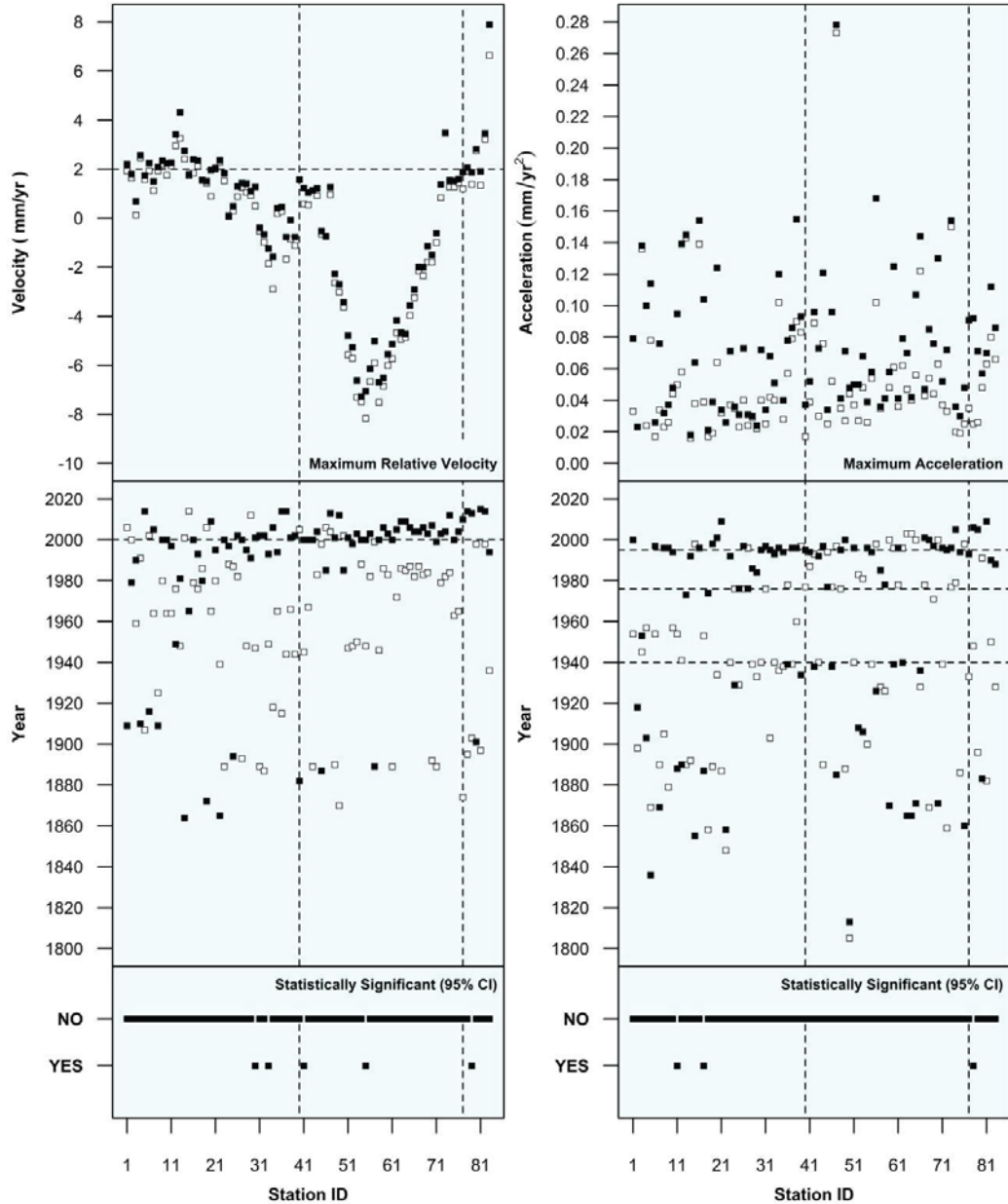
Figure 6.4: Temporal characteristics of mean sea level for the longest records within the study area (Amsterdam, Stockholm, Brest and Swinoujscie).



Notes:

Each site is depicted by a three-panel plot of mean sea level, velocity, and acceleration. The respective scales are identical for all stations for direct comparative purposes.

Figure 6.5: Peak estimates of velocity and acceleration for all stations.



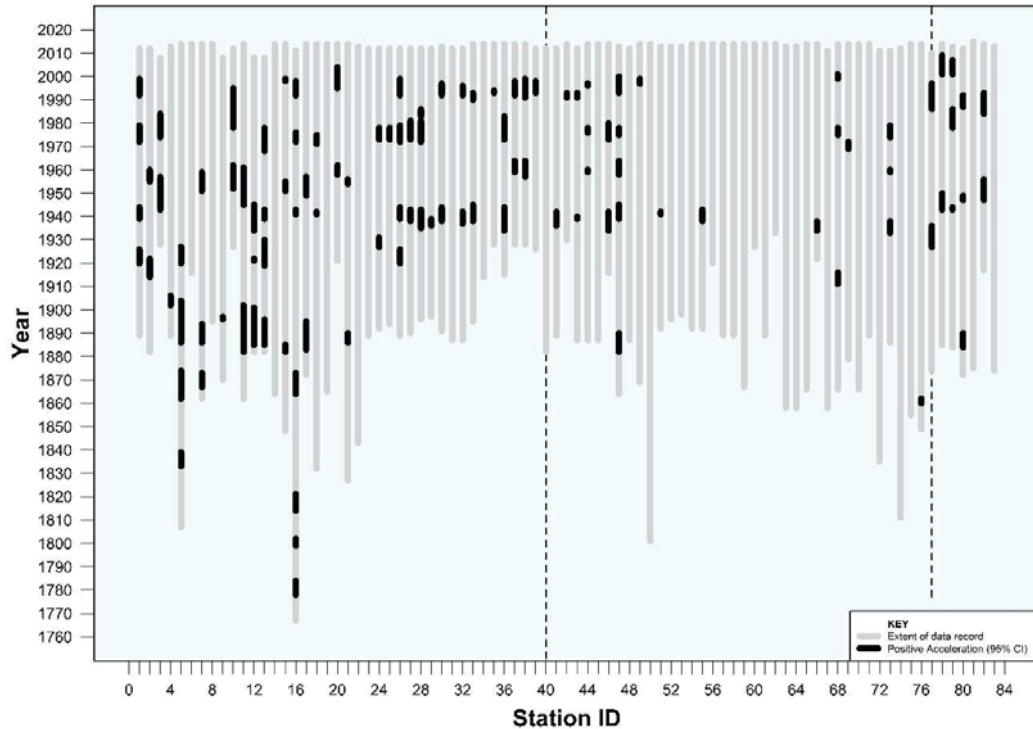
Notes:

Peak metrics are denoted as filled boxes, whilst secondary peaks are denoted by clear boxes. The centre panels indicate the year in which the respective peaks occurred. A vertical dashed line corresponding to station 40 (Gedser, Denmark) and station 77 (Alicante, Spain) denote the commencement of the Baltic Sea stations and Mediterranean Sea and Black Sea stations, respectively. Horizontal lines are provided as visual markers correlating to relevant discussions in the text. The bottom panel provides an indication as to whether the peak metric is statistically different (in this case higher) than all others in the context of the historical record at the 95% confidence level based on the significance testing protocol advised in Wolfe and Hanley (2002). Station ID references are summarised in Table 6.1.

- ❑ Some 52 of the 83 records (63%) have the peak relative velocity occurring on or after 2000 though within this figure there are some interesting spatial features. In particular, this figure rises to 80% of the stations in the semi-enclosed seas (Baltic, Mediterranean and Black Seas), contrasting to only 44% of the stations positioned along the North Atlantic coastline. Some 10 of these peaks coincide with the most recent data point in the time series (Brest, France [ID=5]; Bergen, Norway [ID=36]; Heimsjo, Norway [ID=37]; Mem, Sweden [ID=47]; Swinoujscie, Poland [ID=74]; Alicante, Spain [ID=77]; Marseille, France [ID=78]; Genova, Italy [ID=79]; Trieste, Italy [ID=81]; and Tuapse, Russian Federation [ID=82]);
- ❑ Mean maximum acceleration measured across all records is approximately 0.074 ± 0.042 mm/yr² (1σ) with no particular spatial patterns evident;
- ❑ There is however strong spatial coherence around the timing of the primary and secondary peaks in mean sea level acceleration (middle right panel) with nearly 34% of the peak acceleration focussed within a band between 1994 and 2000. Other bands of acceleration are clearly evident centred around 1940 and 1976; and
- ❑ Most significantly, from an analysis of the peak velocities and accelerations for all records considered within the study area, only 5 peak velocities (Hornbaek, Denmark [ID=30]; Smögen, Sweden [ID=33]; København, Denmark [ID=41]; Furuögrund, Sweden [ID=55]; and Genova, Italy [ID=79]) and 3 peak accelerations (Vlissingen, Netherlands [ID=11]; IJmuiden, Netherlands [ID=17]; and Marseille, France [ID=78]) are statistically different (or higher) than other peaks observed elsewhere over the historical record (95% confidence level). Of these 8 statistically significant peaks, all except the peak accelerations measured at Vlissingen and Ijmuiden occur after 1990.

Figure 6.6 provides an assessment of the extent and temporal distribution of positive acceleration in all records (i.e. statistically different to zero). Such analyses provide an alternative form of assessment for investigating subtleties of acceleration when the metrics are comparatively low. A mere 7.4% of the 10,941 station years of records available exhibit a positive acceleration different to zero at the 95% confidence level. However, there is some evidence of a more sustained period of positive acceleration between ≈ 1880 and 1910 from the longer records available for the southern portion of the North Atlantic coastline.

Figure 6.6: Periods of positive acceleration (95% CI).

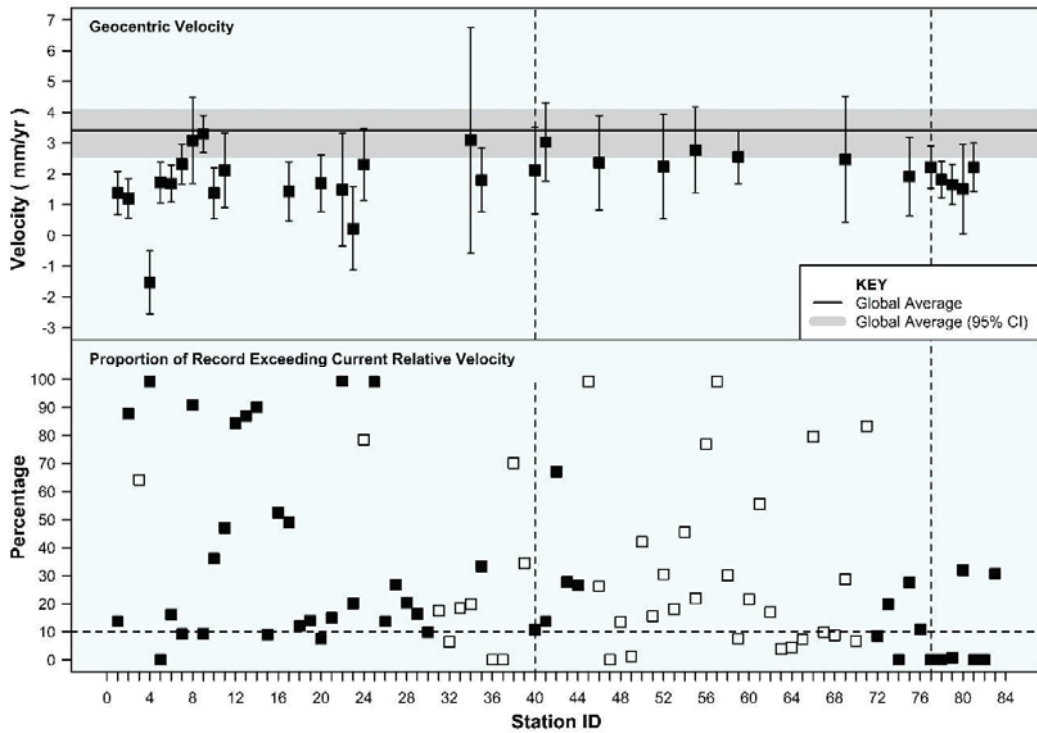


Elsewhere the temporal signatures mirror the peak accelerations discussed previously concerning Figure 6.5. Results displayed in Figure 6.6 also highlight a difference within the Baltic Sea compared to the rest of the study area. Specifically, only 2.6% of station years exhibit a positive acceleration different to zero with some 54% of the Baltic records indicating no positive acceleration throughout the time series (95% CI).

Figure 6.7 provides an appraisal of the current rate of geocentric sea-level rise across the tide gauge network by correcting the relative velocity at the recent end of the record with GPS derived vertical land movement rates from SONEL (refer Table 6.1), noting that only 30 records (or 36%) have an associated SONEL station available with updated ULR6a solutions (Santamaría-Gómez *et al.*, 2012; SONEL, 2016). There are a number of key features evident from this graphical analysis, including no evident spatial trend across Europe from the current geocentric velocities. Further, none of the geocentric velocities determined exceed the global average of 3.4 ± 0.4 mm/yr (Nerem *et al.*, 2010; University of Colorado, 2016) at the 95% confidence level. Though, some 10 stations are lower than the global average (95% CI), of

which 8 are located along the North Atlantic coastline between Lagos, Portugal (ID=1) and Esbjerg, Denmark (ID=23).

Figure 6.7: Estimates of Current Geocentric Rate of Sea-Level Rise (95% CI).



Notes:

“Current” refers to the last date in the respective data time series. Estimates based on real-time relative velocity derived from *msltrend* decomposition corrected by vertical land movement velocities provided by SONEL. The vertical dashed lines demarcate the three respective spatial subregions analysed (North Atlantic Ocean, Baltic Sea, and Mediterranean Sea; refer to Table 6.1). Clear boxes in the bottom panel represent stations in which relative sea-level fall is evident over the course of the record. Data sources and station ID references are summarised in Table 6.1.

The bottom panel of Figure 6.7, although highlighting no particular spatial pattern across Europe, indicates that only 25 of 83 stations (or 30%) exhibit a current velocity exceeded by less than 10% of the historical record. For these stations, this indicates the latter portions of these records are within the upper bracket of velocities recorded over the historical record, providing tangible (albeit limited) evidence of recent acceleration in mean sea-level across the European region.

6.6 Discussion

As advised in Chapter 5 (Section 5.5), ocean water level time series data from tide gauge stations are a complex amalgam of key physical contributors which include:

- ❑ **Factor 1:** land movement at the tide gauge site;
- ❑ **Factor 2:** dynamic influences of largely oceanographic, atmospheric or gravitational origins operating on differing temporal and spatial scales; and
- ❑ **Factor 3:** low amplitude signal of mean sea level rise driven by climate change influences (principally melting of snow and ice reserves bounded above sea level (directly adding water), and thermal expansion of the ocean water mass).

Specifically within the European context, factors 1 and 2 are particularly complex. The study area encompasses sites ranging from those that exhibit high rates of vertical land motion due to post-glacial rebound (e.g., Baltic Sea) to areas where significant ongoing subsidence is prevalent (e.g., eastern margins of the Black Sea). In addition to this, the semi-enclosed margins of the Black, Mediterranean and Baltic Seas drain annual continental water discharges from large tracts of Europe.

Deshayes and Frankignoul (2008) note the North Atlantic Ocean is a key element of the earth's climate. In particular, the cyclonic circulation at depth along the boundaries, the deep western boundary current, is the deep limb of the Atlantic meridional overturning circulation (AMOC) that contributes substantially to the energy balance of the earth. The state of the North Atlantic Oscillation (NAO) imposes a strong constraint on the circulation of the North Atlantic (Getzlaff *et al.*, 2005) and is considered to be a singular major atmospheric, basin scale pattern that affects sea level around Europe and further afield (Tsimplis *et al.*, 2006; Wakelin *et al.*, 2003; Woolf *et al.*, 2003).

In addition to the afore-mentioned studies, numerous published works have been dedicated to examining linkages between dominant NAO drivers and sea level anomalies throughout the study area (e.g., Calafat *et al.*, 2012; Dangendorf *et al.*, 2012; Gomis *et al.*, 2006, 2008, Jevrejeva, *et al.*, 2005; Lehmann *et al.*, 2011; Tsimplis *et al.*, 2008; Tsimplis and Shaw, 2008; Vigo *et al.*, 2005).

The necessity to remove these influences from the data to enhance acceleration estimates is well noted in the literature (e.g., Calafat *et al.*, 2012; Calafat and Chambers, 2013; Chambers *et al.*, 2012; Dangendorf *et al.*, 2014; Douglas, 1992; Haigh *et al.*, 2014).

The NAO was one of the key dynamic features embedded within the synthetic data set (Watson, 2015) used to test time series analysis techniques for their utility in isolating relative mean sea level from conventional ocean water level data sets with improved accuracy (Watson, 2016a). From this testing, SSA (which underpins the *msltrend* package used to decompose records in this study), proved an optimal technique to separate out these complex oscillatory signals with time-varying amplitudes and noise from the low amplitude and low frequency signal of mean sea-level rising over time. In particular, the estimation of mean sea level via selection of ‘trend-like’ components in which a contribution threshold $\geq 75\%$ is contained within frequency bins ≤ 0.01 (refer Section 5.3, Step 2) provides a necessary assurance that these dynamic contaminating influences are removed.

The detailed analysis undertaken highlights that velocity time series associated with relative mean sea-level at each site, are distinctly non-linear, in turn reflective of associated acceleration continually varying over time. With relatively small kinematic properties evident over the course of the lengthy records available (see Figure 6.4), different diagnostic approaches are proving necessary to infer an acceleration in mean sea level records or to detect change points in records that might be reflective of an altered climate-related forcing. The relative mean sea-level velocity and acceleration time series enable subtle changes to be more readily or intuitively detected, moving beyond the encumbrances and inherent limitations of the overly-used linear regression and quadratic techniques to estimate velocity and acceleration, respectively (refer Section 5.5.3).

6.6.1. Reconciling historical and future projected MSL accelerations

As indicated above, the scale of velocities and accelerations measured within this study (e.g., Figure 6.4) remain lower than those associated with forecasts from physics-based climate models over the course of the 21st century and beyond (Church *et al.*, 2013a; IPCC, 2013b). Under forecasts of high simulated radiative (or external) forcing (RCP8.5 scenario), the current rate of global averaged sea-level rise of 3.4 ± 0.4 mm/yr (Nerem *et al.*, 2010; University of

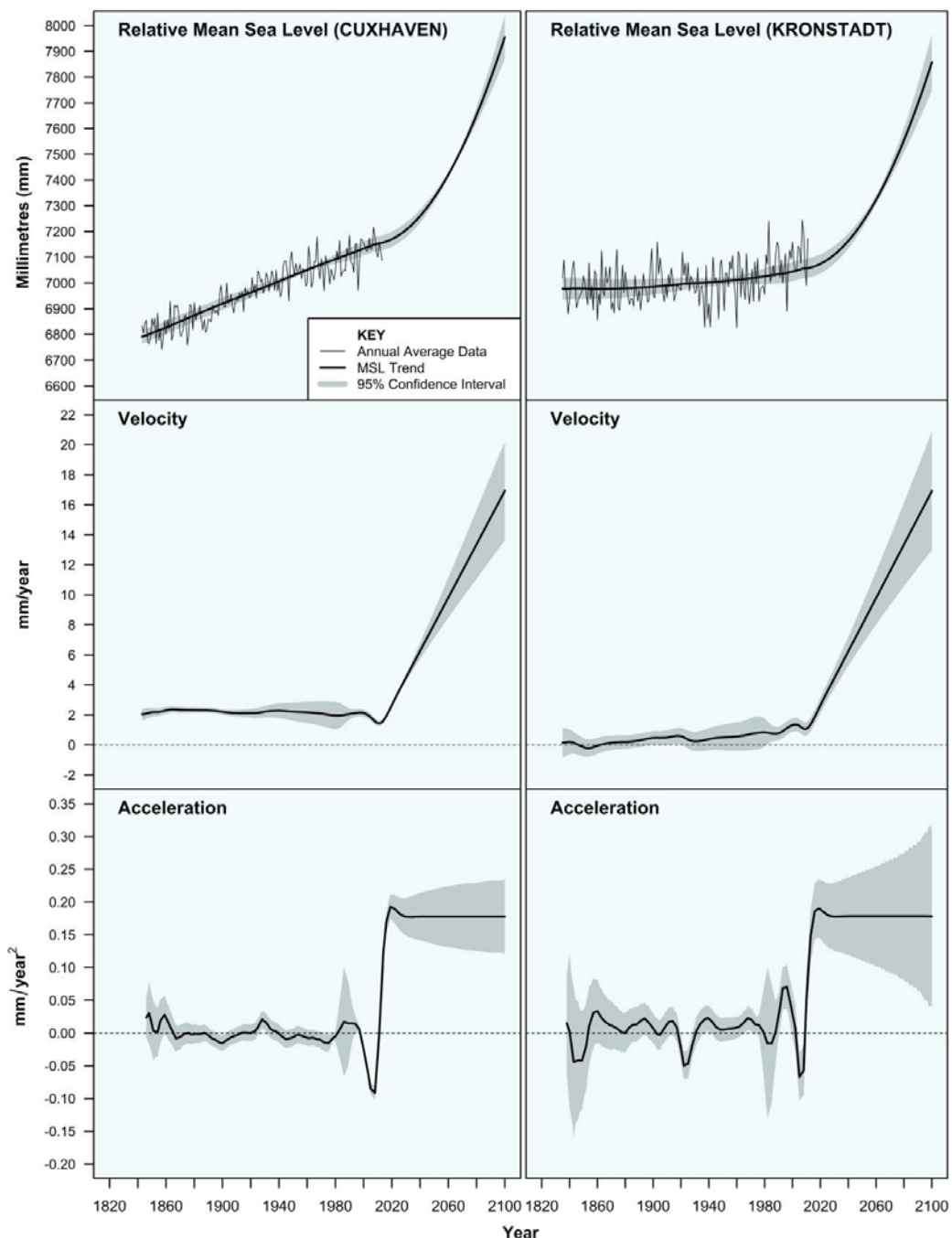
Colorado, 2016) is expected to increase to rates of the order of 8 - 16 mm/yr by 2100 (refer Chapter 1, Figures 1.1 and 1.2).

Figure 6.8 provides a visual comparative analysis of how the velocity and acceleration time series might change at Cuxhaven, Germany and Kronstadt, Russian Federation, based on a relative mean sea-level rise of 800 mm from present to 2100. Under such a scenario, which assumes simple equations of motion and uniform acceleration, the necessary and significant changes in velocities and accelerations compared to those measured over the historical record, are likely to be readily apparent well within the next 20 years. For example, accelerations at both stations will, under such a scenario, have to rise to $\approx 0.18 \text{ mm/yr}^2$ within the next 10 years and be sustained to 2100. By contrast, only one European record (Mem, Sweden) has experienced a measured acceleration of this order from the 10,941 station years analysed (Figure 6.5) and from all of these records, a mere 7.4% exhibit a positive acceleration different to zero at the 95% confidence level (Figure 6.6).

One should caution these forecasts are highly idealistic and preliminary. They are advised in order to provide a sense of perspective regarding the timing of necessary changes to the kinematic properties of mean sea-level at these locations, in order to give effect to such projections.

It is recognised that the atmosphere is regarded as having a very short memory while the oceans and ice sheets, due to their enormous thermal inertia, provide much longer memory for climate variations (Dangendorf *et al.*, 2015; Levermann *et al.*, 2013; Marcos *et al.*, 2017; Trenberth and Hurrell, 1994). This inertia and long term memory relate to the ability and time for the ocean to store and transport heat and temperature anomalies throughout the water mass to great depth (Goosse *et al.*, 2004; Goosse and Renssen, 2005). Whilst these facets are built into coupled ocean–atmosphere general circulation models (OAGCMs) to study the characteristics of the large-scale ocean circulation and its climatic impacts, the trajectory of the oceanic response remains uncertain with potential lags not yet fully understood. From this perspective it is imperative to appreciate the importance of ongoing efforts to identify, with improved accuracy, critical change points in the long time series of mean sea level records available.

Figure 6.8. Indicative implications of projected sea-level rise of 800 mm at Cuxhaven, Germany, and Kronstadt, Russian Federation, from 2015 to 2100.



Notes:

Projections based on simple equations of motion with uniform acceleration. Error margins noted are 95% confidence levels.

Whilst the techniques espoused in this research represent a concerted effort to test and specifically identify enhanced techniques to isolate mean sea level with improved temporal accuracy (Watson, 2015, 2016a,c,e) this work should be considered a staging point for ongoing improvements in such critical areas, in particular the identification of statistically robust change points in the record.

6.6.2. Selected Literature concerning MSL acceleration around Europe

Woodworth (1990) remains one of the seminal papers in the literature concerning mean sea level accelerations focusing on the extensive network of European time series records. This work concluded that European tide gauge records since 1870 showed little evidence for significant accelerations, either positive or negative, in regional mean sea levels, with on average a weak deceleration observed. This study however, based estimates of acceleration on simple quadratic coefficients, which (from a more contemporary understanding) have significant limitations (refer Section 5.5.3).

No comparable studies of this scale regarding mean sea level acceleration across Europe have been undertaken since Woodworth (1990). Though considerable attention has been given to investigations on smaller scales such as the North Sea (e.g., Shennan and Woodworth, 1992; Wahl *et al.*, 2013), English Channel, UK (e.g., Haigh *et al.*, 2009), German Bight (e.g., Wahl *et al.*, 2010; Wahl *et al.*, 2011) and Baltic Sea (e.g., Donner *et al.*, 2012; Hünicke and Zorita, 2016; Spada *et al.*, 2014). Shennan and Woodworth (1992) analysed records from the UK and North Sea, developing a de-trended 'Regional Sea-Level Index', confirming the previous results of Woodworth (1990) with no evidence in the region for an acceleration of sea-level trends in recent decades (that is up to 1992).

Haigh *et al.* (2009) provide a detailed appraisal of available records around the English Channel. Acceleration in mean sea level was observed by considering overlapping 10, 25 and 50-year periods, for the four longest and most complete records. The analysis concluded that recent high rates of change in mean sea level were not unusual compared to those that had occurred at other times during the 20th century, with no evidence as yet (at 2009) for any acceleration in sea level rise over the 20th century around the English Channel.

Wahl *et al.* (2011) provides a detailed assessment of 13 tide gauge records covering the entire German North Sea coastline with particular consideration given to the investigation of non-linear (acceleration) behaviour. One method involves the establishment of a 'virtual' station time series smoothed using SSA (with an embedding dimension of 15 years) in combination with Monte-Carlo-Autoregressive Padding (used previously in Wahl *et al.*, 2010) in a novel approach designed to limit the ubiquity of end effects associated with filtering of time series. Rates of change are then considered via first differences. This work concluded that an acceleration of sea level rise commenced at the end of the nineteenth century with another distinct period of acceleration starting in the 1970s and intensifying from the 1990s, but the high rates of sea level rise during this period are comparable with rates at other times during the last 166 years.

Similar periods of key acceleration are confirmed in the current study, though Wahl *et al.* (2011) do not find evidence of acceleration around 1940 that is clearly evident in the current study and that of others (e.g., Woodworth *et al.*, 2009). Of particular interest Wahl *et al.* (2011) also conclude recent (that is post 1990) rates of rise from non-linear smoothing in the order of 4 – 6 mm/yr for the southern part of the German Bight and 7 – 8 mm/yr for the eastern part. Although the current study finds high recent (post 1990) rates of relative sea level rise for records around the German Bight, the maximum rates determined are only of the order of ≈ 2 mm/yr.

The discrepancy in the rates between the studies might, in part, rest with the comparatively narrow embedding dimension (or window length [L]) of 15 years used for the SSA analysis in the Wahl *et al.* (2011) study. The selection of small window lengths risks sub-optimal separability and potential mixing of signals where the singular values of the decomposition are close. The smaller the embedding space, the shorter the length of the window over which the resolved components are calculated, and the less resolved is each component (Moore *et al.*, 2005). In effect, small SSA windows act like smoothing linear filters of width $2L-1$, thereby retaining (albeit smoothed) contaminating power bands, as distinct from their isolation and removal.

Hein *et al.* (2011) analysed similar German Bight data to Wahl *et al.* (2011) using a similar approach but further develop the method through use of the second derivative to predict

boundary values and calculate the white noise Monte Carlo simulation in the frequency space. By removing major frequency bands identified at approximately 35 and 75 years, Hein *et al.* (2011) concluded no long-term trend of acceleration evident in mean sea level around the German Bight.

Wahl *et al.* (2013) provides a detailed analysis of the North Sea regional sea level records, updating the prior work of Shennan and Woodworth (1992) by considering 3 separate 'Regional Sea-Level Indices' for the North Sea, Inner North Sea and English Channel. This body of work concluded that recent rates of sea level rise (i.e. over the last two to three decades) were high compared to the long-term average, but comparable to those observed at other times in the late 19th and 20th Century. This investigation considers non-linear (acceleration) behaviour using a similar technique to that espoused in Wahl *et al.* (2011).

Donner *et al.* (2012) provides a detailed examination of Baltic Sea records, examining measures of acceleration through the application of a fitted AR[1] model and performing separate (two-sided) t-tests and Mann-Kendall tests for 1000 realisations of each model. This work observed that by comparing the empirical values of the test statistics with those obtained for AR[1] surrogates adjusted to the data, all accelerating trends in the 10% and 50% quantiles become insignificant with respect to both t and Mann-Kendall test. Whilst seasonal influences appear to have been accounted for, there appears no evident ability of this approach to remove the contaminating decadal and multi-decadal variability from the trends.

Intuitively, this would increase the likelihood of statistically measured accelerations, but, in accordance with the approach and tests adopted, they were not realised. Despite differences in approaches, this analysis also highlights the substantial absence of any periods of positive acceleration in mean sea level at the 95% confidence level across the Baltic Sea margin (refer Figure 6.6).

A detailed study of the Baltic mean sea level records by Spada *et al.* (2014) observed an anomaly in the long-term acceleration explained by classical post-glacial rebound theory and numerical modelling of glacial isostasy. This work however, is based upon the use of quadratic coefficients which have significant limitations for the purpose at hand (Watson, 2016c). As

previously advised, this analysis finds no measureable acceleration in mean sea level within the Baltic Sea.

6.7 Conclusion

Watson (2016e) notes the implications of sea-level rise, particularly the much larger projected rates of rise under future climate change modelled scenarios (e.g., Church *et al.*, 2013a; Mengel *et al.*, 2016) are profound with far reaching social, economic and environmental implications (amongst others) foreshadowed over the course of the 21st century and beyond. These are well described for the European context in the *ClimateCost Project* undertaken for the European Union (Brown *et al.*, 2011; Watkiss, 2011).

The impacts associated with relative mean sea level rise across Europe are quite varied, principally due to the associated vertical land motions which range from high rates of land uplift associated with post-glacial rebound experienced within the Fennoscandian Region (up to ≈ 9 mm/yr) to areas experiencing ongoing land subsidence (e.g., northern British Isles and the eastern portions of the Mediterranean and Black Seas). Areas experiencing land subsidence will be impacted upon more urgently and directly by rising global mean sea level. By contrast, depending on the trajectory of future sea level rise, the northern land margins of Fennoscandia might still be rising faster than global mean sea level for the larger part of the 21st century, with no apparent issue for coastal dwelling communities until the rate of sea level rise begins to overwhelm the rate of uplift from post-glacial rebound.

Mean sea level records are pivotal data sources as they provide one of the key proxies by which to measure the impact of a changing climate system. With the very ethos of the climate change science and projection modelling underpinned by accelerations in mean sea level (refer Chapter 1), numerous works in the scientific literature have been dedicated to measuring accelerations that might provide improved instruction on the extent to which external (climate change) forcings are manifesting to assist strategic planning, adaptive responses and policy development in readiness for the challenges ahead.

Atlantic mean sea level records could be considered one of the key “canaries in the coal mine” for climate change research given the North Atlantic Ocean is a key element of the earth’s climate (Deshayes and Frankignoul, 2008) and in particular, the role of the AMOC as a key

means by which heat anomalies are sequestered into the ocean's interior and thus modulate the trajectory of climate change (Buckley and Marshall, 2016).

The analytical techniques espoused in this research improve estimates of mean sea level from conventional, long, annual time series by more efficiently removing decadal to inter-decadal (and longer) dynamic influences. By virtue, associated kinematic properties of the mean sea level signal (velocity, acceleration) are also enhanced.

In addition to the use of improved analytical techniques, the search for accelerations in mean sea level records will require more intuitive, diagnostic considerations (such as those considered in this research) until such time as the mean sea level signal is sufficiently large not to be obscured by complex dynamic influences and other background noise.

Although there has been a general tendency for velocity in mean sea level to increase over time, inferring an acceleration to do so, these kinematic properties of the mean sea level signal around Europe have continued to vary over the course of the historical records available at generally low measured rates. The analysis suggests key periods of acceleration centred in bands around \approx 1880 to 1910, 1940, 1976 and a strong spatially coherent signal between 1994 and 2000 consistent with the general findings of previous researchers using different techniques (e.g., Wahl *et al.*, 2013; Woodworth *et al.*, 2009). Significantly, only one record within the study area exhibits a peak acceleration occurring after 1990 (Marseille, France) that is statistically different (or higher) than other peaks observed elsewhere over the historical record (95% confidence level).

Similarly only 5 of the 83 records analysed exhibited a peak velocity occurring after 1990 statistically different (or higher) than other peaks observed elsewhere over the historical record (95% confidence level). The European-wide context of these findings accord with the prior findings of studies on the English Channel (Haigh *et al.*, 2009) and North Sea (Dangendorf *et al.*, 2014; Wahl *et al.*, 2013).

When relative mean sea level velocities are corrected for available vertical land motions, none of the geocentric velocities determined at the end of the available time series record exceed

the global average rate of 3.4 ± 0.4 mm/yr (Nerem *et al.*, 2010; University of Colorado, 2016) at the 95% confidence level.

The results and findings from this large study of European mean sea level records are broadly consistent with those for the complementary study of the mainland USA records (Watson, 2016e). Whilst the accelerated climate change influence is not yet statistically evident in these records, depending on the climate change trajectory, it is highly likely that such changes will take at least 15 - 20 years to manifest in the network of tide gauge records examined within this analysis.

6.8 Acknowledgements

I would like to acknowledge the publicly available data archives of the PSMSL and the extended data sets kindly provided by Peter Hogarth that have been used for this study. Similarly, I would like to extend my appreciation to the SONEL data centre for kindly providing the updated ULR6a solutions used to estimate geocentric sea level rise and acknowledge Dr Sally Brown (Tyndall Centre for Climate Change Research, University of Southampton, UK) and Dr Sönke Dangendorf (Research Institute for Water and Environment, University of Siegen, Germany) for suggestions that improved this aspect of the study program and associated published paper (Watson, 2017).

Chapter 7

Conclusions and Recommendations

The projected impacts of climate change over the course of the 21st Century and beyond are profound and far reaching. Sea level rise is but one of the inevitable side effects of a warming climate system, due principally to melting of land-based glaciers, ice sheets and ice shelves above sea level and thermal expansion of the ocean water mass. These impacts present formidable challenges in managing adaptation endeavours into the future because whilst higher sea level only directly affects coastal areas, these are the most densely populated and economically active land areas on Earth (McGranahan *et al.*, 2007; Nicholls and Cazenave, 2010; Sachs *et al.*, 2001). The continued trend for coastal global population migration (Neumann *et al.*, 2015) has fuelled increasing projected risks associated with sea level rise.

The prominence of the climate change issue has placed more emphasis on examination of the extensive global repository of relative mean sea level records (Holgate *et al.*, 2012), which along with temperature and carbon dioxide, remain the key proxy data sets used to monitor and quantify changes in the global climate system (refer Chapter 1).

With the very ethos of the climate change science and projection modelling underpinned by accelerations in mean sea level, numerous works in the scientific literature have been dedicated to measuring accelerations that might provide improved instruction on the extent to which external (climate change) forcings are manifesting to assist strategic planning, adaptive responses and policy development in readiness for the challenges ahead (refer Chapter 1). However, these research endeavours fit within a broader, integrated framework of sea level science designed to understand sea level change and its implications both present and future (e.g. Intergovernmental Panel on Climate Change; World Climate Research Programme, etc).

Improving knowledge of acceleration in mean sea level lies principally with improving the temporal resolution of the trend signal. This is no trivial task given contemporary ocean water level time series records are a complex composite of numerous dynamic influences operating on differing temporal and spatial scales, superimposed on a comparatively low amplitude trend of sea level rise driven by climate change influences (refer Chapter 3).

This research program has been designed with careful attention to objectives (which are encapsulated in self-contained Chapters 2 to 6) in order to give effect to the key aim of developing improved techniques (and associated tools) for estimating mean sea level and

associated real-time velocity and acceleration from long individual ocean water level time series to augment climate change research. Numerous techniques have been applied in the literature to estimate acceleration in the trend of mean sea level (Visser *et al.*, 2015), each providing varying (and at times controversial) results. Differentiating key, robust findings from those unwittingly contaminated by the limitations inherent with particular techniques (Rahmstorf and Vermeer, 2011) have not been vigorously prosecuted in the literature to date (Watson, 2016a).

The *msltrend* package and associated methods developed via this research program to enhance estimates of trend, velocity and acceleration in relative mean sea level are long overdue, but welcome advancements for improving sea level research. The research program has given rise to a wide range of key learnings and insights (refer Section 7.1, Table 7.1) that will prove invaluable to sea level researchers. The techniques espoused in this research form an integral part of the evolutionary process by which to estimate mean sea level and associated velocity and acceleration with improving robustness and consistency (refer Chapters 4, 5 and 6).

The findings and tools developed through this research program have profound implications for various science, climate modelling, engineering and coastal planning sectors. Improving the precision in estimating the mean sea level (or externally forced) signal from long tide gauge records will contribute to improved understanding of sea level change (and associated climate change influences) at increasingly more localised scales. Enhancing the precision of the mean sea level trend from long ocean water level time series also provides an improved reference frame in which to augment contemporary processes for the evaluation of climate models and associated sea level projections.

Similarly, by improving the estimation of the mean sea level signal from long tide gauge records, coastal scientists and engineers will have the benefit of more precise trend analysis which in turn, will improve statistical analyses for extreme water level phenomena to better inform coastal design processes and coastal hazard and risk assessments where coastal sea level change has significant ramifications. Further, the earlier identification of key change points in these records will provide better instruction on the likely sea level projection

pathway committed, to enable more targeted coastal planning and adaptation endeavours into the foreseeable future.

Nonetheless this work should be considered a staging point for ongoing improvements in the area of sea level research. A range of potential research projects that can build on the outputs of this thesis to further progress sea level (and climate change) research, are discussed in Section 7.2.

7.1 Key Learnings and Insights from Research

The development of the synthetic data (Chapter 2) and the extensive associated time series analysis testing (Chapter 3) provide a novel, landmark attempt to build a robust and unique framework within which to identify the optimal analytical methods for isolating the mean sea level trend with improved temporal accuracy (Visser *et al.*, 2015). The scale of testing undertaken (over 29 million individual time series analyses) is unprecedented for sea level research purposes.

Key findings from the testing included that enhanced accuracy in resolving the temporal resolution of the trend is achieved through using a combination of:

- ❑ annual average mean sea level data;
- ❑ minimum length data of ≈ 80 years; and
- ❑ “data adaptive” analytics, in particular, Singular Spectrum Analysis (SSA) and multi-resolution wavelet decomposition.

In moving forward to develop a general purpose analysis tool to enhance sea level research, SSA is the more instructive and convenient given the technique provides a superior capability to separate key time varying harmonic components of the time series (refer Chapters 3 and 4).

It is surprising that despite the evident utility of SSA for mean sea level analysis (Chapter 3), there have been comparatively limited examples of its application for this purpose in the literature (e.g., Hein *et al.*, 2011; Holgate *et al.*, 2007; Jevrejeva *et al.*, 2006, 2008; Mather, 2007; Unal and Ghil, 1995; Wahl *et al.*, 2010, 2011, 2013). The parameterization of SSA applied

in the afore-mentioned studies differs considerably, ostensibly based on user intuition and experience, but, none have benefitted from specific optimisation or testing.

Based upon detailed decomposition and analysis of more than 50 of the world's longest records in the Permanent Service for Mean Sea Level (PSMSL) data holdings, the parameterization and performance of SSA has been specifically optimised through this research (Chapter 4) and integrated into an extension package titled *msltrend* (Section 4.6) within the R Project for Statistical Computing to isolate the mean sea level (or trend) signal from long ocean water level data sets with improved temporal resolution and accuracy.

In particular, from the aforementioned analysis, the component(s) from the SSA decomposition which best represent the trend of mean sea level can be effectively isolated using spectral thresholding techniques that capture and reconstruct only components in which 75% of the contribution for each component is confined within the low frequency band [0 - 0.01]. The fitting of a cubic smoothing spline to the isolated trend enables velocity and acceleration (as the first and second derivatives) in mean sea level to be determined at each time step in the original time series with improved resolution.

Key functions and settings within *msltrend* have been specifically optimised and “hard-wired” into the scripting code to prevent inexperienced or untrained sea level analysts from producing misleading results. With the inclusion of a range of output options and a forecasting module to consider the implication of user-defined quantum of sea level rise between the end of the available historical record and the year 2100, *msltrend* is a powerful, freely available, diagnostic research tool that enhances contemporary sea level research appreciably.

The application of the *msltrend* package to the various GMSL reconstructions (Watson, 2016d) and data rich margins of continental USA (Chapter 5) and Europe (Chapter 6), highlight the value of improving the temporal accuracy of the mean sea level signal by removing the contaminating dynamic influences and noise. It is clear from these studies that mean sea level velocity time series are distinctly non-linear, in turn reflective of associated acceleration varying over time. These regional studies are the largest and most detailed works of their type undertaken across both margins, providing pivotal and more instructive knowledge and

conclusions on the nature of acceleration in mean sea level than previously possible (refer Table 7.1).

These studies also highlight the comparatively low time varying velocities and associated accelerations evident over the period of historical records. Until such time as the velocities and accelerations in mean sea level are sufficiently large not to be obscured by complex influences inducing decadal to multi-decadal variability and other background noise, the search for accelerations in ocean water level records require more intuitive, diagnostic considerations (refer Chapters 4, 5 and 6).

For example, the search for acceleration is perhaps more practically inferred by considering whether or not peaks in the instantaneous velocity and acceleration time series are increasing, becoming more sustained or statistically abnormal (or different) over time in the context of the historical record. These diagnostic approaches will continue to be important until the extent of sea level rise (due to climate change) is sufficient to be statistically differentiated from the remnant historical record with widespread spatial coherence (refer Chapters 5 and 6).

Table 7.1: Snapshot of Key Findings and Learnings.

Key Finding	Further Information
Singular Spectrum Analysis (SSA) is an optimal analytic for isolating mean sea level with improved temporal resolution and accuracy from dynamic influences embedded within ocean water level time series	Chapter 3
Conditioning the input data and optimisation of the parameterisation of SSA (specific to ocean water level time series) enhances the accuracy of the estimate of mean sea level	Chapter 4, Table 4.3
Real-time measured velocity and acceleration provide an improved understanding of the time-varying properties of mean sea level	Chapters 4, 5, 6
The comparatively low time varying velocities and associated accelerations evident over the majority of historical records analysed, deem that acceleration is unwisely measured as a simple metric. Until such time as the apparent real-time velocities and accelerations in the mean sea level signal are sufficiently large not to be obscured by complex influences inducing decadal to multi-decadal variability and other background noise, the search for accelerations in these records require more intuitive, diagnostic considerations.	Chapters 5, 6

Table continued over page.

Table 7.1 (cont)

For example, the search for acceleration is perhaps more practically inferred by considering whether or not peaks in the instantaneous velocity and acceleration time series are increasing, becoming more sustained or statistically abnormal (or different) over time in the context of the historical record. This type of approach will continue to be important until the extent of sea level rise (due to climate change) is sufficient to be statistically differentiated from the remnant historical record with widespread spatial coherence.	Chapters 5, 6
Although sea level has risen around continental USA over the period of available tide gauge records (1853 - 2014), clear and differing spatial signatures in sea level rise have emerged between the Central Pacific and west coast compared to those within the Gulf of Mexico and along the east coast.	Chapter 5
No evidence of acceleration in mean sea level across the Central Pacific and along the west coast of the USA to the end of 2014.	Chapter 5
Subtle evidence of a more recent acceleration in mean sea level within the Gulf of Mexico and along the east coast of the USA. It is possible that the recent increase in instantaneous velocities and accelerations within these margins might signal the onset of large projected sea level rises due to climate change forecasts over the course of the 21st century (and beyond).	Chapter 5
Current (2014) geocentric sea level rise around the USA highlights the spatial fingerprint of the sea level rise phenomena. The average rate for the Central Pacific and west coast stations is 1.20 ± 0.45 mm/yr compared to the Gulf of Mexico and along the east coast where the average rate is some 80% higher at 2.19 ± 0.58 mm/yr (95% CI).	Chapter 5
No evidence to support the various recent published works alluding to a so-called 'hotspot' of accelerated sea level rise, particularly along the US east coast margin north of Cape Hatteras.	Chapter 5
Although there has been a general tendency for velocity in mean sea level to increase over time, inferring an acceleration to do so, these kinematic properties of the mean sea level signal around Europe have continued to vary over the course of the historical records available at generally low measured rates. The analysis suggests key periods of acceleration centred in bands around ≈ 1880 to 1910, 1940, 1976 and a strong spatially coherent signal between 1994 and 2000 consistent with the general findings of previous researchers using different techniques.	Chapter 6
The results and findings from the large study of European mean sea level records are broadly consistent with those for the complementary study of the mainland USA records. Whilst the accelerated climate change influence is not yet statistically evident in these records, depending on the climate change trajectory, it is highly likely that such changes will take at least 15 - 20 years to manifest in the network of tide gauge records examined.	Chapters 5, 6

7.2 Future Research

Moving forward, there are a range of potential research projects that can build on the outputs of this thesis to further progress sea level (and climate change) research, summarised in priority order in Table 7.2 (following page).

Table 7.2: Priority Research Projects.

Priority	Research Task
1	Investigating the utility of long tide gauge records and the refined mean sea level signal derived from <i>msslrend</i> to augment existing protocols for evaluating sea surface height projections from climate models (Flato <i>et al.</i> , 2013). Presently, global Archiving, Validation and Interpretation of Satellite Oceanographic (AVISO) data products currently used to evaluate Coupled Model Intercomparison Project (or CMIP) dynamic sea surface heights are only 20–25 years in length. Therefore, the longer decadal and multi-decadal influences are not readily isolated from these satellite data products at this point in time. The real-time velocities determined from long, quality tide gauge records might be useful in augmenting the much shorter global AVISO products at a finer localised scale.
2	Improving estimates of vertical land motion at tide gauges via comparison between geocentric satellite altimetry products and relative tide gauge time series. Various techniques have been proposed in this space over recent years (e.g., Pfeffer and Allemand (2016); Ostanciaux <i>et al.</i> (2012)) to augment the network of direct collocated GPS measurements (Santamaría-Gómez <i>et al.</i> , 2012; SONEL, 2016), but continued research and development in this area with lengthening altimetry records makes this a crucial imperative to improve estimates of geocentric mean sea level from valuable, long, tide gauge records. This research initiative might also consider investigating improved time series techniques to determine the non-linear characteristics of vertical land motion (VLM) measured at tide gauges (highlighted in Section 5.5.1) moving beyond the comparatively simple linear regression techniques commonly applied in this area.
3	Continued data archaeology efforts to find and digitise long tide gauge records to fill spatial gaps, principally in the southern hemisphere to augment the data repository of the PSMSL. Watson <i>et al.</i> (2012) notes that only 2 of some 123 records held by the PSMSL that pre-date 1900 are located within the southern hemisphere, i.e. Fort Denison (1886) and Fremantle (1897). However, this work notes that several additional sites around Australia commenced tide gauge recording dating back to 1858. In addition to the southern hemisphere, the search for additional tide gauge data records of sufficient length (at least 75-80 years) should be focused around important margins including the southern coasts of the African continent and along the coastlines of China. Extensive work in this area has already begun (e.g., Hogarth, 2012; Talke and Jay, 2013) but needs to be further supported and expanded.
4	Continued time series analysis research and development to provide the earliest identification of change points in recent portions of mean sea level records that are reflective of a fundamental change in the external (or radiative) forcings associated with climate change.
5	rolling some of the above-mentioned elements into a more advanced version of the <i>msslrend</i> package.

Chapter 8

Bibliography

- ABC-TV, 2011. Australian Broadcasting Corporation Television (ABC-TV) website. Episode 25: “Ask the Experts” Media Watch Program, 1 August.
URL: <http://www.abc.net.au/mediawatch/transcripts/s3282940.htm>
- Alexandrov, T., Bianconcini, S., Dagum, E.B., Maass, P. and McElroy, T.S., 2012. A review of some modern approaches to the problem of trend extraction. *Econometric Reviews*, 31(6), pp.593-624.
- Alexandrov, T., and Golyandina, N., 2005. Automatic extraction and forecast of time series cyclic components within the framework of SSA. In: *Proc. of the 5th St. Petersburg Workshop on Simulation*, St.Petersburg State University, St.Petersburg, pp.45-50. June.
- Andres, M., Gawarkiewicz, G.G., and Toole, J.M., 2013. Interannual sea level variability in the western North Atlantic: Regional forcing and remote response. *Geophysical Research Letters*, 40(22), pp.5915-5919.
- Aoki, S., 2002. Coherent sea level response to the Antarctic Oscillation. *Geophysical Research Letters*, 29(20), 11(1)-11(4).
- Arabelos, D.N., Papazachariou, D.Z., Contadakis, M.E., and Spatalas, S.D., 2011. A new tide model for the Mediterranean Sea based on altimetry and tide gauge assimilation. *Ocean Science*, 7(3), pp.429-444.
- Argus, D.F., Peltier, W.R., Drummond, R., and Moore, A.W., 2014. The Antarctica component of postglacial rebound model ICE-6G_C (VM5a) based on GPS positioning, exposure age dating of ice thicknesses, and relative sea level histories. *Geophysical Journal International*, 198(1), pp.537-563.
- Australia, 2011. House of Representatives—Debates, 20 September, pp.10778–10780.
- Avsar, N.B., Jin, S.; Kutoglu, H., and Gurbuz, G., 2016. Sea level change along the Black Sea coast from satellite altimetry, tide gauge and GPS observations. *Geodesy and Geodynamics*, 7(1), pp.50-55.
- Baart, F., Van Koningsveld, M., and Stive, M., 2012a. Trends in sea-level trend analysis. *Journal of Coastal Research*, 28(2), pp.311–315.
- Baart, F., van Gelder, P.H.A.J.M., de Ronde, J.; van Koningsveld, M., and Wouters, B., 2012b. The Effect of the 18.6-Year Lunar Nodal Cycle on Regional Sea-Level Rise Estimates. *Journal of Coastal Research*, 28(2), pp.512–516.
- Bakan, G., and Büyükgüngör, H., 2000. The black sea. *Marine Pollution Bulletin*, 41(1), pp.24-43.
- BAS, 2013. British Antarctic Survey (BAS), Natural Environment Research Council, UK website, accessed December 2013. URL: <http://www.antarctica.ac.uk/met/gjma/sam.html>

- Beckers, J.M. and Rixen, M., 2003. EOF calculations and data filling from incomplete oceanographic datasets. *Journal of Atmospheric and Oceanic Technology*, 20(12), pp.1839-1856.
- Bevis, M., Scherer, W. and Merrifield, M., 2002. Technical issues and recommendations related to the installation of continuous GPS stations at tide gauges. *Marine Geodesy*, 25(1-2), pp.87-99.
- Bindoff, N.L., Willebrand, J., Artale, V., Cazenave, A., Gregory, J.; Gulev, S., Hanawa, K., Le Quéré, C., Levitus, S.; Nojiri, Y., Shum, C.K., Talley, L.D., and Unnikrishnan, A., 2007. Observations: Oceanic Climate Change and Sea Level. In: *Climate Change 2007: The Physical Science Basis*. Contribution of Working Group I to the Fourth Assessment Report of the Intergovernmental Panel on Climate Change [Solomon, S., Qin, D., Manning, M., Chen, Z., Marquis, M., Averyt, K.B., Tignor, M., and Miller, H.L., (eds.)]. Cambridge University Press, Cambridge, United Kingdom and New York, NY, USA.
- Bingham, R.J., and Hughes, C.W., 2009. Signature of the Atlantic meridional overturning circulation in sea level along the east coast of North America. *Geophysical Research Letters*, 36(2), doi: 10.1029/2008GL036215.
- BoM, 2013. Bureau of Meteorology (BoM) website, accessed December 2013.
URL: <http://www.bom.gov.au/climate/current/soihtm1.shtml>.
- Boon, J.D., 2012. Evidence of sea level acceleration at US and Canadian tide stations, Atlantic Coast, North America. *Journal of Coastal Research*, 28(6), pp.1437-1445.
- Boon, J.D., and Mitchell, M., 2015. Nonlinear change in sea level observed at North American tide stations. *Journal of Coastal Research*, 31(6), pp.1295-1305.
- Bowman, D.C., and Lees, J.M., 2013. The Hilbert–Huang transform: A high resolution spectral method for nonlinear and nonstationary time series. *Seismological Research Letters*, 84(6), pp.1074-1080.
- Breaker, L.C., and Ruzmaikin, A., 2011. The 154-year record of sea level at San Francisco: extracting the long-term trend, recent changes, and other tidbits. *Climate Dynamics*, 36(3-4), pp.545-559.
- Breaker, L.C. and Ruzmaikin, A., 2013. Estimating rates of acceleration based on the 157-year record of sea level from San Francisco, California, USA. *Journal of Coastal Research*, 29(1), pp.43-51.
- Bromirski, P.D., Miller, A.J., Flick, R.E., and Auad, G., 2011. Dynamical suppression of sea level rise along the Pacific coast of North America: Indications for imminent acceleration. *Journal of Geophysical Research: Oceans*, 116(C7), doi: 10.1029/2010JC006759.

- Broomhead, D.S., and King, G.P., 1986. Extracting qualitative dynamics from experimental data. *Physica D: Nonlinear Phenomena*, 20(2), pp.217-236.
- Brown, S., Nicholls, R.J., Vafeidis, A., Hinkel, J., and Watkiss, P., 2011. The impacts and economic costs of sea-level rise in Europe and the costs and benefits of adaptation. Summary of results from the *EC RTD ClimateCost Project*. Watkiss, P (editor).
- Buckley, M.W., and Marshall, J., 2016. Observations, inferences, and mechanisms of the Atlantic Meridional Overturning Circulation: A review. *Reviews of Geophysics*, 54, pp.5–63.
- Bungenstock, F., and Schäfer, A., 2009. The Holocene relative sea-level curve for the tidal basin of the barrier island Langeoog, German Bight, Southern North Sea. *Global and Planetary Change*, 66(1), pp.34-51.
- Calafat, F.M., Chambers, D.P., and Tsimplis, M.N., 2012. Mechanisms of decadal sea level variability in the eastern North Atlantic and the Mediterranean Sea. *Journal of Geophysical Research: Oceans*, 117(C9), doi: 10.1029/2012JC008285.
- Calafat, F., and Chambers, D., 2013. Quantifying recent acceleration in sea level unrelated to internal climate variability. *Geophysical Research Letters*, 40(14), pp.3661-3666.
- Carton, J.A., and Wahr, J.M., 1986. Modelling the pole tide and its effect on the Earth's rotation. *Geophysical Journal of the Royal Astronomical Society*, 84, pp.121–137.
- Cazenave, A., Henry, O., Munier, S., Delcroix, T., Gordon, A., Meyssignac, B., Llovel, W., Palanisamy, H., and Becker, M., 2012. Estimating ENSO influence on the global mean sea level, 1993–2010. *Marine Geodesy*, 35(sup1), pp.82-97.
- Chambers, D.P., Merrifield, M.A., and Nerem, R.S., 2012. Is there a 60-year oscillation in global mean sea level? *Geophysical Research Letters*, 39(18), doi: 10.1029/2012GL052885.
- Chao, B.F., O'Connor, W.P., Zheng, D., and Au, A.Y., 2001. Reply to comment by Wunsch, C on "Wind stress forcing of the North Sea pole tide". *Geophysical Journal International*, 146, 266.
- Cherniawsky, J.Y., Foreman, M.G.G., Kang, S.K.; Scharroo, R., and Eert, A.J., 2009. 18.6-year lunar nodal tides from altimeter data. *Continental Shelf Research*, 30, pp.575–587.
- Church, J.A., White, N.J., Coleman, R., Lambeck, K., and Mitrovica, J.X., 2004. Estimates of the regional distribution of sea level rise over the 1950-2000 period. *Journal of Climate*, 17(13), pp.2609-2625.
- Church, J.A., and White, N.J., 2006. A 20th century acceleration in global sea-level rise. *Geophysical Research Letters*, 33(1), doi: 10.1029/2005GL024826.
- Church, J.A., and White, N.J., 2011. Sea level rise from the late 19th to the early 21st century. *Survey of Geophysics*, 32, pp.585-602.

- Church, J.A. Clark, P.U., Cazenave, A., Gregory, J.M., Jevrejeva, S., Levermann, A., Merrifield, M.A., Milne, G.A., Nerem, R.S., Nunn, P.D., Payne, A.J., Pfeffer, W.T., Stammer, D., and Unnikrishnan, A.S., 2013a. Sea Level Change. In: *Climate Change 2013: The Physical Science Basis*. Contribution of Working Group I to the Fifth Assessment Report of the Intergovernmental Panel on Climate Change [Stocker, T.F., Qin, D., Plattner, G-K., Tignor, M., Allen, S.K., Boschung, J., Nauels, A., Xia, Y., Bex, V., and Midgley, P.M., (eds.)]. Cambridge University Press, Cambridge United Kingdom and New York, NY, USA.
- Church, J.A. Clark, P.U., Cazenave, A., Gregory, J.M., Jevrejeva, S., Levermann, A., Merrifield, M.A., Milne, G.A., Nerem, R.S., Nunn, P.D., Payne, A.J., Pfeffer, W.T., Stammer, D., and Unnikrishnan, A.S., 2013b. Sea Level Change Supplementary Material. In: *Climate Change 2013: The Physical Science Basis*. Contribution of Working Group I to the Fifth Assessment Report of the Intergovernmental Panel on Climate Change [Stocker, T.F., Qin, D., Plattner, G-K., Tignor, M., Allen, S.K., Boschung, J., Nauels, A., Xia, Y., Bex, V., and Midgley, P.M., (eds.)]. Cambridge University Press, Cambridge United Kingdom and New York, NY, USA.
- Cleveland, R.B., Cleveland, W.S., McRae, J.E., and Terpenning, I., 1990. STL: A seasonal-trend decomposition procedure based on loess. *Journal of Official Statistics*, 6(1), pp.3-73.
- Conomos, T.J., 1979. Properties and circulation of San Francisco Bay waters. In: Conomos, T.J., Leviton, A.E., and Berson, M., (eds.), *San Francisco Bay: The Urbanized Estuary*. Lawrence, Kansas: Allen Press, pp.47–84.
- CRU, 2013. Climatic Research Unit (CRU), University of East Anglia, UK website, accessed December 2013.
URL: <http://www.cru.uea.ac.uk/cru/dat/noa/>.
- Currie, R.G., 1975. Period, Qp and amplitude of the pole tide. *Geophysical Journal International*, 43(1), pp.73-86.
- Dangendorf, S., Wahl, T., Hein, H., Jensen, J., Mai, S., and Mudersbach, C., 2012. Mean sea level variability and influence of the North Atlantic Oscillation on long-term trends in the German Bight. *Water*, 4(1), pp.170-195.
- Dangendorf, S., Calafat, F.M., Arns, A., Wahl, T., Haigh, I.D., and Jensen, J., 2014. Mean sea level variability in the North Sea: processes and implications. *Journal of Geophysical Research: Oceans*, 119(10), doi: 10.1002/2014JC009901.
- Dangendorf, S., Marcos, M., Müller, A., Zorita, E., Riva, R., Berk, K., and Jensen, J., 2015. Detecting anthropogenic footprints in sea level rise. *Nature Communications*, 6, doi: 10.1038/ncomms8849.

- Daubechies, I., 1988. Orthonormal bases of compactly supported wavelets. *Communications on Pure and Applied Mathematics*, 41(7), pp.909-996.
- Daubechies, I., 1992. *Ten lectures on wavelets*. Philadelphia: Society for Industrial and Applied Mathematics (SIAM).
- Daubechies, I., Lu, J., and Wu, H.T., 2011. Synchrosqueezed wavelet transforms: an empirical mode decomposition-like tool. *Applied and Computational Harmonic Analysis*, 30(2), pp.243-261.
- Desai, S.D., 2002. Observing the pole tide with satellite altimetry. *Journal of Geophysical Research: Oceans* (1978-2012), 107 (C11), 1:7 – 1:13.
- Deser, C., Alexander, M.A., Xie, S.P. and Phillips, A.S., 2010. Sea surface temperature variability: Patterns and mechanisms. *Annual review of marine science*, 2, pp.115-143.
- Deshayes, J., and Frankignoul, C., 2008. Simulated variability of the circulation in the North Atlantic from 1953 to 2003. *Journal of Climate*, 21(19), pp.4919-4933.
- Di Lorenzo, E., Schneider, N., Cobb, K.M., Franks, P.J.S., Chhak, K., Miller, A.J., McWilliams, J.C., Bograd, S.J., Arango, H., Curchitser, E., and Powell, T.M., 2008. North Pacific Gyre Oscillation links ocean climate and ecosystem change. *Geophysical Research Letters*, 35(8), doi: 10.1029/2007GL032838.
- Domingues, C.M., Church, J.A., White, N.J., Gleckler, P.J., Wijffels, S.E., Barker, P.M., and Dunn, J.R., 2008. Improved estimates of upper-ocean warming and multi-decadal sea-level rise. *Nature*, 453(7198), pp.1090-1093.
- Donner, R.V., Ehrcke, R., Barbosa, S.M., Wagner, J., Donges, J.F., and Kurths, J., 2012. Spatial patterns of linear and nonparametric long-term trends in Baltic sea-level variability. *Nonlinear Processes in Geophysics*, 19(1), pp.95-111.
- Donoghue, J.F., and Parkinson, R.W., 2011. Discussion of: Houston, J.R., and Dean, R.G., 2011. Sea-Level Acceleration Based on U.S. Tide Gauges and Extensions of Previous Global-Gauge Analyses. *Journal of Coastal Research*, 27(3), pp.409–417, *Journal of Coastal Research*, 994-996, Online publication date: 1 Sep 2011.
- Douglas, B.C., 1992. Global sea level acceleration. *Journal of Geophysical Research: Oceans* (1978–2012), 97(C8), pp.12699-12706.
- Douglas, B.C., 1997. Global sea rise: a redetermination. *Surveys in Geophysics*, 18(2-3), pp.279-292.
- Douglas, B.C., 2001. Sea level change in the era of the recording tide gauge. *International Geophysics*, 75, pp.37-64.

- Douglas, B.C., 2008. Concerning evidence for fingerprints of glacial melting. *Journal of Coastal Research*, 24(sp2), pp.218-227.
- Durbin, J., and Koopman, S.J., 2012. *Time Series Analysis by State Space Methods (No. 38)*. Oxford University Press.
- Eilers, P.H., and Marx, B.D., 1996. Flexible smoothing with B-splines and penalties. *Statistical Science*, 11(2), pp.89-102.
- Ekman, M. and Stigebrandt, A., 1990. Secular change of the seasonal variation in sea level and of the pole tide in the Baltic Sea. *Journal of Geophysical Research: Oceans*, 95(C4), pp.5379-5383.
- Emery, K.O., and Aubrey, D.G., 1991. *Sea Levels, Land Levels, and Tide Gauges*. Springer-Verlag Publishing, New York.
- Ericson, J.P., Vörösmarty, C.J., Dingman, S.L., Ward, L.G., and Meybeck, M., 2006. Effective sea-level rise and deltas: causes of change and human dimension implications. *Global and Planetary Change*, 50(1), pp.63-82.
- Eyring, V., Bony, S., Meehl, G.A., Senior, C.A., Stevens, B., Stouffer, R.J., and Taylor, K.E., 2016. Overview of the Coupled Model Intercomparison Project Phase 6 (CMIP6) experimental design and organization. *Geoscientific Model Development*, 9(5), pp.1937-1958.
- Ezer, T., Atkinson, L.P., Corlett, W.B., and Blanco, J.L., 2013. Gulf Stream's induced sea level rise and variability along the US mid-Atlantic coast. *Journal of Geophysical Research: Oceans*, 118(2), pp.685-697.
- Fasullo, J.T., Boening, C., Landerer, F.W., and Nerem, R.S., 2013. Australia's unique influence on global sea level in 2010–2011. *Geophysical Research Letters*, 40(16), pp.4368-4373.
- Fasullo, J.T., Nerem, R.S. and Hamlington, B., 2016. Is the detection of accelerated sea level rise imminent? *Scientific Reports*, 6, doi: 10.1038/srep31245.
- Flato, G., Marotzke, J., Abiodun, B., Braconnot, P., Chou, S.C., Collins, W., Cox, P., Driouech, F., Emori, S., Eyring, V., *et al.*, 2013. Evaluation of Climate Models. In *Climate Change 2013: The Physical Science Basis*. Contribution of Working Group I to the Fifth Assessment Report of the Intergovernmental Panel on Climate Change [Stocker, T.F., Qin, D., Plattner, G-K., Tignor, M., Allen, S.K., Boschung, J., Nauels, A., Xia, Y., Bex, V., and Midgley, P.M., (eds.)]. Cambridge University Press, Cambridge United Kingdom and New York, NY, USA.
- Foreman, M.G.G., 1977. *Manual for tidal heights analysis and prediction*. Pacific Marine Science Report No. 77–10, Institute of Ocean Sciences, Patricia Bay, Sidney, BC, 66pp.
- Foster, G., and Brown, N., 2015. Time and tide: analysis of sea level time series. *Climate Dynamics*, 45, pp.291–308.

- Garcia, D., Vigo, I., Chao, B.F., and Martinez, M.C., 2007. Vertical crustal motion along the Mediterranean and Black Sea coast derived from ocean altimetry and tide gauge data. *Pure and Applied Geophysics*, 164(4), pp.851-863.
- Getzlaff, J., Böning, C.W., Eden, C., and Biastoch, A., 2005. Signal propagation related to the North Atlantic overturning. *Geophysical Research Letters*, 32(9), doi: 10.1029/2004GL021002.
- Ghil, M., Allen, M.R., Dettinger, M.D., Ide, K., Kondrashov, D., Mann, M.E., Robertson, A.W., Saunders, A., Tian, Y., Varadi, F., and Yiou, P., 2002. Advanced spectral methods for climatic time series. *Reviews of Geophysics*, 40(1), doi: 10.1029/2000RG000092.
- Gillett, N.P., Arora, V.K., Zickfeld, K., Marshall, S.J., and Merryfield, W.J., 2011. Ongoing climate change following a complete cessation of carbon dioxide emissions. *Nature Geoscience*, 4(2), pp.83-87.
- Goddard, P.B., Yin, J., Griffies, S.M., and Zhang, S., 2015. An extreme event of sea-level rise along the Northeast coast of North America in 2009–2010. *Nature Communications*, 6, doi: 10.1038/ncomms7346.
- Godin, G., 1972. *The Analysis of Tides*. University of Toronto Press, Toronto, Ontario, 264pp.
- Golyandina, N., Nekrutkin, V., and Zhigljavsky, A.A., 2001. *Analysis of time series structure: SSA and related techniques*. Chapman and Hall/CRC Press.
- Golyandina, N., and Korobeynikov, A., 2014. Basic singular spectrum analysis and forecasting with R. *Computational Statistics & Data Analysis*, 71, pp.934-954.
- Golyandina, N. and Osipov, E., 2007. The "Caterpillar"-SSA method for analysis of time series with missing values. *Journal of Statistical Planning and Inference*, 137(8), pp.2642–2653.
- Golyandina, N. and Shlemov, A., 2014. Variations of singular spectrum analysis for separability improvement: non-orthogonal decompositions of time series. *arXiv preprint arXiv:1308.4022*.
- Golyandina, N. and Zhigljavsky, A., 2013. *Singular Spectrum Analysis for time series*. Springer Science & Business Media.
- Gomis, D., Tsimplis, M.N., Martín-Míguez, B., Ratsimandresy, A.W., García-Lafuente, J., and Josey, S.A., 2006. Mediterranean Sea level and barotropic flow through the Strait of Gibraltar for the period 1958–2001 and reconstructed since 1659. *Journal of Geophysical Research: Oceans*, 111(C11), doi: 10.1029/2005JC003186.
- Gomis, D., Ruiz, S., Sotillo, M.G., Álvarez-Fanjul, E., and Terradas, J., 2008. Low frequency Mediterranean sea level variability: the contribution of atmospheric pressure and wind. *Global and Planetary Change*, 63(2), pp.215-229.

- Gong, D. and Wang, S., 1999. Definition of Antarctic oscillation index. *Geophysical research letters*, 26(4), pp.459-462.
- Goosse, H., Masson-Delmotte, V., Renssen, H., Delmotte, M., Fichefet, T., Morgan, V., Van Ommen, T., Khim, B.K., and Stenni, B., 2004. A late medieval warm period in the Southern Ocean as a delayed response to external forcing? *Geophysical Research Letters*, 31(6), doi: 10.1029/2003GL019140.
- Goosse, H., and Renssen, H., 2005. A simulated reduction in Antarctic sea-ice area since 1750: implications of the long memory of the ocean. *International Journal of Climatology*, 25(5), pp.569-579.
- GRETl, 2013. Gnu Regression, Econometrics and Time series Library (GRETl) website, accessed July 2013. URL: <http://www.gretl.sourceforge.net/>.
- Grieser, J., Trömel, S., and Schönwiese, C.D., 2002. Statistical time series decomposition into significant components and application to European temperature. *Theoretical and Applied Climatology*, 71, pp.171-183.
- Gross, R.S., 2000. The excitation of the Chandler wobble. *Geophysical Research Letters*, 27(15), pp.2329-2332.
- Grossmann, A., and Morlet, J., 1984. Decomposition of Hardy functions into square integrable wavelets of constant shape. *SIAM Journal on Mathematical Analysis*, 15(4), pp.723-736.
- Grossmann, A., Kronland-Martinet, R., and Morlet, J., 1989. Reading and understanding continuous wavelet transforms. In: *Wavelets* (pp. 2-20). Springer Berlin Heidelberg.
- Haigh, I., Nicholls, R., and Wells, N., 2009. Mean sea level trends around the English Channel over the 20th century and their wider context. *Continental Shelf Research*, 29(17), pp.2083-2098.
- Haigh, I.D., Wahl, T., Rohling, E.J., Price, R.M., Pattiaratchi, C.B., Calafat, F.M., and Dangendorf, S., 2014. Timescales for detecting a significant acceleration in sea level rise. *Nature Communications*, 5, doi: 10.1038/ncomms4635.
- Hallegatte, S., Green, C., Nicholls, R.J. and Corfee-Morlot, J., 2013. Future flood losses in major coastal cities. *Nature climate change*, 3(9), pp.802-806.
- Hamlington, B.D., Leben, R.R., Nerem, R.S., Han, W., and Kim, K.Y., 2011. Reconstructing sea level using cyclostationary empirical orthogonal functions. *Journal of Geophysical Research: Oceans*, 116(C12), doi: 10.1029/2011JC007529.
- Hamlington, B.D., Leben, R.R., Strassburg, M.W., Nerem, R.S., and Kim, K.-Y., 2013. Contribution of the Pacific Decadal Oscillation to global mean sea level trends. *Geophysical Research Letters*, 40, pp.5171-5175.

- Han, J., and van der Baan, M., 2013. Empirical mode decomposition for seismic time-frequency analysis. *Geophysics*, 78(2), pp.9-19.
- Hanna, E., Navarro, F.J., Pattyn, F., Domingues, C.M., Fettweis, X., Ivins, E.R., Nicholls, R.J., Ritz, C., Smith, B., Tulaczyk, S. and Whitehouse, P.L., 2013. Ice-sheet mass balance and climate change. *Nature*, 498(7452), pp.51-59.
- Hannah, J., 1990. Analysis of mean sea level data from New Zealand for the period 1899–1988. *Journal of Geophysical Research*, 95(B6), pp.12,399–12,405.
- Hannah, J., 2004. An updated analysis of long-term sea level change in New Zealand. *Geophysical Research Letters*, 31, L03307, doi: 10.1029/2003GL019166.
- Hannah, J. and Bell, R.G., 2012. Regional sea level trends in New Zealand. *Journal of Geophysical Research: Oceans*, 117(C1), doi: 10.1029/2011JC007591.
- Hansen, J.M., Aagaard, T., and Binderup, M., 2012. Absolute sea levels and isostatic changes of the eastern North Sea to central Baltic region during the last 900 years. *Boreas*, 41(2), pp.180-208.
- Hassani, H., Mahmoudvand, R., and Zokaei, M., 2011. Separability and window length in singular spectrum analysis. *Comptes Rendus Mathématique*, 349(17), pp.987-990.
- Haubrich, R. and Munk, W., 1959. The pole tide. *Journal of Geophysical Research*, 64(12), pp.2373-2388.
- Hay, C.C., Morrow, E., Kopp, R.E., and Mitrovica, J.X., 2015. Probabilistic reanalysis of twentieth-century sea-level rise. *Nature*, 517(7535), pp.481-484.
- Hein, H., Mai, S., and Barjenbruch, U., 2011. What tide gauges reveal about the future sea level. *Proceedings of the Aqua Alta*, Hamburg.
- Hendricks, J.R., Leben, R.R., Born, G.H., and Koblinsky, C.J., 1996. Empirical orthogonal function analysis of global TOPEX/POSEIDON altimeter data and implications for detection of global sea level rise. *Journal of Geophysical Research: Oceans*, 101(C6), pp.14131-14145.
- Higginson, S., Thompson, K.R., Woodworth, P.L., and Hughes, C.W., 2015. The tilt of mean sea level along the east coast of North America. *Geophysical Research Letters*, 42(5), pp.1471-1479.
- Hogarth, P., 2014. Preliminary analysis of acceleration of sea level rise through the twentieth century using extended tide gauge data sets (August 2014). *Journal of Geophysical Research: Oceans*, 119(11), pp.7645-7659.
- Holgate, S., Jevrejeva, S., Woodworth, P., and Brewer, S., 2007. Comment on “A semi-empirical approach to projecting future sea-level rise”. *Science*, 317(5846), pp.1866b-1866b.

- Holgate, S.J., Matthews, A., Woodworth, P.L., Rickards, L.J., Tamisiea, M.E., Bradshaw, E., Foden, P.R., Gordon, K.M., Jevrejeva, S., and Pugh, J., 2012. New data systems and products at the permanent service for mean sea level. *Journal of Coastal Research*, 29(3) pp.493-504.
- Houser, T., Hsiang, S., Kopp, R. and Larsen, K., 2015. *Economic risks of climate change: an American prospectus*. Columbia University Press.
- Houston J.R., and Dean R.G., 2011a. Sea-level acceleration based on U.S. tide gauges and extensions of previous global-gauge analyses. *Journal of Coastal Research*, 27(3), pp.409-417.
- Houston, J.R., and Dean, R.G., 2011b. Reply to: Rahmstorf, S., and Vermeer, M., 2011. Discussion of: Houston, J.R., and Dean, R.G., 2011. Sea-Level Acceleration Based on U.S. Tide Gauges and Extensions of Previous Global-Gauge Analyses. *Journal of Coastal Research*, 27(3), pp.409–417, *Journal of Coastal Research*, pp.788-790. Online publication date: 1 Jul 2011.
- Houston, J.R., and Dean, R.G., 2011c. Accounting for the nodal tide to improve estimates of sea level acceleration. *Journal of Coastal Research*, 27(5), pp.801–807.
- Houston, J.R., and Dean, R.G., 2013. Effects of sea-level decadal variability on acceleration and trend difference. *Journal of Coastal Research*, 29(5), pp.1062-1072.
- Houston, J.R., 2016. Discussion of: Boon, J.D., and Mitchell, M., 2015. Nonlinear change in sea level observed at North American tide stations. *Journal of Coastal Research*, 31(6), pp.1295-1305, *Journal of Coastal Research*, 32(4), pp.983-987.
- Huang, N.E., Shen, Z., Long, S.R., Wu, M.C., Shih, E.H., Zheng, Q., Tung, C.C., and Liu, H.H., 1998. The empirical mode decomposition and the Hilbert spectrum for nonlinear and non-stationary time series analysis. *Proceedings of the Royal Society of London. Series A: Mathematical, Physical and Engineering Sciences*, 454(1971), pp.903–995.
- Hughes, C.W., Woodworth, P.L., Meredith, M.P., Stepanov, V., Whitworth, T., and Pyne, A.R., 2003. Coherence of Antarctic sea levels, Southern Hemisphere Annular Mode, and flow through Drake Passage. *Geophysical Research Letters*, 30(9), 1464.
- Hünicke, B. and Zorita, E., 2016. Statistical Analysis of the Acceleration of Baltic Mean Sea-Level Rise, 1900–2012. *Frontiers in Marine Science*, 3, p.125.
- Hurrell, J.W., 1995. Decadal trends in the North Atlantic Oscillation: regional temperatures and precipitation. *Science*, 269, pp.676–679.
- Hyndman, R.J., and Khandakar, Y., 2008. Automatic Time Series Forecasting: The Forecast Package for R. *Journal of Statistical Software*, 26(3), pp.1-22.
- IERS, 2013. International Earth Rotation and Reference Systems Services (IERS) website, accessed November 2013,

URL: http://www.iers.org/nn_10398/IERSE/Science/EarthRotation/PolarMotion.html.

- IPCC, 2007. *Climate Change 2007: The Physical Science Basis. Contribution of Working Group I to the Fourth Assessment Report of the Intergovernmental Panel on Climate Change* [Solomon, S., Qin, D., Manning, M., Chen, Z., Marquis, M., Averyt, K.B., Tignor, M., and Miller, H.L. (eds.)]. Cambridge University Press, Cambridge, United Kingdom and New York, NY, USA, 996 pp.
- IPCC, 2013a. *Climate Change 2013: The Physical Science Basis. Contribution of Working Group I to the Fifth Assessment Report of the Intergovernmental Panel on Climate Change* [Stocker, T.F., Qin, D., Plattner, G.-K., Tignor, M., Allen, S.K., Boschung, J., Nauels, A., Xia, Y., Bex, V., and Midgley, P.M. (eds.)]. Cambridge University Press, Cambridge, United Kingdom and New York, NY, USA, 1535 pp, doi: 10.1017/CBO9781107415324.
- IPCC, 2013b. Summary for Policymakers. In: *Climate Change 2013: The Physical Science Basis. Contribution of Working Group I to the Fifth Assessment Report of the Intergovernmental Panel on Climate Change* [Stocker, T.F., Qin, D., Plattner, G.-K., Tignor, M., Allen, S.K., Boschung, J., Nauels, A., Xia, Y., Bex, V., and Midgley, P.M., (eds.)]. Cambridge University Press, Cambridge United Kingdom and New York, NY, USA.
- IPCC, 2014: *Climate Change 2014: Impacts, Adaptation, and Vulnerability. Part A: Global and Sectoral Aspects. Contribution of Working Group II to the Fifth Assessment Report of the Intergovernmental Panel on Climate Change* [Field, C.B., V.R. Barros, D.J. Dokken, K.J. Mach, M.D. Mastrandrea, T.E. Bilir, M. Chatterjee, K.L. Ebi, Y.O. Estrada, R.C. Genova, B. Girma, E.S. Kissel, A.N. Levy, S. MacCracken, P.R. Mastrandrea, and L.L. White (eds.)]. Cambridge University Press, Cambridge, United Kingdom and New York, NY, USA, 1132 pp.
- Iz, H.B., 2006. How do unmodeled systematic mean sea level variations affect long-term sea level trend estimates from tide gauge data. *Journal of Geodesy*, 80, pp.40-46.
- Jessen, A., 1964. Chandler's period in the mean sea level. *Tellus*, 16(4), pp.513-516.
- Jevrejeva, S., Moore, J.C., Woodworth, P.L., and Grinsted, A., 2005. Influence of large-scale atmospheric circulation on European sea level: results based on the wavelet transform method. *Tellus A*, 57(2), pp.183-193.
- Jevrejeva, S., Grinsted, A., Moore, J., and Holgate, S., 2006. Nonlinear trends and multiyear cycles in sea level records. *Journal of Geophysical Research: Oceans* (1978–2012), 111(C9), doi: 10.1029/2005JC003229.
- Jevrejeva, S., Moore, J.C., Grinsted, A., and Woodworth, P.L., 2008. Recent global sea level acceleration started over 200 years ago? *Geophysical Research Letters*, 35(8), doi: 10.1029/2008GL033611.

- Jevrejeva, S., Moore, J., Grinsted, A., Matthews, A., and Spada, G., 2014. Trends and acceleration in global and regional sea levels since 1807. *Global and Planetary Change*, 113, pp.11-22.
- JISAO, 2014. Joint Institute for the Study of the Atmosphere and Ocean (JISAO), College of the Environment, University of Washington, USA, website accessed January 2014.
URL: <http://www.jisao.washington.edu/pdo/PDO.latest>
- Johns, C.J., Nychka, D., Kittel, T.G.F. and Daly, C., 2003. Infilling sparse records of spatial fields. *Journal of the American Statistical Association*, 98(464), pp.796-806.
- Jolliffe, I., 2002. *Principal component analysis*. John Wiley & Sons, Ltd.
- Jones, P.D., Jónsson, T., and Wheeler, D., 1997. Extension to the North Atlantic Oscillation using early instrumental pressure observations from Gibraltar and south-west Iceland. *International Journal of Climatology*, 17, pp.1433–1450.
- Jones, P.D., Osborn, T.J., Briffa, K.R., Folland, C.K., Horton, E.B., Alexander, L.V., Parker, D.E., and Rayner, N.A., 2001. Adjusting for sampling density in grid box land and ocean surface temperature time series. *Journal of Geophysical Research*, 106, pp.3371–3380.
- Kaplan, A., Kushnir, Y., Cane, M.A. and Blumenthal, M.B., 1997. Reduced space optimal analysis for historical data sets: 136 years of Atlantic sea surface temperatures. *Journal of Geophysical Research: Oceans*, 102(C13), pp.27835-27860.
- Katsumata, K., Ichiyanagi, M., Miwa, M., Kasahara, M. and Miyamachi, H., 1995. Aftershock distribution of the October 4, 1994 Mw8. 3 Kurile islands earthquake determined by a local seismic network in Hokkaido, Japan. *Geophysical research letters*, 22(11), pp.1321-1324.
- Kemp, A.C., Horton, B.P., Culver, S.J., Corbett, D.R., van de Plassche, O., Gehrels, W.R., Douglas, B.C., and Parnell, A. C., 2009. Timing and magnitude of recent accelerated sea-level rise (North Carolina, United States). *Geology*, 37(11), pp.1035-1038.
- Kemp, A.C., Horton, B.P., Donnelly, J.P., Mann, M.E., Vermeer, M., and Rahmstorf, S., 2011. Climate related sea-level variations over the past two millennia. *Proceedings of the National Academy of Sciences*, 108(27), pp.11017-11022.
- Kemp, A.C., Horton, B.P., Vane, C.H., Bernhardt, C.E., Corbett, D.R., Engelhart, S.E., Anisfeld, S.C., Parnell, A.C., and Cahill, N., 2013. Sea-level change during the last 2500 years in New Jersey, USA. *Quaternary Science Reviews*, 81, pp.90-104.
- Kemp, A.C., Bernhardt, C.E., Horton, B.P., Kopp, R.E., Vane, C.H., Peltier, W.R., Hawkes, A.D., Donnelly, J.P., Parnell, A.C., and Cahill, N., 2014. Late Holocene sea-and land-level change on the US southeastern Atlantic coast. *Marine Geology*, 357, pp.90-100.

- Kemp, A.C., Hawkes, A.D., Donnelly, J.P., Vane, C.H., Horton, B.P., Hill, T.D., Anisfeld, S.C., Parnell, A.C., and Cahill, N., 2015. Relative sea-level change in Connecticut (USA) during the last 2200 yrs. *Earth and Planetary Science Letters*, 428, pp.217-229.
- Killick, R., and Eckley, I., 2014. Changepoint: An R package for changepoint analysis. *Journal of Statistical Software*, 58(3), pp.1-19.
- Kim, D., and Oh, H.S., 2009. EMD: a package for empirical mode decomposition and Hilbert spectrum. *The R Journal*, 1(1), pp.40-46.
- Kim, D., Kim, K.O., and Oh, H.S., 2012. Extending the scope of empirical mode decomposition by smoothing. *EURASIP Journal on Advances in Signal Processing*, pp.1-17, doi: 10.1186/1687-6180-2012-168.
- Kondrashov, D., and Ghil, M., 2006. Spatio-temporal filling of missing points in geophysical data sets. *Nonlinear Processes in Geophysics*, 13(2), pp.151-159.
- Kopp, R.E., 2013. Does the mid-Atlantic United States sea level acceleration hot spot reflect ocean dynamic variability? *Geophysical Research Letters*, 40(15), pp.3981-3985.
- Kopp, R.E., Kemp, A.C., Bittermann, K., Horton, B.P., Donnelly, J.P., Gehrels, W.R., Hay, C.C., Mitrovica, J.X., Morrow, E.D., and Rahmstorf, S., 2016. Temperature-driven global sea-level variability in the Common Era. *Proceedings of the National Academy of Sciences*, 113(11), pp. E1434–E1441.
- Korotaev, G., Oguz, T., Nikiforov, A., and Koblinsky, C., 2003. Seasonal, interannual, and mesoscale variability of the Black Sea upper layer circulation derived from altimeter data. *Journal of Geophysical Research: Oceans*, 108(C4), doi: 10.1029/2002JC001508.
- Kubryakov, A.A., and Stanichnyi, S.V., 2013. The Black Sea level trends from tide gages and satellite altimetry. *Russian Meteorology and Hydrology*, 38(5), pp.329-333.
- Kullenberg, G., 1981. Physical oceanography. In: A. Voipio (Ed.), *The Baltic Sea*, Elsevier Oceanography Series 30, pp.135–182. Amsterdam: Elsevier.
- Lambeck, K., Smither, C., and Johnston, P., 1998. Sea-level change, glacial rebound and mantle viscosity for northern Europe. *Geophysical Journal International*, 134(1), pp.102-144.
- Lehmann, A., Getzlaff, K., and Harlaß, J., 2011. Detailed assessment of climate variability of the Baltic Sea area for the period 1958-2009. *Climate Research*, 46, pp.185-196.
- Leithe-Eriksen, R., (ed.), 1992. *Greenpeace - The seas - The Baltic Sea*, RVG-Interbook, 144 pp.
- Leppäranta, M., and Myrberg, K., 2009. *Physical Oceanography of the Baltic Sea*. Springer Science & Business Media.

- Levermann, A., Clark, P.U., Marzeion, B., Milne, G.A., Pollard, D., Radic, V. and Robinson, A., 2013. The multimillennial sea-level commitment of global warming. *Proceedings of the National Academy of Sciences*, 110(34), pp.13745-13750.
- Lichter, M., Vafeidis, A.T., Nicholls, R.J. and Kaiser, G., 2010. Exploring data-related uncertainties in analyses of land area and population in the “Low-Elevation Coastal Zone”(LE CZ). *Journal of Coastal Research*, 27(4), pp.757-768.
- Loder, J.W. and Garrett, C., 1978. The 18.6-year cycle of sea surface temperature in shallow seas due to variations in tidal mixing. *Journal of Geophysical Research: Oceans*, 83(C4), pp.1967-1970.
- Maksimov, IV and Karklin, VP 1965. The Pole Tide in the Baltic Sea. *Dokl. Akad. Nauk SSSR*, Vol 161, pp. 580–582 (in Russian).
- Malkin, Z., and Miller, N., 2010. Chandler wobble: two more large phase jumps revealed. *Earth, Planets and Space*, 62(12), pp.943-947.
- Mandic, D.P., ur Rehman, N., Wu, Z., and Huang, N.E., 2013. Empirical mode decomposition-based time-frequency analysis of multivariate signals: the power of adaptive data analysis. *IEEE Signal Processing Magazine*, 30(6), pp.74-86.
- Marcos, M., Marzeion, B., Dangendorf, S., Slangen, A.B., Palanisamy, H. and Fenoglio-Marc, L., 2017. Internal Variability Versus Anthropogenic Forcing on Sea Level and Its Components. *Surveys in Geophysics*, 38(1), pp.329-348.
- Markovsky, I., 2012. *Low rank approximation: algorithms, implementation, applications*. Springer Science & Business Media.
- Marshall, G.J., 2003. Trends in the Southern Annular Mode from observations and reanalyses. *Journal of Climate*, 16(24), pp.4134-4143.
- Mather, A.A., 2007. Linear and nonlinear sea-level changes at Durban, South Africa. *South African Journal of Science*, 103(11-12), pp.509-512.
- Maul, G.A., and Martin, D.M., 1993. Sea level rise at Key West, Florida, 1846-1992: America's longest instrument record? *Geophysical Research Letters*, 20(18), pp.1955-1958.
- McGranahan, G., Balk, D., and Anderson, B., 2007. The rising tide: assessing the risks of climate change and human settlements in low elevation coastal zones. *Environment and Urbanization*, International Institute for Environment and Development (IIED), 19(1), pp.17–37.
- Medvedev, I.P., Rabinovich, A.B. and Kulikov, E.A., 2017. The Pole Tide/14-Month Oscillations in the Baltic Sea during the 19th and 20th Centuries: Spatial and Temporal Variations. *Continental Shelf Research*, 137, pp.117-130.

- Meehl, G.A., Stocker, T.F., Collins, W.D., Friedlingstein, P., Gaye, A.T., Gregory, J.M., Kitoh, A., Knutti, R., Murphy, J.M., Noda, A., Raper, S.C.B., Watterson, I.G., Weaver, A.J., and Zhao, Z-C., 2007. *Global Climate Projections*. In: *Climate Change 2007: The Physical Science Basis*. Contribution of Working Group I to the Fourth Assessment Report of the Intergovernmental Panel on Climate Change [Solomon, S., Qin, D., Manning, M., Chen, Z., Marquis, M., Averyt, K.B., Tignor, M., and Miller, H.L., (eds.)]. Cambridge University Press, Cambridge, UK, pp.433-497.
- Melillo, J.M., Richmond, T.T., and Yohe, G.W., 2014. *Climate change impacts in the United States: The Third National Climate Assessment*. U.S. Global Change Research Program, 841 p.
- Mengel, M., Levermann, A., Frieler, K., Robinson, A., Marzeion, B., and Winkelmann, R., 2016. Future sea level rise constrained by observations and long-term commitment. *Proceedings of the National Academy of Sciences*, 113(10), pp.2597-2602.
- Meredith, M.P., Woodworth, P.L., Hughes, C.W., and Stepanov, V., 2004. Changes in the ocean transport through Drake Passage during the 1980s and 1990s, forced by changes in the Southern Annular Mode. *Geophysical Research Letters*, 31(21), L21305, doi: 10.1029/2004GL021169.
- Merrifield, M., Merrifield, S., and Mitchum, G., 2009. An anomalous recent acceleration of global sea level rise. *Journal of Climate*, 22(21), pp.5772-5781.
- Merrifield, M.A., Thompson, P.R., and Lander, M., 2012. Multidecadal sea level anomalies and trends in the western tropical Pacific. *Geophysical Research Letters*, 39, L13602, doi: 10.1029/2012GL052032.
- Meysignac, B., Becker, M., Llovel, W., and Cazenave, A., 2012a. An assessment of two-dimensional past sea level reconstructions over 1950–2009 based on tide-gauge data and different input sea level grids. *Surveys in Geophysics*, 33(5), pp.945-972.
- Meysignac, B., Salas, D., Melia, Y., Becker, M., Llovel, W., and Cazenave, A., 2012b. Tropical pacific spatial trend patterns in observed sea level: Internal variability and/or anthropogenic signature? *Climate of the Past*, 8, pp.787-802.
- Miller, A.J., Cayan, D.R., Barnett, T.P., Graham, N.E., and Oberhuber, J.M., 1994. The 1976–77 climate shift of the Pacific Ocean. *Oceanography*, 7(1), pp.21-26.
- Miller, S.P., 1973. *Observations and interpretation of the pole tide* (Doctoral dissertation, Massachusetts Institute of Technology).
- Miller, S.P., and Wunsch, C., 1973. The pole tide. *Nature*, 246, pp.98-102.

- Minobe, S., 1999. Resonance in bidecadal and pentadecadal climate oscillations over the North Pacific: Role in climatic regime shifts. *Geophysical Research Letters*, 26(7), pp.855-858.
- Minshull, T.A., White, N.J., Edwards, R.A., Shillington, D.J., Scott, C.L., Demirer, A., Shaw-Champion, M., Jones, S.M., Erduran, M., Besevli, T., and Coskun, G., 2005. Seismic data reveal eastern Black Sea Basin structure. *EOS: Transactions American Geophysical Union*, 86(43), pp.413-419.
- Moore, J.C., Grinsted, A., and Jevrejeva, S., 2005. New tools for analyzing time series relationships and trends. *Eos, Transactions American Geophysical Union*, 86(24), pp.226-232.
- Moser, S.C., Davidson, M.A., Kirshen, P., Mulvaney, P., Murley, J.F., Neumann, J.E., Petes, L., and Reed, D., 2014. Coastal zone development and ecosystems. *Climate change impacts in the United States: The Third National Climate Assessment*, pp.579-618.
- Moss, R.H., Edmonds, J.A., Hibbard, K.A., Manning, M.R., Rose, S.K., Van Vuuren, D.P., Carter, T.R., Emori, S., Kainuma, M., Kram, T. and Meehl, G.A., 2010. The next generation of scenarios for climate change research and assessment. *Nature*, 463(7282), pp.747-756.
- Munk, W.H., and Macdonald, G.J.F., 1960. *The Rotation of the Earth: A Geophysical Discussion*. Cambridge University Press, New York, NY, USA, 323 pp.
- Nerem, R.S., Chambers, D.P., Leuliette, E.W., Mitchum, G.T. and Giese, B.S., 1999. Variations in global mean sea level associated with the 1997–1998 ENSO event: Implications for measuring long term sea level change. *Geophysical research letters*, 26(19), pp.3005-3008.
- Nerem, R.S., Chambers, D.P., Choe, C., and Mitchum, G.T., 2010. Estimating Mean Sea Level Change from the TOPEX and Jason Satellite Altimeter Missions. *Marine Geodesy*, 33(S1), pp.435-446.
- Neumann, J., Hudgens, D., Herter, J., and Martinich, J., 2011. The economics of adaptation along developed coastlines. *Wiley Interdisciplinary Reviews: Climate Change*, 2(1), 89-98.
- Neumann, B., Vafeidis, A.T., Zimmermann, J., and Nicholls, R.J., 2015. Future coastal population growth and exposure to sea-level rise and coastal flooding-a global assessment. *PLoS one*, 10(3), 0118571, <https://doi.org/10.1371/journal.pone.0118571>.
- Newman, M., Compo, G.P. and Alexander, M.A., 2003. ENSO-forced variability of the Pacific decadal oscillation. *Journal of Climate*, 16(23), pp.3853-3857.
- Nicholls, R.J., and Cazenave, A., 2010. Sea-level rise and its impact on coastal zones. *Science*, 328(5985), pp.1517-1520.
- NOAA, 2012. *NOAA's State of the Coast. Economy: Ports - Crucial Coastal Infrastructure*. Department of Commerce, National Oceanic and Atmospheric Administration.

- NWS, 2013. National Weather Service (NWS), Climate Prediction Center, National Oceanic and Atmospheric Administration, US Department of Commerce website, accessed December 2013. URL: http://www.cpc.ncep.noaa.gov/products/precip/CWlink/daily_ao_index/ao/ao.shtml
- O'Connor, W.P., 1986. The 14 month wind stressed residual circulation (pole tide) in the North Sea. *NASA Technical Memorandum 87800*.
- O'Connor, W.P., Chao, B.F., Zheng, D. and Au, A.Y., 2000. Wind stress forcing of the North Sea 'pole tide'. *Geophysical Journal International*, 142(2), pp.620-630.
- Ostanciaux, É., Husson, L., Choblet, G., Robin, C., and Pedoja, K., 2012. Present-day trends of vertical ground motion along the coast lines. *Earth-Science Reviews*, 110(1), pp.74-92.
- O'Sullivan, F., 1986. A statistical perspective on ill-posed inverse problems. *Statistical Science*, 1(4), pp.502-518.
- O'Sullivan, F., 1988. Fast computation of fully automated log-density and log-hazard estimators. *SIAM Journal on Scientific and Statistical Computing*, 9(2), pp.363-379.
- Panin, N., and Jipa, D., 2002. Danube River sediment input and its interaction with the north-western Black Sea. *Estuarine, Coastal and Shelf Science*, 54(3), pp.551-562.
- Park, J., and Sweet, W., 2015. Accelerated sea level rise and Florida Current transport. *Ocean Science*, 11(4), pp.607-615.
- Peltier, W.R., 2004. Global Glacial Isostasy and the Surface of the Ice-Age Earth: The ICE-5G(VM2) model and GRACE. *Annual Review of Earth and Planetary Sciences*, 32, pp.111-149.
- Peltier, W.R., Argus, D.F., and Drummond, R., 2015. Space geodesy constrains ice age terminal deglaciation: The global ICE-6G_C (VM5a) model. *Journal of Geophysical Research: Solid Earth*, 120(1), pp.450-487.
- Percival, D.B., and Mofjeld, H.O., 1997. Analysis of subtidal coastal sea level fluctuations using wavelets. *Journal of the American Statistical Association*, 92(439), pp.868-880.
- Percival, D.B., and Walden, A.T., 2006. *Wavelet Methods for Time Series Analysis (Vol. 4)*. Cambridge University Press.
- Pfeffer, J. and Allemand, P., 2016. The key role of vertical land motions in coastal sea level variations: a global synthesis of multisatellite altimetry, tide gauge data and GPS measurements. *Earth and Planetary Science Letters*, 439, pp.39-47.
- Piecuch, C.G., Dangendorf, S., Ponte, R.M. and Marcos, M., 2016. Annual sea level changes on the North American Northeast Coast: influence of local winds and barotropic motions. *Journal of Climate*, 29(13), pp.4801-4816.

- Pinheiro, J., Bates, D., DebRoy, S., Sarkar, D., and the R Development Core Team, 2013. nlme: Linear and Nonlinear Mixed Effects Models. R package version 3.1-111.
- Plag, H.P., 1988. *A regional study of Norwegian coastal long period sea level variations and their causes: with special emphasis on the pole tide* (Doctoral dissertation, Verlag von Dietrich Reimer, Berlin).
- Pollock, D.S.G., 2008. IDEOLOG: A Program for Filtering Econometric Data - A Synopsis of Alternative Methods. *Discussion Papers in Economics 08/21*, Department of Economics, University of Leicester.
- Power, S. and Colman, R., 2006. Multi-year predictability in a coupled general circulation model. *Climate Dynamics*, 26(2-3), pp.247-272.
- PSMSL, 2014. Permanent Service for Mean Sea Level (PSMSL) website, accessed February 2014. URL: <http://www.psmsl.org>.
- PSMSL, 2016. Permanent Service for Mean Sea Level (PSMSL) website, accessed 2 January 2016. URL: <http://www.psmsl.org>.
- Pugh, D.T., 1987. *Tides, Surges and Mean Sea Level*. Wiley Publishing, 472 pp.
- Pugh, D.T., 1996. *Tides, Surges and Mean Sea-Level (reprinted with corrections)*. John Wiley & Sons Ltd.
- Qiu, B., 2002. Large-scale variability in the midlatitude subtropical and subpolar North Pacific Ocean: Observations and causes. *Journal of Physical Oceanography*, 32(1), pp.353-375.
- Qiu, B., and Chen, S., 2012. Multidecadal sea level and gyre circulation variability in the northwestern tropical Pacific Ocean. *Journal of Physical Oceanography*, 42(1), pp.193-206.
- R Core Team, 2013. R: A language and environment for statistical computing. R Foundation for Statistical Computing, Vienna, Austria. ISBN 3-900051-07-0. URL: <http://www.R-project.org/>.
- R Core Team, 2014. R: A language and environment for statistical computing. R Foundation for Statistical Computing, Vienna, Austria. ISBN 3-900051-07-0. URL: <http://www.R-project.org/>.
- R Core Team, 2015. R: A language and environment for statistical computing. R Foundation for Statistical Computing, Vienna, Austria. ISBN 3-900051-07-0. URL: <http://www.R-project.org/>.
- R Core Team, 2016. R: A language and environment for statistical computing. R Foundation for Statistical Computing, Vienna, Austria. ISBN 3-900051-07-0. URL: <http://www.R-project.org/>.
- Rahmstorf, S., and Vermeer, M., 2011. Discussion of: Houston, J.R., and Dean, R.G., 2011. Sea-Level Acceleration Based on U.S. Tide Gauges and Extensions of Previous Global-Gauge Analyses. *Journal of Coastal Research*, 27(3), pp.409-417. *Journal of Coastal Research*, pp.784-787. Online publication date: 1 Jul 2011.

- Ray, R.D., and Douglas, B.C., 2011. Experiments in reconstructing twentieth-century sea levels. *Progress in Oceanography*, 91(4), pp.496-515.
- Reynolds, R.W. and Smith, T.M., 1994. Improved global sea surface temperature analyses using optimum interpolation. *Journal of climate*, 7(6), pp.929-948.
- Rintoul, S., 2011. Sea-level rises are slowing, tidal gauge records show, *The Australian*, News Limited, 22 July.
- Rossby, C.G., 1939. Relation between variations in the intensity of the zonal circulation of the atmosphere and the displacements of the semi-permanent centers of action. *Journal of Marine Research*, 2(1), pp.38-55.
- Rossby, T., Flagg, C.N., Donohue, K., Sanchez-Franks, A., and Lillibridge, J., 2014. On the long-term stability of Gulf Stream transport based on 20 years of direct measurements. *Geophysical Research Letters*, 41(1), pp.114-120.
- Sachs, J.D., Mellinger, A.D., and Gallup, J.L., 2001. The geography of poverty and wealth. *Scientific American*, 284, pp.70-75.
- Sallenger Jr, A.H., Doran, K.S., and Howd, P.A., 2012. Hotspot of accelerated sea-level rise on the Atlantic coast of North America. *Nature Climate Change*, 2(12), pp.884-888.
- Santamaría-Gómez, A., Gravelle, M., Collilieux, X., Guichard, M., Míguez, B.M., Tiphaneau, P., and Wöppelmann, G., 2012. Mitigating the effects of vertical land motion in tide gauge records using a state-of-the-art GPS velocity field. *Global and Planetary Change*, 98, pp.6-17.
- Schneider, N. and Cornuelle, B.D., 2005. The forcing of the Pacific decadal oscillation. *Journal of Climate*, 18(21), pp.4355-4373.
- Schneider, T., 2001. Analysis of incomplete climate data: Estimation of mean values and covariance matrices and imputation of missing values. *Journal of Climate*, 14(5), pp.853-871.
- Senjyu, T., 2006. Spatiotemporal variability of interdecadal sea level oscillations in the North Pacific. *Journal of Geophysical Research*, 111, C07022, doi: 10.1029/2005JC003053.
- Shennan, I., and Woodworth, P.L., 1992. A comparison of late Holocene and twentieth-century sea-level trends from the UK and North Sea region. *Geophysical Journal International*, 109(1), pp.96-105.
- Shepherd, A., Ivins, E.R., Geruo, A., Barletta, V.R., Bentley, M.J., Bettadpur, S., Briggs, K.H., Bromwich, D.H., Forsberg, R., Galin, N. and Horwath, M., 2012. A reconciled estimate of ice-sheet mass balance. *Science*, 338(6111), pp. 1183-1189.
- Sherwood, S.C., 2000. Climate signals from station arrays with missing data, and an application to winds. *Journal of Geophysical Research: Atmospheres*, 105(D24), pp.29489-29500.

- Sirosh, J., 2015. Cortana Intelligence and Machine Learning Blog. 'Microsoft Closes Acquisition of Revolution Analytics'. Available at:
<https://blogs.technet.microsoft.com/machinelearning/2015/04/06/microsoft-closes-acquisition-of-revolution-analytics/> [Accessed 21 Jul. 2016].
- Smith, K., 2011. We are seven billion. *Nature Climate Change*, 1(7), pp.331-335.
- Smith, T.M., Reynolds, R.W., Livezey, R.E. and Stokes, D.C., 1996. Reconstruction of historical sea surface temperatures using empirical orthogonal functions. *Journal of Climate*, 9(6), pp.1403-1420.
- SONEL (Systeme d'Observation Du Niveau Des Eaux Littorales), 2016.
URL: <http://www.sonel.org/-Vertical-land-movement-estimate-.html>
- Spada, G., Olivieri, M., and Galassi, G., 2014. Anomalous secular sea-level acceleration in the Baltic Sea caused by isostatic adjustment. *Annals of Geophysics*, 57(4), p.S0432.
- Stanev, E.V., 2005. Black Sea Dynamics. *Oceanography*, 18(2), pp.56-75.
- Stineman, R.W., 1980. A consistently well-behaved method of interpolation. *Creative Computing*, 6(7), pp.54-57.
- Sturges, W., 1974. Sea level slope along continental boundaries. *Journal of Geophysical Research*, 79(6), pp.825-830.
- Sturges, W., and Douglas, B.C., 2011. Wind effects on estimates of sea level rise. *Journal of Geophysical Research: Oceans*, 116(C6), doi: 10.1029/2010JC006492.
- Swiss Re, 2016. URL: http://media.swissre.com/documents/sigma1_2016_en.pdf (Accessed: 8 April 2016).
- Szabo, S., Brondizio, E., Renaud, F.G., Hetrick, S., Nicholls, R.J., Matthews, Z., Tessler, Z., Tejedor, A., Sebesvari, Z., Foufoula-Georgiou, E., Costa, S. and Dearing, J.A., 2016. Population dynamics, delta vulnerability and environmental change: comparison of the Mekong, Ganges–Brahmaputra and Amazon delta regions. *Sustainability Science*, 11(4), pp.539-554.
- Talke, S.A., and Jay, D.A., 2013. Nineteenth century North American and Pacific tidal data: Lost or just forgotten? *Journal of Coastal Research*, 29(6a), pp.118-127.
- Tamino, 2011. How not to analyze tide gauge data. Open Mind -Science, Politics, Life, the Universe, and Everything BLOG, 22 July.
URL: <https://tamino.wordpress.com/2011/07/22/how-not-to-analyze-tide-gauge-data/>
- Tary, J.B., Herrera, R.H., Han, J., and Baan, M., 2014. Spectral estimation—What is new? What is next? *Reviews of Geophysics*, 52(4), pp.723-749.

- Thakur, G., Brevdo, E., Fučkar, N.S., and Wu, H.T., 2013. The synchrosqueezing algorithm for time-varying spectral analysis: robustness properties and new paleoclimate applications. *Signal Processing*, 93(5), pp.1079-1094.
- Thompson, D.W.J., and Wallace, J.M., 2000. Annular modes in the extratropical circulation, Pt I: Month-to-month variability. *Journal of Climate*, 13, pp.1000–1016.
- Torrence, C., and Compo, G.P., 1998. A practical guide to wavelet analysis. *Bulletin of the American Meteorological society*, 79(1), pp.61-78.
- Torres, M.E., Colominas, M.A., Schlotthauer, G., and Flandrin, P., 2011. A complete ensemble empirical mode decomposition with adaptive noise. In: *2011 IEEE International Conference on Acoustics, Speech and Signal Processing (ICASSP)*, May 22–27, Prague Congress Center, Prague, Czech Republic, pp.4144–4147.
- Trenberth, K.E., and Hurrell, J.W., 1994. Decadal atmosphere-ocean variations in the Pacific. *Climate Dynamics*, 9(6), pp.303-319.
- Trenberth, K.E., Stepaniak, D.P., and Smith, L., 2005. Inter-annual variability of the patterns of atmospheric mass distribution. *Journal of Climate*, 18, pp.2812-2825.
- Trenberth, K.E., Jones, P.D., Ambenje, P., Bojariu, R., Easterling, D., Klein Tank, A., Parker, D., Rahimzadeh, F., Renwick, J.A., Rusticucci, M., Soden, B., and Zhai, P., 2007. Observations: Surface and Atmospheric Climate Change. In: *Climate Change 2007: The Physical Science Basis. Contribution of Working Group I to the Fourth Assessment Report of the Intergovernmental Panel on Climate Change* [Solomon, S., Qin, D., Manning, M., Chen, Z., Marquis, M., Averyt, K.B., Tignor, M., and Miller, H.L., (eds.)]. Cambridge University Press, Cambridge, United Kingdom and New York, NY, USA.
- Trupin, A., and Wahr, J., 1990. Spectroscopic analysis of global tide gauge sea level data. *Geophysical Journal International*, 100(3), pp.441-453.
- Tsimplis, M.N., Flather, R.A. and Vassie, J.M., 1994. The North Sea pole tide described through a tide-surge numerical model. *Geophysical research letters*, 21(6), pp.449-452.
- Tsimplis, M.N., and Josey, A.S., 2001. Forcing of the Mediterranean Sea by atmospheric oscillations over the North Atlantic. *Geophysical Research Letters*, 28, pp.803-806.
- Tsimplis, M.N., Shaw, A.G.P., Flather, R.A., and Woolf, D.K., 2006. The influence of the North Atlantic Oscillation on the sea-level around the northern European coasts reconsidered: the thermosteric effects. *Philosophical Transactions of the Royal Society A*, 364, pp.845-856.
- Tsimplis, M., Marcos, M., Somot, S., and Barnier, B., 2008. Sea level forcing in the Mediterranean Sea between 1960 and 2000. *Global and Planetary Change*, 63(4), pp.325-332.

- Tsimplis, M.N., and Shaw, A.G., 2008. The forcing of mean sea level variability around Europe. *Global and Planetary Change*, 63(2), pp.196-202.
- Tushingham, A., and Peltier, W.R., 1991. Ice-3G: A new global model of late Pleistocene deglaciation based upon geophysical predictions of post-glacial relative sea level change. *Journal of Geophysical Research: Solid Earth*, 96(B3), pp.4497-4523.
- Unal, Y.S., and Ghil, M., 1995. Interannual and interdecadal oscillation patterns in sea level. *Climate Dynamics*, 11(5), pp.255-278.
- United Nations, Department of Economic and Social Affairs, Population Division, 2015. *World Population Prospects: The 2015 Revision, Key Findings and Advance Tables*. Working Paper No. ESA/P/WP.241.
- University of Colorado, 2016. URL: <http://sealevel.colorado.edu/content/map-sea-level-trends>.
- US Census Bureau, 2009. *X-12-ARIMA Reference Manual Version 0.3*. Washington, DC: US Census Bureau, US Department of Commerce.
- Van Der Veen, A.J., Deprettere, E.F. and Swindlehurst, A.L., 1993. Subspace-based signal analysis using singular value decomposition. *Proceedings of the IEEE*, 81(9), pp.1277-1308.
- Vautard, R., and Ghil, M., 1989. Singular spectrum analysis in nonlinear dynamics, with applications to paleoclimatic time series. *Physica D: Nonlinear Phenomena*, 35(3), pp.395-424.
- Vigo, I., Garcia, D., and Chao, B.F., 2005. Change of sea level trend in the Mediterranean and Black seas. *Journal of Marine Research*, 63(6), pp.1085-1100.
- Visser, H., Dangendorf, S., and Petersen, A.C., 2015. A review of trend models applied to sea level data with reference to the “acceleration-deceleration debate”. *Journal of Geophysical Research: Oceans*, 120(6), pp.3873-3895.
- Volkov, D.L., and Landerer, F.W., 2015. Internal and external forcing of sea level variability in the Black Sea. *Climate Dynamics*, 45(9-10), pp.2633–2646.
- Wahl, T., Jensen, J., and Frank, T., 2010. On analysing sea level rise in the German Bight since 1844. *Natural Hazards and Earth System Science*, 10(2), pp.171-179.
- Wahl, T., Jensen, J., Frank, T., and Haigh, I.D., 2011. Improved estimates of mean sea level changes in the German Bight over the last 166 years. *Ocean Dynamics*, 61(5), pp.701-715.
- Wahl, T., Haigh, I.D., Woodworth, P.L., Albrecht, F., Dillingh, D., Jensen, J., Nicholls, R.J., Weisse, R., and Wöppelmann, G., 2013. Observed mean sea level changes around the North Sea coastline from 1800 to present. *Earth-Science Reviews*, 124, pp.51-67.
- Wakelin, S.L., Woodworth, P.L., Flather, R.A., and Williams, J.A., 2003. Sea-level dependence on the NAO over the NW European Continental Shelf. *Geophysical Research Letters*, 30(7), 1403.

- Watkiss, P., 2011. *The ClimateCost Project*. Final Report, Volume 1: Europe. Stockholm Environmental Institute, Sweden. ISBN 978-91-86125-35-6.
- Watson, C.S., White, N.J., Church, J.A., King, M.A., Burgette, R.J. and Legresy, B., 2015. Unabated global mean sea-level rise over the satellite altimeter era. *Nature Climate Change*, 5(6), pp.565-568.
- Watson, P.J., 2011. Is There Evidence Yet of Acceleration in Mean Sea Level Rise Around Mainland Australia. *Journal of Coastal Research*, 27(2), pp.368-377.
- Watson, P.J., Commins, R., Janssen, V., McElroy, S., Batman, G. and Connors, D., 2012. Augmenting the utility of NSW longest tide gauge records with continuous GNSS technology. Proceedings: 21st Annual NSW Coastal Conference, Kiama, NSW, Australia, November.
- Watson, P.J., 2015. Development of a unique synthetic data set to improve sea-level research and understanding. *Journal of Coastal Research*, 31(3), pp.758-770.
- Watson, P.J., 2016a. Identifying the best performing time series analytics for sea-level research. In: Rojas, I., and Pomares, H. (eds.), *Time Series Analysis and Forecasting: Contributions to Statistics*. Springer International Publishing, pp.261-278, doi: 10.1007/978-3-319-28725-6.
- Watson, P.J., 2016b. msltrend: Improved Techniques to Estimate Trend, Velocity and Acceleration from Sea Level Records. *R Project for Statistical Computing*, published 12 January.
URL: <http://cran.ms.unimelb.edu.au/web/packages/msltrend/index.html>
- Watson, P.J., 2016c. How to improve estimates of real-time acceleration in the mean sea level signal. In: Vila- Concejo, A.; Bruce, E.; Kennedy, D.M., and McCarroll, R.J. (eds.), Proceedings of the 14th International Coastal Symposium (Sydney, Australia). *Journal of Coastal Research*, Special Issue, No. 75, pp.780-784. Coconut Creek (Florida), ISSN 0749-0208.
- Watson, P.J., 2016d. A new perspective on global mean sea level (GMSL) acceleration. *Geophysical Research Letters*, 43(12), pp.6478-6484.
- Watson, P.J., 2016e. Acceleration in US Mean Sea Level? A New Insight using Improved Tools. *Journal of Coastal Research*, 32(6), pp.1247-1261.
- Watson, P.J., 2017. Acceleration in European Mean Sea Level? A New Insight Using Improved Tools. *Journal of Coastal Research*, 33(1), pp.23-38.
- Wenzel, M., and Schröter, J., 2014. Global and regional sea level change during the 20th century. *Journal of Geophysical Research: Oceans*, 119(11), pp.7493-7508.
- Wolfe, R., and Hanley, J., 2002. If we're so different, why do we keep overlapping? When 1 plus 1 doesn't make 2. *Canadian Medical Association Journal*, 166(1), pp.65-66.
- Wood, S., 2006. *Generalized additive models: an introduction with R*. CRC press, Boca Ratan, FL.

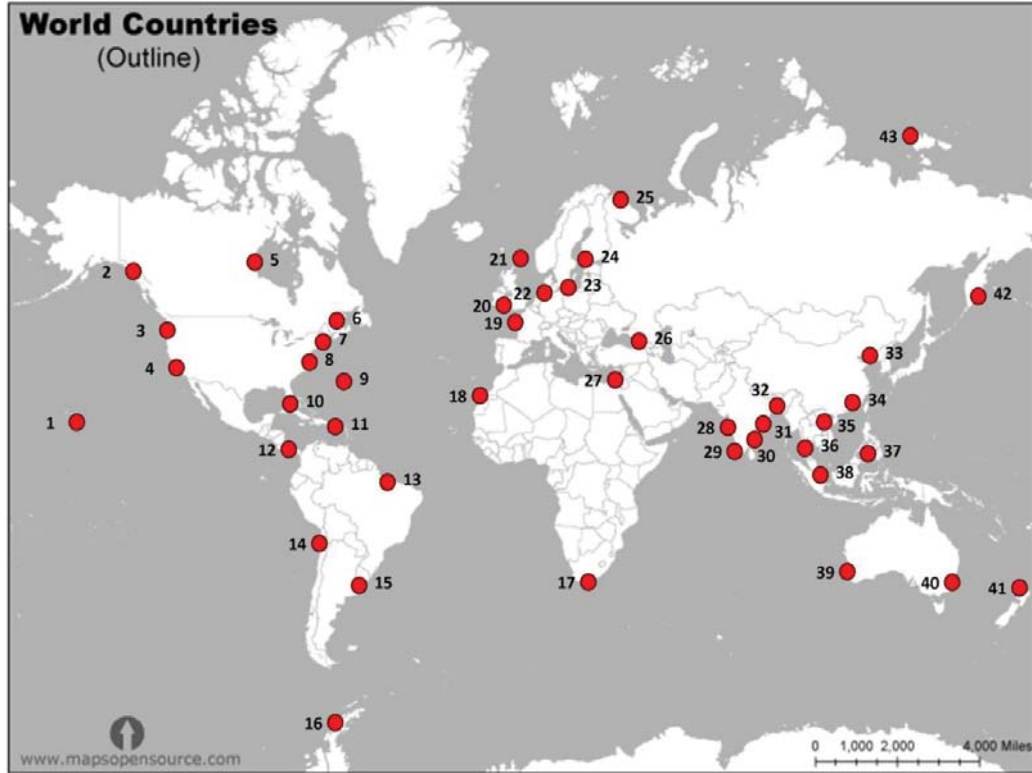
- Woodworth, P.L., 1990. A search for accelerations in records of European mean sea level. *International Journal of Climatology*, 10(2), pp.129-143.
- Woodworth, P.L., White, N.J., Jevrejeva, S., Holgate, S.J., Church, J.A., and Gehrels, W.R., 2009. Review - Evidence for the accelerations of sea level on multi-decade and century timescales. *International Journal of Climatology*, 29, pp.777-789.
- Woodworth, P.L., 2012. A Note on the Nodal Tide in Sea Level Records (Editorial). *Journal of Coastal Research*, 28(2), pp.316-323.
- Woodworth, P.L., Maqueda, M.Á.M., Roussenov, V.M., Williams, R.G., and Hughes, C.W., 2014. Mean sea-level variability along the northeast American Atlantic coast and the roles of the wind and the overturning circulation. *Journal of Geophysical Research: Oceans*, 119(12), pp.8916-8935.
- Wolf, D.K., Shaw, A.G.P., and Tsimplis, M.N., 2003. The influence of the North Atlantic Oscillation on sea level variability in the North Atlantic Region. *The Global Atmosphere and Ocean System*, 9(4), pp.145-167.
- Wöppelmann, G., Pouvreau, N. and Simon, B., 2006. Brest sea level record: a time series construction back to the early eighteenth century. *Ocean Dynamics*, 56(5-6), pp.487-497.
- Wöppelmann, G., and Marcos, M., 2012. Coastal sea level rise in southern Europe and the non-climate contribution of vertical land motion. *Journal of Geophysical Research: Oceans*, 117(C1), doi: 10.1029/2011JC007469.
- Wu, Z., and Huang, N.E., 2009. Ensemble empirical mode decomposition: a noise-assisted data analysis method. *Advances in Adaptive Data Analysis*, 1(01), pp.1-41.
- Wunsch, C., 1974. Dynamics of the pole tide and the damping of the Chandler wobble. *Geophysical Journal International*, 39(3), pp.539-550.
- Wunsch, C., 1986. Dynamics of the North Sea pole tide reconsidered. *Geophysical Journal International*, 87(3), pp.869-884.
- Wunsch, C., 2001. Comments on 'Wind stress forcing of the North Sea "Pole Tide"' by WP O'Connor, BF Chao, D. Zheng and AY Au. *Geophysical Journal International*, 146(1), pp.264-265.
- Xie, L. and Dickman, S.R., 1995. North Sea pole tide dynamics. *Geophysical Journal International*, 121(1), pp.117-135.
- Xie, L., and Dickman, S.R., 1996. Tide gauge data analysis of the pole tide in the North Sea. *Geophysical Journal International*, 126, pp.863-870.

- Yan, Z., Tsimplis, M.N., and Woolf, D., 2004. An analysis of relationship between the North Atlantic Oscillation and sea level changes in NW Europe. *International Journal of Climatology*, 24, pp.743-758.
- Yin, J., and Goddard, P.B., 2013. Oceanic control of sea level rise patterns along the East Coast of the United States. *Geophysical Research Letters*, 40(20), pp.5514-5520.
- Zeileis, A., and Grothendieck, G., 2005. zoo: S3 Infrastructure for Regular and Irregular Time Series. *Journal of Statistical Software*, 14(6), pp.1–27. URL: <http://www.jstatsoft.org/v14/i06/>.
- Zervas, C., Gill, S., and Sweet, W., 2013. *Estimating vertical land motion from long-term tide gauge records*. NOAA Technical Report. NOS CO-OPS, 65, p.22.
- Zhang, X., and Church, J.A., 2012. Sea level trends, inter-annual and decadal variability in the Pacific Ocean. *Geophysical Research Letters*, 39, L21701, doi: 10.1029/2012GL053240.
- Zickfeld, K., Eby, M., Alexander, K., Weaver, A.J., Crespin, E., Fichefet, T., Goosse, H., Philippon-Berthier, G., Edwards, N.R., Holden, P.B. and Eliseev, A.V., 2013. Long-term climate change commitment and reversibility: An EMIC intercomparison. *Journal of Climate*, 26(6), pp.5782-5809.
- Zwally, H.J., Li, J., Robbins, J.W., Saba, J.L., Yi, D. and Brenner, A.C., 2015. Mass gains of the Antarctic ice sheet exceed losses. *Journal of Glaciology*, 61(230), pp.1019-1036.

Appendix A

PSMSL Stations Used to Develop Core Synthetic Data Set

Figure A1: Location of PSMSL stations used to derive seasonal components.



Data source: <<https://mapsopensource.com>>

Table A1: Summary of PSMSL stations used to derive seasonal components.

Ref No.	PSMSL Station Location	Ref No.	PSMSL Station Location
1	Honolulu (USA)	23	Swinoujscie (Poland)
2	Yakutat (Canada)	24	Helsinki (Finland)
3	Seattle (USA)	25	Murmansk (Russia)
4	San Francisco (USA)	26	Poti (Georgia)
5	Churchill (Canada)	27	Alexandria (Egypt)
6	Trois-Rivieres (Canada)	28	Mumbai (India)
7	New York (USA)	29	Cochin (India)
8	Baltimore (USA)	30	Chennai (India)
9	Bermuda (Bermuda)	31	Visakhapatnam (India)
10	Key West (USA)	32	Diamond Harbour (India)
11	Magueyes Island (Puerto Rico)	33	Dalian (China)
12	Balboa (Republic of Panama)	34	Macau (Macau)
13	Belem (South America)	35	Hondau (Vietnam)
14	Antofagasta (South America)	36	Ko Taphao Noi (Thailand)
15	Buenos Aries (South America)	37	Jolo (Philippines)
16	Argentine Islands (Antarctica)	38	Sembawang (Singapore)
17	Mossel Bay (South Africa)	39	Fremantle (Australia)
18	Arrecife (Canary Islands, Spain)	40	Fort Denison (Australia)
19	Brest (France)	41	Auckland (New Zealand)
20	Newlyn (UK)	42	Petropavlovsk (Russia)
21	Lerwick (UK)	43	Kotelnyi (Russia)
22	Cuxhaven (Germany)		

Notes: Refer Figure A1 for station location.

Appendix B

Extraction of Noise Component from PSMSL Stations Used to Develop Synthetic Data Set

Figure B1: Noise component of PSMSL station records used for synthetic data set.

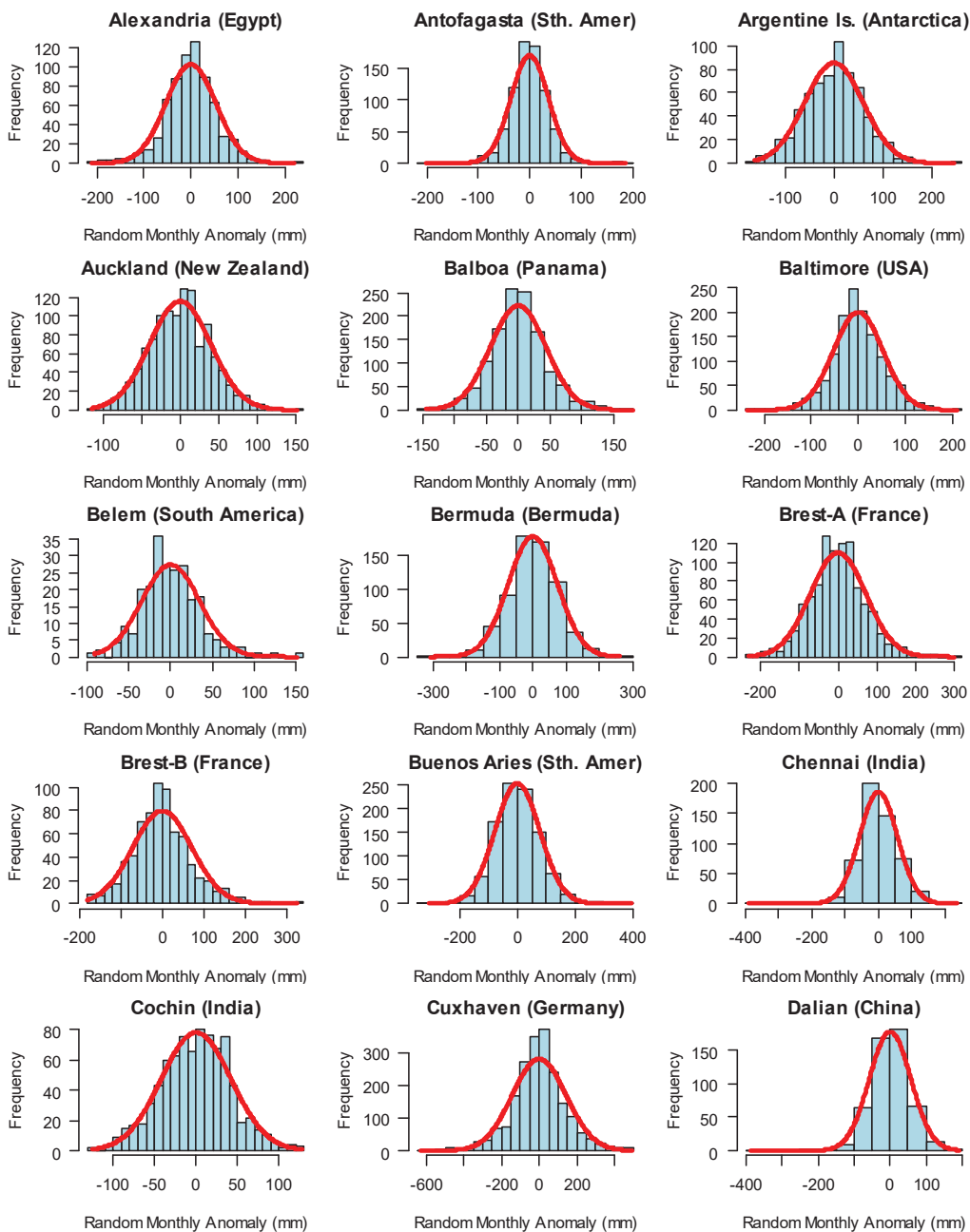


Figure B1 (cont): Noise component of PSMSL station records used for synthetic data set.

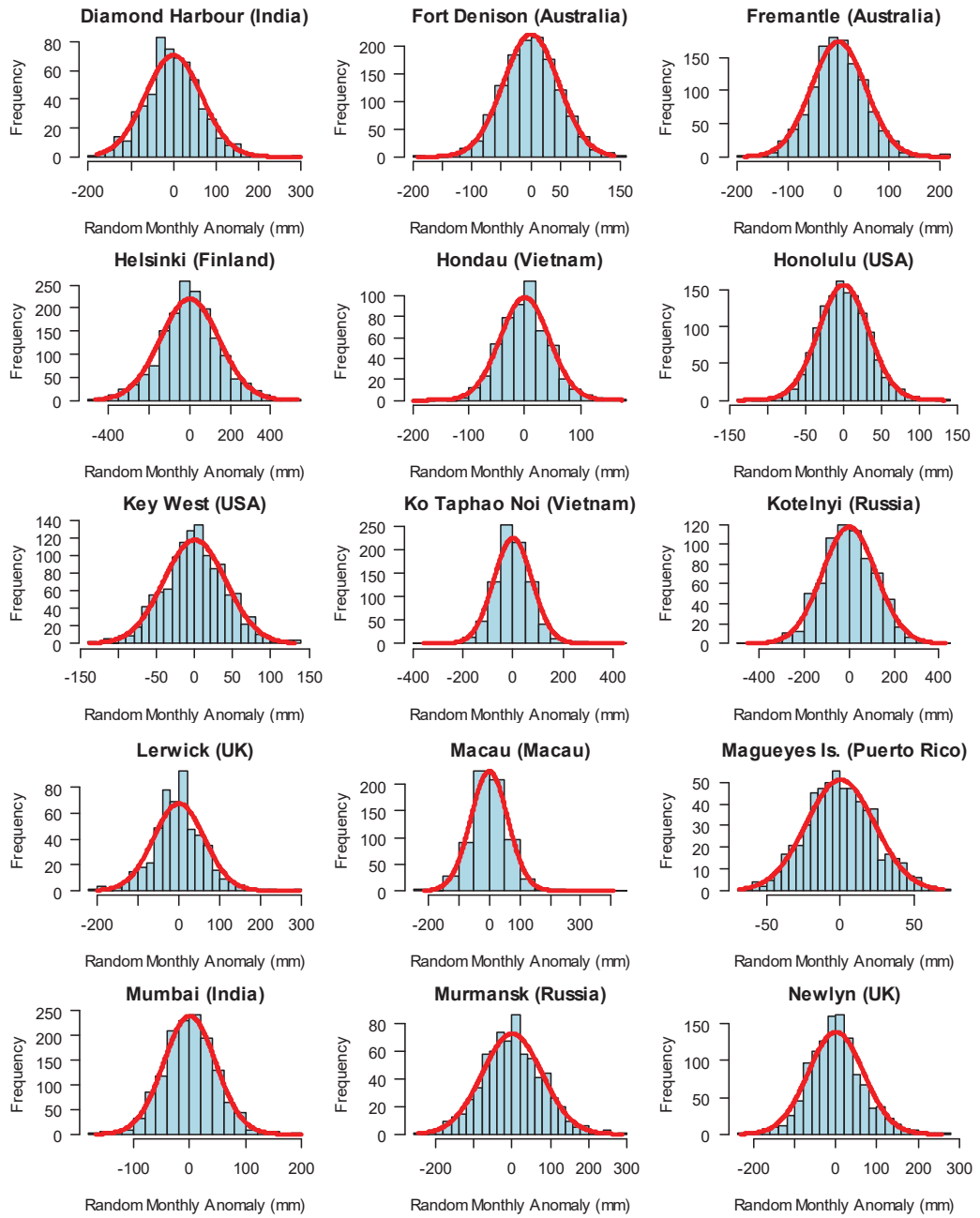
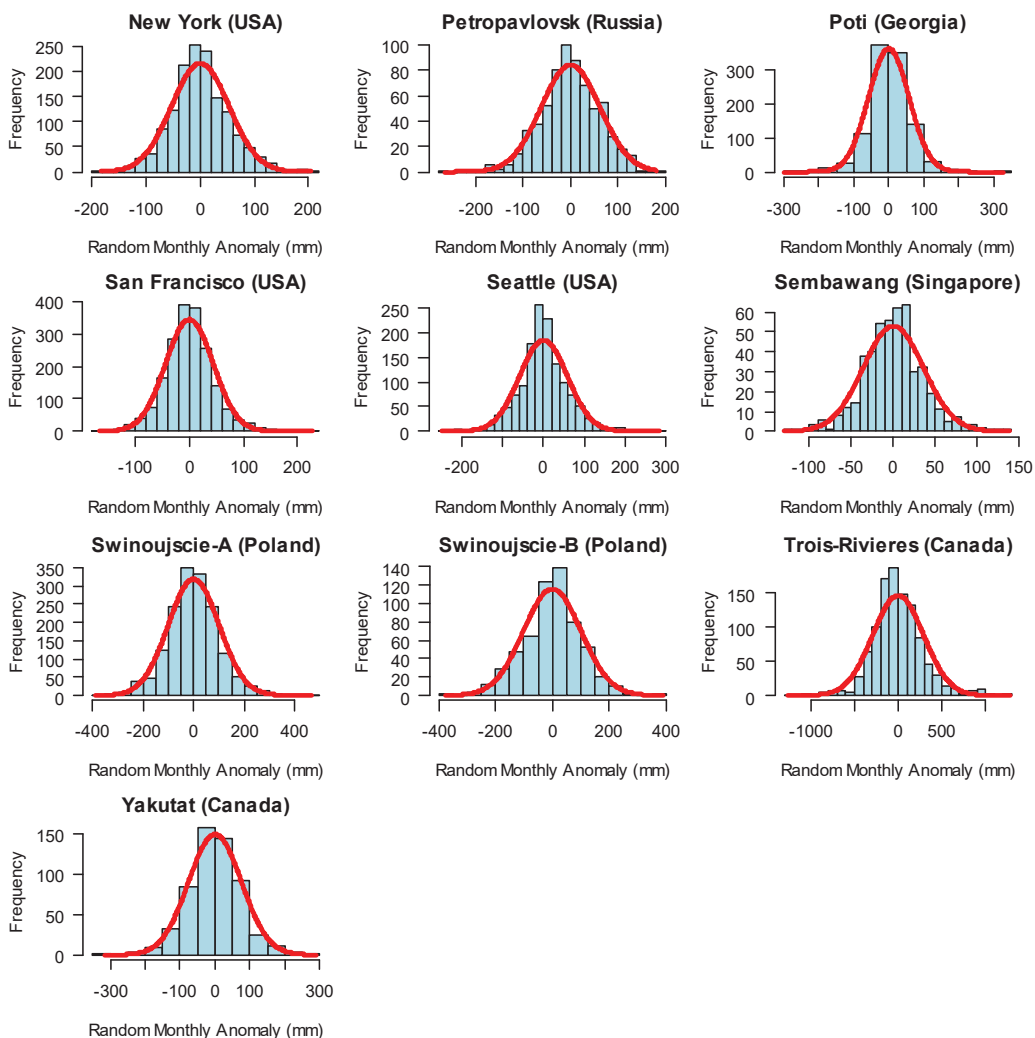


Figure B1 (cont): Noise component of PSM SL station records used for synthetic data set.



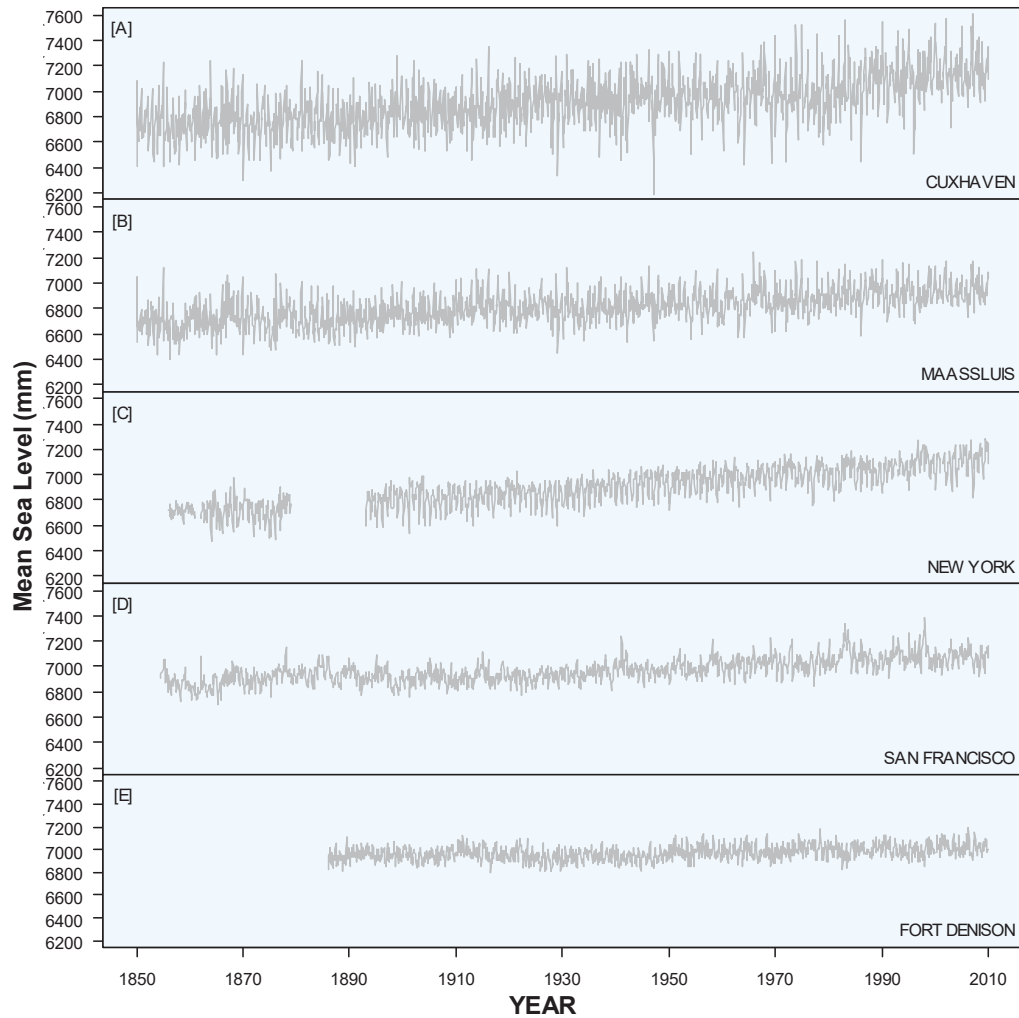
Notes:

1. Histograms of monthly white noise anomalies (residuals) for each station record determined in accordance with the procedure espoused in Section 2.4.5; and
2. Theoretical normal (Gaussian) distribution depicted on histograms (in red).

Appendix C

Comparison of Real and Synthetic Data Set Mean Sea Level Time Series

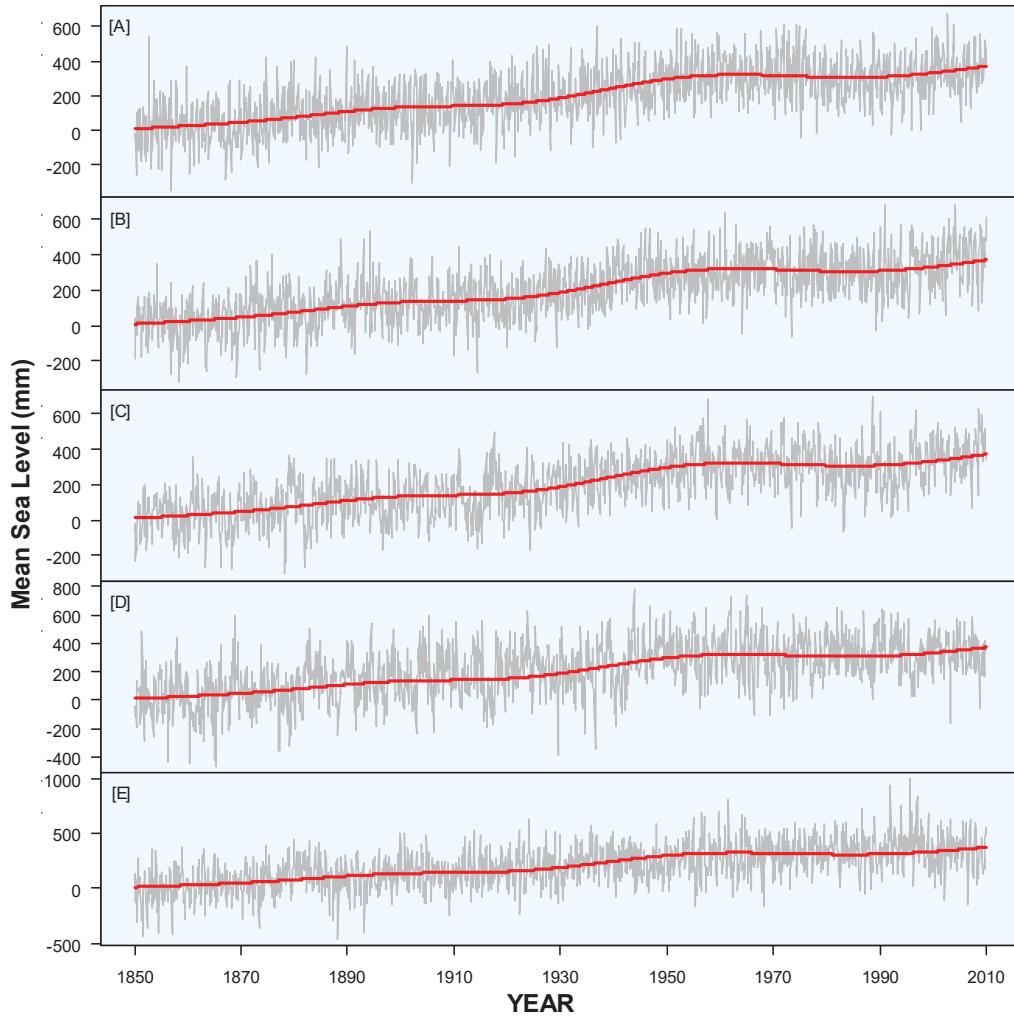
Figure C1: Selected monthly average ocean water level data sets from PSMSL.



Notes:

Selected long monthly average ocean water level data sets obtained from Permanent Service for Mean Sea Level (PSMSL).

Figure C2: Selected monthly average ocean water level time series from synthetic data set.



Notes:

1. Time series depicted above (Panels [A] to [E]) are the first 5 randomly generated monthly average ocean water level time series within the synthetic data set (20,000 time series);
2. Fixed Mean Sea Level indicated in red on each of the generated monthly time series; and
3. Refer Chapter 2 for details on the construction of the synthetic data set (refer also Tables 2.1 and 2.2).

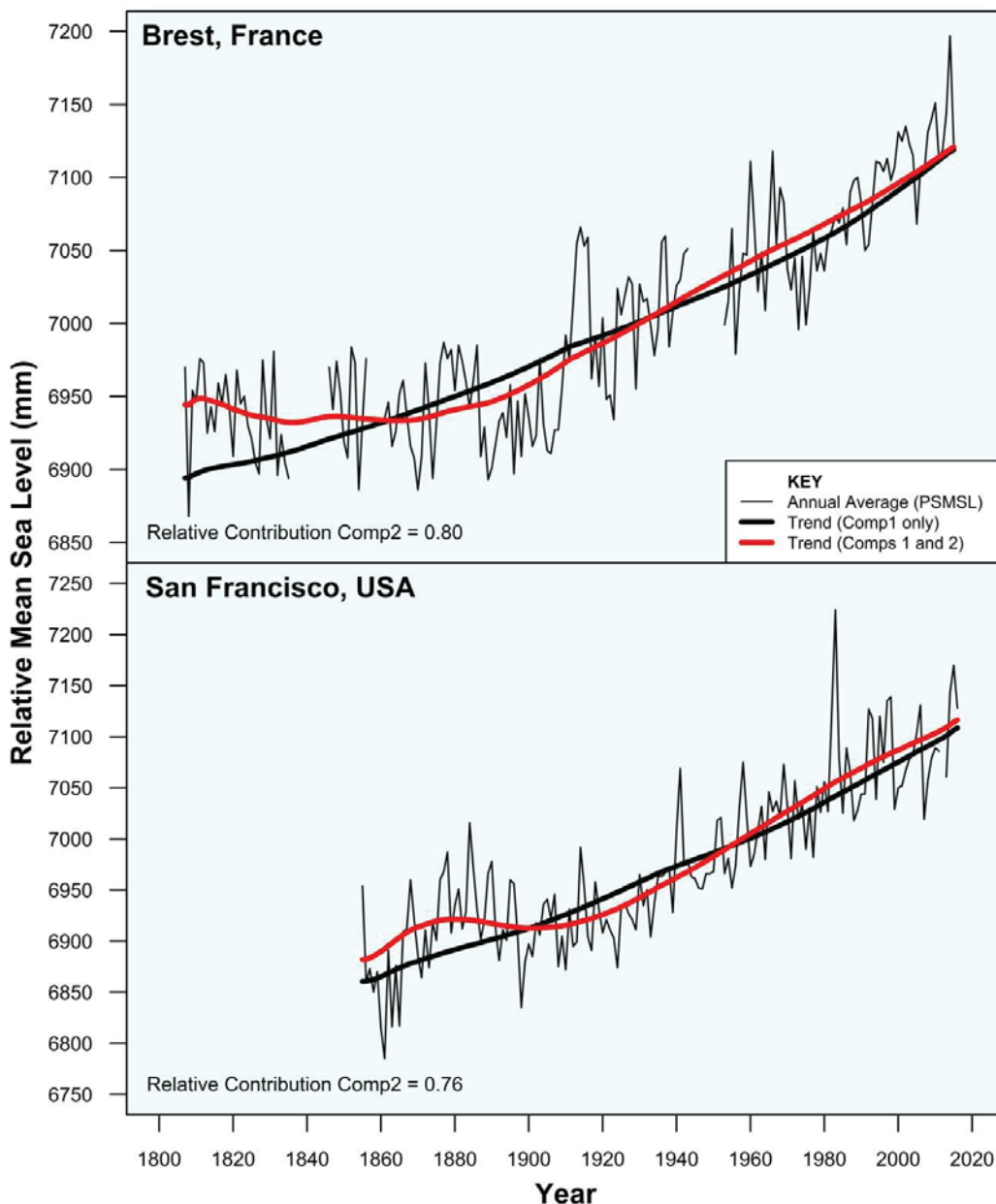
Appendix D

Comparison of Components 1 and 2 to optimise and automate SSA decomposition

The optimisation process involved Singular Spectrum Analysis decomposition of all records in the Permanent Service for Mean Sea Level exceeding 100 years in length (refer Section 4.3.3). For the majority of these records, the trend was wholly contained within the leading component. However, some 12 records also indicated “trend-like” power in the 2nd component as well (i.e. dominant relative contribution in the lowest frequency bin [0 – 0.01]).

This appendix provides a visual inspection of the component 1 and 2 outputs for these 12 records of interest to assist in determining an appropriate cut-off level for isolating distinctly “trend-like” components based on the relative contribution of the singular value in the lowest frequency bin [0 – 0.01]).

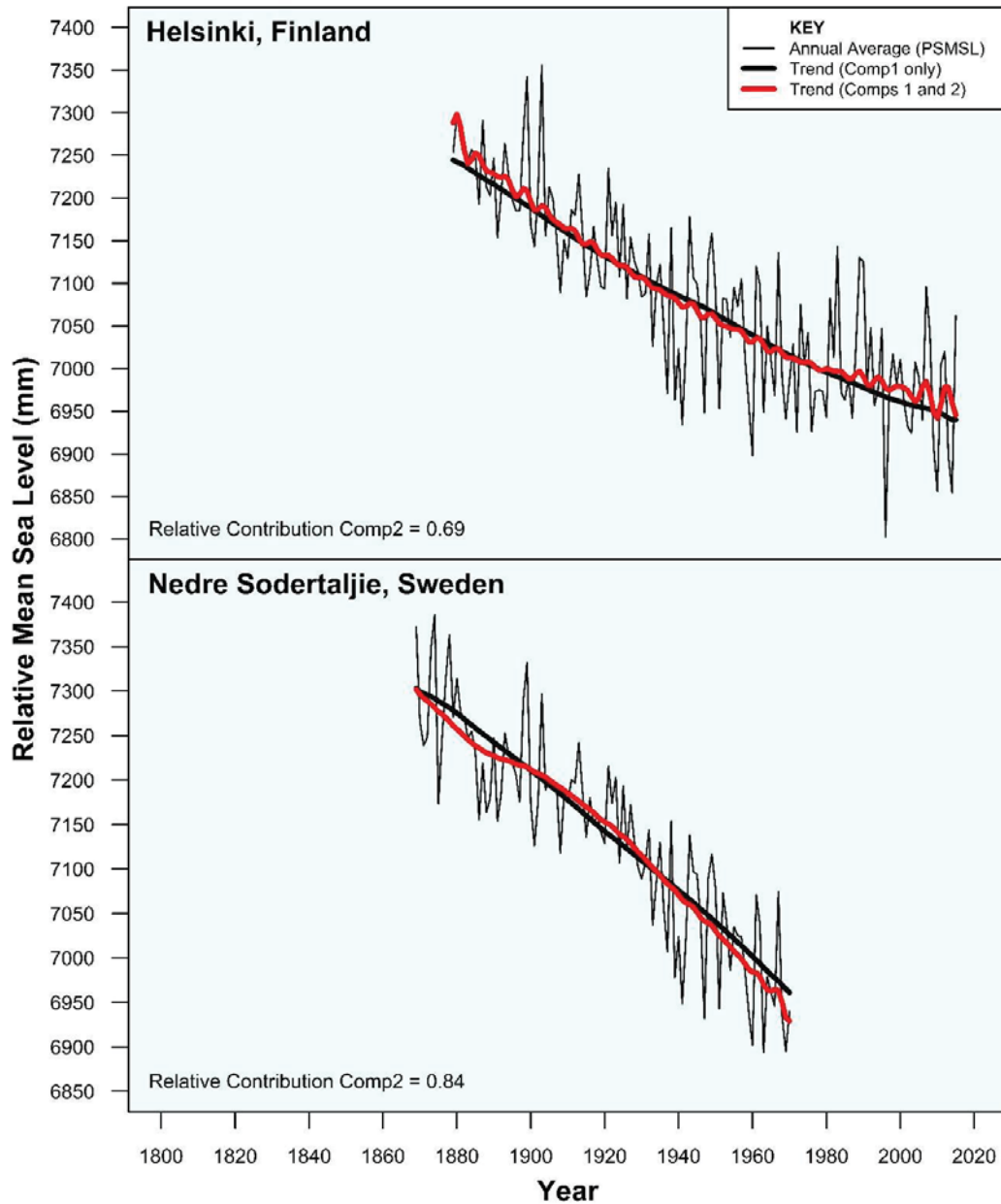
Figure D1: Leading 2 components of SSA decomposition for Brest and San Francisco mean sea level records.



Notes:

1. For further details on SSA decomposition, testing and parameterisations used, refer Section 4.3.3, Table 4.1 and Figure 4.1; and
2. The relative contribution of the singular value in the lowest frequency bin [0 – 0.01] is depicted in the lower left corner of each panel.

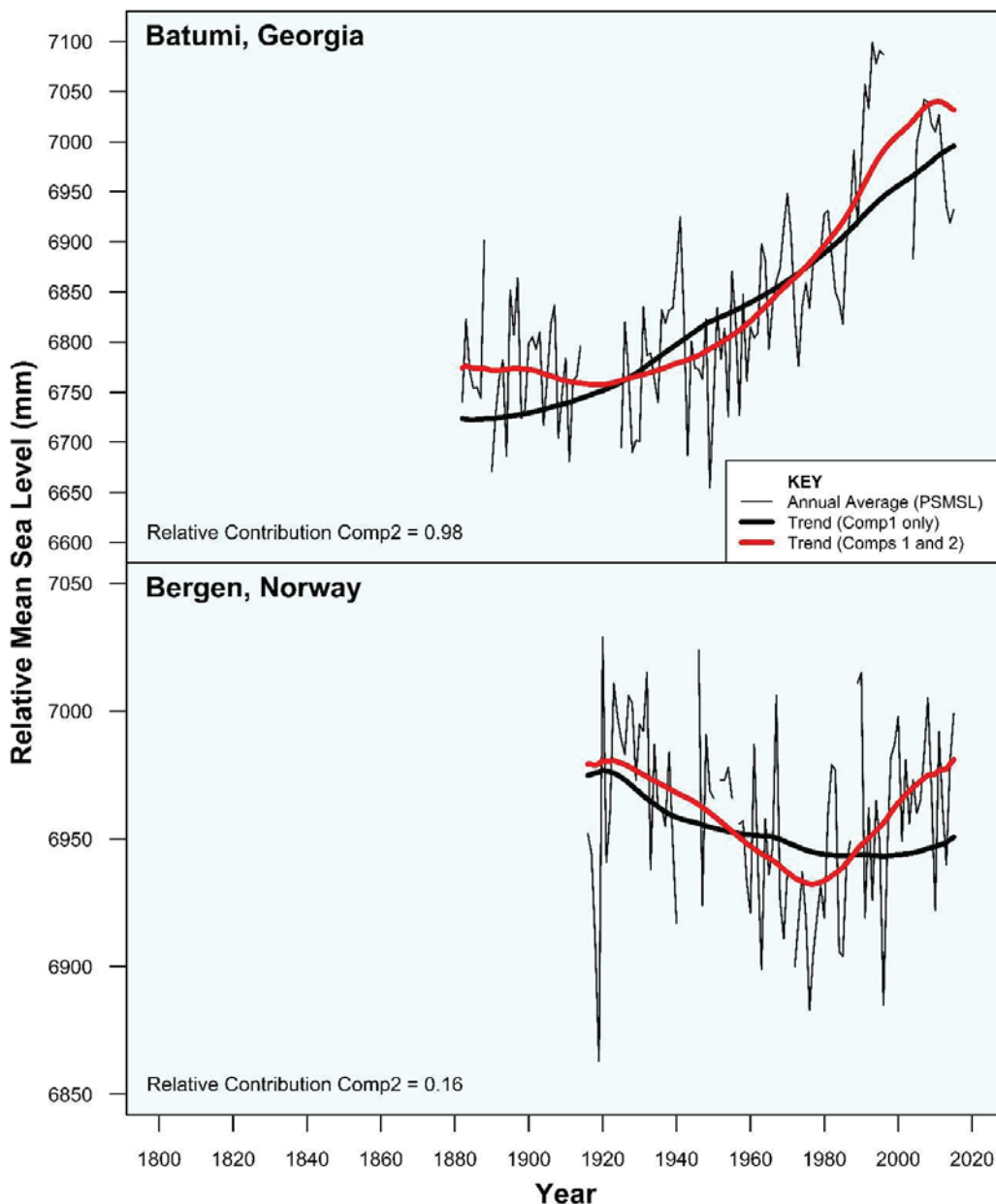
Figure D2: Leading 2 components of SSA decomposition for Helsinki and Nedre Sodertalje mean sea level records.



Notes:

1. For further details on SSA decomposition, testing and parameterisations used, refer Section 4.3.3, Table 4.1 and Figure 4.1; and
2. The relative contribution of the singular value in the lowest frequency bin [0 – 0.01] is depicted in the lower left corner of each panel.

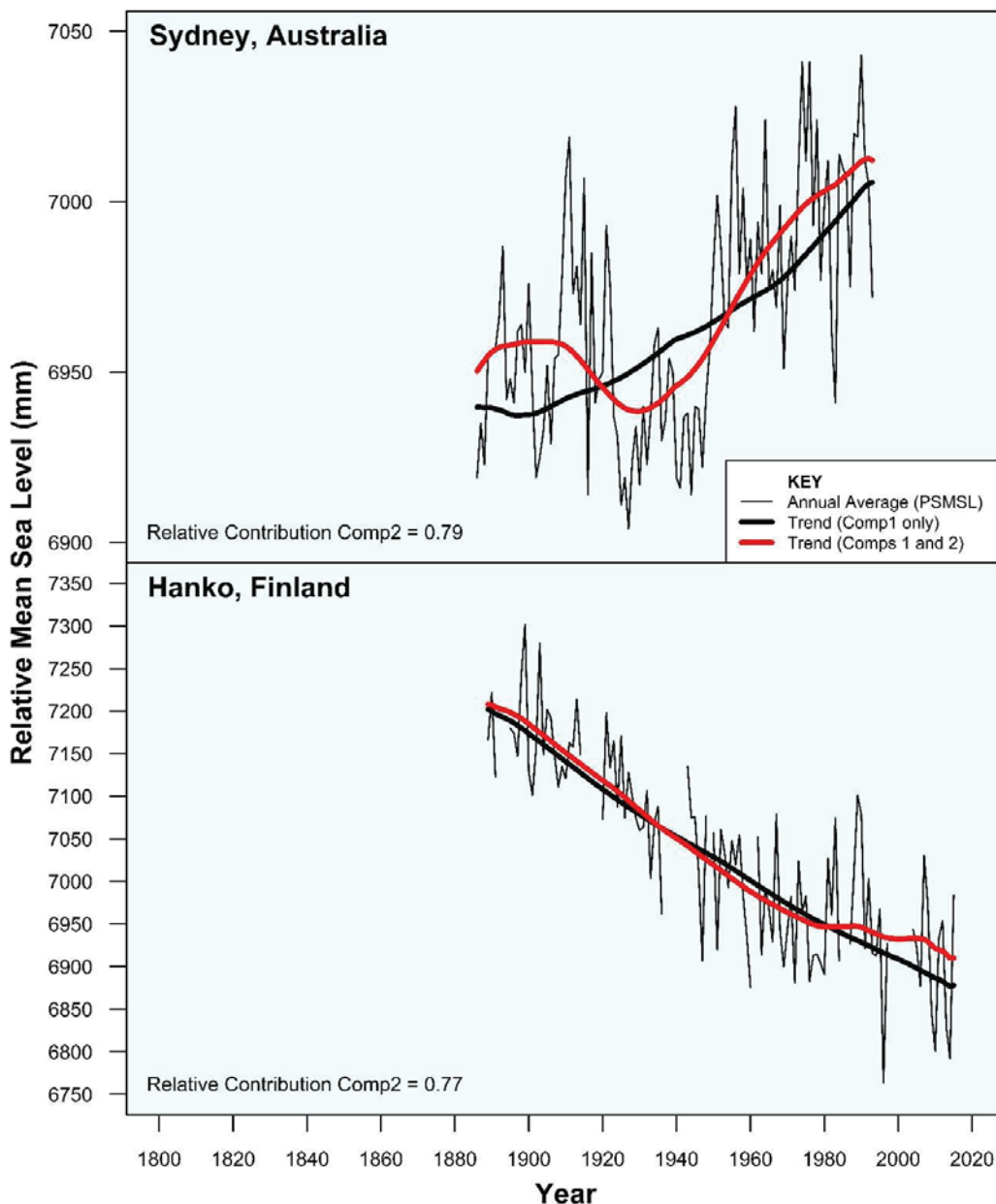
Figure D3: Leading 2 components of SSA decomposition for Batumi and Bergen mean sea level records.



Notes:

1. For further details on SSA decomposition, testing and parameterisations used, refer Section 4.3.3, Table 4.1 and Figure 4.1; and
2. The relative contribution of the singular value in the lowest frequency bin [0 – 0.01] is depicted in the lower left corner of each panel.

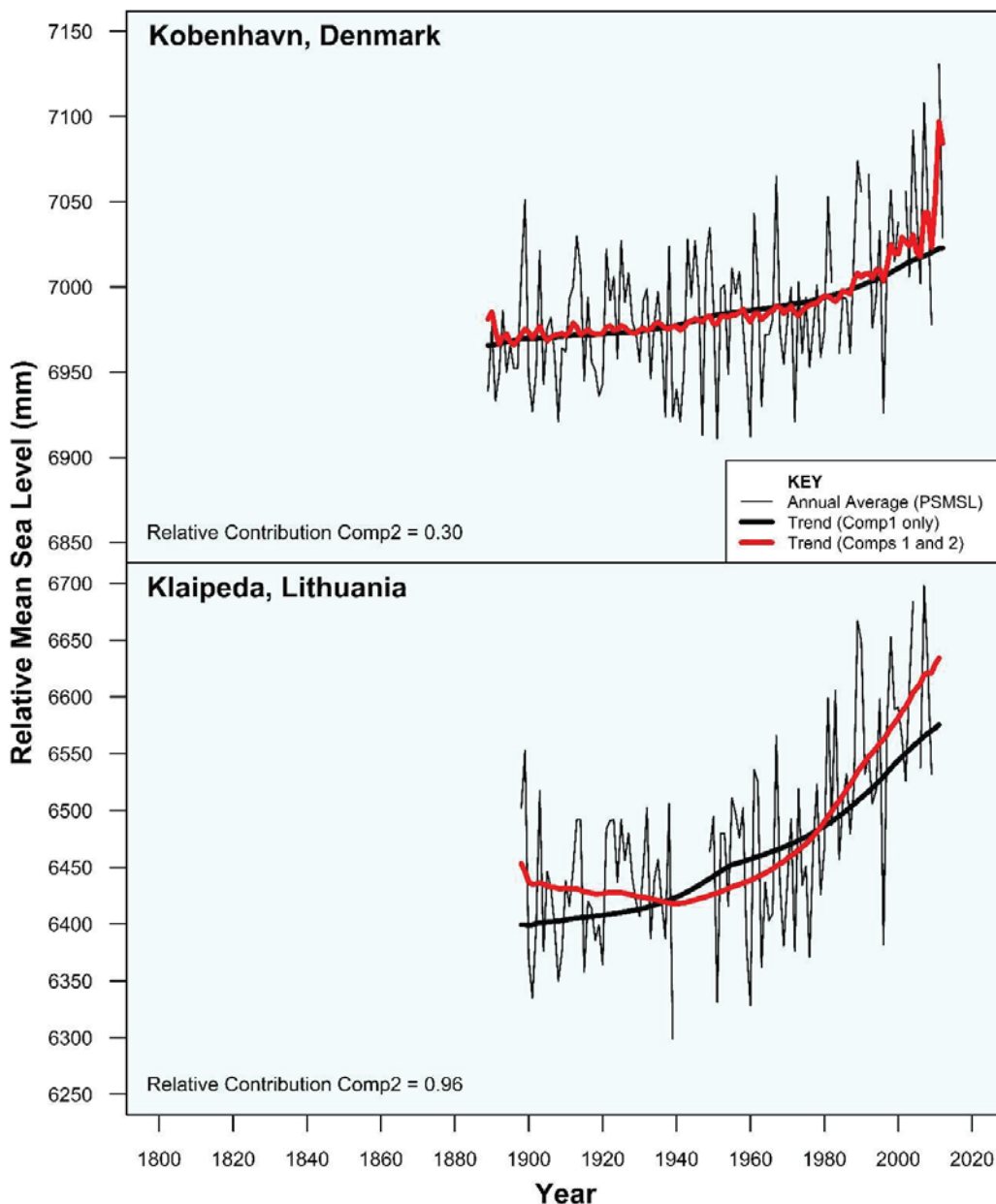
Figure D4: Leading 2 components of SSA decomposition for Sydney and Hanko mean sea level records.



Notes:

1. For further details on SSA decomposition, testing and parameterisations used, refer Section 4.3.3, Table 4.1 and Figure 4.1; and
2. The relative contribution of the singular value in the lowest frequency bin [0 – 0.01] is depicted in the lower left corner of each panel.

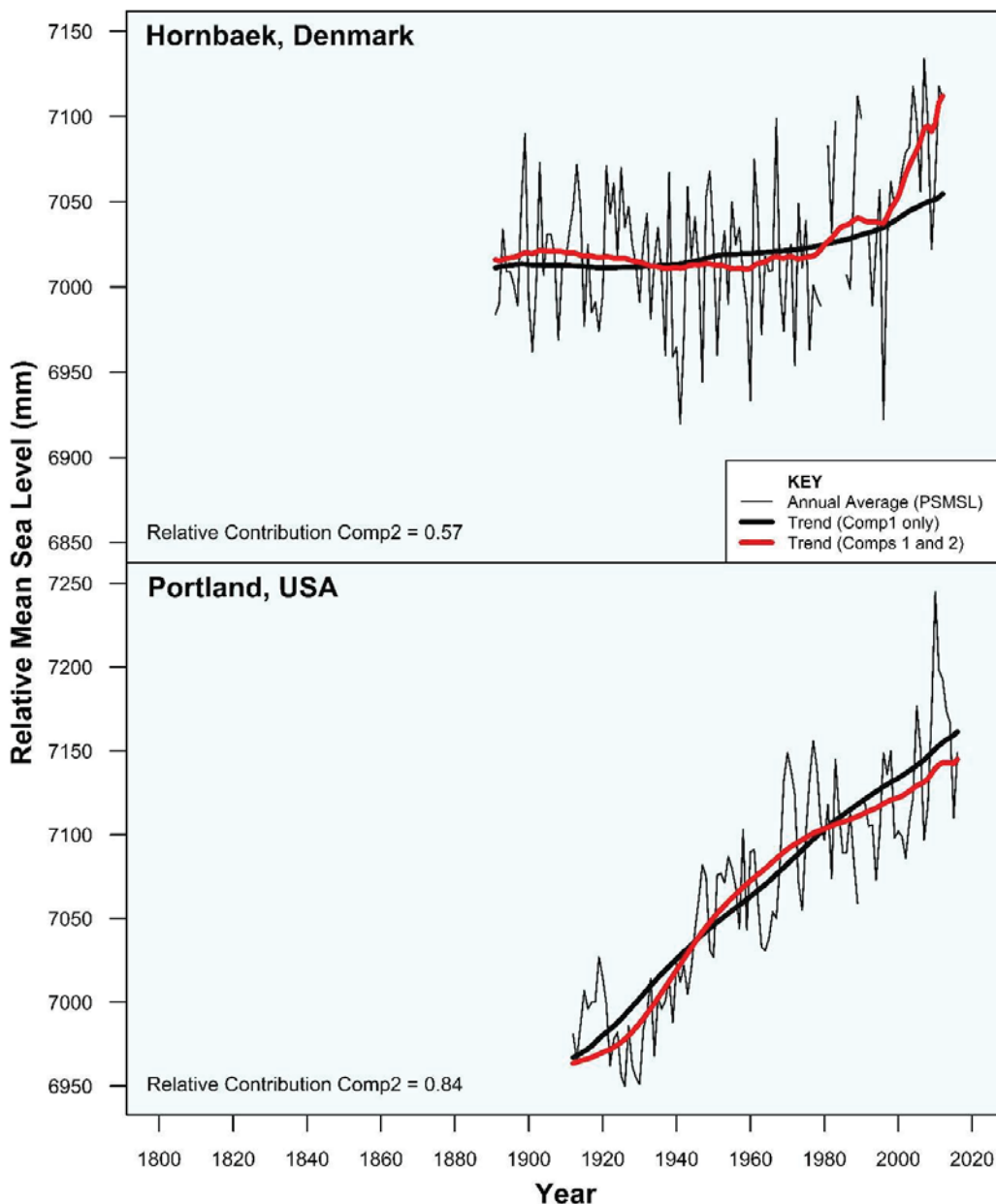
Figure D5: Leading 2 components of SSA decomposition for Kobenhavn and Klaipeda mean sea level records.



Notes:

1. For further details on SSA decomposition, testing and parameterisations used, refer Section 4.3.3, Table 4.1 and Figure 4.1; and
2. The relative contribution of the singular value in the lowest frequency bin [0 – 0.01] is depicted in the lower left corner of each panel.

Figure D6: Leading 2 components of SSA decomposition for Hornbaek and Portland mean sea level records.



Notes:

1. For further details on SSA decomposition, testing and parameterisations used, refer Section 4.3.3, Table 4.1 and Figure 4.1; and
2. The relative contribution of the singular value in the lowest frequency bin [0 – 0.01] is depicted in the lower left corner of each panel.

Appendix E

“Msltrend” User Manual

The “msltrend” package User Manual is available as a pdf document for download from the Comprehensive R Archive Network (CRAN) at the following URL:

<https://cran.r-project.org/web/packages/msltrend/index.html>.

Package ‘msltrend’

January 12, 2016

Type Package

Title Improved Techniques to Estimate Trend, Velocity and Acceleration from Sea Level Records

Version 1.0

Depends R (>= 3.2.2)

Date 2016-01-11

Description Analysis of annual average ocean water level time series from long (minimum length 80 years) individual records, providing improved estimates of trend (mean sea level) and associated real-time velocities and accelerations. Improved trend estimates are based on Singular Spectrum Analysis methods. Various gap-filling options are included to accommodate incomplete time series records. The package also contains a forecasting module to consider the implication of user defined quantum of sea level rise between the end of the available historical record and the year 2100. A wide range of screen and pdf plotting options are available in the package.

Author Phil J Watson <philwatson.slr@gmail.com>

Maintainer Phil J Watson <philwatson.slr@gmail.com>

License GPL (>= 3)

LazyData TRUE

Imports changepoint (>= 2.1.1), forecast (>= 6.2), plyr (>= 1.8.3), Rssa (>= 0.13-1), tseries (>= 0.10-34), zoo (>= 1.7-12)

Repository CRAN

NeedsCompilation no

RoxygenNote 5.0.1

Date/Publication 2016-01-12 08:46:00

R topics documented:

Balt	2
mssl.forecast	3
mssl.pdf	4

2		<i>Balt</i>
	mssl.plot	6
	mssl.trend	7
	mssl.trend	10
	s	10
	summary	11
	t	12
Index		14

Balt *Ocean water level data for Baltimore, USA*

Description

Annual average ocean water level data from Permanent Service for Mean Sea Level (UK).

Usage

`data(Balt)`

Format

Time series data file with the first column the year and the second column the corresponding annual average ocean water level (mm). File contains 112 records spanning the period from 1904 to 2014 with a single missing value in 1990.

Details

The raw (*.csv) form of this data set is used extensively in the examples throughout this manual.

Source

Permanent Service for Mean Sea Level (2015)

References

Holgate, S.J., Matthews, A., Woodworth, P.L., Rickards, L.J., Tamisiea, M.E., Bradshaw, E., Foden, P.R., Gordon, K.M., Jevrejeva, S. and Pugh, J., 2013. New data systems and products at the Permanent Service for Mean Sea Level. *Journal of Coastal Research*, 29(3), pp. 493-504.

See Also

`mssl.trend`, `mssl.forecast`, `mssl.plot`, `mssl.pdf`, `summary`.

Examples

```
data(Balt)
plot(Balt, type = "l", xlab = "Year", ylab = "Annual Average Mean Sea Level (mm)",
main = 'BALTIMORE, USA')
str(Balt) # check structure of data file
```

mssl.forecast

3

<code>mssl.forecast</code>	<i>Projected sea level rise integrated with historical record.</i>
----------------------------	--

Description

Projected sea level rise integrated with historical record.

Usage

```
mssl.forecast(object, slr = 800, plot = TRUE)
```

Arguments

<code>object</code>	of class "mssl.trend" (see <code>mssl.trend</code> and <code>s</code>).
<code>slr</code>	numeric, enables a user defined amount of projected sea level rise in millimetres. The user range is [200 to 1500] where 800 is the default setting.
<code>plot</code>	logical, if 'TRUE' then the original time series is plotted to the screen along with the trend component, the result of gap filling (where necessary) and the added quantum of sea level rise selected. 95% confidence intervals have also been applied. Default = TRUE.

Details

This routine adds a user specified quantum of sea level rise from the end of the deconstructed historical record to the year 2100. All internal parameters captured in the `mssl.trend` object are passed directly to `mssl.forecast`.

Value

An object of class "mssl.forecast" is returned with the following elements:

\$Station.Name: the name of the data record.

\$Summary: a summary data frame of relevant attributes relating to the trend and the inputted annual average data set extended to 2100 with projected sea level rise, including:

- **\$Year:** input data;
- **\$MSL:** input data;
- **\$Trend:** mean sea level trend;
- **\$TrendSD:** standard deviation of the determined mean sea level trend;
- **\$Vel:** velocity (or first derivative) of mean sea level trend (mm/year);
- **\$VelSD:** standard deviation of the velocity of the mean sea level trend;
- **\$Acc:** acceleration (or second derivative) of mean sea level trend (mm/year/year);
- **\$AccSD:** standard deviation of the acceleration of the mean sea level trend; and
- **\$FilledTS:** gap-filled time series (where necessary).

\$Velocity: outputs the peak velocity and the year in which it occurs.

\$Acceleration: outputs the peak acceleration and the year in which it occurs.

\$Historical.Record: outputs details of the start, end and length of the input data set.

\$Historical.Fillgaps: outputs the extent of missing data (years) in the original record and the gap filling method used (where necessary).

\$Projected.SLR: details the amount of sea level rise applied between the end of the historical record and the year 2100.

\$Bootstrapping.Iterations: outputs the number of iterations used to generate the respective standard deviations for error margins.

See Also

`msl.trend`, `msl.plot`, `msl.pdf`, `summary`, `Balt`, `s`, `t`.

Examples

```
# -----
# Isolate trend from Baltimore record, filling gaps with spline interpolation,
# 500 iterations and adding 1000 mm of slr to 2100. Use raw 'Balt.csv' data file.
# Note: ordinarily user would call 'File.csv' direct from working directory
# using the following sample code:
# s <- msl.trend('Balt.csv', fillgaps = 3, iter = 500, 'BALTIMORE, USA')
# t <- msl.forecast(s, slr = 1000)
# -----

data(s) # msl.trend object from above-mentioned example
data(t) # msl.forecast object from above-mentioned example
str(t) # check structure of msl.forecast object
msl.plot(s, type=2) # check screen output of gapfilling and trend estimate
msl.plot(t, type=2) # check screen output of adding 1000 mm of sea level rise
```

msl.pdf

Pdf plotting options.

Description

Pdf plotting options.

Usage

```
msl.pdf(x, file_name = " ", type = 1, ci = 1)
```

mssl.pdf

5

Arguments

<code>x</code>	object of class “ <code>mssl.trend</code> ” (see <code>mssl.trend</code> and <code>s</code>) or “ <code>mssl.forecast</code> ” (see <code>mssl.forecast</code> and <code>t</code>).
<code>file_name</code>	is a character string indicating the name of the pdf output file. If this field is left blank the output file will be automatically saved in the working directory under the default name “ <code>File1.pdf</code> ”.
<code>type</code>	numeric, enables a user defined input to select the type of chart to be plotted. The default setting (<code>type = 1</code>) provides 3 charts in the same plot area with the time series in the top panel, instantaneous velocity in the middle panel and instantaneous acceleration in the bottom panel. The alternatives (2, 3 and 4) are single panel plots of time series, instantaneous velocity and instantaneous acceleration, respectively.
<code>ci</code>	numeric, enables a user defined input to select the type of confidence interval to be displayed on the plots. The default setting (<code>ci = 1</code>) corresponds to a 95% confidence interval whilst <code>ci=2</code> provides a 99% confidence interval.

Details

This routine provides a range of pdf plotting options for both “`mssl.trend`” (see `mssl.trend`) and “`mssl.forecast`” (see `mssl.forecast`) objects. Three panel plots (`type 1` or default) are formatted with width = 16.54 inches and height = 20 inches. Single panel plots (`types 2, 3, 4`) are formatted with width = 16.54 inches and height = 15 inches. All plots are designed to be proportionally correct when imported into documents and re-sized to the width of a standard A4 page. The same range of alternative screen plotting options are available via `mssl.plot`.

See Also

`mssl.trend`, `mssl.forecast`, `mssl.plot`, `Balt`, `s`, `t`.

Examples

```
# -----
# Isolate trend from Baltimore record, filling gaps with spline interpolation,
# 500 iterations and adding 1000 mm of slr to 2100. Use raw 'Balt.csv' data file.
# Note: ordinarily user would call 'File.csv' direct from working directory
# using the following sample code:
# s <- mssl.trend('Balt.csv', fillgaps = 3, iter = 500, 'BALTIMORE, USA')
# t <- mssl.forecast(s, slr = 1000)
# -----

data(s) # mssl.trend object from above-mentioned example
data(t) # mssl.forecast object from above-mentioned example

# default output, 3 panels, 95% confidence intervals.
mssl.pdf(s)
# Check 'File1.pdf' in working directory

# pdf plot time series, 95% confidence intervals.
mssl.pdf(s, file_name = 'Series.pdf', type = 2)
```

```

# Check 'Series.pdf' file in working directory

# pdf plot instantaneous velocity, 95% confidence intervals.
mssl.pdf(s, file_name = 'Velocity.pdf', type = 3)
# Check 'Velocity.pdf' file in working directory

# pdf plot instantaneous acceleration, 99% confidence intervals.
mssl.pdf(s, file_name = 'Acceleration.pdf', type = 4, ci = 2)
# Check 'Acceleration.pdf' file in working directory

# default output, 3 panels, 95% confidence intervals.
mssl.pdf(t, file_name = 'Forecast.pdf')
# Check 'Forecast.pdf' file in working directory

```

mssl.plot

Screen plotting options.

Description

Screen plotting options.

Usage

```
mssl.plot(x, type = 1, ci = 1)
```

Arguments

x	object of class “mssl.trend” (see <code>mssl.trend</code> and <code>s</code>) or “mssl.forecast” (see <code>mssl.forecast</code> and <code>t</code>).
type	numeric, enables a user defined input to select the type of chart to be plotted. The default setting (<code>type = 1</code>) provides 3 charts in the same plot area with the time series in the top panel, instantaneous velocity in the middle panel and instantaneous acceleration in the bottom panel. The alternatives (2, 3 and 4) are single panel plots of time series, instantaneous velocity and instantaneous acceleration, respectively.
ci	numeric, enables a user defined input to select the type of confidence interval to be displayed on the plots. The default setting (<code>ci = 1</code>) corresponds to a 95% confidence interval whilst <code>ci=2</code> provides a 99% confidence interval.

Details

This routine provides a range of screen plotting options for both “mssl.trend” (see `mssl.trend`) and “mssl.forecast” (see `mssl.forecast`) objects. The same range of alternative pdf plotting options are available via `mssl.pdf`.

See Also

`mssl.trend`, `mssl.forecast`, `mssl.pdf`, `Balt`, `s`, `t`

mssl.trend

7

Examples

```

# -----
# Isolate trend from Baltimore record, filling gaps with spline interpolation,
# 500 iterations and adding 1000 mm of slr to 2100. Use raw 'Balt.csv' data file.
# Note: ordinarily user would call 'File.csv' direct from working directory
# using the following sample code:
# s <- mssl.trend('Balt.csv', fillgaps = 3, iter = 500, 'BALTIMORE, USA')
# t <- mssl.forecast(s, slr = 1000)
# -----

data(s) # mssl.trend object from above-mentioned example
data(t) # mssl.forecast object from above-mentioned example
mssl.plot(s) # default screen plot output, 3 panels, 95% confidence intervals
mssl.plot(s, type = 2) # plot time series, 95% confidence intervals
mssl.plot(s, type = 3) # plot instantaneous velocity, 95% confidence intervals
mssl.plot(s, type = 4, ci = 2) # plot acceleration, 99% confidence intervals
mssl.plot(t) # default screen plot output, 3 panels, 95% confidence intervals
mssl.plot(t, type = 2) # plot time series, 95% confidence intervals
mssl.plot(t, type = 3) # plot instantaneous velocity, 95% confidence intervals
mssl.plot(t, type = 4, ci = 2) # plot acceleration, 99% confidence intervals

```

*mssl.trend**Isolate trend component from mean sea level records.***Description**

Isolate trend component from mean sea level records.

Usage

```
mssl.trend(file, station_name = " ", fillgaps = 1, iter = 10000,
           plot = TRUE)
```

Arguments

file csv format input file **with no header row** of annual average water levels. This file must contain 2 columns with the first column the time period (in years) and the second column annual average ocean water levels (in millimetres). Missing data must be denoted by "NA". Missing data and maximum missing data gap are limited to 15% and 5%, respectively, of the data record. The minimum length data record processed by the package is 80 years.

Warning: If input data files do not conform to these pre-conditions, the analysis will be terminated. It should be further noted that the existence of quasi 60 year oscillations in global mean sea level have been well recognised in the literature. Therefore, in order to be effective for climate change and sea level research, only input files with a minimum length exceeding 80 years have been considered in order that the package can identify and isolate such signals.

station_name	character string, providing the name of the data record. Note: This field can be left blank, however, it is retained for use in banner labelling of all plotting and pdf outputs.
fillgaps	numeric, provides 3 alternative gap filling procedures for missing data. The default procedure (fillgaps = 1) is based on iterative gap filling using Singular Spectrum Analysis (refer <code>igapfill</code>). The alternatives (2 and 3) are based on linear interpolation and cubic spline interpolation, respectively (refer <code>na.approx</code>). Note: Gap filled portions of the time series are denoted in red on the default screen plot. This is done specifically to provide ready visual observation to discern if the selected gap filling method provides an appropriate estimate within the gaps in keeping with the remainder of the historical record. Depending on the nature of the record and extent of gaps, some trial and error between alternatives might be necessary to optimise gap filling.
iter	numeric, enables a user defined number of iterations for bootstrapping to determine error margins. The user range is [500 to 10000] where 10000 is the default setting. Warning: Although the default setting provides a more accurate basis for estimating error margins, the degree of iterations slows the analysis and can take several minutes to run.
plot	logical, if 'TRUE' then the original time series is plotted to the screen along with the trend component and the result of gap filling (where necessary). 95% confidence intervals have also been applied. Default = TRUE.

Details

This is the key entry point to the package. This function deconstructs annual average time series data into a trend and associated real-time velocities and accelerations, filling necessary internal structures to facilitate all other functions in this package. The trend is isolated using Singular Spectrum Analysis, in particular, aggregating components whose low frequency band [0 to 0.01] exceed a threshold contribution of 75%. Associated velocities and accelerations are determined through the fitting of a cubic smoothing spline to the trend with 1 degree of freedom per every 8 years of record length. Refer Watson (2016a,b) for more detail.

Value

An object of class "msl.trend" is returned with the following elements:

\$Station.Name: the name of the data record.

\$Summary: a summary data frame of the relevant attributes relating to the trend and the inputted annual average data set, including:

- \$Year: input data;
- \$MSL: input data;
- \$Trend: mean sea level trend;
- \$TrendSD: standard deviation of the determined mean sea level trend;
- \$Vel: velocity (or first derivative) of mean sea level trend (mm/year);
- \$VelSD: standard deviation of the velocity of the mean sea level trend;

- **\$Acc**: acceleration (or second derivative) of mean sea level trend (mm/year/year);
- **\$AccSD**: standard deviation of the acceleration of the mean sea level trend;
- **\$Resids**: time series of uncorrelated residuals; and
- **\$FilledTS**: gap-filled time series (where necessary).

\$Velocity: outputs of the peak velocity and the year in which it occurred.

\$Acceleration: outputs of the peak acceleration and the year in which it occurred.

\$Record.Length: outputs details of the start, end and length of the input data set.

\$Fillgaps: outputs the extent of missing data (years) in the original record and the gap filling method used (where necessary).

\$Bootstrapping.Iterations: outputs the number of iterations used to generate the respective standard deviations for error margins.

\$Changepoints: outputs the number and time at which changepoints in the variance of the uncorrelated residuals occur (if any). Where changepoints are identified, block bootstrapping procedures are used with residuals quarantined between changepoints.

References

Watson, P.J., 2016a. Identifying the best performing time series analytics for sea-level research. In: *Time Series Analysis and Forecasting, Contributions to Statistics*, ISBN 978-3-319-28725-6, Springer International Publishing (in press).

Watson, P.J., 2016b. How to improve estimates of real-time acceleration in the mean sea level signal. In: Vila-Concejo, A., Bruce, E., Kennedy, D.M., and McCarroll, R.J. (eds.), Proceedings of the 14th International Coastal Symposium (Sydney, Australia). *Journal of Coastal Research*, Special Issue, No. 75. Coconut Creek (Florida), ISSN 0749-0208 (in press).

See Also

mssl.forecast, mssl.plot, mssl.pdf, summary, Balt, s.

Examples

```
# -----
# Isolate trend from Baltimore record, filling gaps with spline interpolation and
# 500 iterations. Use raw 'Balt.csv' data file. Note: ordinarily user would call
# 'File.csv' direct from working directory using the following sample code:
# s <- mssl.trend('Balt.csv', fillgaps = 3, iter = 500, 'BALTIMORE, USA') # DONT RUN
# -----

data(s) # mssl.trend object from above-mentioned example
str(s) # check structure of mssl.trend object
mssl.plot(s, type=2) # check screen output of gapfilling and trend estimate
```

msltrend	<i>msltrend: A package providing improved techniques to estimate trend, velocity and acceleration from sea level records.</i>
----------	---

Description

The 'msltrend' package provides improved estimates of trend (mean sea level) and associated real-time velocities and accelerations from long (minimum 80 years), individual, annual average ocean water level data records. Improved trend estimates are based on Singular Spectrum Analysis methods. Various gap-filling options are included to accommodate incomplete time series records. The package also contains a forecasting module to consider the implication of user defined quantum of sea level rise between the end of the available historical record and the year 2100. A wide range of screen and pdf plotting options are available within the package.

msltrend functions

The `msl.trend` function is the key entry point to the package deconstructing annual average time series data records into a trend and associated real-time velocities and accelerations, filling necessary internal structures which facilitate all functions in this package (Refer Watson 2016a,b for more detail).

The `msl.forecast` function enables a user defined quantum of sea level rise to be added from the end of the deconstructed historical record to the year 2100. Similarly, this function estimates real-time velocities and accelerations from the start of the available historical record to the year 2100.

References

Watson, P.J., 2016a. Identifying the best performing time series analytics for sea-level research. In: *Time Series Analysis and Forecasting, Contributions to Statistics*, ISBN 978-3-319-28725-6, Springer International Publishing (in press).

Watson, P.J., 2016b. How to improve estimates of real-time acceleration in the mean sea level signal. In: Vila-Concejo, A., Bruce, E., Kennedy, D.M., and McCarroll, R.J. (eds.), Proceedings of the 14th International Coastal Symposium (Sydney, Australia). *Journal of Coastal Research*, Special Issue, No. 75. Coconut Creek (Florida), ISSN 0749-0208 (in press).

s	<i>sample 'm_{sl}.trend' object</i>
---	---

Description

Output of call to `msl.trend` used extensively in examples throughout this Manual.

Usage

`data(s)`

summary

11

Format`mssl.trend` object**Details**

This `mssl.trend` object is used extensively in the examples throughout this manual in order to call the object direct rather than producing the same via original code which can be computationally expensive. This object results from a decomposition of the Baltimore record, filling gaps with spline interpolation and using 500 iterations to generate error margins via bootstrapping.

Note: Ordinarily the user would call 'File.csv' direct from working directory, creating the 'mssl.trend' object using the following sample code:

```
s <- mssl.trend('Balt.csv', fillgaps = 3, iter = 500, 'BALTIMORE, USA') # DON'T RUN
```

See Also

`mssl.trend`, `mssl.forecast`, `mssl.plot`, `mssl.pdf`, `summary`, `Balt`.

Examples

```
data(s)
str(s) # check structure of object
```

*summary**Summary outputs of decomposed time series.*

Description

Summary outputs of decomposed time series.

Usage

```
summary(object)
```

Arguments

`object` of class "mssl.trend" (see `mssl.trend`) or "mssl.forecast" (see `mssl.forecast`).

Details

This routine provides a screen summary of the respective outputs from a `mssl.trend` or `mssl.forecast` object. The summary produced is identical to `str()` for an object of class "mssl.trend" (see `mssl.trend`) or "mssl.forecast" (see `mssl.forecast`).

See Also

`mssl.trend`, `mssl.forecast`, `Balt`, `s`, `t`.

Examples

```

# -----
# Isolate trend from Baltimore record, filling gaps with spline interpolation,
# 500 iterations and adding 1000 mm of slr to 2100. Use raw 'Balt.csv' data file.
# Note: ordinarily user would call 'File.csv' direct from working directory
# using the following sample code:
# s <- msl.trend('Balt.csv', fillgaps = 3, iter = 500, 'BALTIMORE, USA')
# t <- msl.forecast(s, slr = 1000)
# -----

data(s) # msl.trend object from above-mentioned example
data(t) # msl.forecast object from above-mentioned example
summary(s) # summary for object of class 'msl.trend' object
summary(t) # summary for object of class 'msl.forecast' object

```

t *sample 'msl.forecast' object*

Description

Output of call to `msl.forecast` used extensively in examples throughout this Manual.

Usage

`data(t)`

Format

`msl.forecast` object

Details

This `msl.forecast` object is used extensively in the examples throughout this manual in order to call the object direct rather than producing the same via original code which can be computationally expensive. This object results from a decomposition of the Baltimore record, filling gaps with spline interpolation and using 500 iterations to generate error margins via bootstrapping (see `s`). This `'msl.trend'` object is then parsed to `msl.forecast` with the addition of 1000 millimetres of sea level rise between the end of the historical record and 2100.

Note: Ordinarily the user would call `'File.csv'` direct from working directory, creating the `'msl.trend'` object first, then creating the above-mentioned `msl.forecast` object using the following sample code:

```

s <- msl.trend('Balt.csv', fillgaps = 3, iter = 500, 'BALTIMORE, USA') # DON'T RUN
t <- msl.forecast(s, slr = 1000) # DON'T RUN

```

See Also

`msl.trend`, `msl.forecast`, `msl.plot`, `msl.pdf`, `summary`, `Balt`, `s`.

t

13

Examples

```
data(t)
str(t) # check structure of object
```

Index

*Topic **datasets**

Balt, 2
s, 10
t, 12

Balt, 2, 4–6, 9, 11, 12

igapfill, 8

msl.forecast, 2, 3, 3, 5, 6, 9–12

msl.pdf, 2, 4, 4, 6, 9, 11, 12

msl.plot, 2, 4, 5, 6, 9, 11, 12

msl.trend, 2–6, 7, 10–12

msltrend, 10

msltrend-package (msltrend), 10

na.approx, 8

s, 3–6, 9, 10, 11, 12

summary, 2, 4, 9, 11, 11, 12

t, 4–6, 11, 12